

**INTEGRATED CORE-BASED SEQUENCE STRATIGRAPHY,
CHEMOSTRATIGRAPHY AND DIAGENESIS OF THE LOWER
CRETACEOUS (BARREMIAN–APTIAN), BIYADH AND SHU'AIBA
FORMATIONS, A GIANT OIL FIELD, SAUDI ARABIA**

A Dissertation

by

NASSER MOHAMMAD S. AL-GHAMDI

Submitted to the Office of Graduate Studies of
Texas A&M University
in partial fulfillment of the requirements for the degree of

DOCTOR OF PHLOSOPHY

Chair of Committee,	Michael C. Pope
Committee Members,	Yuefeng Sun
	Ernest A. Mancini
	Hisham Nasr-El-Din
Head of Department,	Rick Giardino

August 2013

Major Subject: Geology

Copyright 2013

ABSTRACT

This study provides the most updated stratigraphic, depositional and diagenetic histories of the Early Cretaceous Biyadh and Shu'aiba formations. Carbon isotope data were integrated with core descriptions and well logs to define the age model beyond the resolution of biostratigraphy; they were also used as a geochronology tool for correlating between wells and across platform to basin transitions.

The Biyadh Formation consists of one 3rd-order sequence of four high-frequency sequences (S1-S4). S1 and S2 are the TST, composed of deep chalky limestone facies. S3 and S4 are the HST composed of skeletal rudist grainstone deposited in shallow water environments. The Biyadh sequence is capped by a regional subaerial boundary (SB1) corresponding to a global sea level fall. The Shu'aiba Formation consists of one 2nd-order sequence of four 3rd-order sequences and ten HFS's (S1-S10). S1 records the initial TST, followed by the regional MFS (K70) of S2. S3 is the late TST and is dominated by *Lithocodium aggregatum*/coral facies. S4 to S6 formed the early HST and are dominated by rudist buildups that transitioned basinward into fore-bank, slope and basinal settings with pronounced clinoform geometries. S7 and S8 are composed of shallow lagoonal milliolid packstone, representing the late HST. S9 and S10 are new identified Upper Aptian prograding sequences that formed during forced regression on the northern-block within platform edge and slope settings.

The correlation between the Arabian Plate stratigraphic record and the standard Tethys isotope record and eustatic sea-level suggests a direct influence of the 3rd-order

sea-level fluctuations on the Biyadh and Shu'aiba formations. This correlation also suggests that the Aptian were mainly controlled by glacio-eustatic fluctuations associated with eccentricity cycles. The Barremian records low magnitude sea-level changes and thinner sequences likely reflecting obliquity cycles. The Shu'aiba Formation records major subaerial hiatus reflecting glacial intervals, interrupted by flooding units reflecting global warming intervals.

Trace elements, microprobe analysis, Cathodoluminescence (CL) and stable isotope data were used to define the diagenetic history of the Shu'aiba Formation within the sequence stratigraphic framework. The Shu'aiba Formation was mainly affected by meteoric diagenesis associated with the major unconformity at top of Shu'aiba.

DEDICATION

This dissertation is dedicated to my mother and father for their encouragement, to my wife and children for their support and patience.

ACKNOWLEDGEMENTS

Thanks are first given to Allah almighty for endless help, guidance and blessings. I would like to thank my committee chair, Dr. Michael Pope, and my committee members, Dr. Yuefeng Sun, Dr. Ernest Mancini and Hisham Nasr-El-Din for their guidance and support throughout the course of this research.

I thank the Exploration Organization and the Reservoir Characterization Department at Saudi Aramco Oil Company for providing data, support and for the permission to publish this work.

Finally, thanks to my mother and father for their encouragement, to my wife and children for their support and patience throughout my work.

TABLE OF CONTENTS

	Page
ABSTRACT	ii
DEDICATION	iv
ACKNOWLEDGEMENTS	v
TABLE OF CONTENTS	vi
LIST OF FIGURES.....	ix
LIST OF TABLES	xiv
 CHAPTER	
I INTRODUCTION.....	1
II STRATIGRAPHIC ARCHITECTURE, FACIES ANATOMIES AND THEIR IMPLICATIONS ON GLOBAL CORRELATION AND PALEOCLIMATE EVALUATION OF THE EARLY CRETACEOUS BARREMIAN AND APTIAN (BIYADH AND SHU'AIBA FORMATIONS) IN A GIANT OIL FIELD, SAUDI ARABIA.....	6
Overview	6
Introduction	9
Geological Setting.....	13
Methodology and Data Sets	16
Facies Description	19
Sequence Stratigraphy.....	33
Introduction	33
Biyadh and Shu'aiba Sequence Stratigraphy.....	39
Parasequences.....	54
Discussion	57
Barremian verses Aptian Sequence Stratigraphy.....	57
Shu'aiba Formation Hierarchy and Platform Evolution.....	59
Maximum Flooding Surfaces.....	61
Anatomy of the Shu'aiba Formation Platform.....	64
Global Correlation.....	78

CHAPTER	Page
Implication and Significance of Global Correlations.....	88
Implication and Significance for Reservoir Geology.....	89
Conclusions	92
III INTEGRATED HIGH-RESOLUTION CHEMOSTRATIGRAPHY AND FACIES-BASED STRATIGRAPHIC ARCHITECTURE OF THE EARLY CRETACEOUS (APTIAN), SHU'AIBA FORMATION, SAUDI ARABIA.....	96
Overview	96
Introduction	98
Methodology	104
Geological Setting.....	105
Stratigraphic Framework.....	106
Chemostratigraphy	110
General Results	110
Carbon Isotope Record.....	114
Oxygen Isotope Record.....	120
Sequence 1.....	122
Sequence 2.....	123
Sequences 3 - 7.....	126
Sequences 8 and 9	127
Discussion	128
Isotopes versus Depositional Facies.....	128
Carbon Isotope Curves versus Stratigraphic Framework and Depositional Settings.....	133
Isotope Stratigraphy versus Global Sea-Level Changes	144
Carbon Isotope Stratigraphy versus High-Frequency Parasequences.....	146
Carbon Isotope and Palaeoclimate Changes	149
Conclusions	151
IV TRACE ELEMENT VARIATIONS, GEOCHEMICAL ANALYSIS AND THEIR IMPLICATIONS ON DIAGENETIC HISTORY OF THE EARLY CRETACEOUS (APTIAN) SHU'AIBA FORMATION.....	155
Overview	155
Introduction	157
Data Sets.....	160

CHAPTER	Page
Results	161
Trace Elements	161
Microprobe Analysis	171
Cathodoluminescence (CL)	175
Isotope Geochemistry	181
Discussions	185
Trace Elements	185
Microprobe Analysis	193
Cathodoluminescence (CL)	195
Isotope Geochemistry	197
Paragenetic Sequence	201
Conclusions	203
V CONCLUSIONS	206
REFERENCES	211

LIST OF FIGURES

FIGURE	Page
1	Aptian paleogeographic map for the Arabian Plate showing the location of study area and the intrashelf basins 10
2	Barremian to Aptian chronostratigraphy of the study area, showing the general sequence stratigraphy 11
3	Base map and facies distribution at S6 of Shu'aiba platform showing three cross-section traverses (A-A', B-B' and C-C') and 55 cored-wells used in this study 15
4	Type composite core description showing general lithofacies description, sequence stratigraphy and gamma ray logs within the marginal setting.... 18
5	Core sample photographs of typical facies in Biyadh Formation 20
6	Core sample photographs of typical deep subtidal and <i>Lithocodium</i> facies in Shu'aiba Formation 21
7	Core sample photographs of typical rudist facies in Shu'aiba Formation.. 22
8	Core sample photographs of typical deep ramp facies and sequence boundaries in Shu'aiba Formation 23
9	Depositional model of Late Barremian Biyadh Formation shows the position of each facies on a low angle homoclinal ramp platform..... 24
10	Depositional model for the Hawar unit showing restricted shallow subtidal/tidal flat environment (condensed unit)..... 25
11	Depositional model for the <i>Lithocodium</i> algal platform of Lower Shu'aiba Formation, HFS's 2 and 3 26
12	Depositional model for HFS's 4-6 within the rudist buildups, showing the position of each facies in a barrier-bank low angle ramp..... 27
13	Depositional model for the Upper Aptian HFS's 9 and 10 showing the shelf marginal edge within the prograding sequences..... 28

FIGURE	Page
14 West-East type chronostratigraphic cross section of the Shu'aiba Formation correlating gamma ray logs and $\delta^{13}\text{C}$ isotope curves	34
15 Detail N-S stratigraphic cross section (D-D') of Biyadh Formation and Hawar Member on the Northern block	35
16 Detail W-E dip oriented stratigraphic cross section of Shu'aiba Formation on the Northern block	36
17 Detail W-E stratigraphic cross section of Shu'aiba Formation on the Southern block	37
18 Detail N-S stratigraphic cross section of Shu'aiba Formation from Southern and Northern blocks across the intraplatform depression	38
19A Schematic stratigraphic profiles of the Shu'aiba Formation showing the evolution of the Shu'aiba platform within the depositional profiles and the Shu'aiba stratigraphic hierarchy	50
19B Legend, symbols and color codes of lithofacies used in the above cross sections	51
20 Facies map at top of HFS 3	66
21 Facies map at top of HFS 4	67
22 Facies map at top of HFS 5	68
23 Facies map at top of HFS 6	69
24 Facies map at top of HFS 7	70
25 Facies map at top of HFS 8	71
26 Facies map of the Upper Aptian sequences 9 and 10	72
27 Composite global correlation between the Arabian Plate Biyadh and Shu'aiba formations and the global stratigraphic records	80
28 Aptian paleogeographic map for the Arabian Plate showing the location of study area and the intrashelf basins	100

FIGURE	Page
29 Base map of Shu'aiba platform showing two cross-section lines (A-A', B-B') and wells used in this study	101
30 Stratigraphic column of the Early Cretaceous strata in Saudi Arabia	102
31 Two-dimensional depositional model showing the evolution of the Shu'aiba platform associated with major facies associations	107
32 Type well (M) showing composite isotope data calibrated with core descriptions and gamma ray logs	111
33 Carbon versus oxygen isotope plots from all 21 wells.....	112
34 Type east-west chronostratigraphic cross section of the Shu'aiba Formation correlating gamma ray logs and $\delta^{13}\text{C}$ isotope curves for five wells versus the Tethyan pelagic curve of Föllmi et al. (2006)	116
35 Integrated west-east cross section showing high-resolution stratigraphic framework, gamma ray logs and $\delta^{13}\text{C}$ isotope curves from platform to basin transition	117
36A Integrated north-south strike trend cross section.....	118
36B Legend, symbols and color codes of lithofacies used in the above cross sections.....	119
37 Correlation of oxygen isotope curves from several wells in the shelf-marginal setting showing major sequence boundaries.....	121
38 Core sample photographs of some important boundaries and facies	125
39 Carbon isotope curves from all wells plotted against depth.....	135
40 Carbon isotope curves from the deep-lagoonal setting	136
41 Carbon isotope curves from the shelf-marginal setting	137
42 Carbon isotope curves from the back-bank/platform-interior setting	138
43 Carbon isotope curves from the slope and open-marine settings.....	139
44 Carbon isotope curves from the basinal setting	140

FIGURE	Page
45 Carbon isotope correlation of the west-east platform to basin transition illustrating how biostratigraphy and chemostratigraphy data are integrated to determine the stratigraphic geometry of the Shu'aiba Formation and agecdifference between the Lower Aptian platform sequences and the Upper Aptian prograding.....	141
46 Carbon isotope curve in a higher resolution scale from Well H, plotted against core description of Well H.....	148
47 Base map with the Shu'aiba platform facies showing well locations.....	158
48 Trace elements from rudist buildup setting of Well-52 plotted against depth and superimposed by major sequence boundaries	163
49 Trace elements from rudist buildup setting of Well-6 plotted against depth and superimposed by major sequence boundaries	166
50 Trace elements from slope/shelf edge setting of Well-55 plotted against depth and superimposed by major sequence boundaries	168
51 Trace elements from open marine setting of Well-19 plotted against depth.....	170
52 Thin sections samples of different cements show the location of the microprobe analysis.....	173
53 Thin sections samples of different cements show the location of the microprobe analysis.....	174
54 Plain light and Cathodoluminescence petrography zones of rudist fragments within rudist buildups	178
55 Plain light and Cathodoluminescence petrography zones of rudist fragments within rudist facies and slope setting	179
56 Plain light and Cathodoluminescence petrography zones of large blocky calcite	180
57 Cross plot of carbon and oxygen isotope data of both mud matrix (blue) and cements (red)	182

FIGURE	Page
58 Strontium isotope curves ($^{87}\text{Sr}/^{86}\text{Sr}$) linked to core descriptions and sequence stratigraphy	184
59 Major trace elements from different wells plotted against depth.....	188
60 Cross plot of Fe and Mn from all data	189
61 Magnesium concentration plotted against concentrations of Fe, Sr and Mn	192
62 Cross plot of carbon and oxygen isotope data from calcite cements	199
63 Paragenetic sequences of the main events from early to late diagenesis ...	202

LIST OF TABLES

TABLE		Page
1A	Summary of Lithofacies in shelf margin settings.....	29
1B	Summary of Lithofacies in open marine and basinal settings.....	30
2	Trace elements from all wells with range and average for each trace element	162
3	Summary of microprobe analysis from eight thin sections of 39 samples.	172

CHAPTER I

INTRODUCTION

The Cretaceous carbonate platforms are some of the largest and most widespread sedimentary successions in the stratigraphic records (Simo et al., 1993). They contain approximately 16% of the world's hydrocarbon reserves (Carmatt and St. John, 1986; Klemme and Ulmishek, 1991 in Scott et al., 1993). The Lower Cretaceous Barremian and Aptian, Biyadh and Shu'aiba formations are one of the main prolific oil reservoirs in the Middle East (Alsharhan and Nairn 1986; Alsharhan, 1995; van Buchem et al. 2010; AL-Ghamdi and Read, 2010). The Shu'aiba and Biyadh formations are composed mainly of pure carbonate successions and are separated by dense argillaceous carbonate units that act as a seal between the two reservoirs. These carbonate successions contain distinctive buildup facies of rudists, corals, stromatoporoids and *Lithocodium* algal platform with distinct dominance of certain organisms according to their stratigraphic and depositional settings. The Aptian Shu'aiba Formation is one of the largest and most geologically and petrophysically complex hydrocarbon reservoir in the Middle East, due to facies heterogeneities, syn-depositional faulting and diagenetic overprints. Understanding the distribution of these facies within stratigraphic framework is the key for developing better 3-D reservoir and simulation models.

This study focuses on developing a high-resolution core-based chronostratigraphic model using an integrated approach, where stable-isotope data are linked to well-logs and core descriptions to constrain the age model of the Biyadh and

Shu'aiba formations. Therefore, this study provides the most updated and accurate high-resolution sequence and chemostratigraphic frameworks that cover the entire Shu'aiba platform using all available cored wells (50 wells), including carbon isotope profiles from 26 wells. This study identified new Upper Aptian prograding sequences that occurred within the northern platform edges. The study also analyzed and interpreted a wide range of lithofacies and depositional settings. The Shu'aiba Formation records complex facies architectures that changed laterally from lagoonal settings on the western flank to platform interiors and rudist margin in the middle to slope and open marine settings on the eastern flank.

Carbonate platforms contain wealth of information about paleoenvironments, paleoclimate, ocean chemistry and sea level fluctuations. Therefore, they represent an archive for these global changes along with processes that are driving them. The early Cretaceous successions of Biyadh and Shu'aiba formations provides a good opportunity for analyzing these changes using excellent core converges along with wireline logs and stable-isotope data. The integration of stable-isotope geochemistry with sequence stratigraphy help analyze the effects of the perturbation of carbon cycles occurred during these times that expressed by carbon-isotope excursions. It also helps evaluate the effect of rapid climate changes during the Early Cretaceous. These changes include warming events associated with global transgressive related to the global methane disassociation, followed by the development of the global Oceanic Anoxic Event 1a and then followed by cooling intervals associated with global regressions of sea level.

This dissertation is divided into three main projects, each of which presents a complete individual paper design for journal publication. However, these projects are directed into three major objectives. These major objectives includes; (1) developing a new detail high-resolution stratigraphic and facies architectures for the Biyadh and Shu'aiba formations for reservoir characterization and development; (2) understanding the diagenesis history and porosity evolution to define flow units and barriers within the reservoir; (3) evaluating the effect of global eustatic sea level fluctuations and stable-isotope geochemistry with their implications on global correlations and paleoclimate changes within the Barremian and Aptian stages.

Chapter two is focusing on the descriptions of lithofacies with their relationship to depositional environments and sequence stratigraphy. Five detail depositional models were constructed to illustrate the evolution of the Biyadh and Shu'aiba platforms within the sequence stratigraphic framework. Four detailed stratigraphic cross sections were generated to illustrate the new refined stratigraphic frameworks with new additional Upper Aptian sequences identified on the north-eastern flank of the platform edge. Facies maps of each sequence were generated showing the distribution of lithofacies and the evolution of the rudist buildups. These maps are significant in generating reservoir model and will also be used in predicting the spatial and temporal variations of lithofacies with their implication on reservoir quality. A refined global correlation between the Lower Cretaceous stratigraphic records and the global sea level curve, global isotope profile and orbital sea level model has been established. This correlation provides better correlation that fit with the global stratigraphic records including the

oceanic anoxic event 1a and repositioning the major maximum flooding surfaces K70 and K80.

Chapter three is focusing on the stable isotope chemostratigraphy analysis and how carbon isotope data were integrated with core data to develop a higher resolution age model, especially within the slope and open marine settings. The integration of carbon isotope data with core data suggest that the carbon isotope record of the Shu'aiba platform represents the original marine signature and their fluctuations represents the global signature. Oxygen and strontium isotope data were also incorporated into this study, but were not as useful as the carbon isotope data due to the effect of the diagenesis. The effects of depositional environments and lithofacies on the carbon and oxygen isotope data were also analyzed and interpreted. The relationship between carbon isotope profiles and global sea level changes were also investigated to evaluate the hypotheses of using the isotope data as a proxy of global sea level fluctuations.

Chapter four is focusing on the diagenesis history of the Shu'aiba Formation with some emphasize on trace element variations, and microprobe analysis and their relationships with sequence stratigraphy and depositional settings. Trace elements from five wells representing different facies and depositional settings were plotted against depth and superimposed by major sequence boundaries to analyze their variations and determine the major diagenetic environments. Microprobe analysis were done on selective samples to investigate different type of cements and diagenetic features and then linked to cathodoluminescence stages. Other data such as petrography,

cathodoluminescence and stable isotope data were analyzed and incorporated to define paragenetic sequences and understanding how porosity formed.

CHAPTER II

**STRATIGRAPHIC ARCHITECTURE, FACIES ANATOMIES AND THEIR
IMPLICATIONS ON GLOBAL CORRELATION AND PALEOCLIMATE
EVALUATION OF THE EARLY CRETACEOUS BARREMIAN AND APTIAN
(BIYADH AND SHU'AIBA FORMATIONS) IN A GIANT OIL FIELD, SAUDI
ARABIA**

Overview

A high-resolution core-based sequence stratigraphic framework with new facies and depositional anatomies are constructed for the Lower Cretaceous Barremian-Aptian Biyadh and Shu'aiba Formations in a giant hydrocarbon reservoir in Saudi Arabia. The integrated dataset, including fifty-five cored wells calibrated with gamma ray logs, biostratigraphy and stable isotope chemostratigraphy, constrains the internal correlation of this field and indicates a platform-to-basin transition and prograding clinoform geometries during falling sea level. This model will be used for constructing a new higher resolution 3-D reservoir models and when integrated with petrophysics, should enhance the simulation model and provide a better production plan for the reservoir. The Shu'aiba platform is divided into two distinct blocks (north and south) by syn-depositional fault systems. Each block has distinctive reservoir and facies characteristics.

The Biyadh Formation consists of one 3rd-order sequence composed of four high-frequency sequences (S1-S4). Sequences 1 and 2 formed the TST of the composite

sequence with a deeper subtidal platform of chalky mudstone/wackestone facies. Sequences 3 and 4 formed the HST and are composed of high-energy shallow subtidal facies dominated by Caprotinid rudists and peloidal grainstone. The entire Shu'aiba Formation forms a 2nd-order composite sequence, comprised of four 3rd-order sequences and ten high-frequency sequences (S1-S10). 3rd-order sequence 1 is comprised of S1-S3; 3rd-order sequence 2 is comprised of S4-S6; 3rd-order sequence 3 is comprised of S7 and S8 and 3rd-order sequence 4 is comprised of S9 and S10. S1 records the initial TST with the deposition of Hawar Member, followed by deposition of the deepest water facies during S2 including the regional MFS (K70). S3 is the late TST of the Shu'aiba composite sequence and is characterized by the extensive *Lithocodium aggregatum*/coral facies. During this sequence the platform differentiated producing platform to basin settings with slight clinoform and backstepping geometries. S4-S6 marks the onset of rudist buildup facies with a well established platform-margin setting that changed laterally from back-bank and lagoonal settings into bank-crest then the fore-bank, slope and basinal settings with a pronounced basinward clinoform geometry. 3rd-order sequence 2 has a transgressive lag at the base dominated by *glossomyophorus* rudists that deepen upward to the MFS of the Shu'aiba 2nd-order composite sequence (K80) and is overlain by massive high-energy bank-crest facies of *in situ* caprinid rudist rudstone that passes upward into well-rounded rudist fragments formed in beach environments. A subaerial exposure surface (SB 7) caps sequence 6 on top of the rudist buildups. S7 and S8 are dominated by shallow lagoonal peloidal milliolid packstone facies associated with

local *Agriopleura* floatstone, deposited during the HST of the Shu'aiba composite sequence.

The Upper Aptian sequences S9 and S10 are newly identified sequences recorded on the northern-block within the platform edge and slope settings recording progradational systems formed during a major forced regression. These sequences were determined on the basis of chemostratigraphic analysis calibrated with available biostratigraphy. These sequences compose a lowstand wedge of argillaceous mudstone facies that may act as a reservoir baffle zone, changing upward to high-energy marginal facies of mixed rudist and stromatoporoid/coral facies. Regional correlation suggest that more prograding sequences likely formed basinward during the prolonged exposure of the platform.

A proposed correlation between the Arabian Plate and global stratigraphic records has significant implications on the evaluation of paleoclimate and glacio-eustatic controls of the Lower Cretaceous Barremian and Aptian. Of particular importance in this study is the refined position of the regional flooding events K70 and K80 and their relation with the global sea-level changes and perturbations in the global Earth's system during the Aptian stage. Evidences of glacial events during the Aptian are recorded within the Shu'aiba sequences alternating with warming events associated with nannoconids crisis and Oceanic Anoxic Event (OAE 1a). The stratigraphic record in this study and their global correlation suggests that the Barremian stage was dominated by warm greenhouse interval, followed by rapid climate change of possibly more transitional interval in the Aptian associated with glacial events.

Introduction

The Lower Cretaceous Shu'aiba Formation is one of the main oil producers in the United Arab Emirates, Oman, Qatar and Saudi Arabia (Alsharhan and Nairn 1986; Alsharhan, 1995; Hughes, 2000; Borgomano et al, 2002; van Buchem et al. 2002; Immenhauser et al. 2004; van Buchem et al. 2010; AL-Ghamdi and Read, 2010). The Lower Cretaceous Barremian and Aptian successions of Biyadh and Shu'aiba Formations (Figures 1 and 2), are NE-trending carbonate rudist build-up with average thickness of 600 ft (183 m) located in a remote area within the Empty Quarter. The Shu'aiba carbonate build-up in the study area formed on the edge of a shallow ramp bordering the adjacent intra-shelf basin (Figure 1). The Shu'aiba Formation has complex facies architecture with heterogeneous reservoir quality, due to the development of rudist banks, syn-depositional faulting and later diagenetic overprinting. Sequences within the build-up are difficult to map, likely because of growth faulting, depositional topography, rapid facies changes and stacking and shingling of rudist banks. The Shu'aiba reservoir in the study area has been producing for 14 years and a high-resolution sequence stratigraphic framework is essential to build a secondary development plan for this giant oil field.

Early description for the Shu'aiba Formation was conducted by Ziegler (1976). The first geological model for reservoir modeling was produced by Aktas and Hughes (1998). However, the descriptive framework was mainly in terms of depositional setting rather than rock types. A detailed description of biofacies and their environments was provided by Hughes (2000). A higher resolution stratigraphic model and detailed

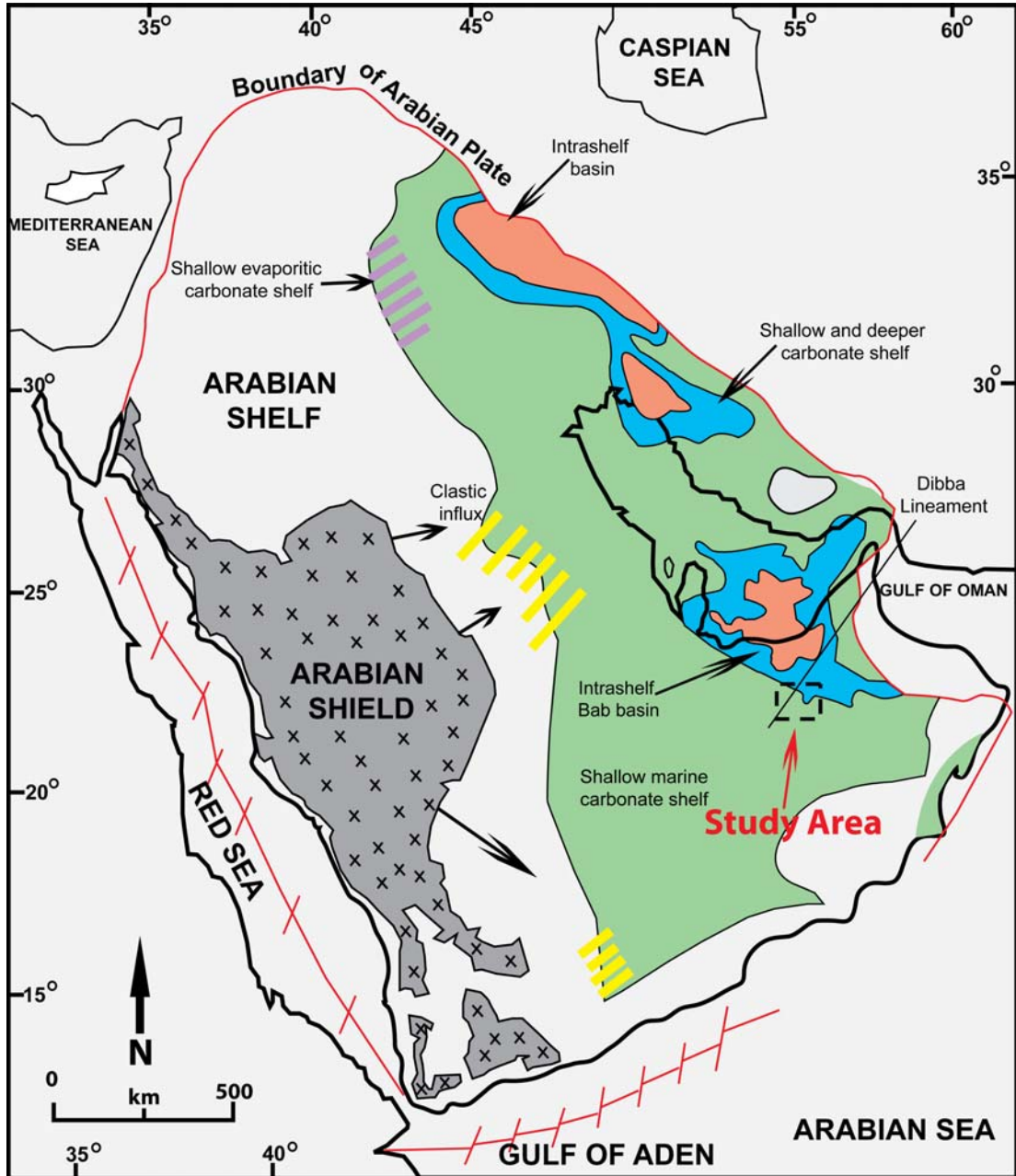


Figure 1. Aptian paleogeographic map for the Arabian Plate showing the location of study area and the intrashelf basins. Modern plate boundaries are shown with red lines.

description, including the first clinoform geometries on the platform margin was outlined by AL-Ghamdi and Read (2010). However, this model was only based on 14 wells, limited stable isotope and biostratigraphic data. This study presents a new high-resolution rock-based, sequence-stratigraphic model, refining the 2-D reservoir facies anatomy using 55 cored-wells, gamma ray logs and extensive isotope data (26 wells). This detailed framework will be integrated with petrophysical and engineering data to build new 3-D reservoir and simulation models and it should provide insights for new horizontal drilling locations and secondary and tertiary hydrocarbon recovery.

The Aptian stage provide one of most prominent time in geological history that records dramatic changes in biota and environmental conditions associated with the perturbation of global carbon cycles (Föllmi et al., 1994; Jenkyns, 2003; Weissert and Erba, 2004.). The Lower Cretaceous Barremian and Aptian record global high sea-level changes, that greatly influenced the stratigraphic records (Matthews and Frohlich, 2002; Immenhauser and Matthews, 2004; Al-Husseini and Matthews, 2010; Droste, 2010). High-resolution orbital cyclostratigraphy of the Aptian suggests that the main driving mechanism are the ~ 400 and ~ 100 k.y eccentricity orbital cycles (Al-Husseini and Mathews, 2010; Huang et al., 2010). The high-resolution rock-based stratigraphic framework in this study will be tied to and compared with global sea-level charts (Rohl and Ogg, 1998; Hardenbol et al., 1998; Haq and Schutter, 2005), the standard carbon isotope curve (Follmi et al., 2006) and cyclostratigraphy (Al-Husseini and Mathews, 2010) to evaluate the influence of global sea-level changes on the evolution of the Shu'aiba platform. This global correlation is the key to understand and evaluate the

regional stratigraphic framework and hierarchy of the Early Cretaceous Arabian Plate presented in van Buchem et al. (2010). It also help refine our understanding of global climate during the Early Cretaceous Barremian and Aptian, because it was suggested that the Aptian may record a time of global cooling interval, within the prevailing Cretaceous greenhouse system, possibly associated with glaciation in the poles (Frakes et al., 1999; Alley and Frakes, 2003; AL-Ghamdi and Read, 2010). The global correlation will help improve our understanding of the Biyadh and Shu'aiba stratigraphic architecture, thus providing a better chronostratigraphic model for reservoir development and possible exploration potential in the area and around the world.

Geological Setting

The present Arabian Plate (Figure 1) is bordered to the north by a convergent margin with the Eurasian Plate, forming the fold and thrust belt of the Taurus and Zagros Mountains. To the west and southwest, are the divergent rift zones in the Gulf of Aden and Red Sea. The northwestern margin is bounded by strike-slip faults in the Gulf of Aqaba and the Dead Sea region. The Arabian Shield, a block of Precambrian basement, in the western part of the Arabian Peninsula, periodically provided siliciclastic sediments to the Arabian shelf, that formed on the eastern Arabian Peninsula. The Arabian shelf thus consists of both siliciclastic and carbonates rocks and started as an intra-cratonic phase from Proterozoic to Middle Permian, followed by a passive margin phase in the Mesozoic. This culminated in the active margin phase in the Cenozoic that persists to the present-day (Harris et al., 1984; Christian, 1997; Sharland et al., 2001).

The Early Cretaceous is marked by rifting of the Indian, Australian and Antarctic plates away from the African and Arabian plates. The Arabian Plate separated from Africa and moved toward the Neo-Tethys Ocean and developed passive margins on its north, northeast, and southeast margins. The eastern margin of the Arabian Plate faced the open Neo-Tethys Ocean, and lay several degrees south of the equator. Early Cretaceous intra-shelf basins were created by intra-Cambrian Hormuz salt movement (Sharland et al., 2001; Ziegler, 2001). Rudist banks, such as those in the Shaybah region, were deposited on the margins of these intra-shelf basins during the Aptian. The intra-shelf basins were separated from the open Neo-Tethys Ocean by a narrow carbonate barrier system (Christian, 1997; Sharland et al., 2001; Ziegler, 2001; Greselle and Pittet, 2005).

The Shu'aiba Formation described in this field study is located on a northeast-trending, doubly plunging anticline, and is divided by a zone of EW-trending faults into northern and southern blocks (Figure 3). The regional structure was mainly affected by northeast-trending faulting parallel to the Dibba Lineament, and sub-parallel to the trend of Shaybah field. The field is located on a basement uplift that appears to have influenced the growth of the build-up, implying syn-sedimentary tectonics (AL-Ghamdi and Read, 2010). This syn-depositional faulting influenced the stratigraphic framework, the thickness and facies distribution of the Shu'aiba successions. The field was divided into two depositional blocks by an E-NE-trending growth fault zone; each block has its own distinctive facies architecture and sequence-stratigraphic development. The present-day Shaybah structure was developed during the Cenomanian in response to intra-

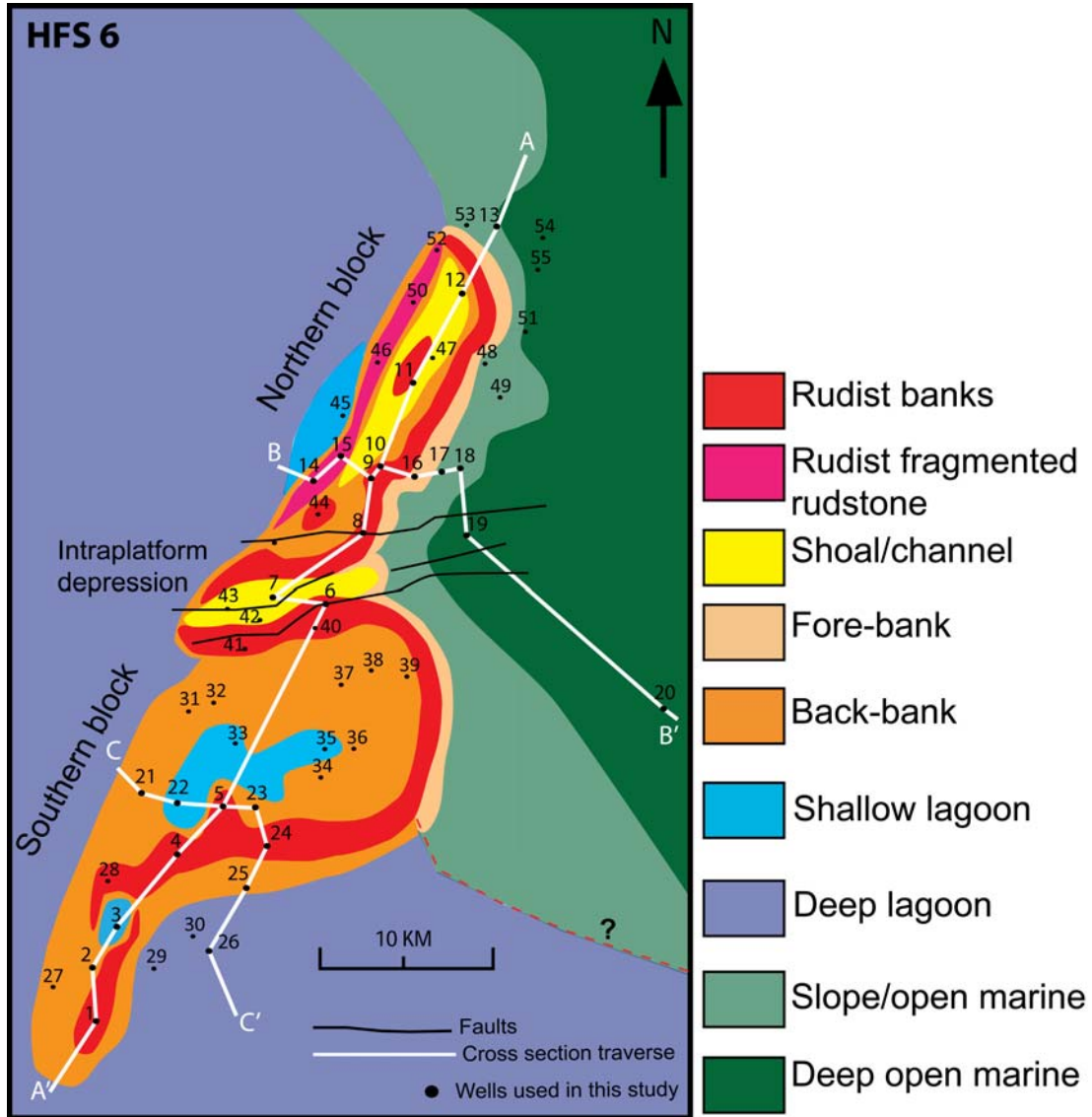


Figure 3. Base map and facies distribution at S6 of Shu'aiba platform showing three cross-section traverses (A-A', B-B' and C-C') and 55 cored-wells used in this study.

oceanic compressional tectonics in the Neo-Tethys region, and was truncated by pre-Aruma erosion (Middle Turonian unconformity) related to uplift of ophiolitic nappes in Oman (Aktas and Hughes, 1998).

Methodology and Data Sets

Fifty five cored wells, averaging 450 ft (140 m) each, totaling 16142 ft (4,920 m) of cores, penetrating the Shu'aiba Formation were logged bed-by-bed and examined using a binocular microscope. Three Wells (12, 11 and 9) penetrate deeper into the Barremian Biyadh Formation, providing the first opportunity to describe and evaluate this succession. Core descriptions included gross lithology (shale, limestone and dolomite), rock type, grain-size, shape and sorting, vertical succession of lithologies, location of bounding surfaces, types of biotic constituents and pore system distribution. Microfacies analysis were examined using thin sections during the core logging to confirm the types of constituents (including foraminifera) and diagenetic modifications of grains and matrix. Stable carbon and oxygen isotope data from 26 wells also were collected and calibrated with core descriptions to constrain the age model of the Shu'aiba Formation especially in the slope and open marine settings where the Lower/Upper Aptian boundary occurred (Figure 4).

A generalized type core description of the entire study interval (Figure 4) calibrated to its gamma ray log provides the basis for a 1-D interpretation of lithofacies and sequence stratigraphy. Sequence boundaries, maximum flooding surfaces and various scales of sequences and parasequences were picked on the logged sections

(Figure 4). Sequence boundaries were picked at significant erosional surfaces above successions of parasequences that progressively shallowed and or thinned up-section. Maximum flooding surfaces (MFS) or units (MFU) were placed at the base of the deepest water facies within a sequence and at the tops of upward deepening trends of parasequence sets. Where possible, parasequence boundaries and maximum flooding surfaces were traced across the build-ups, to generate a depositional model. Facies cross-sections within this sequence-stratigraphic framework were made by interpolating between cored wells using Walther's law within the conceptual ramp depositional model.

In order to correlate the sequences, the base of the Shu'aiba Formation (the top of Hawar unit) was used as a datum for the cross-sections because it has distinctive high gamma-ray response in all wells associated with a thin stylolitic shale layer. The northern and southern blocks were correlated using the top Shu'aiba unconformity to bridge the medial fault zone. Seismic data were examined to constrain the sequence picks along the margin of the build-up where clinoform development was likely (e.g Yose et al., 2010); however, it proved of limited value, due to the absence of a clear reflector at the top of the Shu'aiba Formation, and the occurrence of multiple artificial reflections within this unit.

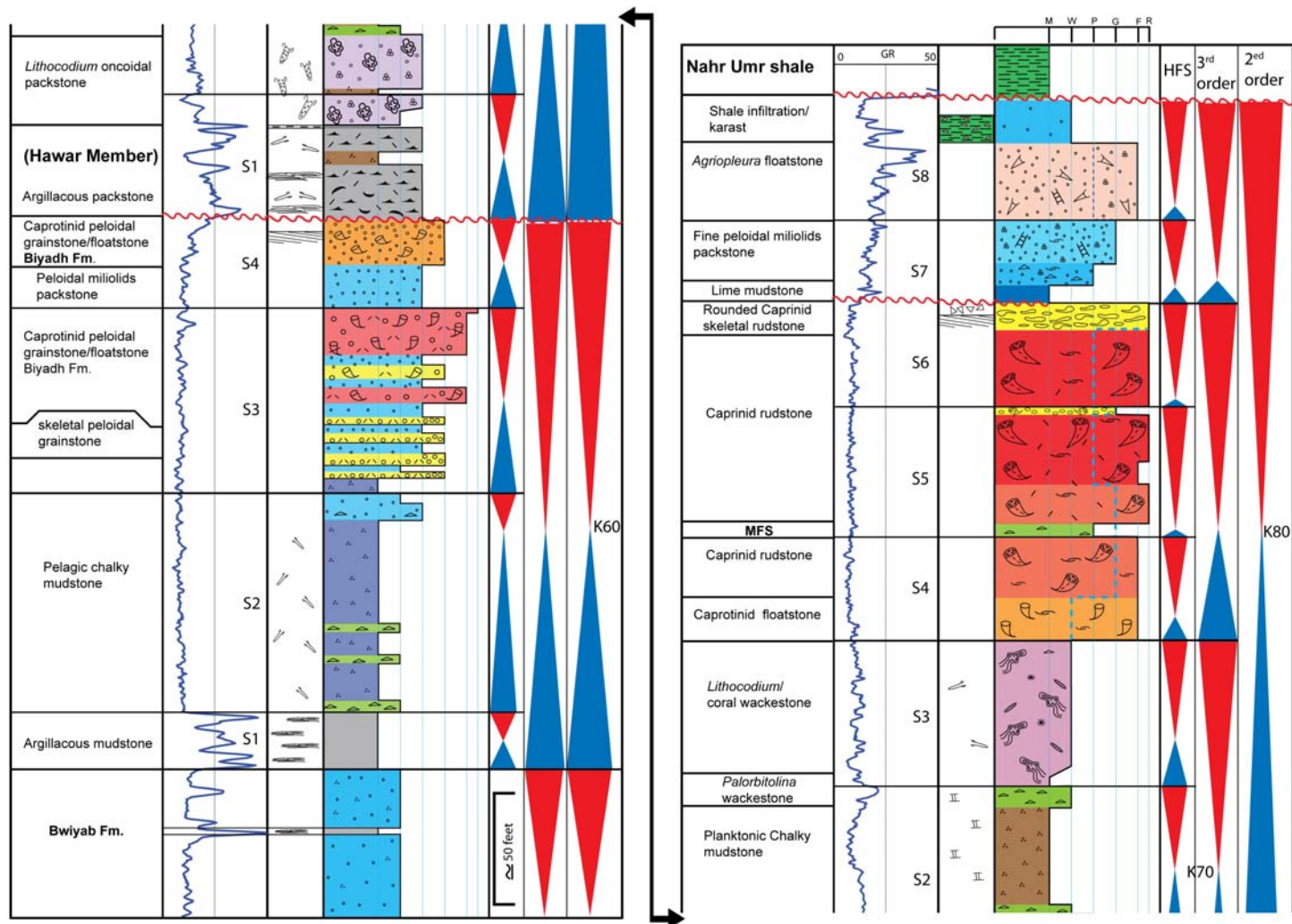


Figure 4. Type composite core description showing general lithofacies description, sequence stratigraphy and gamma ray logs within the marginal setting.

Facies Description

The lithofacies of the Shu'aiba Formation were previously described and interpreted by AL-Ghamdi and Read (2010); using 14 cored wells. A detail biofacies and depositional environment study was conducted by Hughes (2000). This paper presents more updated lithofacies descriptions using cores and petrographic analysis from 55 cored-wells located across the entire field (Figure 3). This extensive data set resulted in newly recognized facies (e.g shoal facies complex and the upper Aptian facies; Figures. 5 - 8) and also helped refine the interpretation of depositional environments and produces more accurate facies maps and depositional cross-sections of the Biyadh and Shu'aiba Formations. The detail facies descriptions are summarized in Tables 1A & B and the facies are illustrated in Figures (5 - 8). Figures 9 - 13 illustrates the position of each lithofacies within a low angle ramp model. These depositional models especially, Figure 12 show lateral facies transition from inner ramp/lagoon, back-bank, bank-crest, fore-bank, slope to basin settings in the Far East. Seventeen significant lithofacies were determined in this study on the basis of fossil assemblages, rock type, texture and sediment constituents. These lithofacies were grouped into four major facies associations (lagoonal facies, shelf marginal facies, Open marine/slope facies and basinal facies) that are linked to major depositional environments (Tables 1A & B). However, smaller-scale lithofacies also were recognized and interpreted, such as platy coral versus branching coral or rudist *in situ* floatstone versus rudist *in situ* rudstone facies. These facies with subtle differences in their characteristics or their environments were lumped with other

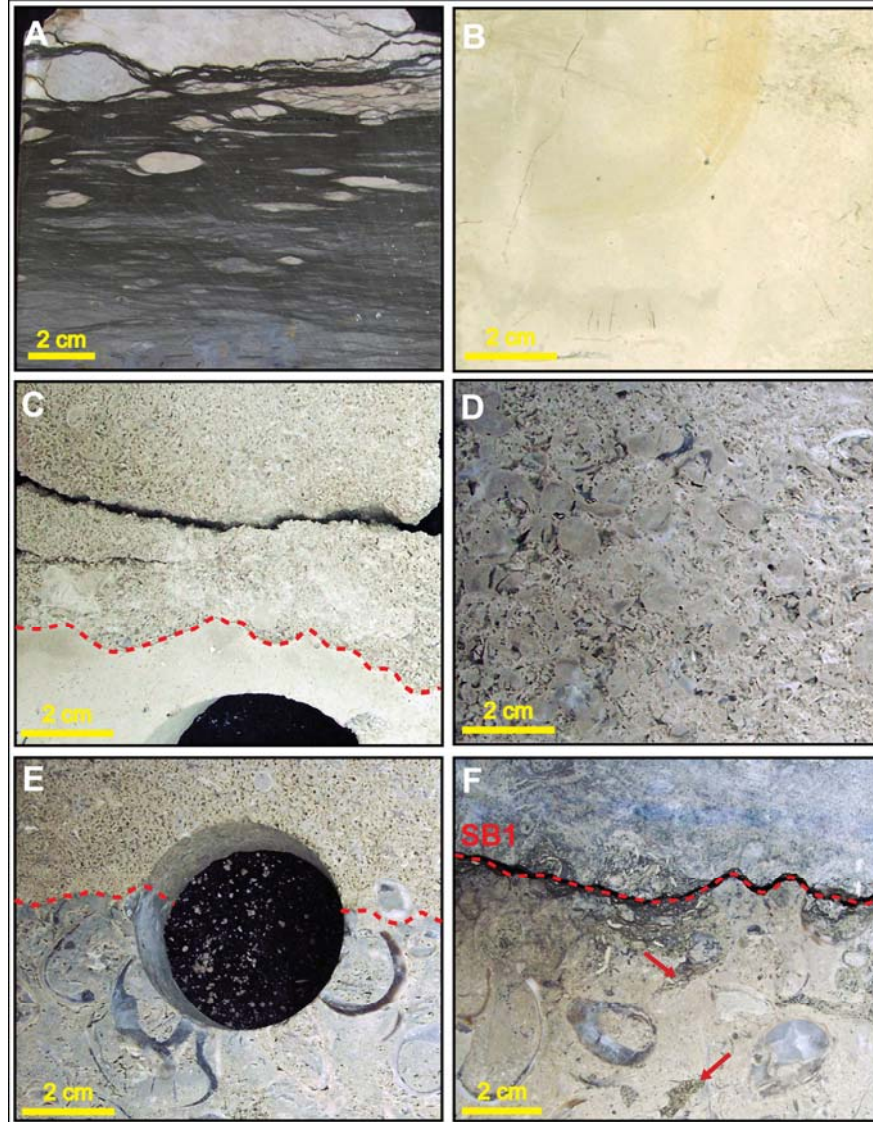


Figure 5. Core sample photographs of typical facies in Biyadh Formation. (A) Argillaceous black, dense mudstone, overlain by sharp contact and white carbonate of Biyadh Formation. (B) clean chalky mudstone facies within the Lower part of Biyadh Formation, representing the maximum flooding unit (K60). (C) Sharp erosional contact at top of cycle within HFS 3 of Biyadh Formation, separating subtidal wackestone facies, from the peloidal grainstone facies. (D) Oncoidal coral skeletal grainstone facies in HFS 3 of Biyadh Formation. (E) *Glassomyophorus* rudist floatstone facies from HFS 4 of Biyadh Formation, overlain by sharp contact (cycle top) and skeletal peloidal grainstone facies. (F) *Glassomyophorus* rudist floatstone facies, capped by a scalloped surface and major sequence boundary (SB1) at the top of the Biyadh Formation, overlain by dark-gray argillaceous *Palorbitolina* packstone of Hawar unit. Arrows indicate karst fill from Hawar unit infiltrated into the rudist facies of Biyadh Formation.

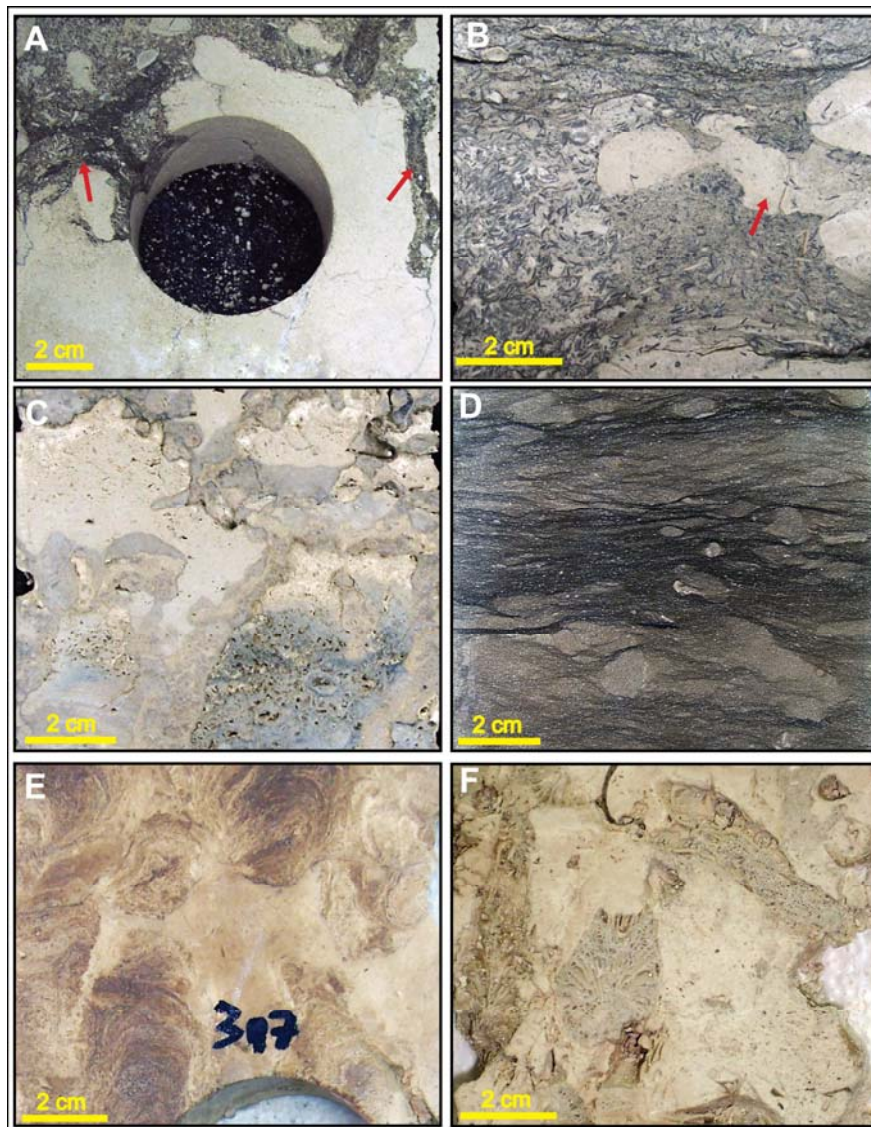


Figure 6. Core sample photographs of typical deep subtidal and *Lithocodium* facies in Shu'aiba Formation. (A) Karst fill (arrows) from Hawar unit infiltrated into the rudist facies of Biyadh Formation at SB1. (B) Dark gray *Palorbitolina* packstone of Hawar "dense" unit. Burrowing and bioturbation occurred on the right hand side (arrow). (C) Bioturbated oncolidal *Lithocodium* miliolid packstone facies at basal Shu'aiba Formation (shallow subtidal, upper ramp environment). (D) Black, wispy-laminated mudstone/wackestone facies (deep lagoon/deep restricted environments). (E) *Lithocodium* aggregatum wackestone/boundstone facies, columnar-laminated morphology (open-marine algal platform). (F) Platy coral floatstone includes extensive leaching (open-marine algal platform).

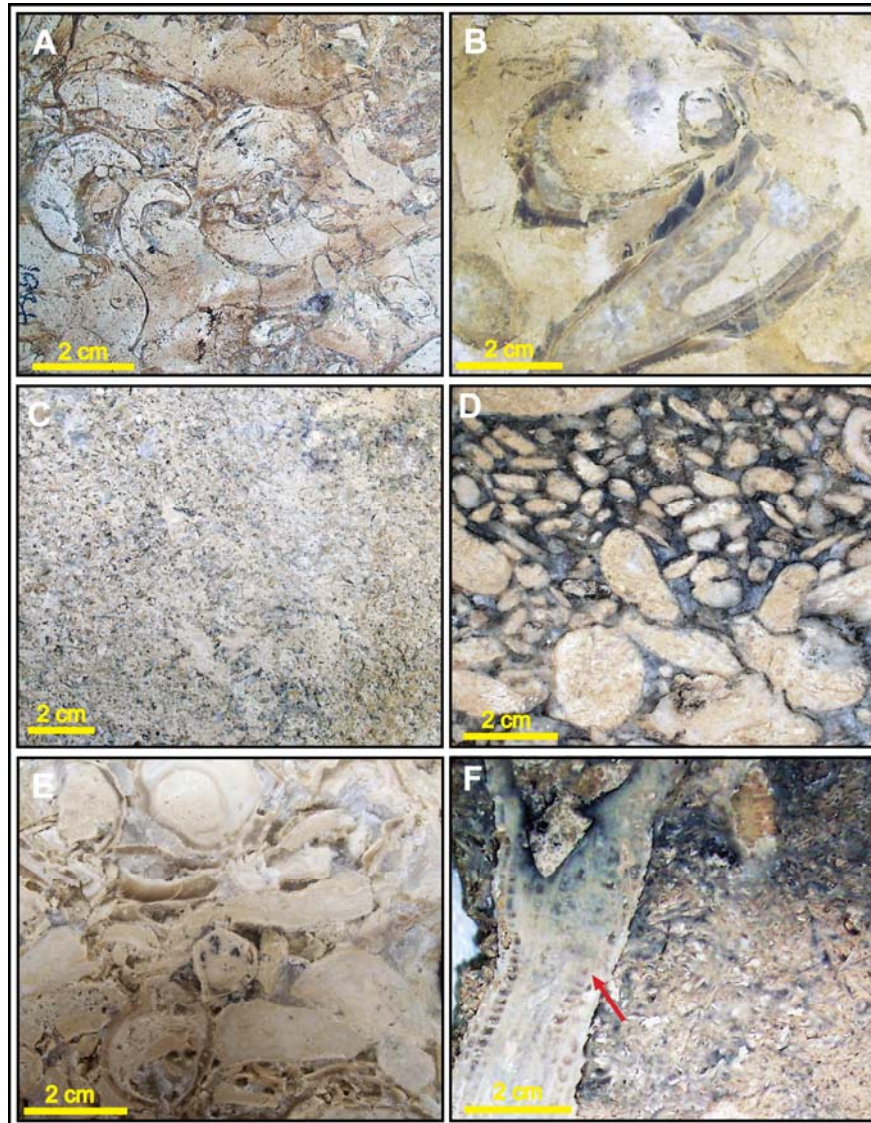


Figure 7. Core sample photographs of typical rudist facies in Shu'aiba Formation. (A) Caprotinid *Glassomyophorus* floatstone (back-bank). (B) *Agriopleura* floatstone (shallow lagoon/inner ramp). (C) Skeletal debris grainstone (shoal/channel). (D) Well rounded, cemented *Offneria* rudstone (high-energy beach/shoal). (E) Caprinid rudist debris *Offneria* rudstone (high-energy bank-crest/shoal). (F) *In-situ* (life position) caprinid *Offneria* floatstone (bank-crest). Arrow points out to live-position *Offneria* rudist.

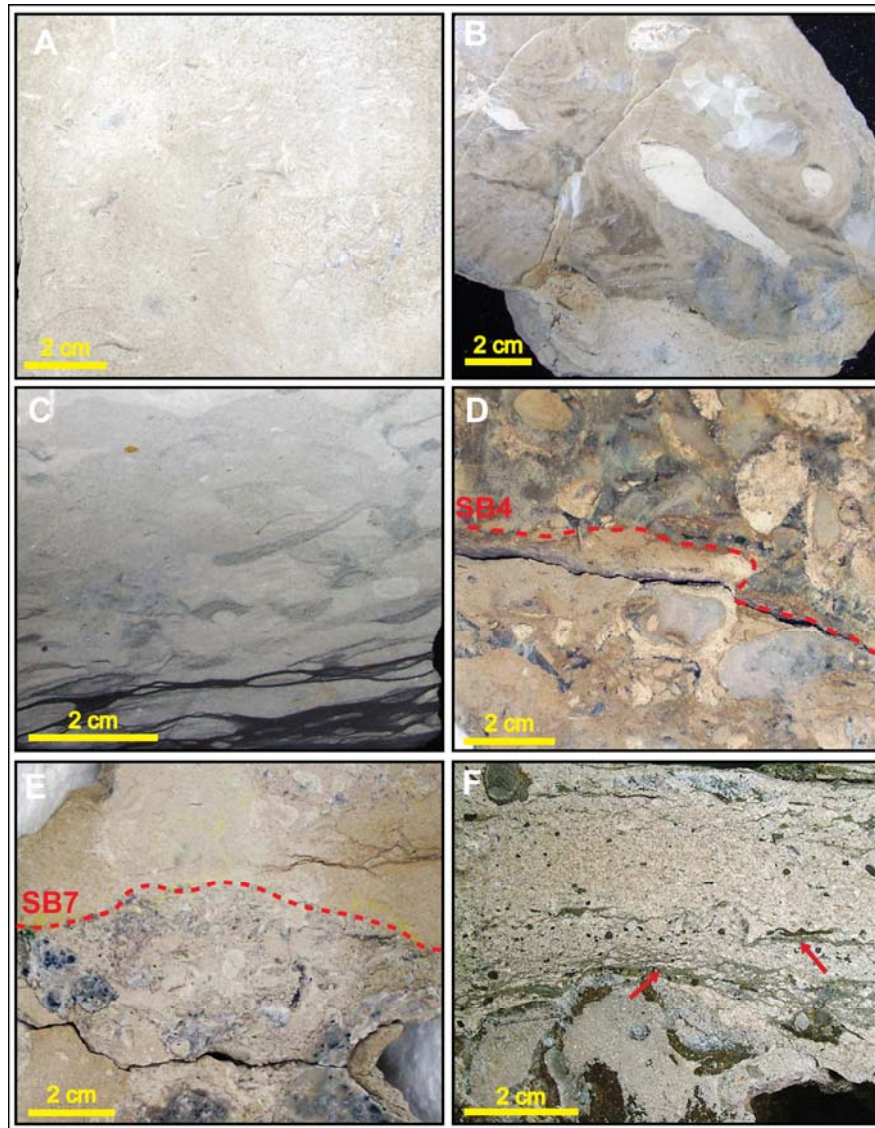


Figure 8. Core sample photographs of typical deep ramp facies and sequence boundaries in Shu'aiba Formation. (A) *Palorbitolina* wackestone (deep open-marine). (B) Massive stromatoporoid boundstone, (Upper Aptian marginal setting). (C) Dark wispy-stylolite argillaceous mudstone (Upper Aptian Boundary). (D) Sequence boundary 3 (SB3), separating *Lithocodium* facies below from the overlying rudist facies. (E) Sequence boundary 7 (SB7) at top of the rudist buildups, marking the termination of the Lower Aptian Caprinid rudist associated with subaerial exposure surface. (F) Nahr Umr green shale (arrows) infiltrated into the upper part of Shu'aiba during karstification associated with the major late Aptian unconformity.

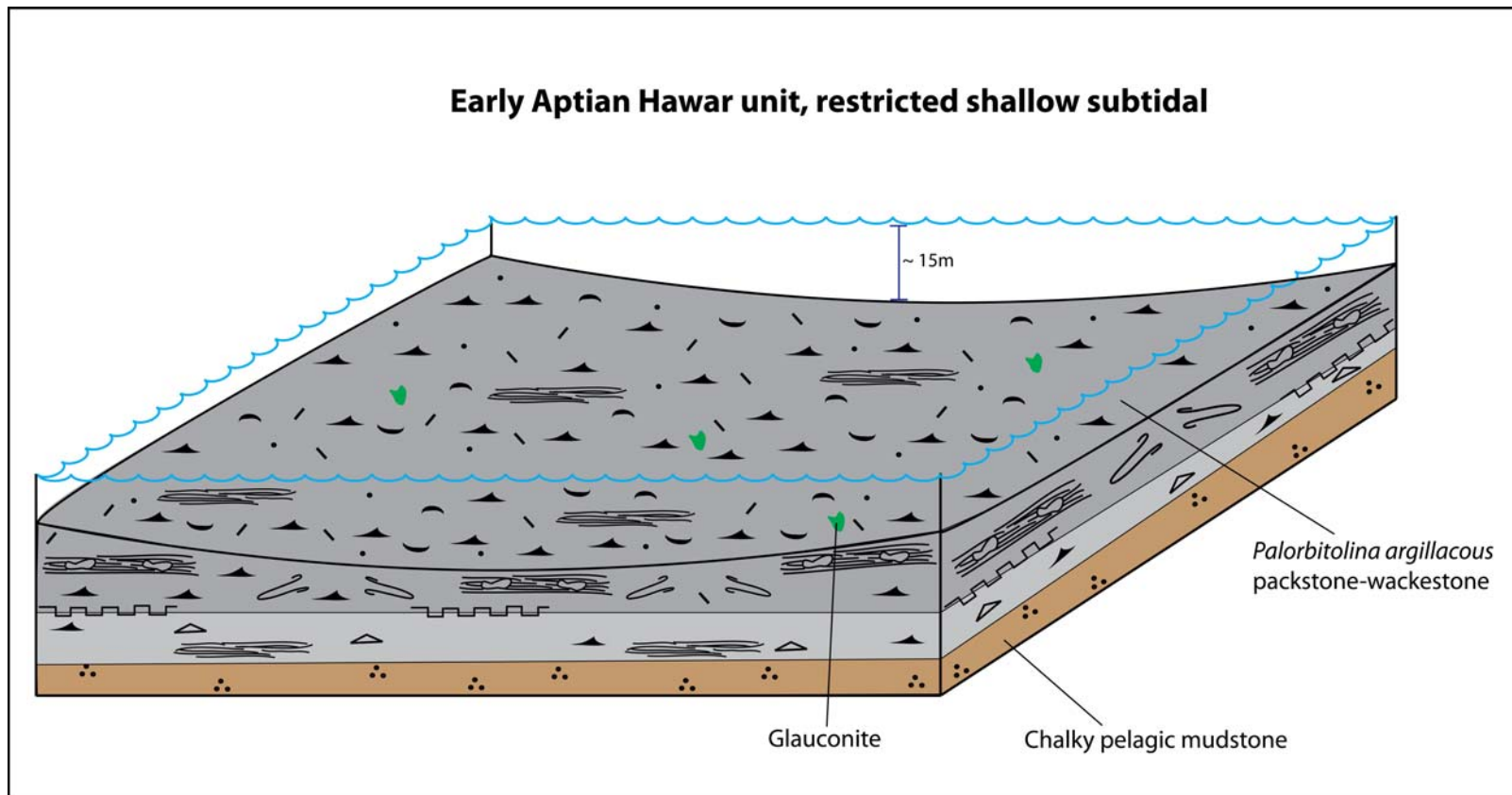


Figure 10. Depositional model for the Hawar unit showing restricted shallow subtidal/tidal flat environment (condensed unit).

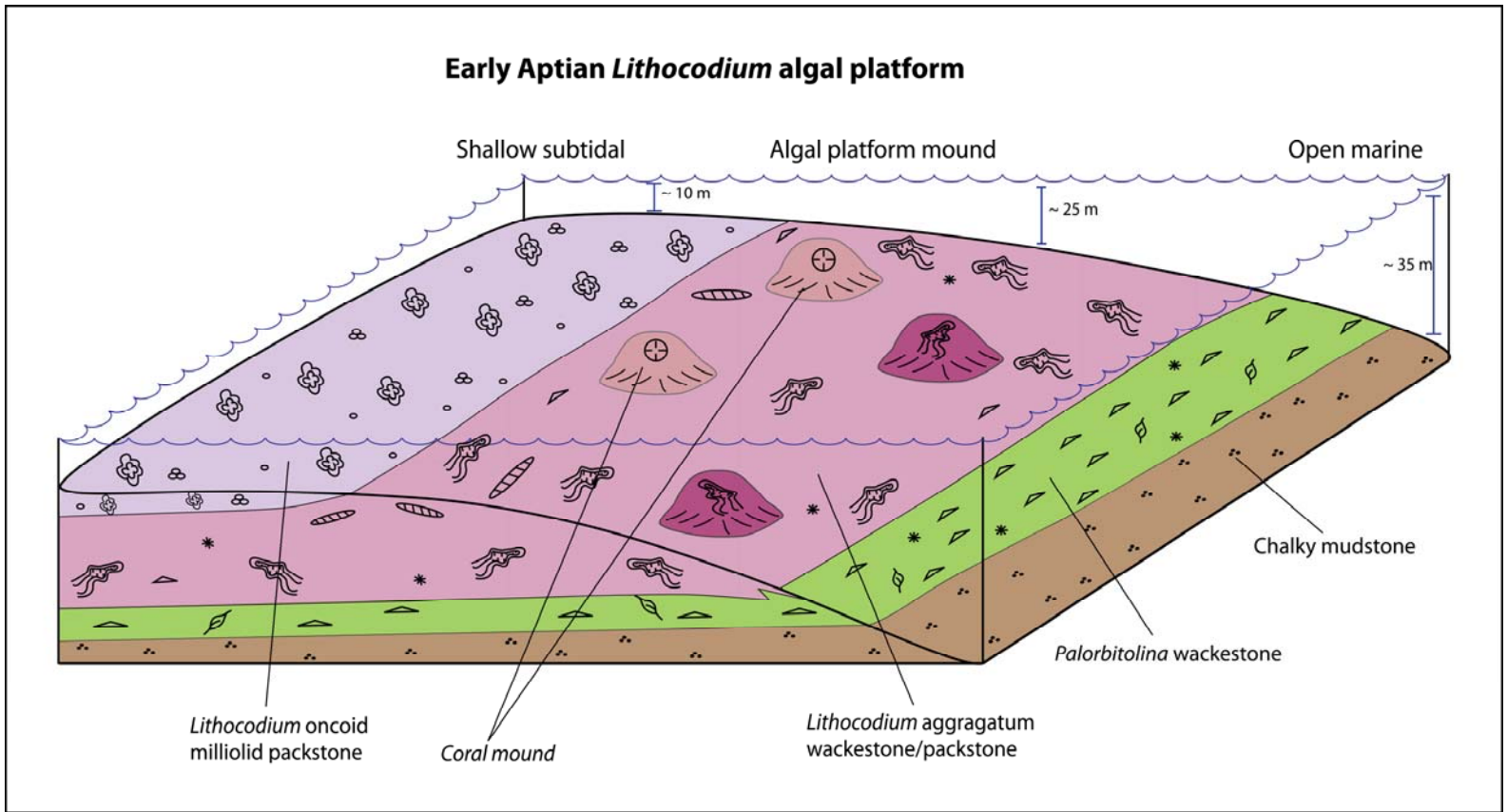


Figure 11. Depositional model for the *Lithocodium* algal platform of Lower Shu'aiba Formation, HFS's 2 and 3.

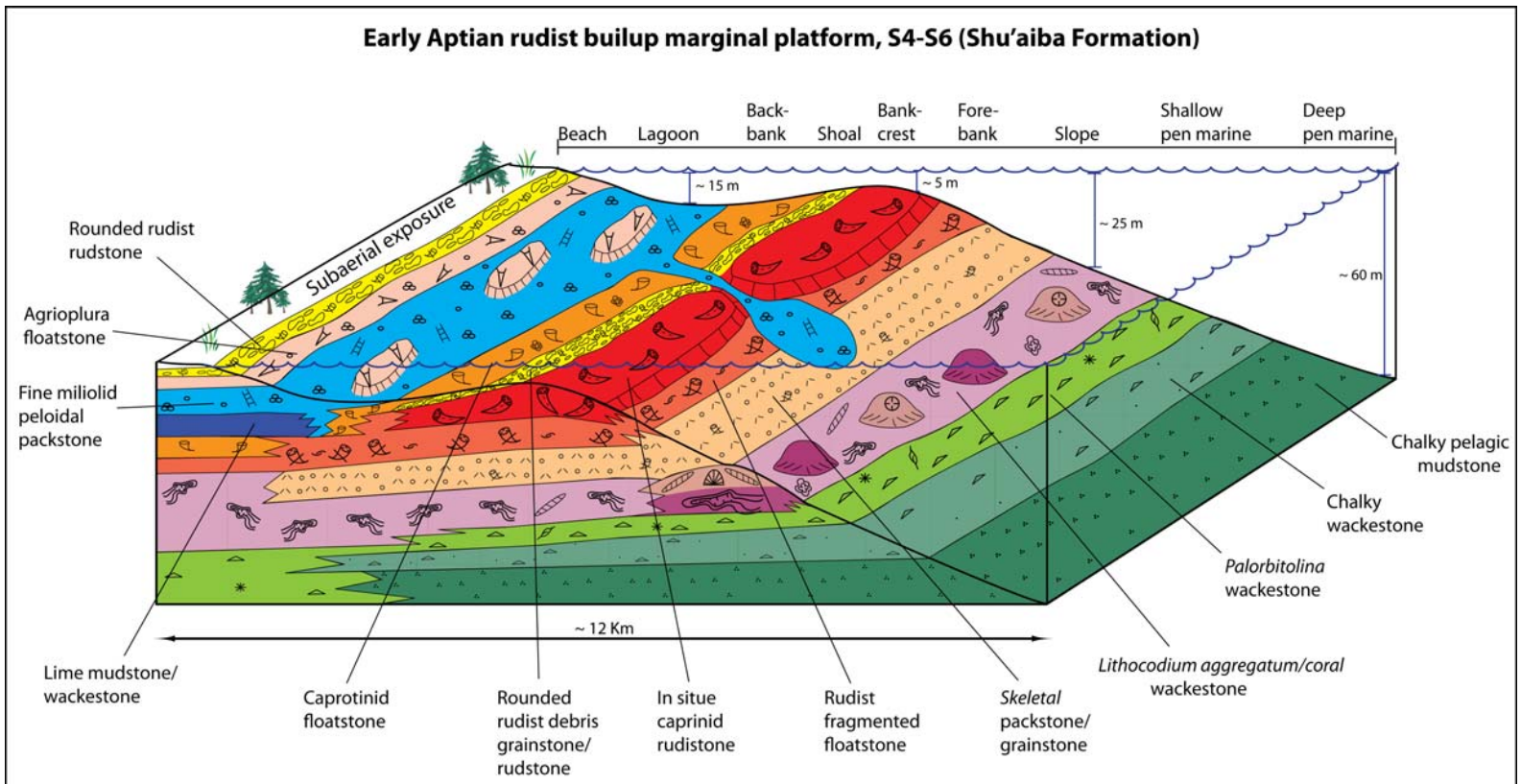


Figure 12. Depositional model for HFS's 4-6 within the rudist buildups, showing the position of each facies in a barrier-bank low angle ramp.

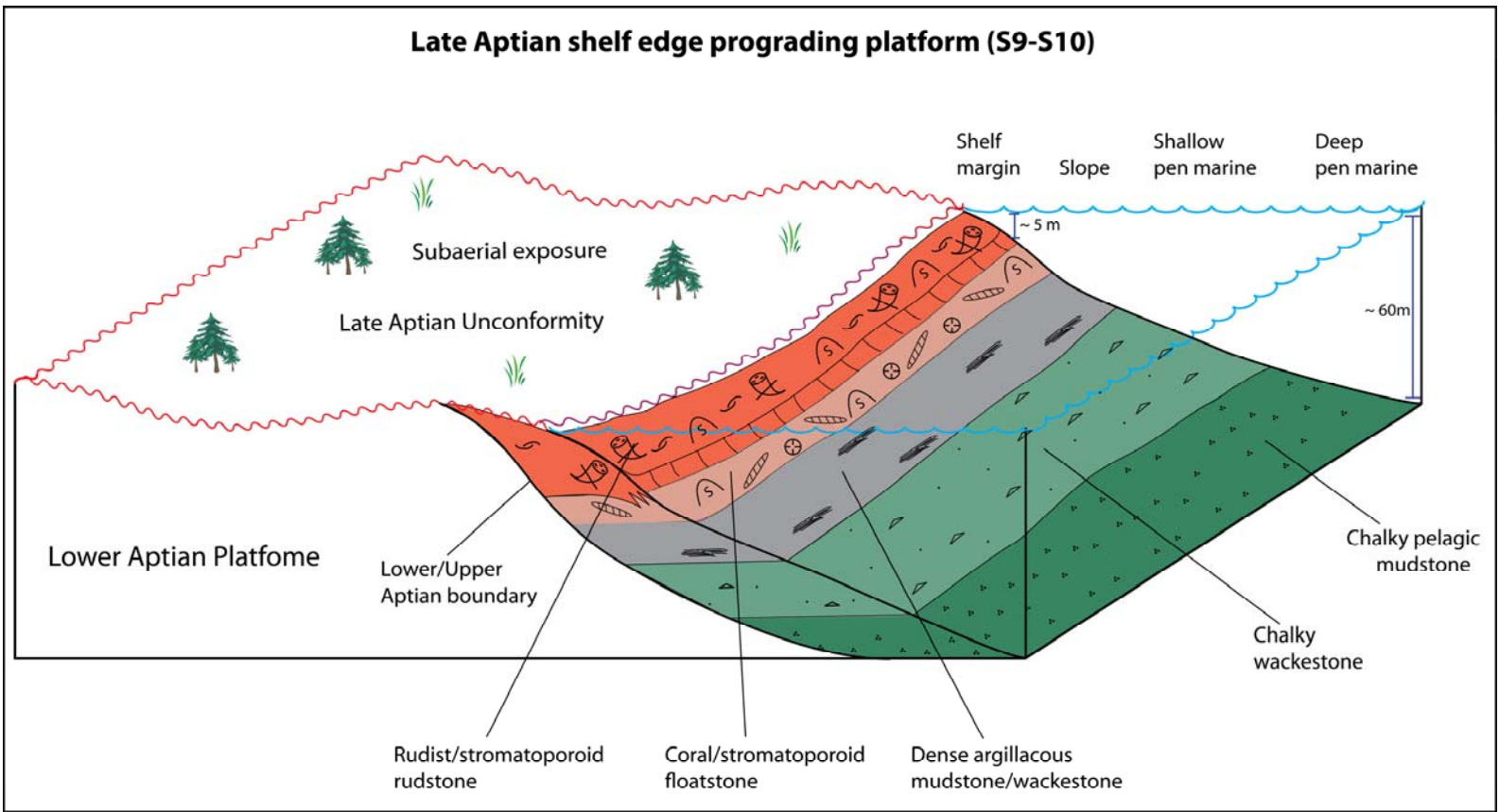
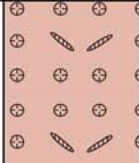
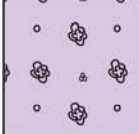


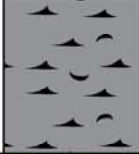

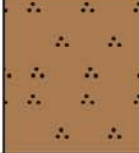



Figure 13. Depositional model for the Upper Aptian HFS's 9 and 10 showing the shelf marginal edge within the prograding sequences. The pre-existing Early Aptian platform was subaerially exposed during this time.

Table 1A. Summary of Lithofacies in shelf margin settings.

Facies Association	Facies	color code	Description	Sed. structure	Matrix (in rudstone/floatstone)	Fossils	Energy	Pore type	Depth (Estimated)	Environments
Inner Ramp/Lagoon	Very fine skeletal peloidal packstone/grainstone		Very fine-fine-medium grained, moderately well sorted, rounded, abundant skeletal grains, common peloids, rare pelletal grains, intergranular cement	Low angle cross beds		Abundant miliolids, textularids, <i>Vercorsella areneta</i> , <i>Debarina hahounerensis</i> , high-trochoid <i>Palorbitolina</i> , common dasyclad alga, rare <i>Lithocodium</i> , common (<i>Agriopleura</i>)	Low to moderate	Common MO and micro porosity	5-10 m	Shallow lagoon
	<i>Agriopleura</i> packstone/floatstone		Pebble-gravel size rudists, elongate V-shape and U-shape		Fine skeletal peloidal packstone/grainstone	Abundant - common <i>Agriopleura</i> , common miliolids), low-trochoid <i>Palorbitolina</i>	Low to moderate	Common MO and micro porosity	5-15 m	Shallow-moderately deep lagoon
	Lime mudstone/wackestone		Silty to very fine grains, abundant mud, argillaceous, chert	Abundant and large burrows, microstylolites, nodular bedding		Abundant miliolids and benthonic forams (<i>Textularia</i> , <i>Vercorsella</i> , <i>Debarina</i>), common <i>Palorbitolina</i> , common to rare <i>Lithocodium</i> , locally planktic forams	Very low	Micro porosity rare MO	25-35 m	Deep Lagoon
Shelf margin	Well rounded rudist debris rudstone/grainstone		Granule - pebble to coarse sand, well rounded, well sorted, mud-free, may occur as well cemented below sequence boundary or very porous shoal debris/channel	Cross beds	Grainstone	Abundant caprinid rudist debris of (<i>Offneria murgensis</i>)	Very high	Abundant VG and MO	< 5 m	Beach/shoal or channel
	Rudist-fragmented packstone/grainstone		Fine-coarse skeletal grains, angular-moderately rounded, moderately sorted, fine-coarse equant calcite cements	Cross beds		Mainly caprinid skeletal debris of <i>Offneria</i> , rare caprotinid debris, common coral and echinoderms, common benthonic foraminifera	Moderately high	Common VG, MO, less common micro porosity	5-15 m	Shallow-forebank
	<i>In situ</i> caprinid rudstone/floatstone		Pebble-gravel size rudists, angular-moderately rounded, poorly sorted, <i>in situ</i> rudist (unbroken)		Packstone-wackestone, mudstone (locally)	Large <i>in situ</i> caprinid rudist (<i>offneria</i>)	High to locally moderately low	Abundant VG and MO, Common micro porosity	5-10 m	Bank-crest (<i>in situ</i>)
	Caprinid skeletal floatstone/rudstone		Pebble-very coarse grains, poorly-moderately sorted, rudist and bivalve skeletal debris		Grainstone/packstone, mudstone (locally)	Abundant caprinid rudist (<i>Offneria</i>) less common caprotinid (<i>Glossomyophorus</i>)	High	Abundant VG and MO	5 -10 m	Bank-crest/proximal bank-edge/shoal
	Caprotinid floatstone		Coarse-sand to pebble-size grains, poorly sorted		wackestone/mud-rich packstone	Abundant caprotinid rudist (<i>Glossomyophorus costatus</i>), common <i>Palorbitolina</i> , less common (<i>Agriopleura</i>) less common <i>Lithocodium</i>	Low to moderate	Common MO and micro-porosity, rare VG	5-30 m	Back bank, relatively deep, transgressive rudist
	Fine-medium skeletal packstone		Medium sand size, moderately rounded, well sorted, common peloids, common fine-medium intergranular equant calcite cements			Skeletal debris of mainly <i>Offneria</i> , bivalve, oyster, common foraminifera include; <i>Textularia</i> and <i>Palorbitolina</i>	Moderate	Abundant MO	20-30 m	Deep forebank/shallow slope

Table 1B. Summary of Lithofacies in open marine and basinal settings.

Facies Association	Facies	color code	Description	Sed. structure	Matrix (in rudstone/floatstone)	Fossils	Energy	Pore type	Depth (Estimated)	Environments
Open marine / slope	Coral packstone/floatstone		Pebble-coarse grains, elongate-rounded shape, moderately sorted		Mudstone/wackestone	Abundant branching or platy coral, some massive coral heads, debris of echinoderm, bivalve, common <i>Lithocodium</i> , rare <i>Palorbitolina</i>	Low to moderate	Abundant MO and VG, common microporosity	10-30 m	Open marine/lagoon
	<i>Lithocodium</i> oncoid miliolid packstone		Fine-medium sand size, poorly sorted, peloids, pebble size <i>Lithocodium</i> lumps, oncoid, lime mud	Highly bioturbated, large irregular borrows		Abundant miliolids, <i>Textularia</i> , common <i>Lithocodium</i> lumps, (NO <i>Palorbitolina</i>)	Moderately high-energy	Common MO and microporosity	10-15 m	Shallow carbonate platform
	<i>Lithocodium aggregatum</i> wackestone/bindstone		Encrusting <i>Lithocodium</i> , fine-medium sand-size, poorly sorted	Abundant-common burrows, wispy microstylolites	Chalky mudstone/wackestone	Abundant <i>Lithocodium aggregatum</i> , common, coral, echinoderm debris, skeletal fragments of bivalve, abundant/common (<i>Textularia</i> , <i>Vercorsella arenata</i> , <i>Debarina hahounerensis</i>), <i>Palorbitolina</i> , miliolids. Rare planktic forams	Moderate-low	Abundant micro porosity	20-35 m	Open marine algal platform / lagoon
Deep Marine / Basin	<i>Palorbitolina</i> wackestone		Chalky-fine grains, common, moderately friable	Common burrow and microstylolites		Abundant low-trochoid <i>Palorbitolina</i> abundant/common; (<i>Textularia</i> , <i>Vercorsella</i> , <i>Debarina</i>) common miliolids, rare/common planktic forams, common <i>Lithocodium</i> common echinoderm debris, common <i>Gastropodes</i>	Low	Abundant micro porosity	< 25-30 m	Open marine
	Dark argillaceous <i>Palorbitolina</i> packstone		Dark gray, granule size <i>Palorbitolina</i> , Fine-medium sand size, dense, poorly sorted peloids, common glauconite and pyrite, highly argillaceous and organic matters, reddish oxidized materials	Abundant burrows, hard grounds, normal-graded scour fills, wispy microstylolites		Abundant low-trochoid <i>Palorbitolina</i> , high diversity of benthonic foraminifera, common textularids, common echinoderm and bivalve debris	Low	Dense, Rare micro porosity	10-25 m	Condensed section, relatively shallow marine
	Chalky pelagic wackestone/mudstone		Fine-medium sand size, moderately-well rounded, well sorted, common peloids, common fine-medium intergranular equant calcite cements	Common burrows		Skeletal debris of rudist, bivalve, oyster, common foraminifera include; <i>Textularia</i> and <i>Palorbitolina</i>	Low	Microporosity, MO	25-30 m	Deep slope, open marine
	Planktonic lime mudstone		White-light gray, clay size, chalky, very friable, structureless, semi-pelagic	Common burrows		Abundant planktic foraminifera (<i>Hedbergella</i>), abundant/common <i>Palorbitolina</i> , textularids, <i>Rotalids</i> , <i>Lenticulina</i>	Very low	Abundant micro porosity	40- 50 m	Deep open marine, deepest water facies
	Shaly lime mudstone/shale (intrashelf basin)		Black-dark gray, muddy-silty grains, highly argillaceous, highly organic, common siliciclastic (quartz)				Very low		50-70 m	very deep open marine intrashelf basin

similar facies to simplify the stratigraphic cross sections and to make facies distribution less complicated in the 3-D reservoir modeling. In addition, these 17 lithofacies also were sub-divided on the basis of their significant petrophysical properties and hence their impact on reservoir performance. The following is a brief summary of these four major facies associations:

1. Inner ramp/lagoonal facies association (Table 1A). This facies association occurs mainly in the upper part of Biyadh Formation and in the upper part of the Shu'aiba Formation. These facies were deposited in moderate-to-low energy inner ramp/lagoonal setting with a maximum of 10-15 m water depth in a moderate to low energy (Hughes, 2000; AL-Ghamdi and Read, 2010). These lithofacies include: peloidal milliolid packstone/wackestone, *Agriopleura* floatstone and deep lagoonal mudstone/wackestone facies. However, the deeper lagoonal facies were deposited in restricted deeper water environments, or in restricted ponds within the platform interior.
2. Shelf marginal rudist buildup facies association (Table 1A). This facies association formed mainly within the middle part of the Shu'aiba Formation forming thick and massive rudist buildups. It also formed in the uppermost part of the Biyadh Formation. Lithofacies includes; *in situ* and rudist facies (mainly *Offneria* type) within bank-crest, reworked rudist debris rudstone/grainstone, Caprotinid rudist floatstone (back-bank) and skeletal grainstone/packstone of fore-bank/shallow slope.

3. Open marine algal platform facies association (Table 1B). This facies association includes the algal platform of *Lithocodium*/coral facies, oncoidal *Lithocodium* packstone facies, argillaceous packstone of Hawar unit and the *Palorbitolina* wackestone. These units are generally characterized by mud-dominated matrix and high diversity of associated biota, including foraminifera. These facies were deposited in a relatively deep open marine setting within the lower part of the Shu'aiba Formation. The exception of these lithofacies is the *Palorbitolina* argillaceous packstone of the Hawar unit that was deposited in a more restricted shallow marine subtidal environment (van Buchem et al., 2002; 2010).

4. Deep open marine basinal facies association (Table 1B). This facies association is the deepest water facies within the Shu'aiba and Biyadh formations. Lithofacies include chalky pelagic mudstone within the deep open-marine settings occurred far east toward the basin, planktonic *Hedbergella* mudstone within the lower part of the Shu'aiba Formation representing a major flooding unit (K70) and the argillaceous intrashelf basin that formed far to the east within the Bab basin.

Sequence Stratigraphy

Introduction

The sequence stratigraphic framework presented here builds on the rock-based stratigraphic framework of AL-Ghamdi and Read (2010), using more core data, stable isotope chemostratigraphy and available biostratigraphic data. This study also presents the first stratigraphic framework for the Biyadh Formation in Saudi Arabia with new core data (Figures 4 and 15). The stratigraphic frameworks of the Biyadh and Shu'aiba formations in this study are compared with the regional Lower Cretaceous 2nd- and 3rd-order sequence stratigraphic model of van Buchem et al. (2010). However, some differences occurred between the frameworks presented here and van Buchem et al., (2010), such as the location of the major MFS of Shu'aiba sequence and the hierarchy of the Shu'aiba Formation. This study presents a more detailed high-resolution stratigraphic framework on the order of 400 k.y (HFS's) and higher-scale parasequences that control the reservoir facies anatomy and hence, reservoir quality. The type core description with associated gamma ray logs, interpreted sequences are shown in Figure 4, summarizing the sequence stratigraphic framework of the Biyadh and Shu'aiba Formations. Integrated carbon isotope data, gamma ray and sequence stratigraphy were integrated to better define the age model of the Shu'aiba Formation, particularly defining the Lower/Upper Aptian boundaries on the platform edges (Figure 14). Four detailed stratigraphic cross sections (Figures 15-18) were constructed; one in Biyadh Formation (Figure 15), two west-east dip trending sections in Shu'aiba Formation (Figures 16 and 17) and one

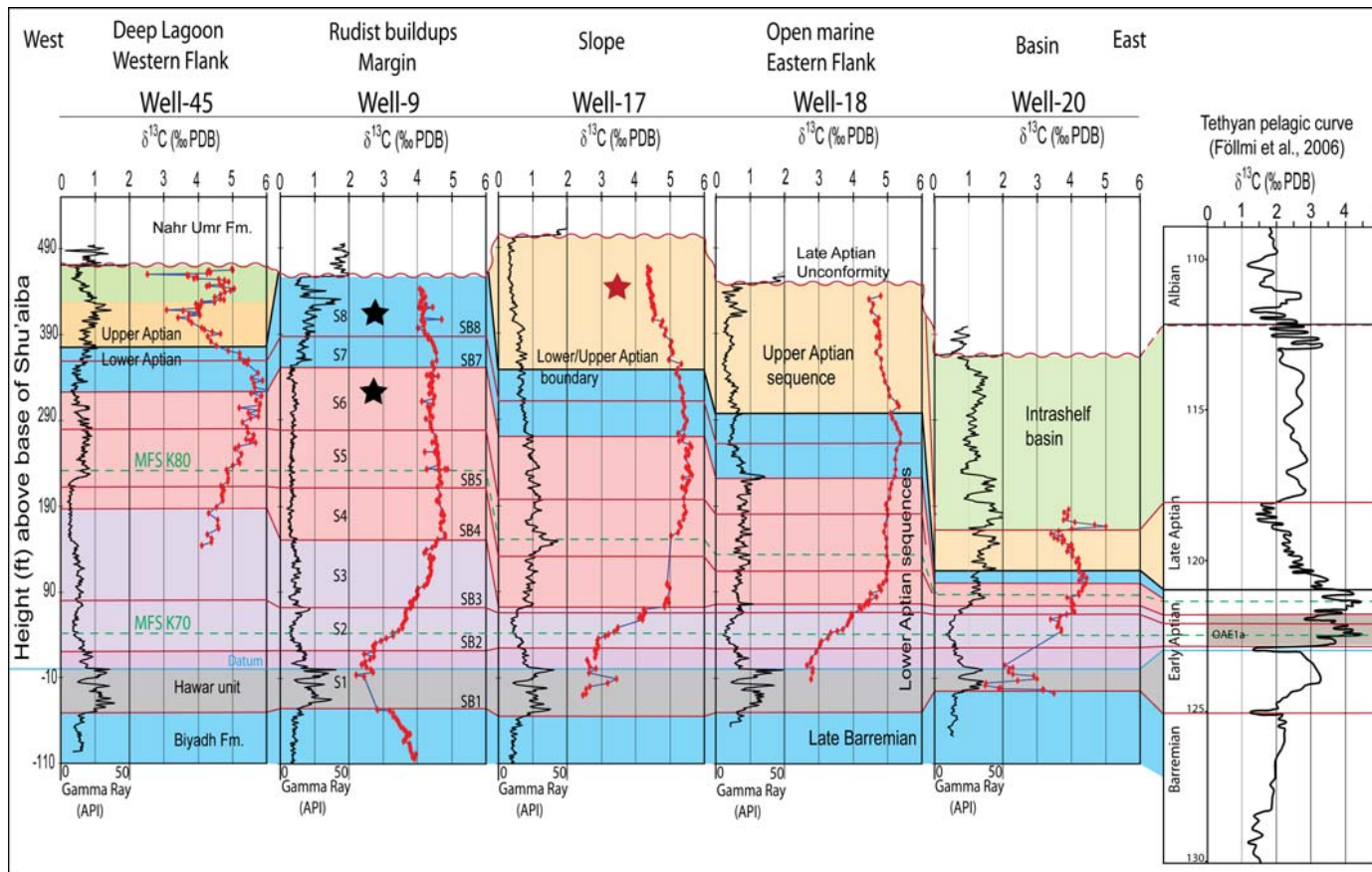


Figure 14. West-East type chronostratigraphic cross section of the Shu'aiba Formation correlating gamma ray logs and $\delta^{13}\text{C}$ isotope curves. The carbon isotopes are correlated with the Tethyan pelagic curve of Föllmi et al., (2006). Major sequence boundaries are shown in red. The purple shaded zone is the *Lithocodium* algal platform facies that corresponds to major global positive excursion in the early Aptian that is related to Oceanic Anoxic Event 1a. Upper Aptian prograding sequences are shown in orange and green. Red star indicates late Aptian rudist *Horiopleura* of the Polyconitidae family, while black stars indicate early Aptian rudist Caprinid *Offneria* below SB6 and Caprotinid *Agriopleura* above SB6.

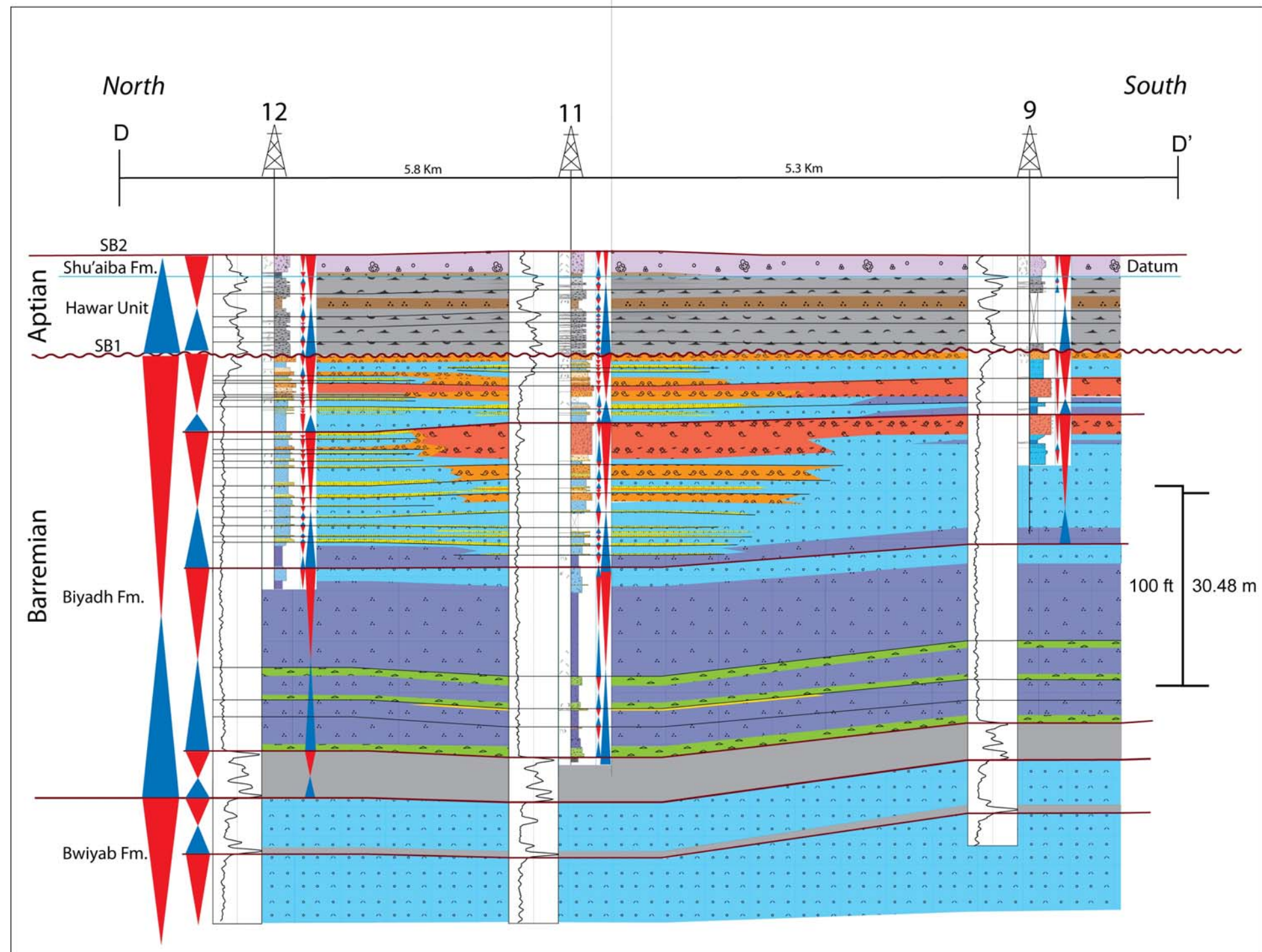


Figure 15. Detail N-S stratigraphic cross section (D-D') of Biyadh Formation and Hawar Member on the Northern block. This cross section illustrates the layer-cake stratigraphy of these units along with high scale parasequences. See figure 3 for location.

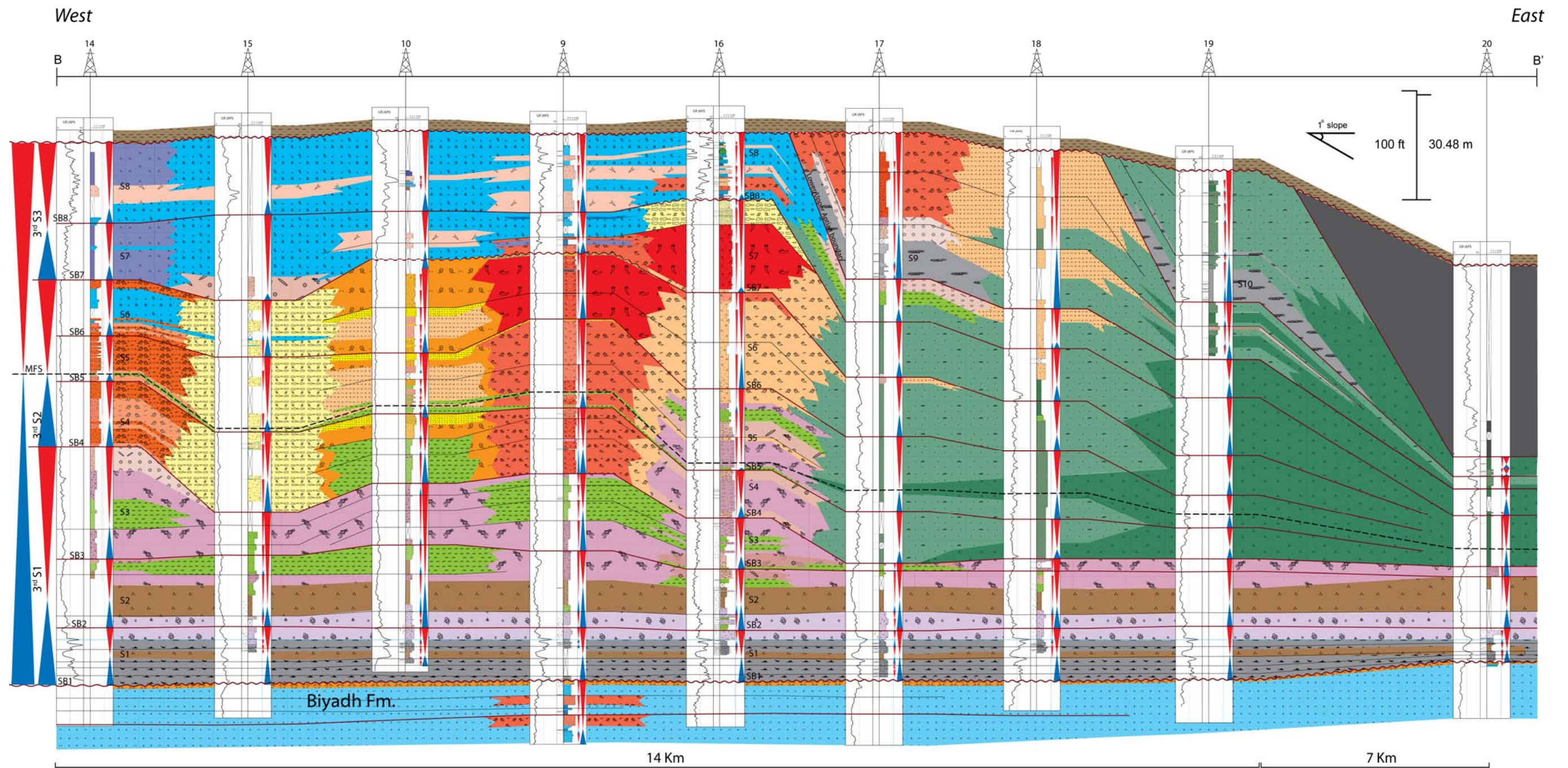


Figure 16. Detail W-E dip oriented stratigraphic cross section of Shu'aiba Formation on the Northern block. The prograding Upper Aptian sequences produced clinoform geometries on the eastern platform edge. Note the lateral facies changes across the platform to basin transition. Ramp crest commonly grew more than surrounding area leading to differential accommodation. See figure 3 for location.

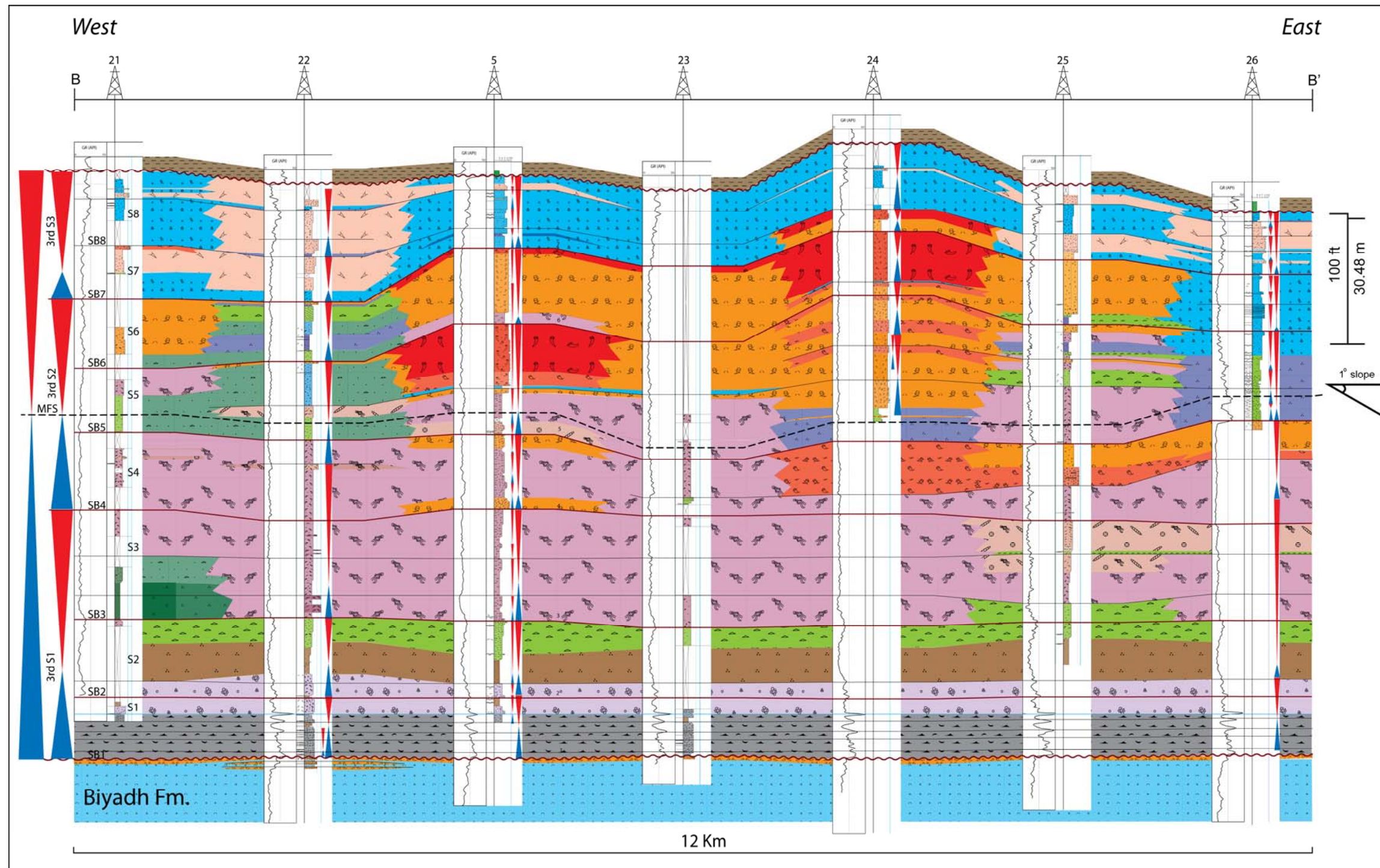


Figure 17. Detail W-E stratigraphic cross section of Shu'aiba Formation on the Southern block. This cross section shows thicker *Lithocodium* facies and less stratigraphic complexity than the northern block. See figure 3 for location.

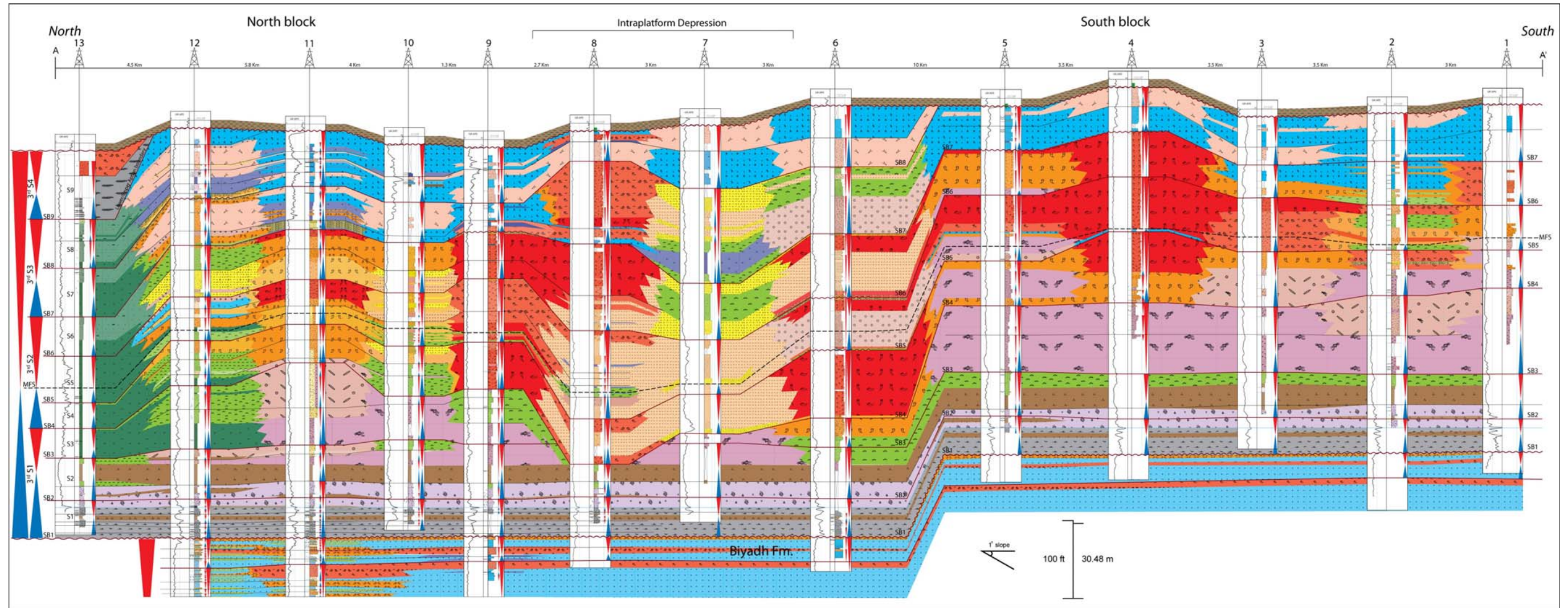


Figure 18. Detail N-S stratigraphic cross section of Shu'aiba Formation from Southern and Northern blocks across the intraplatform depression. Note how the intraplatform depression is dominated by skeletal debris packstone surrounding by rudist buildups. See figure 3 for location.

north-south strike trending section in Shu'aiba Formation (Figure 18).

The stratigraphic successions of Biyadh and Shu'aiba Formations are part of one large scale second order super sequence with a duration of about 17 My. This super sequence is bounded at the base by the Late Valanginian unconformity and is capped by the Late Aptian unconformity (Sharland et al., 2001). The Biyadh Formation occurs within the TST, while the Shu'aiba Formation occurs within the HST of the super sequence.

Biyadh and Shu'aiba Sequence Stratigraphy

The following are brief descriptions of each sequence within the Biyadh and the Shu'aiba Formations, focusing on the high-frequency sequences (HFS type sequence). The term "sequence, or S" refers here to the high-frequency sequences that range in duration from 400 k.y to 1 m.y at maximum, whereas the longer-term 3rd-order sequences and smaller-scale parasequences will be specified when mentioned.

Late Barremian Sequence

The Late Barremian Biyadh Formation is penetrated in three wells beneath the Shu'aiba Formation (Wells 11, 12 and 9). It is equivalent to the Arabian Plate Barremian 2 sequence of the Barremian supersequence of van Buchem et al., (2010). The Late Barremian succession is composed of one 3rd-order composite sequence and four high-frequency sequences (Figure 15). S 1 starts with a TST of black argillaceous dense mudstone (Figure 5A) at the base of Biyadh Formation characterized by its high gamma ray values representing the initial TST of the composite sequence. This dense unit is

similar in sedimentology and log characteristics to the Hawar unit at the base of the Shu'aiba Formation, but it does not contain abundant *Palorbitolina*. Due to the limited core materials in this interval, it is not clear if this argillaceous unit is dominated by *Palorbitolina* deposited in a shallow restricted environment similar to the Hawar unit or if this is deeper basinal facies without *Palorbitolina*. Abundant *Palorbitolina* occur in equivalent units in the region (van Buchem et al., 2010).

S 2 contains a thick bioturbated marly lime mudstone facies representing the late TST with the maximum flooding interval of the 3rd-order composite sequence. This is a deep shelf or open marine facies of uniform thickness that is interbedded with thin *Palorbitolina* wackestone units. The MFS of S 2 occurs in the middle part of the sequence containing abundant deep chalky mudstone (Figure 5B). This MFS also is the major MFS for the late Barremian composite sequence, corresponding to MFS K60 of Sharland et al. (2001). This high frequency sequence is capped by shallow skeletal packstone facies with common gastropods and *Textularid* foraminifera.

Sequences 3 and 4 record changes in facies and depositional environment from deeper open marine pelagic mudstone to shallow subtidal rudist caprotinid facies. These sequences start with initial flooding unit ~10 ft (3 m) of lower shoreface mudstone that gradually shallows upward to peloidal/oncolidal grainstone/packstone facies associated with branching corals. These sequences are capped by thick upper shoreface rudist barrier facies composed mainly of caprotinid *Glassomyophorus* rudist floatstone. In addition, these S3 and S4 are characterized by meter- to decimeter scale parasequences, possibly fifth-order cycles or higher (Figure 15). These small-scale parasequences have sharp, erosional, irregular surfaces at their base with clean coarse grainstone facies

composed of *Palorbitolina*, peloids, oncoidal and skeletal fragments deposited during flooding events (Figures 5C and 5D). These grainstone facies deepen upward to fine skeletal packstone/wackestone facies and are capped by another sharp and irregular contact overlain by the next parasequence. The correlation between different wells suggests that these parasequences can extend for long distances (up to ~ 5 km), and can be mapped on their log characteristics (Figure 15). These small-scale parasequences are unique in the Barremian Biyadh Formation and do not occur in the Shu'aiba Formation.

The upper part of Late Barremian sequence is dominated by the *Glassomyophorus* and *Agriopleura* floatstone associated with clean peloidal miliolid grainstone matrix (Figure 5E). These rudists do not form colonial rudstone buildups as in the Shu'aiba Formation; they form a uniform barrier bank facies possibly developed in the shallow upper shoreface or beach environment (Figure 9) that can be traced field wide. No Caprinid *Offneria* rudist occurred in the Barremian Biyadh Formation.

Lower Aptian Sequence 1 (S1)

This sequence overlies the regional sequence boundary and exposure surface of sequence boundary 1 (SB1) that separates the underlying Late Barremian Biyadh Formation and the overlying Early Aptian Hawar unit of the Shu'aiba Formation (Figure 5F). This boundary represents a subaerial exposure surface that is mapped regionally (van Buchem et al., 2010; Droste, 2010). This boundary also is significant because it corresponds to one of the major global depletion of carbon isotope values during the Early Cretaceous (Figure 14). The Hawar unit, previously known as "Biyadh dense unit" in Saudi Arabia was lithostratigraphically separated from the Shu'aiba Formation and

grouped with the Barremian Biyadh Formation (Ziegler, 1976; Aktas and Hughes; 1998; Hughes, 2000). However, this unit should not be tied to the Biyadh Formation, because it is genetically related to the composite sequence of the Shu'aiba Formation as the TST of sequence 1 and has unique lithological and petrophysical characteristics, acting as a seal between the Shu'aiba and Biyadh formations (Witt Gokdag, 1994; van Buchem et al., 2002). Therefore, this unit is considered here as a separate unit rather than a unit within the Biyadh Formation as interpreted previously.

S1 began with the deposition of a dark-colored argillaceous *Palorbitolina* packstone facies of the base at the Hawar unit. This unit is characterized by abundant black *Palorbitolina*, glauconite, pyrite, reddish oxidized material and marine-cemented hardgrounds (Figures 6A & B). This facies records the regional initial transgression (TS) following platform exposure at the end of the Barremian. This transgression was deposited in relatively shallow water ranging from ~ 10 - 20 m water depth (Figure 10), based on its associated fauna and grainy texture, despite the abundant argillaceous content. Shallow tidal flat facies with subaerial exposure surfaces were documented in a coeval sequence from Oman outcrops (van Buchem et al., 2002 ; 2010). This TS unit has a sheet-like geometry with nearly uniform thickness that is correlated regionally (Figure 16). Moreover, this regional transgression coincides with a global depletion in carbon isotope signature (Figure 14) and it is correlated globally (AL-Ghamdi and Pope, 2011). The MFS of this sequence is a clean, pelagic chalky mudstone facies (brown facies), characterized by low *Palorbitolina* abundance, and lower gamma ray values. This suggests that as water deepened across the platform, fewer or no *Palorbitolina* were deposited, resulting in a clean skeletal facies of predominately planktonic and pelagic

foraminifera. At the top of Hawar unit, gamma ray values record the highest value in all the Shu'aiba Formation associated with deposition of a thin (few centimeters thick) black argillaceous mudstone. This marker is regionally correlated and used here as a datum for all stratigraphic correlations (Figure 16). This sequence is capped by a sharp contact and abrupt change in facies from the dark argillaceous *Palorbitolina* packstone of the Hawar unit to the shallow subtidal, low density white-oncoidal *Lithocodium*/peloidal packstone of basal Shu'aiba Formation. This oncoidal *Lithocodium* facies has a uniform thickness across the platform and records the onset of the porous Shu'aiba successions and it represents the HST of S1 (Figure 6C).

Five high-frequency, decimeter-scale parasequences were identified and mapped throughout the field within the transgressive Hawar unit. These parasequences begin with highly argillaceous bioturbated *Palorbitolina* packstone marking a flooding surface and they deepen upward to lighter-colored, less argillaceous wackestone capped by a marine cemented hardground or firmground surface.

Lower Aptian Sequence 2 (S2)

This sequence begins with a thin flood unit of lime mudstone above SB2 (Figures 16, 17, 18) occurs within the oncoidal *Lithocodium* facies of S1. AL-Ghamdi and Read (2010) picked SB2 higher, at the top of oncoidal *Lithocodium* facies at the base of the pelagic chalky *Hedbergella* mudstone unit that is here interpreted to be the maximum flooding unit (MFU) of S2 rather than both the flooding surface and MFU. This flooding surface is thin but it extends throughout the field and also can be picked on the basis of its thin, high gamma ray value. The TST of this sequence is the oncoidal

Lithocodium/Bacinella packstone facies that deepen upward to the extensive sheet-like deep planktonic *Hedbergella* chalky lime mudstone. This facies is one of the deepest water facies in the Early Aptian Shu'aiba succession and was interpreted to be the MFU of the Shu'aiba composite sequence (AL-Ghamdi and Read, 2010). However, it is interpreted here only as the MFU of S2; equivalent to the regional MFS K70 of Davies et al. (2002). This facies has the lowest gamma ray values in the entire Shu'aiba Formation, due to its clean matrix with no argillaceous or clay materials. This facies grades upward to *Palorbitolina* wackestone with local *Lithocodium aggregatum*, which represent the HST of sequence 2 and is capped by a relatively higher energy facies of *Lithocodium/Palorbitolina* packstone. The top of this facies is a significant time marker associated with high gamma ray signal that is correlatable across the field. This gamma ray marker represents the termination of the sheet-like uniform layers associated with a low angle carbonate ramp, and the onset of a transitional carbonate platform with extensive algal *Lithocodium aggregatum/coral* mounds on the margin passing into an intrashelf basin on the eastern side (Figure 16).

Lower Aptian Sequence 3 (S3)

The base of sequence 3 (SB3) is picked above the *Palorbitolina* packstone associated with of high gamma ray time marker (Figures 16, 17, 18). S3 records a change in platform setting from uniform homogeneous strata to more heterogeneous and mounded like strata with more pronounced lateral changes of depositional settings. This sequence is distinguished by its extensive *Lithocodium aggregatum* wackestone/boundstone interbedded with platy coral floatstone (Figure 6E). The coral

facies have a more grainy texture relative to the *Lithocodium* facies, and are interpreted as parasequence caps (Figure 6F). However, *Lithocodium aggregatum* facies is the dominant facies in this sequence, forming a mound-like topographic high on the middle of the field that builds clinoforms toward the eastern basinal setting (Figure 16). The southern block has a thicker *Lithocodium aggregatum* unit compared to the northern block with columnar growth morphology that extends into the overlying S4 (e.g Wells 21, 22 and 25) (Figure 17). The extensive *Lithocodium* facies shows subtle shallowing upward to *Palorbitolina* wackestone or platy coral floatstone representing the HST of this sequence. This sequence has thicker strata with backstepping geometries on the platform (Figure 16) and thinner strata on the eastern side associated with clinoforms geometry toward the basinal settings where deeper wackestone/mudstone facies were deposited (e.g well 13 on the north, well 17 on the eastern flank).

Lower Aptian Sequences 4-6 (S4-S6)

SB4 is picked at the base of the first occurrence of the rudist buildup facies or its coeval detrital skeletal wackestone facies (Figures 16 and 18). SB4 records a major change in depositional environment with an abrupt change in facies from the algal dominated facies (*Lithocodium*/coral platform) to the shallow water rudist floatstone/rudstone facies on the margin (Figure 8D) and fine skeletal wackestone on the slope and open marine settings. Carbon isotopes record a significant chronostratigraphic marker in all depositional settings at SB4 with an almost constant value of ~ 4.5 ‰ representing an abrupt change in the carbon cycle related to abrupt change in global climate associated with a recovery of carbonate production and the development of

rudist buildup facies (Figure 14);(Follmi et al., 2006, Jynkens 2003; AL-Ghamdi and Pope 2012). Sequences 4-6 are equivalent to the 3rd-order Early Aptian sequence 3 of van Bucum et al. (2002; 2010), which represent the main rudist buildups of the Shu'aiba Formation. S4-S6 form one large 3rd-order shallowing upward sequence capped by subaerial exposure surface of SB6, but this larger 3rd-order sequence is here divided into three HFS's on the basis of the detail core descriptions and stacking patterns. During the deposition of these sequences, a syn-depositional fault system was reactivated creating the intraplatform depression that divided the Shu'aiba platform into northern and southern blocks (Figure 18). These two blocks records different depositional histories, sequence geometries and diagenetic histories (AL-Ghamdi and Read, 2010, Aktas and Hughes, 1998).

On the northern-block marginal setting, the TST of S4 is dominated by the caprotinid type rudist *Glassomyophorus costatus* floatstone (Figure 7A), that deepens slightly upward to the MFS of thin skeletal packstone and then shallows upward into the HST of rudist rudstone at the top of S4. On the eastern flank, lateral facies change occur with equivalent interbedded platy coral floatstone and *Lithocodium* boundstone (e.g well 16), changing laterally to open marine wackestone and then to deep basinal mudstone facies farthest to the east. On the southern block, S4 has only a thin transgressive caprotinid rudist facies that deepen upward to extensive *Lithocodium aggregatum* facies and then shallow upward into thin caprotinid rudist floatstone (Figure 17). Caprinid rudists do not occur in the southern block in this sequence.

Sequence 5 records major deepening indicated by the presence of *Palorbitolina* wackestone within the rudist buildups (e.g wells 14, 10, and 2) (Figures 16 - 18). On the

flanks, major deepening is recorded by extensive black mudstone facies (e.g wells 21 and 26), representing the regional maximum flooding unit of the large scale Shu'aiba composite sequence (Figure 6D). This composite MFS is different than the composite Shu'aiba MFS picked previously (AL-Ghamdi and Read, 2010) in the lower chalky mudstone facies and is also different than the MFS picked by van Buchum et al. (2010) at the uppermost part of "AP 2 sequence" near the contact between the *Lithocodium* facies and the rudist buildups. Regional stratigraphic correlation suggests that this MFS is most likely equivalent to the K80 MFS of Sharland et al. (2001) and Davis et al. (2002), but higher resolution biostratigraphy is required to accurately determine the age of this surface.

On the northern block, the intraplatform depression of S5 is dominated by skeletal peloidal grainstone that was shed from the surrounding rudist buildups (Figure 18). This intraplatform depression formed a channel-like body with high-energy currents winnowing the sediments and forming clean grainstone facies (Wells 7 and 8);(Figure 7C). The northern block platform interior (e.g wells 10, 12 and 11);(Figure 18) is more likely a shoal or back-shoal setting dominated by high-energy environments rather than a restricted back bank as previously interpreted (Aktas and Hughes, 1998; Hughes, 2000; AL-Ghamdi and Read, 2010). This skeletal grainstone facies is similar to the grainstone in the intraplatform depression, however, the location of the grainstone in the intraplatform depression was controlled by syn-depositional faulting rather than a depositional shoal setting. S5 on the southern block also records massive *in situ* rudist buildups, but they are not as abundant as on the northern block. Restricted ponds or a low-energy lagoonal platform interior of *Palorbitolina* wackestone/mudstone facies was

deposited locally between these rudists (e.g Wells 25, 22 and 2). This makes the southern block a low reservoir quality compare to the northern block.

Sequence 6 represents an overall shallowing upward trend within the rudist buildups in all wells, with the development of thick, massive shallow water rudist facies. Also, the lagoonal and platform interior settings have thin rudist units within this sequence. S6 begins with a thin flood of wackestone or *Glassomyophorus* rudist floatstone stacked on the previous rudists buildup of sequences 4 and 5. The rudist buildups of S6 are different from those of S4 and S5, being dominated by *in situ* recumbent caprinid rudist *Offneria murgensis* recording high-energy bank-crest settings with colonized rudist barriers (Figures 7E and F). Sequence 6 is capped by a thin (~1 m) unit of well-rounded, well-sorted rudist rudstone facies that likely developed in a high-energy beach environment and represent the shallowest water facies in the Shu'aiba successions (Figure 7D). This facies is very well cemented, possibly due to the influence of meteoric waters during the exposure of this platform and may act as a reservoir baffle or even barrier zone. A red clay soil content that infiltrates down between the rudist fragments (Figure 8E) indicating a subaerial exposure surface developed on top of this facies (wells 4, 9 and 46). Oxygen isotope values at this sequence boundary shows 1.5 to 2 ‰ depletion, suggesting meteoric diagenesis (AL-Ghamdi and Pope, 2012). Sequence 6 has pronounced lateral facies changes with clinoform geometries from rudist rudstone at the margin to skeletal packstone and wackestone on the slope and in open marine settings with a correlative conformity surface (Figures 19A and 19B). On the southern block, sequence 6 records overall upward shallowing rudist buildups facies, but the high-energy beach facies on top of the rudists are absent. The absence of this high-energy

facies on the southern block suggests that the northern block was influenced by higher energy wave that formed the beach deposits but these were not formed or preserved on the southern block. On southern block, sequence 6 also records the termination of the *Offneria* rudist buildups, whereas the northern blocks contains rudist buildups in the overlying sequences.

Lower Aptian Sequence 7(S7)

On the southern block, sequence 7 represents the end of Aptian sequences and it is capped by the Late Aptian unconformity at top of the Shu'aiba Formation (Figure 17). S7 begins with a thin transgressive unit of deep lagoonal mudstone that shallows upward to shallow lagoonal peloidal miliolid packstone facies. The only rudists occurring in this sequence is the elongate caprotinid *Agriopleura* or *Pachytraga* that form local patchy mounds (Figure 7B). The upper part of this sequence gradually deepens to mudstone facies contains infiltrated shale from the Nhr-Umr Formation beneath the top unconformity. The deepening trend from shallow miliolidal packstone to wackestone/mudstone below the top of the Shu'aiba Formation occurs in most wells. On the northern block, S7 begins with a mudstone flooding surface including rip up clasts and reworked rudist fragments and deepens upward to deep lagoonal mudstone. This mudstone is overlain by the miliolidal packstone facies with local *Agriopleura* floatstone facies. However, thick massive rudist buildups of *Offneria* rudist rudstone still developed local patchy rudist buildups, commonly stacked on rudist buildups that formed in sequence 6 (Wells 8, 12 and 16);(Figure 18). This rudist units do not form continuous barrier banks, but they are patchy mounds surrounded the lagoonal facies

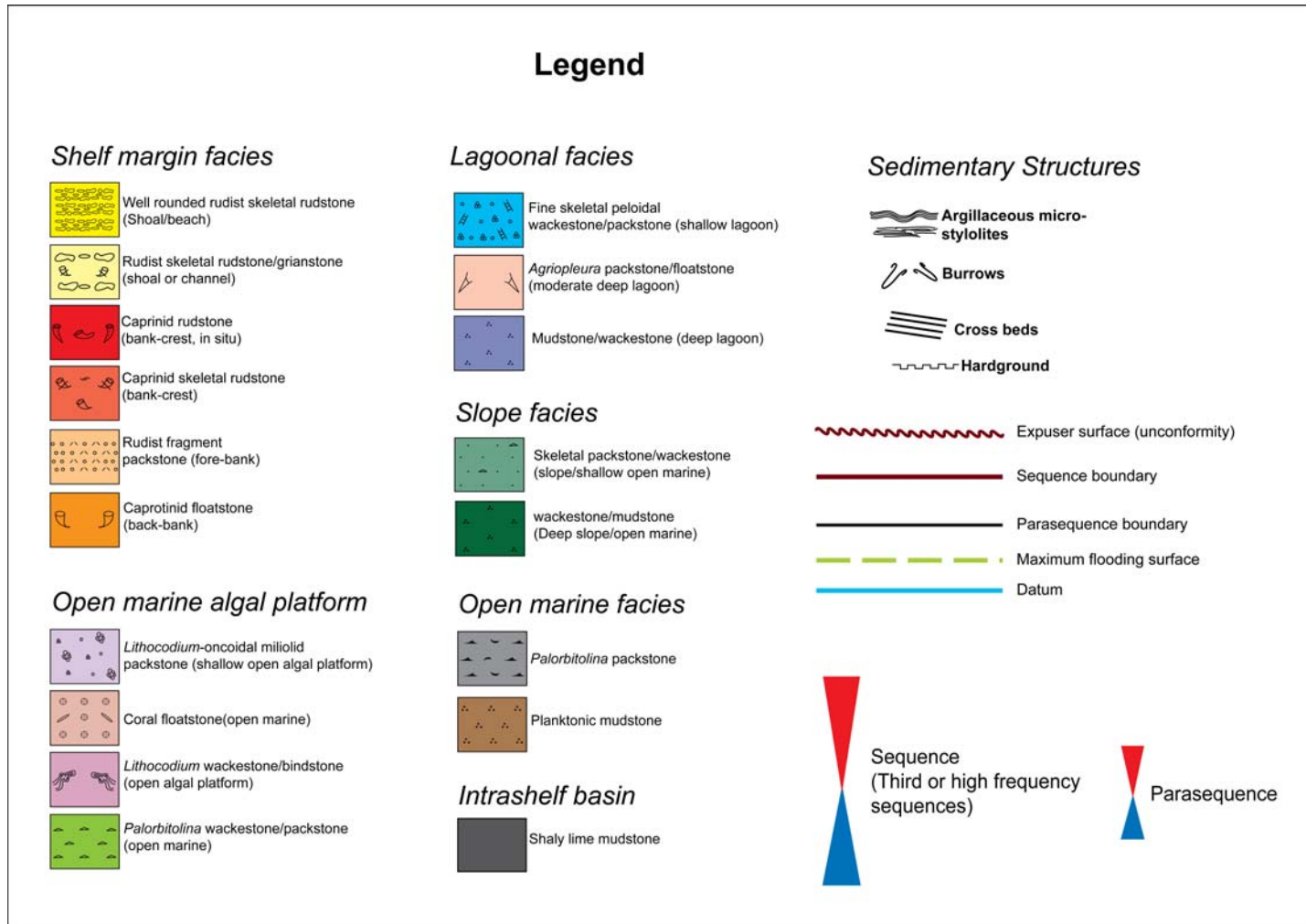


Figure 19B. Legend, symbols and color codes of lithofacies used in the above cross sections.

with a prograding shingled geometry. These patchy rudist buildups are capped by high energy rounded-rudist rudstone formed in a beach environment that was subaerially exposed similar to the facies that cap sequence 6. The top of sequence 7 records the termination of the *in situ* rudist buildups within the Shu'aiba Formation and the demise of the caprinid *Offneria* rudist species (Hughes, 2000).

Lower Aptian Sequence 8 (S8)

This sequence only occurs on the northern block, due to the influence of the syn-depositional subsidence that moved the northern block down and provided accommodation space on the northern block when the south block was exposed and eroded by the Late Aptian unconformity (AL-Ghamdi and Read, 2010; Figure 18). This sequence is the last phase of sedimentation on the Shu'aiba Formation platform margin. However, more sequences are still developed on the eastern platform edges. S8 is dominated by shallow lagoonal peloidal miliolid packstone/wackestone facies interbedded with thin, deeper lagoonal mudstone facies. *Agriopleura* floatstone facies occur as local patchy rudist mounds or as the caps to shallowing upward successions, but no colonized rudist occurred in this sequence. This sequence records a deepening trend of mudstone facies below the Late Aptian unconformity similar to S7 on the southern block. This unconformity formed karst that locally penetrates deeper than 30 ft (10 m) into the top of the Shu'aiba Formation (e.g. wells 16 and 52; Figure 8F).

Upper Aptian Sequences 9 & 10 (S9 & S10)

Sequences 9 and 10 are Upper Aptian sequences identified for the first time in this study. They formed only on the northern block as shelf edge prograding sequences, during which the interior of the Shu'aiba platform was subaerially exposed and eroded (Figures 17 and 19A). These sequences are equivalent to sequences Apt4a and Apt4b of van Buchum et al. (2010). The Lower/Upper Aptian boundary is a conformable surface and was picked initially on the basis of carbon isotope values (Figure 14) and coincides with an abrupt change in facies from fine skeletal and detrital packstone of the Lower Aptian slope of S8 to dark dense argillaceous mudstone facies of S9 (Figure 8C). In addition, nannofossil data from well 19 confirms the Late Aptian age of these sequences with the first occurrence of the nannofossil *Lithraphidites houghtonii* (AL-Ghamdi and Pope, 2012). Thus, biostratigraphy integrated with core description and chemostratigraphy constrain the age of these prograding sequences (AL-Ghamdi and Pope, 2012). The argillaceous mudstone averages about 20 to 30 ft thick (6-9 m) and shallows upward into grainy coral floatstone facies overlain by massive reefal facies containing mixed stromatoporoid and rudist rudstone (Figure 8B). The argillaceous mudstone facies occurring at the base of these sequences possibly represent a lowstand prograding wedge, similar to what has been interpreted by van Buchem et al. (2010) and Yose et al. (2010). The Late Aptian rudists mainly are *Horiopleura* species of the Polyconitidae family (Skelton, 2008, Saudi Aramco internal report), quite different type than the lower Aptian caprinid and caprotinid rudists. The range of *Horiopleura* rudists extends from the Aptian to the lower Albian (Skelton and Masse, 2000). These shelf

edge sequences prograde toward the intrashelf basin with clinoform geometries and laterally change facies to open marine skeletal packstone/wackestone and finally to deep pelagic basinal mudstone. At least nine high-frequency sequences were described from seismic in the coeval Bu-Hasa field, and they prograde > 10 km from the shelf edge toward the basin (Pierson et al., 2010). It is possible that more prograding sequences formed far to the east in the study area, but more data (e.g seismic data) is necessary to confirm this interpretation. The Upper Aptian prograding sequences also occurred in the far northern edge of the platform where wells 53, 13 and 54 have similar depositional settings to the eastern flank with similar facies and similar stacking patterns. Upper Aptian sequences also formed on the northwestern flank as shown in the carbon isotope curve in well 45 (Figure 14), but differ from the eastern flank in that they do not have shallow water rudist facies or slope and open marine settings, instead the Upper Aptian here records restricted lagoonal environments.

Finally, the Bab intrashelf basin occurs on the far eastern side in well 20, and is thought to be the latest Upper Aptian or early Lower Albian (van Bucum et al., 2010). It is the last stage of basin infill and is dominated by organic-rich lime mudstone interbedded with sandstone.

Parasequences

Parasequences are an important component of the stratigraphic framework and reservoir characterization as they control the reservoir properties and hence the simulation model and its fluid flow behavior (Kerans and Tinker, 1997). Therefore,

higher-scale parasequences of the Biyadh and Shu'aiba Formations were identified and mapped to better characterize their reservoirs and to provide a higher-resolution genetic layering scheme for the 3-D reservoir model. Also, their stacking pattern, thickness and magnitude will provide better understanding on the driving mechanism of the stratigraphic records and the effect of climate within a global or regional scale.

Parasequences in Biyadh Formation

There are 34 parasequences identified in Biyadh Formation, most of them can be traced between wells and throughout the field (Figure 15). Of these 34 parasequences, four formed in S1; five formed in S2; 13 formed in S3 and 12 formed in S4. Parasequences in S1 occurred within the argillaceous dense unit at basal Biyadh Formation. No cores penetrate the entire interval of this unit, but four meter-scale (~ 5 ft thick, 1.5 m) cycles can be mapped throughout the area on gamma ray logs. As similar to Hawar unit, the higher gamma ray values of this unit indicate highly argillaceous mudstone representing flooding surface that change upward to more clean, deeper and less argillaceous mudstone. Parasequences within S2 are thicker ~ 15 ft (4.5 m) cycles, that begin with a *Palorbitolina* wackestone and deepen upwards to chalky mudstone facies. Major changes in parasequences pattern occurred at S3 where many more (13) small scale ~ 2-5 ft (0.6-1.5 m) cycles are delineated within the shallow upward S 3. These cycles are characterized by a sharp erosional contact at the base overlain by oncoidal peloid grainstone facies or rudist floatstone representing a flooding surface that shallow upward to less grainy packstone/wackestone facies (Figure 5C). Most of these

cycles can be correlated between the wells and may have some impact on reservoir quality distribution (Figure 15).

Parasequences in Shu'aiba Formation

The Shu'aiba Formation contains at least 37 parasequences within the Early and Late Aptian sequences, 31 parasequences formed in the Lower Aptian back-bank or platform interior settings and at least 6 additional parasequences formed in the Upper Aptian prograding wedges on the flanks. Of the 31 parasequences; seven formed in S1 (including 6 in Hawar unit), whereas S2-S10 include 3-4 parasequences each. Parasequences within S1 and S2 are sheet-like units and are calibrated to gamma-ray logs, thus they can be mapped throughout the field. Parasequences in S3 within the *Lithocodium*/coral mounds have slightly different geometries due to the development of *Lithocodium* mounds on the platform margin and clinoform prograding toward the basin. Therefore, more parasequences are recorded on the platform margin than the slope or open-marine settings. Associated fauna were used to pick some these parasequences, where the relatively deeper water *Lithocodium* facies is interbedded with the relatively shallower coral facies.

Generally, the *in situ* rudist buildups within the bank-crest at S4 - S6 are poorly cyclic and do not record higher-order parasequences, due to their nature as reefal buildups geometry with massive framework and higher sedimentation rate. However, parasequences are better developed on the back-bank, shoal or fore-bank settings. Interbedded of different type of rudists, such as the deeper water *Glassomyophorus*

rudist and the shallow water *Offneria* rudist within these sequence are used as an evidences of cycle changes. These parasequences S4-S6 are locally continued and are rarely mappable over the rudist buildups. In addition, these parasequences cannot be mapped over the open marine settings, due to the unchanged and uniform lithofacies deposited in coeval open marine and basinal settings.

The upper part of the Shu'aiba Formation (S7-S8) has seven parasequences at maximum that can be mapped locally. These parasequences have deep lagoonal mudstone at the base that shallows upward into peloidal miliolid packstone or *Agriopleura* floatstone facies. Exposure surfaces formed locally at the top of these parasequences.

Parasequences in the Upper Aptian sequences 9 and 10 are characterized by a basal dense argillaceous mudstone that changes upward into coral/stromatoporoid floatstone or skeletal packstone facies. These parasequences show clinoform geometries and can be mapped locally, with a top lap geometry against the Upper Shu'aiba Unconformity.

Discussion

Barremian versus Aptian Sequence Stratigraphy

Although there are some similarity in the facies associations between the Late Barremian Biyadh Formation and the Aptian Shu'aiba Formation, there are many differences between the two units with regards to their depositional settings and facies architecture. First, the entire Biyadh Formation is composed of one large scale 3rd-order

shallowing up sequence recording a single long-term sea level rise and fall. Conversely, the Shu'aiba Formation records a large scale composite sequence/or 2nd-order sequence, built by four 3rd-order sequences, built by 10 high frequency sequences. The Biyadh Formation was deposited on a shallow subtidal ramp with relatively thin rudist banks at the upper shoreface environments (Figure 9). The Shu'aiba depositional platform evolved from, restricted subtidal, algal dominated ramp to marginal rudist barrier bank (Figures 10-13). The shallow subtidal ramp of the Biyadh Formation formed sheet-like layers at all scales (3rd-order sequences to parasequences) because there were no tectonic rim developed during this time, therefore, there was no major lateral changes in depositional setting and no intrashelf basinal architecture developed at this time. This is indicated by the uniform sheet-like strata of all the large and small scale parasequences within the Biyadh Formation, they are layer-cake strata and do not have the shingle or clinofom geometries like the overlying Shu'aiba Formation (Figure 15). The rudist facies in Biyadh Formation also correlate as a layer cake unit and are dominated by the elongate caprotinid *Glassomyophorus* and *Agriopleura* species with no evidence of the high-energy reffal caprinid rudist of *Offneria* species.

In addition, the average thickness of the Biyadh sequence is about 220 ft (67 m) whereas the average thickness of the Shu'aiba Formation is about 450 ft (137 m). This is due to the absence of extensive *Lithocodium* aggregatum algal mounds and a colonized rudist buildups in the Biyadh Formation.

Shu'aiba Formation Hierarchy and Platform Evolution

The Shu'aiba Formation, including Hawar unit and the Late Aptian sequences is about 530 ft (160 m) thick and is composed one large scale composite 2nd-order sequence (spanning ~7 My) comprised of four 3rd-order sequences (~ 1 - 2 My each) and 10 high frequency sequences (~ 400 ky - 1 My; Figures 19A). Previous study of AL-Ghamdi and Read (2010), interpreted 7 HFS's in the Shu'aiba platform within the Early Aptian, but did not interpret any 3rd-order sequences, due to the lack of biostratigraphic markers and poor age control within the Shu'aiba platform. This study used much more data than previous study and is also incorporating much more carbon isotope data that helps constrain the ages beyond the resolution of biostratigraphy (Figure 14). Thus, eight HFS's (S1 to S8) were identified and mapped on the Early Aptian Shu'aiba platform, plus two more HFS's (S9 and S10) are mapped on the Late Aptian platform edge, compared to seven HFS's in AL-Ghamdi and Read (2010). The extra sequence in the Early Aptian in this paper is S3 that is a significant chronostratigraphic marker, in addition to its association with a notable change in platform geometry and basin configuration. Thus interpreted as an individual HFS rather than parasequence.

On the basis of stacking patterns, stratigraphic geometry, facies association and carbon isotope curves, the ten HFS's in the Shu'aiba Formation can be grouped into four 3rd-order sequences with possible duration of ~1 - 2 My each. These 3rd-order sequences are abbreviated as 3rd-order S1, 3rd-order S2, 3rd-order S3 3rd-order S4 to differentiate them from the HFS's S1-S10. The first 3rd-order S1 consists of S1, S2 and S3 that are characterized by a transgressive phase associated with sea-level rise, mud-dominated

facies, and open marine algal platform environments, with *Lithocodium*/coral and *Palorbitolina* facies. This 3rd-order sequence represents a global diminish of carbonate production with the absence of rudist buildups that were replaced by extensive *Lithocodium aggregatum* and coral facies (Huck et al., 2012). The second 3rd-order sequence (3rd-order S2) is composed of sequences S4, S5 and S6, associated with the development of massive rudist buildup facies. This sequence is dominated by aggrading geometries and relative sea-level stillstand with high sedimentation rates representing the early HST of the Shu'aiba 2nd-order composite sequence. The 3rd-order S2 also records an individual shallowing upward sequence where the base is dominated by transgressive *Glassomyophorus* rudist facies that shallow upward into a high-energy *Offneria* rudist facies that is capped by rounded rudist debris rudstone facies formed in a beach environment followed by subaerial exposure of the platform. 3rd-S2 here is equivalent to "Apt3" in van Buchem et al. (2010) and Yose et al. (2010).

3rd-order sequence 3 is composed of S7 and S8 and it overlies the SB7 exposure surface that records the termination of the colonized *Offneria* rudist buildups on the southern block. This 3rd-order sequence represents the last stage of deposition on the platform margin with shallow lagoonal miliolids peloidal packstone facies interfingering with local *Agriopleura* rudists. The stratigraphic geometry of this sequence is dominated by late HST of the Shu'aiba composite sequence with slight progradation of the rudist and shallow lagoonal facies toward the basin. This sequence was extensively eroded and karstified during the Late Aptian unconformity that formed during a global sea-level fall (estimated of ~30 m sea-level drop), possibly due to polar glaciation (Al-Husseini and

Matthews, 2010). The fourth 3rd-order sequence (3rd-order S4) is composed of the Upper Aptian (S9 and S10) that prograde from the shelf edge into the intrashelf basin. This sequence was only deposited on the northern platform edge during a forced regression and major sea-level fall in the Late Aptian. Core descriptions integrated with carbon isotope data confirm two prograding sequences formed on the flanks of the Shu'aiba platform, however, more prograding sequences may exist farther east toward the basin (Figure 14). Yose et al. (2010) and Pierson et al. (2010) were able to identify nine prograding sequences on the U.A.E giant field A, using seismic data.

Maximum Flooding Surfaces

The regional maximum flooding surfaces of the Early Cretaceous Biyadh and Shu'aiba Formations have been debated, especially the maximum flooding surfaces K70 and K80. Sharland et al. (2001) defined three major flooding surfaces within the study interval; (K60) in the Late Barremian Biyadh Formation, and (K70 and K80) in the Early Aptian Shu'aiba Formation. Sharland et al., (2001) placed K60 within the unit at the base of the Biyadh Formation, placed K70 at the top of the Hawar dense unit corresponding to the highest gamma ray signal at the contact between Hawar unit and basal Shu'aiba Formation, and placed K80 higher in the Shu'aiba section coeval to the tar unit of intrashelf Bab Member.

K60 in this paper was placed higher in the section within the mudstone facies of S2 at the base of the Biyadh Formation (coeval to Khariab Formation in the U.A.E). It is

similar to the placement of K60 in van Buchem et al. (2010) but different than the K60 of Sharland et al., 2001 that was picked within the dense unit underneath (Figure 15).

Davies et al., (2002) on his updated study, refined the location of K70 and placed it higher in the section within the lower part of the Shu'aiba Formation, corresponding the chalky *Hedbergella* planktonic mudstone facies that also was interpreted to be the deepest water facies of the Shu'aiba Formation (AL-Ghamdi and Read, 2010). In addition, K70 was interpreted to be the MFS of the entire Early Cretaceous supersequence (Sharland et al., 2001; Davies et al., 2002; AL-Ghamdi and Read, 2010). The Hawar unit, was previously interpreted as a deep, open platform with planktonic foraminifera associated with the predominant argillaceous *Palorbitolina* packstone facies (Hughes, 2000). AL-Ghamdi and Read (2010) interpreted the Hawar dense unit as deposited in relatively deep water environments, but with lack of planktonic foraminifera, thus K70 maximum flooding surface was placed higher in the section within the clean chalky planktonic mudstone facies that interpreted to represent the deepest water facies of the Shu'aiba Formation. However, evidence of mud cracks and possible exposure surfaces within the coeval Hawar unit, especially in the outcrop of Jabal Akhdar (Oman), suggests that the Hawar unit may deposit in tidal flat or shallow restricted environments rather than a deep open marine setting and representing the early TST rather than the maximum flooding surface (van Buchem et al., 2002, 2010; Pittet et al., 2002; Stronhmenger et al., 2006).

Van Buchem et al., (2010) however did not recognize K70 as a major surface, they only recognized the K80 as the major MFS of the entire Lower Cretaceous super

sequence. Moreover, van Buchem et al., (2010), Droste, (2010) and others, picked K80 on the basis of the general stratigraphic trend near the contact from the lower Shu'aiba transgressive phase dominated by *Lithocodium/Bacinella* facies to the middle Shu'aiba rudist buildups regressive phase. However, there is no discrete surface that can be identified for this MFS event and gamma ray logs also do not have a significant increase associated with this surface in the region. We agree that the MFS K80 is probably the major MFS for the Shu'aiba composite sequence rather than K70, but we do not agree that it is located at the contact between the *Lithocodium/Bacinella* facies and the rudist buildups facies. This contact is a major sequence boundary (SB 4 in this study and base of Apt3 in van Buchem et al., 2010), marked by a sharp contact and abrupt change in facies (Figure 8D), depositional environment, and also change in the global carbon isotope values, thus it cannot be a sequence boundary and maximum flooding surface at the same time. K80 in this study is placed on a clear physical surface in cores, that is higher in the section than the K80 of van Buchem et al. (2010), within the rudist buildups facies of S5 associated with a major flooding surface and deep water facies recorded in cores associated with higher gamma ray signals, especially on the flanks of the field (Figures 16-19). This is a major drowning event within S5 that occurred across the entire field and also occurred within the *in situ* rudist bank-crest setting, where deeper water *Palorbitolina* mudstone/wackestone was deposited within the rudist buildups indicating major platform drowning event (e.g wells 14, 9, 10 and 12). On the platform edge, major deepening is recorded with the deposition of a thick succession of deeper water, black-laminated mudstone facies. Placing K80 at this surface makes S1 -

S4 the TST of the entire Shu'aiba composite sequence with general aggrading and backstepping geometries. S5 - S8 then become the early HST with aggrading and slight prograding geometries toward the basin. S9 - S10 is the late HST with strong, downstepping and progradational geometries (Figure 19A). In addition, the rudist buildups in S4, beneath the K80 are mainly dominated by the relatively deep water transgressive caprotinid *Glassomyophorus* rudist, but above K80 the caprinid *Offneria* rudists are the predominant rudist type. Therefore, K80 here is the turnover surface (MFS) between the large scale TST and HST of the Shu'aiba composite sequence.

Although K80 is considered the major MFS of the Shu'aiba composite sequence, K70 is still an important flooding unit and it is picked here as the MFS of the HFS S2 and the MFS of the 3rd-order sequence 1. K70 also is an important surface, because it is associated with the onset of the major carbon isotope positive excursion of the Early Cretaceous just beneath the *Lithocodium/Bacinella* facies, coeval to widespread black shale deposited during the global OAE 1a (Immenhauser et al., 2005). It is not clear why this MFS (K70) and its associated facies, the deep planktonic chalky mudstone unit (brown color in the cross sections) was not clearly defined and mapped in the region. This MFS was described as a secondary higher-order flooding event with limited correlation potential (e.g. van Buchem et al., 2010).

Anatomy of the Shu'aiba Formation Platform

A series of facies maps (Figures 20 - 26) were generated for each HFS (S3 - S10) to illustrate the evolution of Shu'aiba platform and to track the changes in its

depositional anatomy to determine its influence on reservoir quality. These facies maps are crucial for constructing a 3-D geocellular model and also for predicting reservoir quality and guiding new drilling programs. They also are important to understand the influence of third order sea-level changes during the Aptian on the Shu'aiba platform and the effect of syn-depositional faulting on facies development. The facies maps were constructed using the 55 cored wells at the top of each sequence representing the HST of each sequence. S1 and S2 were not included in the facies maps, because their facies are sheet-like strata across the region without any lateral facies changes.

Facies anatomy of HFS 3 (S3)

Sequence 3 is dominated by the development of *Lithocodium*/coral algal mounds with subtle lateral facies changes to *Palorbitolina* wackestone (Figure 20). In this sequence, the Shu'aiba platform is dominated by the *Lithocodium* facies associated with global sea-level rise that flooded epicontinental basins around the world during the development of Oceanic Anoxic Event 1a. This *Lithocodium* facies is coeval to black shale and the global OAE 1a elsewhere (Immenhauser et al., 2005). The *Lithocodium* facies in this sequence develop a thick and extensive algal mound on the margin that thins toward the eastern side of the basin and changes to deep, open marine facies (Figure 19A). Patchy coral mounds of mixed platy and massive corals developed locally to the north and south. These coral facies may extend for several kilometers and providing high reservoir quality due to the abundance of intergranular and moldic porosity within the corals (Figure 6F). These coral mounds developed on top of the

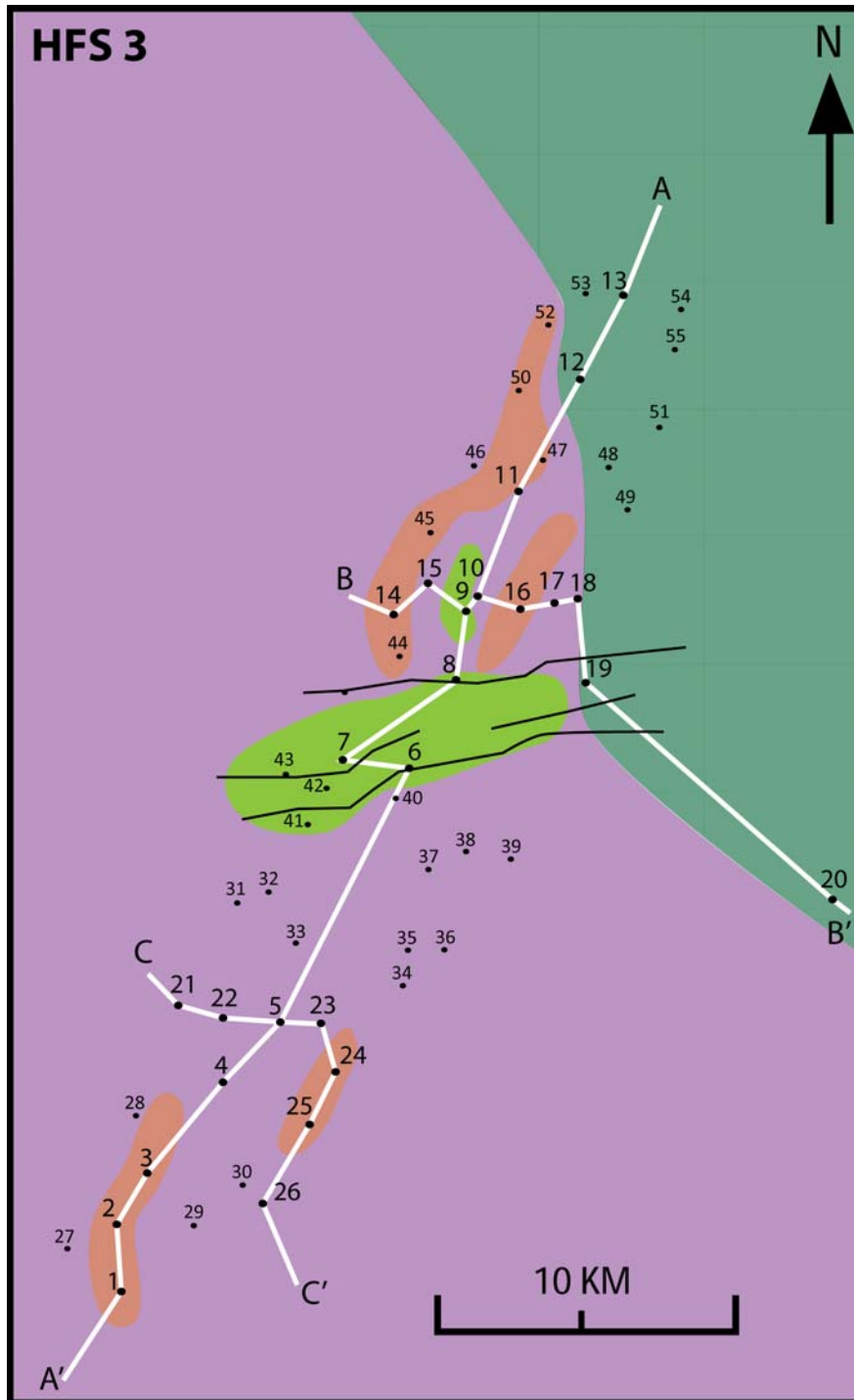


Figure 20. Facies map at top of HFS 3. This facies is dominated by *Lithocodium* facies. Intraplatform depression is dominated by *Palorbitolina* wackestone facies (green). Coral facies form local mounds on the flanks.

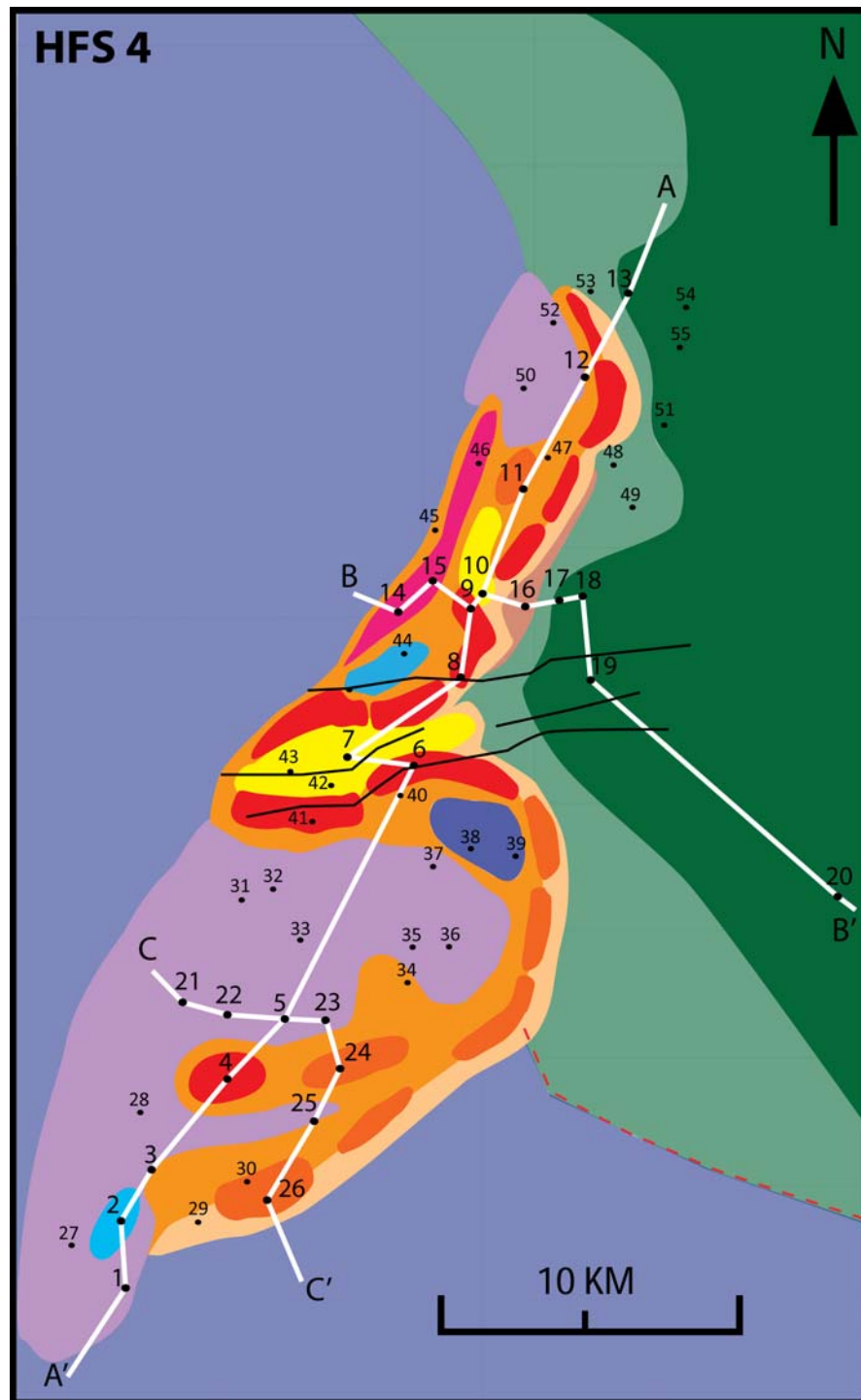


Figure 21. Facies map at top of HFS 4. This map shows the initiation of the rudist buildups. The southern block still develop extensive *Lithocodium* on the western margin.

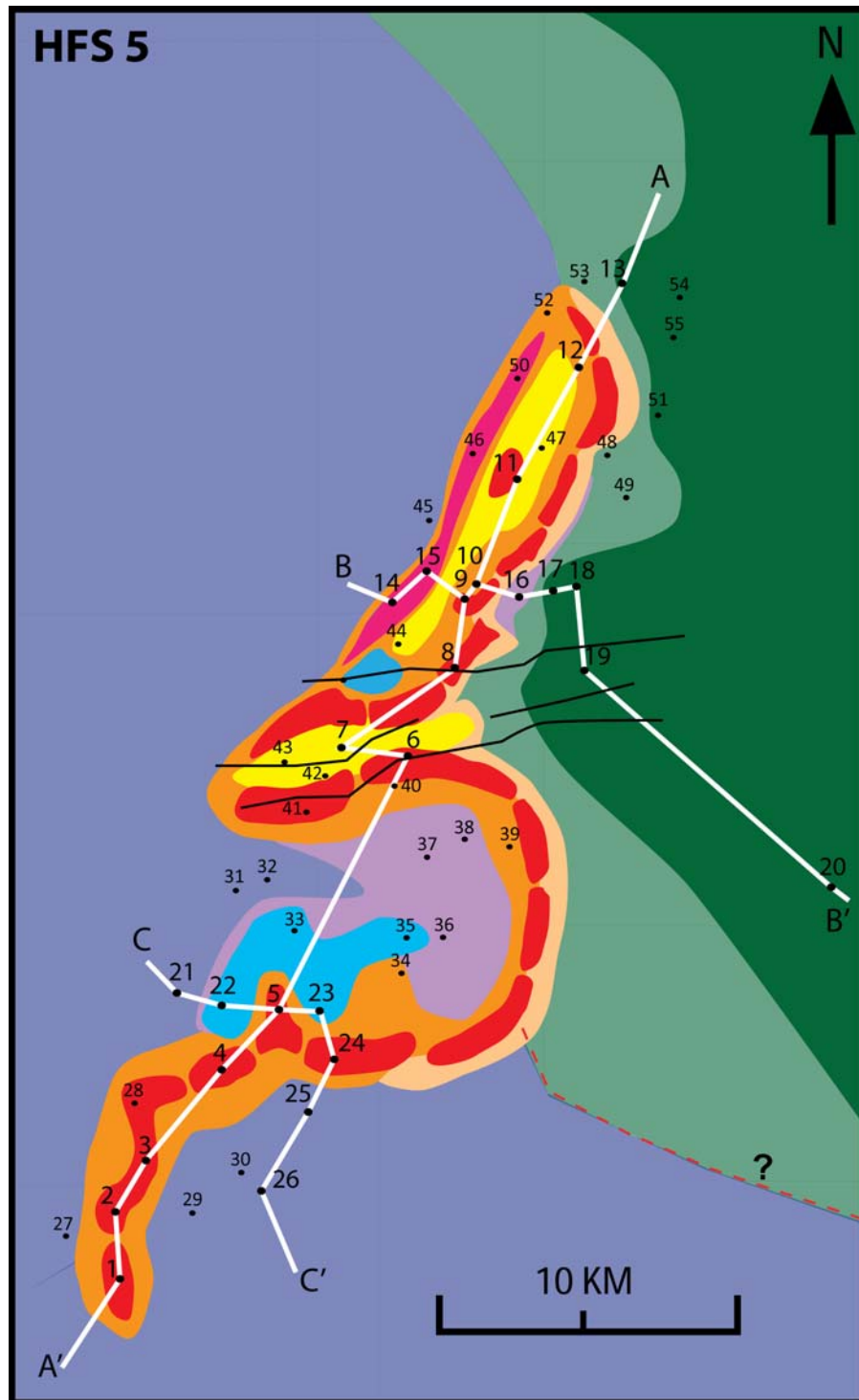


Figure 22. Facies map at top of HFS 5. Rudist buildups rimmed the northern block, while the western side of the southern block is open to deep lagoonal facies.

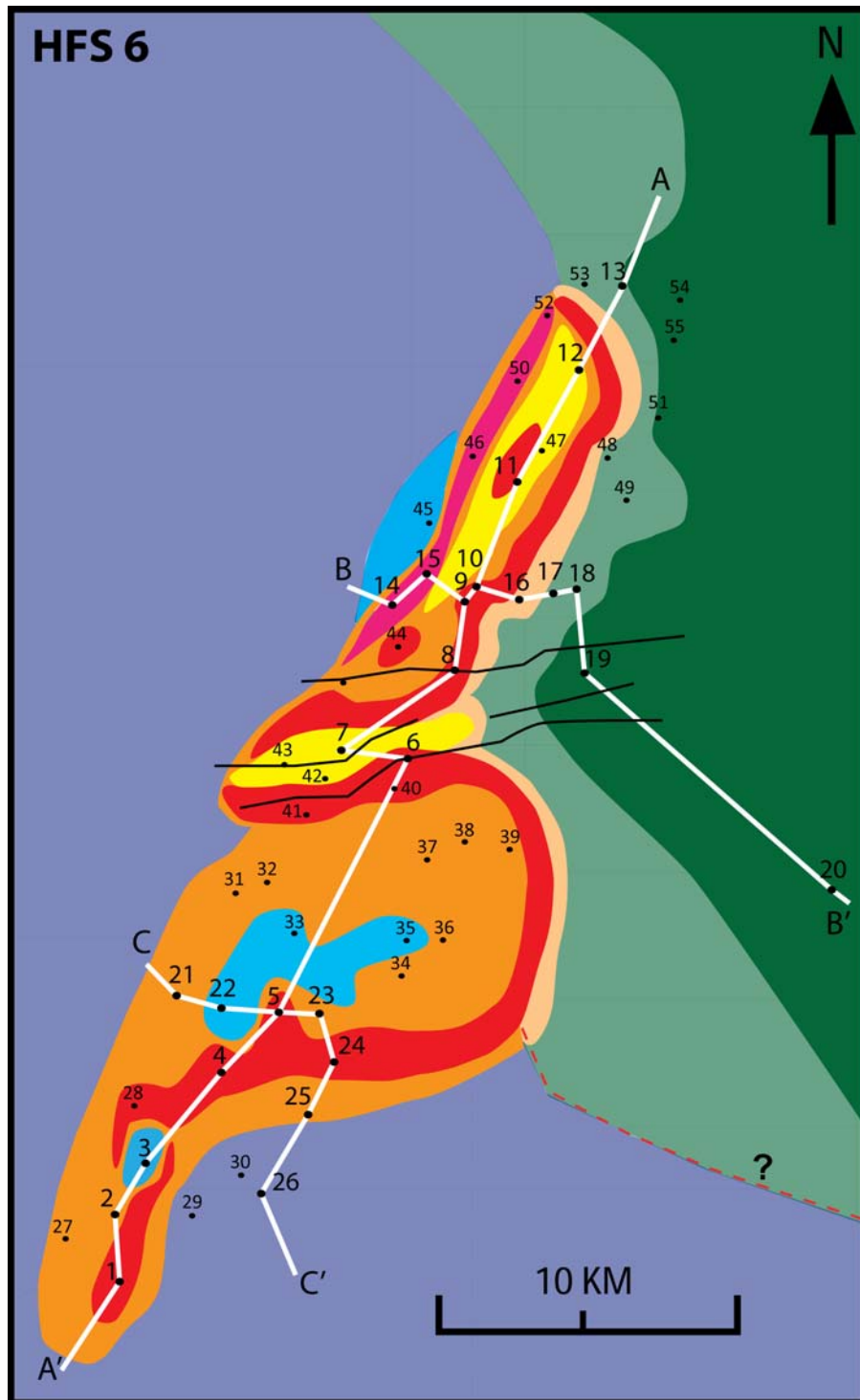


Figure 23. Facies map at top of HFS 6. Extensive and continuous rudists buildups formed around the field.

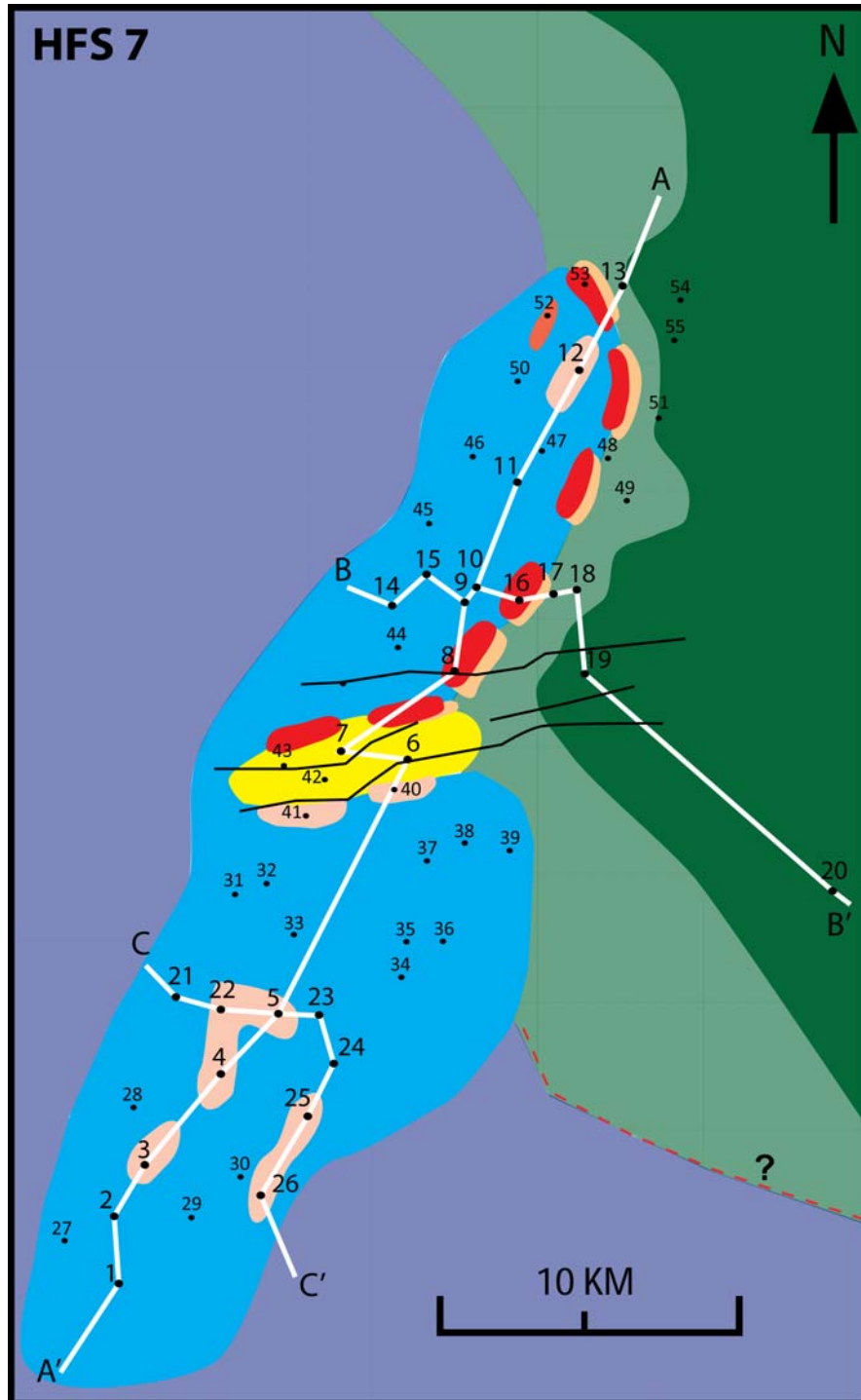


Figure 24. Facies map at top of HFS 7. The platform is dominated by inner ramp lagoonal facies, but rudist buildups still forming in the eastern margin.

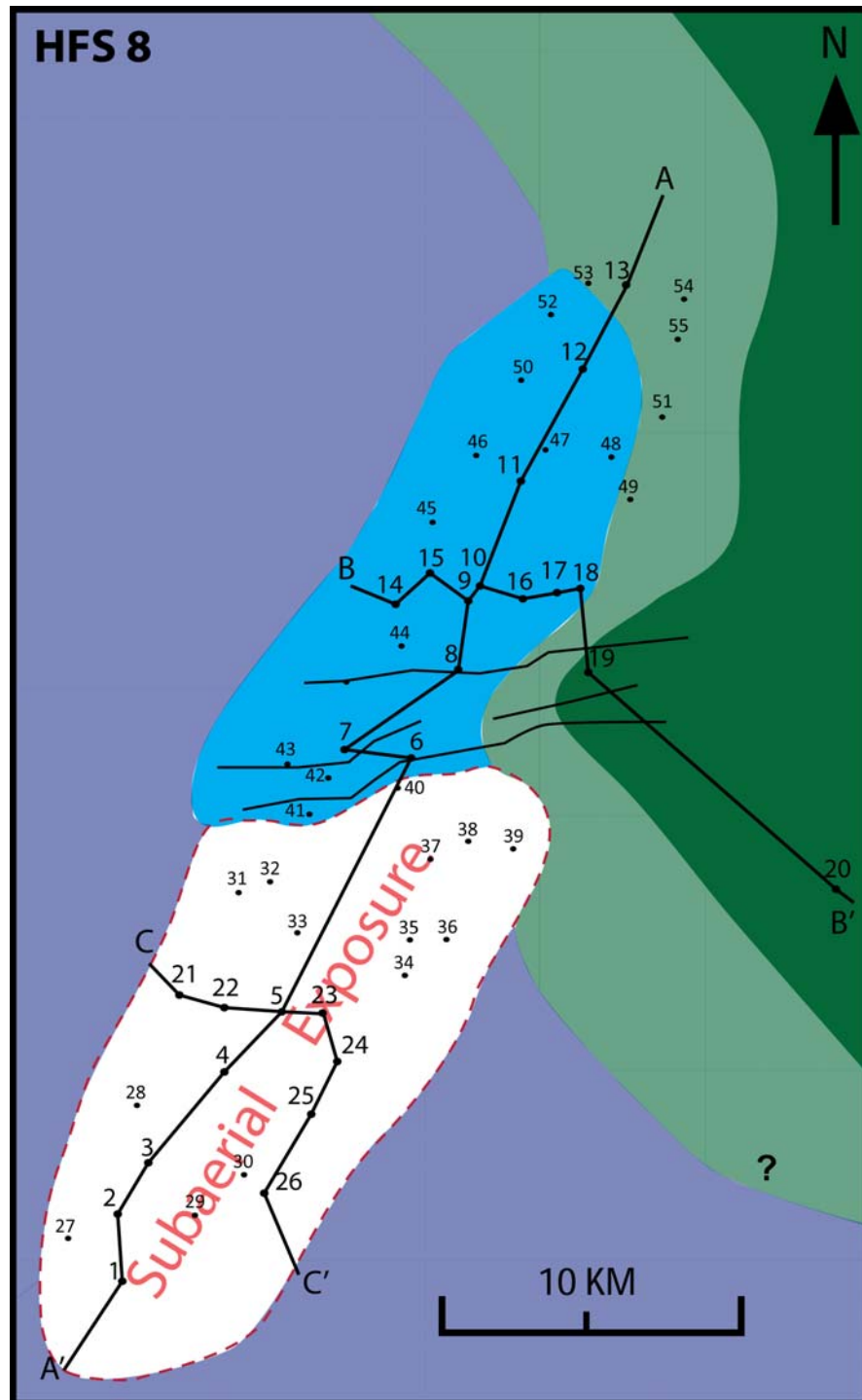


Figure 25. Facies map at top of HFS 8. The southern block is subaerially exposed and the northern block is dominated by inner ramp shallow lagoonal facies.

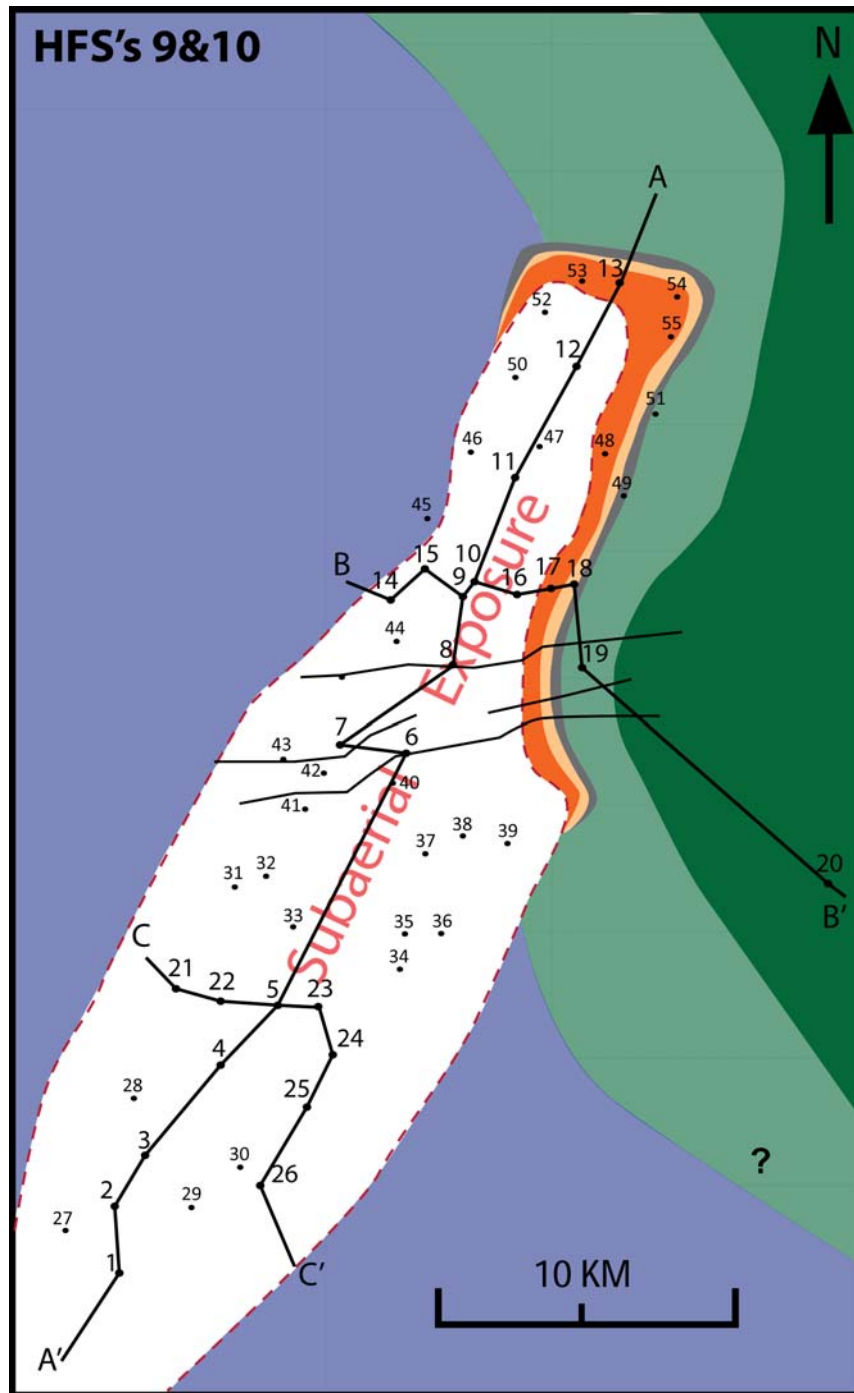


Figure 26. Facies map of the Upper Aptian sequences 9 and 10. The whole platform was subaerially exposed except the north and eastern margins of the northern block, where prograding sequences occurred.

Lithocodium facies as topographically higher coral mounds were suitable place for the rudist buildups to initiate in the following sequences, such as the elongate coral unit on the north that is overlain by the high-energy rudist facies that has the highest reservoir quality in all wells. The intraplatform depression between the northern and southern blocks was dominated by *Palorbitolina* wackestone facies without significant *Lithocodium* or coral developed due to sediment starvation and its topographic low position. Therefore, S3 thins dramatically in this zone or pinches out altogether (Wells 7 and 8)(Figure 18). This change in the facies at the intraplatform depression suggests that the syn-depositional fault systems initiate early in this sequence, because previous sequences were uniform beneath this depression area.

Facies Anatomy of HFS 4 (S4)

Sequence 4 formed at the base of the 3rd-order S2, recording the onset of the rudist buildups along the north and south margins of the platform (Figure 21). The south margin rudist facies passes eastward into an open marine *Lithocodium* algal platform or lagoonal facies, whereas the northern block developed more extensive rudist buildups that transitioned into a fragmented rudist shoal except along the northeastern flanks (Wells 50 and 52) where the *Lithocodium* facies persisted, suggesting an open environment to deeper water facies off the margin. The rudist buildups in this sequence are dominated by mixed *Glassomyophorus* and *Offneria* rudists in the northern and mainly *Glassomyophorus* rudists on the southern block, suggesting the northern block was influenced by higher energy waves than the southern block. The rudist buildups on

the eastern flanks were interpreted as the windward margin whereas the western flank was the leeward margin (AL-Ghamdi and Read, 2010). However, the western flank rudist facies (pink) is dominated by fragmented rudists rudstone in a grainy matrix with abundant moldic and vuggy porosity and was deposited under a higher energy environment than the eastern flank (red) (Figure 7E). Conversely, the eastern flank rudist facies, is dominated by *in situ* rudist rudstone/floatstone with muddy matrix filling and infiltrating the rudists with moderate to good porosity. Rudist buildups in this sequence formed north-south oriented buildups, with discontinuous elongated barriers possibly separated by tidal channels (Figure 12). These discontinuous rudist buildups was conceptually interpreted on the basis of discontinuous barrier banks (or reefs) in modern carbonates platforms such as the Great Pearl Bank barrier of the Arabian Gulf (Hughes, 1997) and the Great Barrier Banks of Australia (J.F Read, personnel com.). The intraplatform depression is dominated by detrital grainstone facies developed in an elongated W-E trending trough with high-energy currents in a channel-like geometry. This detrital grainstones were sourced from the surrounding rudist buildups that developed on the topographically high W-E trending rim created by fault systems, possibly along deep seated basement faults as suggested by seismic data. The platform interior in the northern block is generally dominated by the back-bank *Glassomyophorus* rudist floatstone with no evidence of deep lagoonal ponds or restricted lagoons as previously thought (Hughes, 2000). The southern block, however has deeper back-bank or lagoonal settings dominated by *Lithocodium aggregatum* facies as shown on the western flank (Figure 21).

Facies Anatomy of HFS 5 (S5)

The rudist buildups in this sequence continued to develop a stacked sequence above the previous platform margins, but the buildups extend further around the platform (Figure 22). For instance, rudist buildups were established above the *Lithocodium* facies of S4 on the far south and possibly attached to the previous rudist buildups on the central part at Well 4 with an elongated north-south trend. The northern block has similar rudist trends as the previous sequence, but they also extended into Wells 50 and 52 forming a more continuous rim around the platform over *Lithocodium* facies in S4. A major change in facies in the northern block is the development of a high-energy grainstone shoal (Figure 7C), in the platform interior (yellow zone, Figure 22) as an elongated north-south trending zone. This high energy grainstone in the platform interior was deposited in a shoal or shallow back-bank settings and surrounded by *in situ* rudist buildups on both sides. The southern block, however does not have such high energy shoal facies, instead, the platform interior is dominated by low energy lagoonal wackestone or *Lithocodium*/coral facies (e.g. Wells 33, 23 and 35). The deep lagoonal facies marks a widespread deepening event that were clearly recorded on the flank wells (e.g wells 21, 26, 30 and 45) associated with the regional maximum flooding unit (MFU, K80) of the Shu'aiba 2nd-order composite sequence, coeval to the K80 of Sharland et al. (2001). This MFU is also recorded within the rudist buildup barrier as a thin unit of *Palorbitolina* wackestone facies.

Facies Anatomy of HFS 6 (S6)

Sequence 6 has well established rudist barrier banks around the field and records the shallowest water facies of the Shu'aiba Formation associated with subaerial exposure surface (Figure 23). Rudist buildups are mainly dominated by the high-energy, recumbent *Offneria* rudists (Figure 7F), that formed more continuous *in situ* rudist barriers. Therefore, the rudist facies predominate across the entire platform, either as a rim of barrier banks, or back-bank, or fore-bank fragmented rudist rudstone. The platform interior on the northern block is dominated by high-energy grainstone as well as by a new established local rudist buildups in the central part of the platform (Well 11 and 44). The platform interior in the southern block also is dominated by moderately deep back-bank rudist facies, except where deep restricted ponds in the central part of the platform interior (Wells 22, 12 and 3). The northeastern flanks is dominated by fine skeletal wackestone/mudstone deposited in slope and open marine settings as in previous sequences, but subtle shallowing occurs in this stage to more detrital skeletal packstone. The rudist buildups in this sequence are capped by thin, well-rounded, well-cemented rudist rudstone facies of high-energy beach environments (Figure 7D), followed by an exposure surface, marking the termination of rudist buildups in the southern block and the end of the 3rd-order sequence 2.

Facies anatomy of HFS 7 (S7)

Sequence 7 is dominated by extensive shallow lagoonal/inner ramp environments with fine skeletal peloidal milliolid packstone/wackestone facies on both north and south

blocks (Figure 24). However, the northern block still developed rudist barrier banks on the eastern side, backed by shallow lagoonal sediments. These rudist buildups have similar trends to previous rudist buildups, but are slightly shifted basinward representing slight progradation of the platform margin settings. These rudists are possibly discontinues separated by tidal channels. The intraplatform depression still contains fragmented rudist skeletal grainstone, therefore a rudist buildups likely formed around the trough to source this grainstone facies. The southern block is entirely dominated by the shallow lagoonal sediments excepts where *Agriopleura* rudist floatstone that developed local mounds.

Facies anatomy of HFS 8 (S8)

Sequence 8 only occurs on the northern block, while the southern block was subaerially exposed (Figure 25). The northern block is dominated by shallow lagoonal facies that prograded basinward. The intraplatform channel was buried by the shallow lagoonal facies. Rudist buildups did not form during this sequence.

Facies Anatomy of HFS's 9 and 10 (S9 and S10)

Sequences 9 and 10 are Upper Aptian sequences formed only on the northern lock platform edges as a prograding sequences into the basin during a long-term sea level fall (Figure 26). Facies anatomy of these sequences include shallow water rudist/stromatoporoid/coral marginal facies formed marginal setting on the eastern and around the far northern part of the field. An upper Aptian wedge along the western flank

(Well 45) consists solely of shallow lagoon facies, with no rudist or shallow marginal facies occurred in this wedge. The shallow water marginal facies on the eastern flank passes laterally into slope and deep open marine facies. Moreover, these Upper Aptian sequences begin with a flooding even of an argillaceous mudstone at their base interpreted as low-stand wedges. This argillaceous mudstone is interpreted as a continuous N-S elongate wedge that may act as a reservoir barrier to fluid flow movement. The interpretation of this mudstone as a low-stand wedge may imply a separation in the reservoir units, however, pressure data is required to substantiate this interpretation.

Global Correlation

The Lower Cretaceous Barremian and Aptian successions of the subsurface Biyadh and Shu'aiba Formations record major subaerial sequence boundaries and dramatic facies changes associated with growth and demise of carbonate platforms that can be linked to global changes in sea-level, ocean chemistry, and Milankovitch orbital forcing. To evaluate this relationship, the stratigraphic framework of the Biyadh and Shu'aiba Formations presented in this paper were calibrated to biostratigraphy and stable isotope chemostratigraphy and correlated to: (1) the global sea-level curve of Haq and Schutter (2005); (2) the sequence stratigraphic records from European sections (Hardenbol et al., 1998); (3) the high-resolution sea-level changes recorded in Pacific guyots (Rohl and Ogg, 1998); (4) the high-resolution orbital model sea-level (Al-Hussaini and Matthews, 2010) and (5) the global carbon isotope curve of the Tethyan

pelagic records (Follmi et al., 2006) (Figure 27). This correlation suggests that the 3rd-order sequences of the Biyadh and Shu'aiba Formations formed in response to global sea-level changes and to rapid Earth's climate changes. Also, most HFS's can be correlated globally, but are less pronounced than the 3rd-order sequences. The high-resolution orbital forcing model of Al-Husseini and Matthews, (2010) is controlled by the 405 k.y eccentricity cycles (called stratons), driven mainly by glacio-eustasy. Some of these stratons are correlated directly to some HFS's in this study, especially the HFS's in the Biyadh and the lower part of the Shu'aiba Formations. The following is a brief discussion of each sequence with their correlated sea-level and chemostratigraphic curves and the significant and implications of their global correlations.

3rd-order Barremian Sequence (Biyadh Formation)

The 3rd-order composite sequence of the Biyadh Formation is composed of four HFS's (S1-S4) and is coeval to Ap Bar2 of van Buchem et al. (2010). The correlation suggests that S1 and S2, which are the TST of this sequence, are correlated with Bar 5 in Hardenbol et al. (1998) and formed during one sea-level rise and fall of Haq and Schutter, (2005) and correlates to stratons 326-314 of the orbital sea-level model (Al-Husseini and Mathews, 2010). The extreme spike of the orbital model at straton 315, represents the maximum sea-level rise and is correlated with the MFS of the Biyadh 3rd-order composite sequence corresponding to the deepest water facies in Biyadh

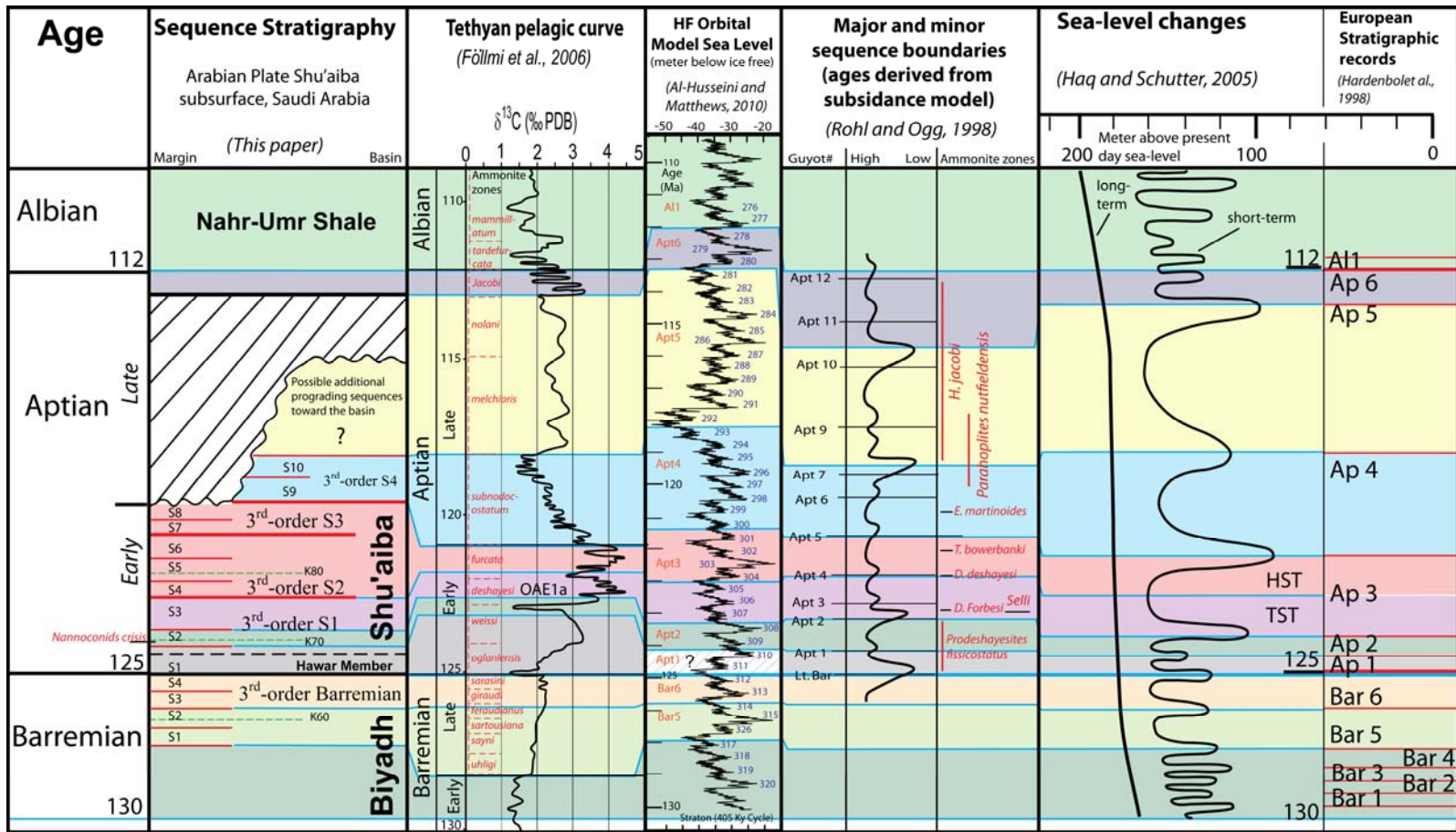


Figure 27. Composite global correlation between the Arabian Plate Biyadh and Shu'aiba formations and the global stratigraphic records. The colors used for each sequence were arbitrary to highlight the sequence.

Formation, which is the chalky mudstone facies at the middle of Biyadh S2. This MFS is well correlated with the 3rd-order regional MFS (K60) of Sharland et al., (2001) and van Buchem et al. (2010). The coeval Tethys carbon isotope curve of this sequence shows subtle change with an overall minor gradual increase from 1.5 ‰ at the base of S1 to 2.2‰ at the top of S2 (Figure 27).

The HST of the 3rd-order Biyadh sequence is composed of two HFS's (S3 and S4) and they are correlated to the global Bar 6 of Hardenbol et al. (1998), and formed during one global sea-level rise and fall of Haq and Schutter (2005). S3 and S4 are well correlated with stratons 313 and 312 of Al-Husseini and Mathews (2010), suggesting that each of these HFS's is an ~ 400 k.y cycle. This correlation suggests that the Biyadh 3rd-order composite sequence can be separated into two smaller scale 3rd-orders sequences, each on the order of ~ 1 to 1.5 m.y duration, where the mud dominated- TST sequences S1 and S2 of the Biyadh Formation comprise one sequence coeval to Bar 5, and the grain-dominated- HST sequences S3 and S4 comprise another sequence coeval subtle change with an overall minor gradual increase from 1.5 ‰ at the base of S1 to 2.2‰ at the top of S2 (Figure 27).

The HST of the 3rd-order Biyadh sequence is composed of two HFS's (S3 and S4) and they are correlated to the global Bar 6 of Hardenbol et al. (1998), and formed during one global sea-level rise and fall of Haq and Schutter (2005). S3 and S4 are well correlated with stratons 313 and 312 of Al-Husseini and Mathews (2010), suggesting that each of these HFS's is an ~ 400 k.y cycle. This correlation suggests that the Biyadh 3rd-order composite sequence can be separated into two smaller scale 3rd-orders

sequences, each on the order of ~ 1 to 1.5 m.y duration, where the mud dominated- TST sequences S1 and S2 of the Biyadh Formation comprise one sequence coeval to Bar 5, and the grain-dominated- HST sequences S3 and S4 comprise another sequence coeval to Bar 6. S3 and S4 contains many small-scale parasequences (13 parasequences for each sequence). Since S3 and S4 are ~ 400 k.y in duration; each parasequence appears to be fifth-order cycles spanning ~ 40 k.y duration and may be related to obliquity orbital forces.

3rd-order Early Aptian Shu'aiba Sequence 1

The Early Aptian 3rd-order sequence 1 is composed of three sequences (S1, S2 and S3) and occurred in the lower part of the Shu'aiba Formation and includes the Hawar unit. This sequence is coeval to the Ap Apt1 and 2 of van Buchem et al. (2010). SB1 is a major sequence boundary that separates the Barremian Biyadh Formation from the Aptian Hawar unit and Shu'aiba Formations and it is linked to the Barremian-Aptian boundary (~125 My) and correlates with the global sequence boundary at the base of Apt 1 in Hardenbol et al. (1998) and Rohl and Ogg (1998). This boundary represents a major high magnitude sea-level fall possibly on the order of tens of meters that can be traced worldwide (Hillgartner et al., 2002; Droste, 2010; Al-Husseini and Matthews, 2010). This boundary is associated with a negative carbon isotope excursion that also is correlated worldwide and is used in this correlation as a datum for the global correlation in figure 27. This boundary also reflects major rapid change in global climate from cooling and sea-level fall during the Late Barremian to global warming and sea-level rise

during the overlain Early Aptian (Jenkyns, 2003; Weissert and Erba, 2004). The major negative carbon isotope excursion in the earliest Early Aptian is related to dissociation of methane hydrates, possibly triggered by an increase in volcanism on the Ontong-Java Plateau (dated ~ 125-119 Ma) with large amount of CO₂ released to the atmosphere causing a greenhouse warm climate and coincident warming of bottom waters on continental shelves that resulted in global warming and sea-level rise in the earliest Early Aptian (Larson and Erba 1999; Weissert and Erba, 2004; Follmi et al., 1994, 2006; Jahren et al., 2001; Jenkens 2003). The Barremian-Aptian boundary in the Shu'aiba Formation is overlain by S1 with the deposition of the argillaceous Hawar unit. S1 is correlated with Apt1 in Hardenbol et al. (1998) and Apt1 in Rohl and Ogg (1998), associated with global sea-level rise in the earliest Aptian (Figure 14). The Early Aptian stratons 311 and 310 are correlated with Apt1 and thus seem to be correlated with the Hawar unit in the Shu'aiba Formation. However, Al-Husseini and Matthews, (2010) correlated these stratons with lowstand wedge sequences only present in the Oman Ocean margin that onlap onto the SB1 sequence boundary (Droste, 2010). Stratons 311 and 310 were interpreted to be coeval to the subaerial exposure of SB1 and thus the Hawar unit is correlated to stratons 309 and 308. This correlation may work as a regional interpretation within the Arabian Plate sequence stratigraphic framework, but when stratons 309 and 308 are correlated globally to Apt1 of Hardenbol et al., (1998), there will be a problem with correlating the rest of the sequences with the sea-level curve and global isotope signature. For instance, if stratons 309 and 308 are linked to the Hawar unit and correlated with the global Apt 2 instead of Apt1, that will make stratons 304-

301 equivalent to Ap3 of Hardenbol et al. (1998), and correlative to the global OAE1a event as interpreted by Al-Husseini and Matthews, (2010). That correlation suggests that the rudist dominated (3rd-order sequence 2) in this study, or the equivalent AP Apt 3 of van Buchem et al. (2010) correlates with the OAE1a (Selli unit) in the standard isotope curve of Follmi et al. (2006). The OAE1a should correlate to the *Lithocodium* dominated interval of the Shu'aiba Formation which is S3 (within the 3rd-order sequence 1) in this study or Ap Apt 2 of van Buchem et al. (2010). The carbon isotope records of Shu'aiba Formation integrated with biostratigraphy (Figure 14) strongly suggest that the Hawar unit is correlated with the first negative excursion above the Barremian-Aptian boundary and hence is correlated to Apt 1 and the sea-level rise above the boundary.

S2 of the Shu'aiba Formation records a major deepening event associated with the deposition of chalky *Hedbergella* mudstone, which is the deepest water facies of the Shu'aiba platform. This flooding event is coeval to K70 of Davis et al. (2001) and it correlates to the onset of the major positive enrichment of carbon isotope values, just beneath OAE1a. MFS K70 is possibly correlated to the highest sea-level rise of straton 308 of Al-Husseini and Matthews, 2010 and to the sea-level rise of Ap 2 of Hardenbol et al. (1998). S2 here with its deeper facies and K70 likely correlates with the Early Aptian nannoconid crisis defined from the Tethyan pelagic sediments. The nannoconid crisis was caused by a reduction in calcification, due to the high atmospheric CO₂ just before the OAE 1a, and is associated with a global warming event and sea-level rise (Luciani et al., 2006).

The Shu'aiba S3 is dominated by an extensive *Lithocodium aggregatum* wackestone and is correlated to the maximum carbon isotope enrichment and to the OAE 1a. S3 possibly correlates to stratons 307-305 and to the TST of the Ap3 of Hardenbol et al. (1998). This correlation differs from the correlation of Al-Husseini and Matthews (2010) that correlate stratons 304-301 to the OAE1a and to the Ap Apt3 of van Buchem et al., (2010). This latter correlation contradicts the biostratigraphic zonation, therefore, the correlation provided here is suggested as an update for correlating the Arabian Plate stratigraphic records to the global records.

3rd-order Early Aptian Shu'aiba Sequence 2

This 3rd-order sequence is a rudist bearing unit composed of three sequences (S4,S5 and S6) that formed in the middle part of the Shu'aiba Formation and it is coeval to the Ap Apt3 of van Buchem et al. (2010). This sequence correlates with the upper part (HST) of Ap 3 of Harndenbol et al. (1998), deposited during the HST of the global sea-level curve of Haq and Schutter (2005). It also correlates to the Apt 4 sequence in the Pacific Guyot of Rohl and Ogg, (1998). This sequence possibly correlates with stratons 304–301 where the maximum sea-level rise occurred within straton 303 coeval to the proposed MFS of the Shu'aiba composite sequence presented here, and corresponding to the regional K80 of Sharland et al. (2001). This MFS occurs within S5 and is well recorded in all wells of the study area. The carbon isotope curve of the Tethys pelagic record of Follmi et al. (2006) correlated to this unit shows enrichment values at the *furcata* ammonite zone corresponding to the maximum sea-level rise. This enrichment of

carbon isotope values should not be confused with the lower major enrichment that correlates to the *deshayesi* ammonite unit related to the global OAE1a. The carbon isotope values of the Shu'aiba platform record within this sequence range from 4.5 to 5 ‰ with more uniform values corresponding to the development of the extensive rudist buildups (Figure 14). Al-Husseini and Mathews (2010), however, correlated stratons 304–301 to Apt 3 of Hardenbol et al. (1998) and to Ap Apt3 of van Buchem et al. (2010), but correlated these stratons to the lower major carbon isotope enrichment of the *deshayesi* ammonite unit associated with the OAE1a. However, this interpretation contradicts with the stratigraphic framework, facies and chemostratigraphy presented here, because both the 3rd-order sequence 2 in this paper and the Ap Apt3 of van Buchem et al. (2010) are rudist-dominated sequences that developed above the OAE1a. The 3rd-order sequence 2 represents a recovery of carbonate productivity after the demise of carbonate buildups in the lower Hawar unit, the nannoconid crisis and the *Lithocodium aggregatum* interval that acts as a substitute to the rudist buildups during the carbon perturbation intervals and OAE1a in the Early Aptian (Immenhauser et al., 2005).

3rd-order Early Aptian Shu'aiba Sequence 3

This 3rd-order sequence consists of S7 and S8 and it is part of the HST of the Shu'aiba composite sequence. This sequence appears to be a regional, rather than a global individual sequence, but when combined with 3rd-order S2, it correlates with the late HST of the global Ap3 of Hardenbol et al. (1998). In the marginal setting, the top of

this sequence records a prominent sea-level fall that correlate with the global sea-level fall at the top of Ap3.

3rd-order Late Aptian Shu'aiba Sequence 4

Late Aptian Shu'aiba sequence 4 formed only on the platform edge as a progradational wedge composed of S9 and S10, representing a forced regression system and is coeval to the Ap Apt4 of van Buchem et al. (2010). It also correlates with Ap4 of Hardenbol et al. (1998) and with Apt5 in Rohl and Ogg (1998). The orbital model shows eight stratons (300-293) correlate to this sequence, suggesting that more progradational sequences may occur basinward in the study area, similar to the nine prograding sequences interpreted from seismic data in nearby fields (Pierson et al., 2010; Yose et al., 2010). The stratigraphic record from the Pacific Guyots shows a maximum of two or three sequences correlated to the eight prograding sequences in the Arabian Plate. This suggests that these prograding sequences might be correlated regionally rather than globally, reflecting more local relative sea-level changes. The carbon isotope curve shows gradual upward depletion in this sequence indicated a cooling interval may have followed the major positive enrichment associated with the OAE 1a.

The global sequence Ap5 of Hardenbol et al. (1998) correlates to Apt9, Apt10 in the Pacific Guyots and to stratons 292-281. This sequence does not form in the Shu'aiba study interval here but may occur in the far eastern part of the Shu'aiba platform as small scale prograding wedges. The orbital cycles in Ap5 suggest a substantial glacio-eustatic lowstand on the order of ~30 m sea-level drop (AL-Husseini and Matthews,

2010). This sea-level drop culminates to the top of Ap5 of Hardenbol et al. (1998) where the largest sea-level drop of the Aptian stage occurred (Haq and Schutter, 2005). The Pacific guyot also records a major sea-level drop just above Apt10 that correlates to the global sea-level curve. The Late Aptian unconformity at the top of the Shu'aiba Formation formed during this major sea-level drop, producing a major subaerial unconformity and karst features. The base of the Nahr-Umr Formation represents the latest Aptian transgression (Al-Husseini and Mathews, 2010) and correlates to Apt 6 of Hardenbol et al. (1998), Apt 12 of the Pacific guyots and the global sea-level curve of Haq and Schutter (2005). Nahr-Umr shale formed above the top Shu'aiba unconformity and record a widespread sea-level rise, possibly representing the meltdown of the Late Aptian glaciations (Al-Husseini and Mathews, 2010); and corresponding to an abrupt positive enrichment in the carbon isotope curve just beneath the Aptian/Albian boundary.

Implication and Significance of Global Correlations

The global correlation presented above suggests that the Biyadh and Shu'aiba Formations records a strong influence of the 3rd-order global sea-level changes associated with changes in carbon isotope signature, ocean chemistry and global climate on the development of Biyadh and Shu'aiba platforms. This correlation suggests major differences in the sea-level magnitude are associated with changes in stratigraphic accumulation between the Barremian and the Aptian stages (Figure 27). The Barremian stage has lower amplitude sea-level fluctuations with relatively thinner sequences

compare to the Aptian stage that has higher amplitude sea-level fluctuations associated with thicker sequences and more pronounced condensed sections. Also, the Barremian stage is dominated by a small-scale parasequences (decimeter scale), whereas the Aptian stage is dominated by larger-scale parasequences (meter scale), except the Hawar unit. The Barremian parasequences of the Biyadh Formation have an average duration of 30-40 ky, whereas the Aptian parasequences have an average duration of 100 ky. This suggests that the glacio-eustatic control of the eccentricity orbital cycles were not the main driving mechanism for both the Barremian and Aptian stages. The parasequences of the Barremian Biyadh Formation possibly reflect obliquity cycles, whereas the parasequences of the Aptian Shu'aiba Formation may reflect small-scale eccentricity. Therefore, the Barremian stage may have recorded a warmer global climate, compared to the Aptian that records cooling and warming intervals with possible glaciations recorded during the base (SB1), middle (SB7) and upper part of the Aptian. Thus, the Aptian stage is not a uniform greenhouse period. Instead, it is more transitional time interrupted by glacial events as suggested by stratigraphic records, sea-level fluctuations and isotope data.

Implication and Significance for Reservoir Geology

High-resolution chronostratigraphic frameworks provide the best tool for distributing the petrophysical properties in the interwell space within a 3-D reservoir model (Lucia, 2007). Sequence stratigraphy including high-resolution cyclicity and facies distribution presented in this study will be integrated in future studies with

wireline logs, petrophysical and engineering data to define flow units and barriers within the reservoir. This detailed stratigraphic framework will have a significant impact on the simulation model, thus enhancing production and development plan.

The Biyadh Formation with its homoclinal low angle ramp platform can be easily integrated to wireline logs and petrophysical data in uncored wells to construct a 3-D geological model in the entire field, due to its sheet-like sequences and uniform facies distribution. The initial TST of the Biyadh Formation, which is the argillaceous mudstone "dense unit" at the base of the Biyadh Formation acts as a barrier between Biyadh reservoir and the underlying Bwiyab Formation. The following TST (S2) of the Biyadh Formation is dominated by an extensive mud-dominated facies with low reservoir quality. The HST (S3 and S4) within the Biyadh Formation is dominated by higher energy rudist peloidal grainstone/packstone facies, that are still sheet-like units and can be correlated with wireline logs in uncored wells. The high-frequency cycles within the HST are bounded by hardgrounds or tight exposure surfaces that well correlated for long distances. These surfaces are thin but they are tight and well-cemented, thus may affect vertical fluid flow. Therefore, accurate mapping of these small scale cycles is important to characterize this unit.

The Hawar unit is very tight and dense unit and it acts as a major seal separating the Biyadh reservoir from Shu'aiba reservoir. The lower part of the Shu'aiba Formation is dominated by muddy low reservoir quality facies. However, dissolution of platy corals may develop good reservoir zones with intragranular porosity (Figure 6F). The rudist buildups facies is dominated by porous high-energy facies, however, the top of the rudist

buildups (SB 7) is marked by subaerial surface along with cemented rudists facies. The stratigraphic correlation suggests that this surface is well correlated field wide, thus forming a baffle or barrier zone for vertical fluid flow. This zone is also accompanied by distinct high gamma ray signal that allow for correlation in uncored wells.

The interpretation of the prograding sequences on the shelf edge with clinoform geometries is very significant in determining reservoir continuity and reservoir layering scheme. Previous geological models used to connect layers across the platform edges as a layer-cake geometry, which means connecting two different chronostratigraphic units that are genetically different. The framework presented here more accurately defines the Upper Aptian wedges as prograding sequences that are onlapping onto the top unconformity and are not connecting to the previous Lower Aptian sequences. Moreover, the lower part of the prograding sequences is dominated by a lowstand argillaceous dense mudstone unit that probably acts as reservoir barriers, with possible different oil-water contacts. However, more integrated research with pressure data is required to prove these results. In addition, the interpretation of the Upper Aptian prograding sequences suggests that more prograding sequences may form basinward with the possibility of new reservoir exploration targets off structures controlled by stratigraphic traps. However, seismic data is needed to evaluate the spatial distribution and the extent of the prograding sequences.

Conclusions

A detailed high-resolution rock-based stratigraphic framework of the Lower Cretaceous (Barremian and Aptian) Biyadh and Shu'aiba Formations provides an updated stratigraphic and depositional framework for these units. This framework are developed from 55 cored wells, biostratigraphy and 26 carbon isotope curves, covering the entire Shu'aiba platform in one the most prolific giant carbonate reservoirs in the Middle East. The Late Barremian Biyadh Formation is composed of one 3rd-order composite sequence (~3 My), comprised of four high-frequency sequences (S1-S4). S1 and S2 are the TST of the Barremian composite sequence and K60 is the composite MFS, occurring within S2. These sequences are composed predominantly of relatively deep subtidal mud-dominated *Palorbitolina* chalky wackestone/mudstone facies. S3 and S4 are the HST of the Barremian composite sequence and are composed of high-energy shallow water subtidal with Caprotinid rudist and peloidal grainstone facies. This sequence is capped by a regional subaerial boundary (SB1) recording a global sea level fall.

The entire Shu'aiba Formation formed a 2nd-order composite sequence (~ 7 My duration) composed of four 3rd-order sequences (~1-2 My) and ten HFS's (S1-S10; each ~ 405 Ky - 1 My duration). S1 records the initial TST with the deposition of Hawar unit, followed by S2 that records the deepest water facies and the regional MFS (K70). S3 is the late TST of the Shu'aiba composite sequence and is characterized by the deposition of extensive *Lithocodium aggregatum*/coral facies associated with the onset of differentiated platform-to-basin settings with slight clinof orm and backstepping

geometries. The 3rd-order sequence 2, consisting of S4-S6, records the onset of a well established platform-margin setting containing rudist buildup facies that changed toward the platform interior into lagoonal facies and transitioned basinward into fore-bank, slope and basinal settings with pronounced clinoform geometries. This sequence has a transgressive lag at its base dominated by *Glossomyophorus* rudists that deepen upward to the regional composite MFS (K80). This is followed by the higher energy bank-crest of *in situ* caprinid rudist rudstone facies that is capped by well-rounded rudist fragments deposited in beach environments followed by the development of exposure surface (SB 7). S7 and S8 are dominated by shallow lagoonal peloidal milliolid packstone facies associated with local *Agriopleura* floatstone, representing the HST of the Shu'aiba composite sequence.

The newly identified Upper Aptian sequences S9 and S10 are recorded on the northern-block within prograding platform edge and slope settings that formed during a major forced regression. These sequences were identified on the basis of chemostratigraphic analysis calibrated with biostratigraphy. These sequences form a lowstand wedge of argillaceous wackestone facies that may act as a possible reservoir baffle zone, changing upward to high energy marginal facies of mixed rudist and stromatoporoid/coral facies. Regional correlation suggests that more prograding sequences likely formed basinward.

High-resolution maps of facies distribution were generated to define the depositional anatomy and reservoir facies distribution. These maps are crucial when integrated with petrophysical parameters to determine the 3-D reservoir model, and help

predict the uncertainty between the wells, thus enhancing the 3-D reservoir characterization. The Shu'aiba platform is divided into northern and southern blocks, each with their own distinctive facies distribution and depositional anatomies. The northern block records higher energy facies with grainstone shoals/channels developed in the platform interior, whereas the southern block has thicker *Lithocodium aggregatum* algal platform facies with relatively lower energy environments. The southern block has deeper lagoonal environments within the platform interior.

A refined global correlation between the Arabian Plate and global stratigraphic records and global sea-level curves was generated on the basis of this study. This correlation strongly suggests a direct influence of the 3rd-order sea-level fluctuations in the Biyadh and Shu'aiba Formations. The Shu'aiba Formation records the perturbations of global carbon cycles associated with the nannoconids crisis and OAE1a. The global nannoconids crisis appears to be correlated with the deep chalky mudstone facies associated with the MFS in S2, that is coeval to the regional MFU (K70). The OAE1a with its distinctive carbon isotope values is coeval to the *Lithocodium aggregatum* facies of S3 and correlated to the TST of global sequence AP3. This correlation also suggests that Aptian HFS's were mainly controlled by glacio-eustatic sea-level changes and the long term eccentricity cycles (~ 405 Ky) were the main driving mechanism. The Barremian sequences record low magnitude sea-level changes with relatively thinner sequences compared to the Aptian. Moreover, the Barremian parasequences likely reflect obliquity (~ 40 Ky), whereas the Aptian parasequences are likely controlled by small scale eccentricity (~ 100 Ky) cycles. The Shu'aiba Formation records major

subaerial hiatus reflecting glacial intervals, interrupted by major flooding units reflecting global warming intervals. These changes in the stratigraphic records and sea-level magnitude between the Barremian and Aptian suggest a prevailed greenhouse period during the Barremian, changed rapidly into a transitional climate period in the Aptian interrupted by glacial events.

CHAPTER III

**INTEGRATED HIGH-RESOLUTION CHEMOSTRATIGRAPHY AND FACIES-
BASED STRATIGRAPHIC ARCHITECTURE OF THE EARLY CRETACEOUS
(APTIAN), SHU'AIBA FORMATION, SAUDI ARABIA**

Overview

High-resolution carbon isotope signatures were integrated with core descriptions and gamma ray logs and used as a correlation tool for better age control to refine the sequence stratigraphic framework of the Shu'aiba Formation in Saudi Arabia. The carbon isotope variations of the shallow carbonate Shu'aiba Formation correlate well with the Tethyan pelagic record and indicate an original marine C¹³ signature for the Early Cretaceous (Aptian) Shu'aiba Formation. Carbon isotope values of the Shu'aiba Formation ranges from 1.5 to 6‰ with minimal or no diagenetic effects. Oxygen isotope values range from -2.7 to -6.7‰, but were reset during diagenesis, and cannot be applied for chemostratigraphic analysis. The Shu'aiba strontium isotope records ranges from 0.707356 to 0.707454 and differ slightly from the standard Aptian record due to diagenesis.

The Shu'aiba Formation platform is a large scale composite sequence (~7 My) composed of seven early Aptian high-frequency sequences and two additional late Aptian prograding sequences. Carbon isotope data were calibrated with core descriptions and gamma ray logs to construct two detail high-resolution stratigraphic cross sections.

Carbon isotope data help refine the internal stratigraphic architecture of the Shu'aiba Formation especially on the slope and open marine settings across the Lower/Upper Aptian boundary. The carbon isotope values of the Hawar "dense" unit in the base of Shu'aiba Formation record major depletion corresponding to the global dissociation of methane hydrates, followed by major positive excursion associated with the deposition of *Lithocodium/Bacinella* facies coeval with the global Oceanic Anoxic Event 1a (OAE 1a). The rudist buildups on the platform commence with a value of approximately 4.5‰ in most wells and generally have a uniform carbon isotope trend, followed by gradual depletion to the top of Shu'aiba Formation. Although there are some variations in carbon isotope values associated with the lateral facies change from lagoon, margin, slope, open marine and basinal settings, carbon isotope trends are still similar and can be correlated field-wide. There is little evidence of meteoric diagenesis associated with the depletion of carbon isotope values. However, oxygen isotope records were possibly affected by meteoric diagenesis associated with subaerial exposure surfaces, but did not get affected by the late Aptian unconformity, despite the massive karstification observed in cores. The good correlation between the original carbon isotope fluctuations and the 3rd-order sequence framework of the Shu'aiba Formation fits well with the established carbon isotope curves that have been used as a proxy for global sea-level changes during the Early Cretaceous. This study also shows that small scale parasequences (5th order or higher) can be calibrated with carbon isotope curves, but they most likely represent relative sea-level changes with local effects rather than global signatures. Applications of high-resolution carbon isotope stratigraphy for the Shu'aiba Formation significantly

constrain the stratigraphic framework, and will lead to better geological and simulation models for reservoir characterization and development.

Introduction

Carbon and oxygen isotope data have been used to trace the chemical compositions of the oceans through geologic history. The $\delta^{13}\text{C}$ values are used to examine changes in the ratio of organic relative to inorganic carbon reservoirs in the crust. The $\delta^{18}\text{O}$ values results from climate changes associated with glacial versus non-glacial periods, temperature of water and diagenesis (Weissert and Lini, 1991; Jenkyns, 1995; Weissert et al., 1998; Stoll and Schrag, 2000 and Erbacher et al., 2002). Carbon isotope compositions of carbonate rocks can, therefore, be tied to biostratigraphy and chronostratigraphy, and used as a relative geochronologic tool for the geologic record. Carbon isotope data also can be used as a proxy for sea-level changes where transgressive systems tract and sea-level rise are associated with positive shifts of the global $\delta^{13}\text{C}$, and high stand systems tract and sea-level fall are associated with negative shifts of the global $\delta^{13}\text{C}$ (Föllmi et al., 1994, 2006; Weissert et al., 1998). Several studies on the isotope stratigraphy of shallow carbonate platforms, however, suggest that positive and negative shifts of carbon and oxygen isotopes may not necessarily be related to the global carbon and oxygen isotope compositions of the oceans, but may reflect local diagenetic processes rather than global changes (Immenhauser et al., 2003; Xiong and Heckel, 1996; Patterson and Walter, 1994).

The Lower Cretaceous (Aptian) Shu'aiba Formation in Saudi Arabia (Figures 28 and 29) is a giant carbonate reservoir that was deposited in a shallow carbonate platform bordering an intrashelf basin (Aktas and Hughes, 1998; Hughes 2000; Al-Ghamdi and Read, 2010). The Shu'aiba Formation (Figure 30) is also one of the main oil producers in the United Arab Emirates (U.A.E) and Oman (Alsharhan and Nairn, 1986). A high-resolution sequence stratigraphic framework was established to characterize the reservoir by providing the building blocks for reservoir modeling and simulation (Al-Ghamdi and Read, 2010). Without an accurate age control, however, the correlation of shelf margin to basin successions is difficult due to the lack of subaerial exposure surfaces and flooding surfaces in the open marine and deep water facies. Moreover, the limited resolution of biostratigraphic data makes it hard to accurately constrain the age model especially on the flanks of the platform where upper Aptian prograding sequences may exist (Al-Ghamdi and Read, 2010).

The Early Cretaceous (Aptian) provides one of the best records of carbon variations in the geological record (Weissert and Lini, 1991; Weissert et al., 1998; Föllmi et al., 1994; 2006; Vahrenkamp, 1996; 2010). The carbon isotope variations of the Early Cretaceous (Aptian) Shu'aiba Formation in the Arabian platform record high-resolution carbon fluctuations of the southern Neo-Tethys Ocean, that due to the lack of diagenetic overprint and high sedimentation rate, can be correlated globally with the standard Tethys signature (Vahrenkamp, 1996 and 2010; Immenhauser et al., 2004). Vahrenkamp (1996 & 2010) used bulk carbon isotope data to correlate the Lower Cretaceous successions of the southern Tethys Ocean in the Arabian platform with the

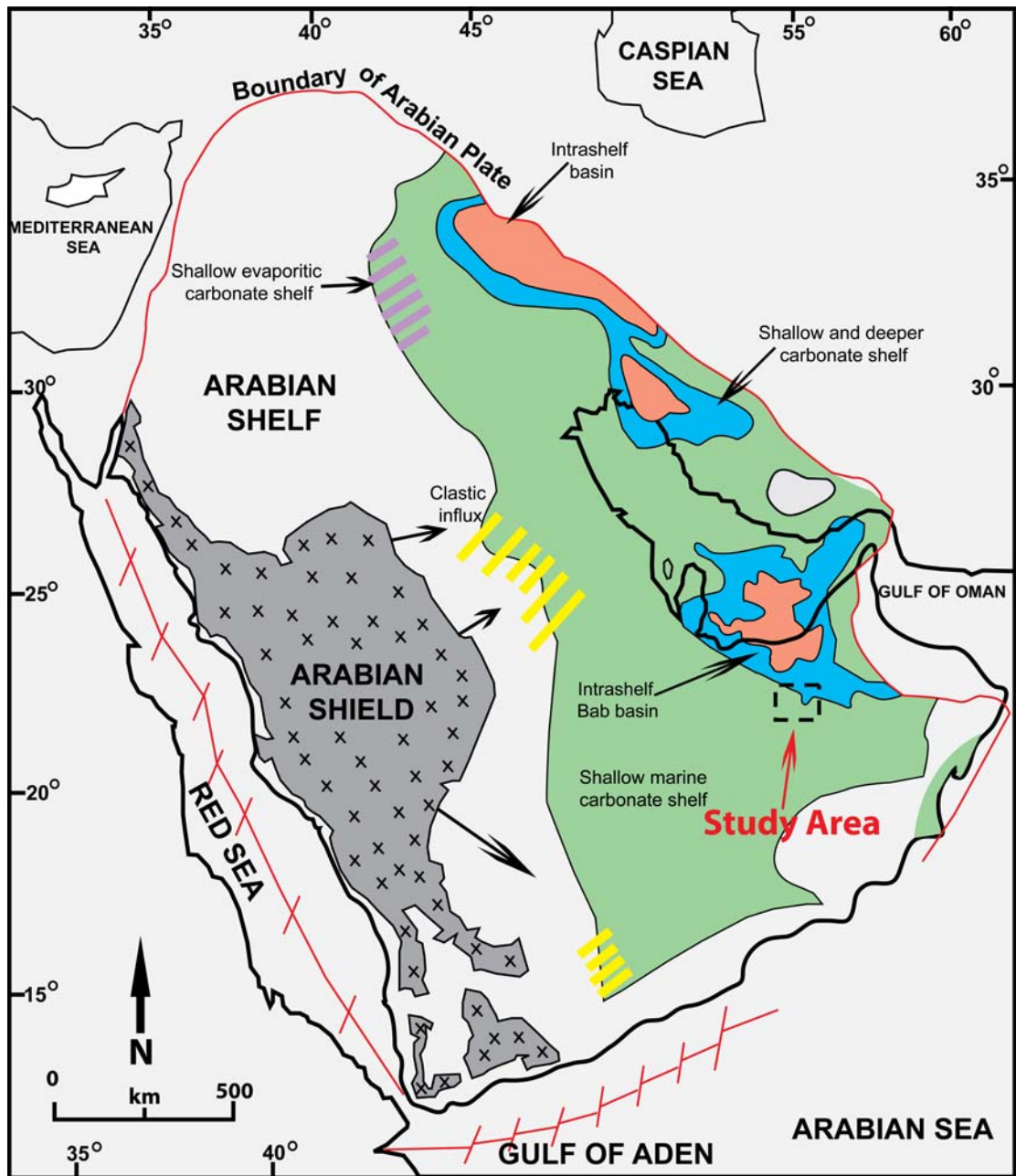


Figure 28. Aptian paleogeographic map for the Arabian Plate showing the location of study area and the intrashelf basins. Modern plate boundaries are shown with red lines.

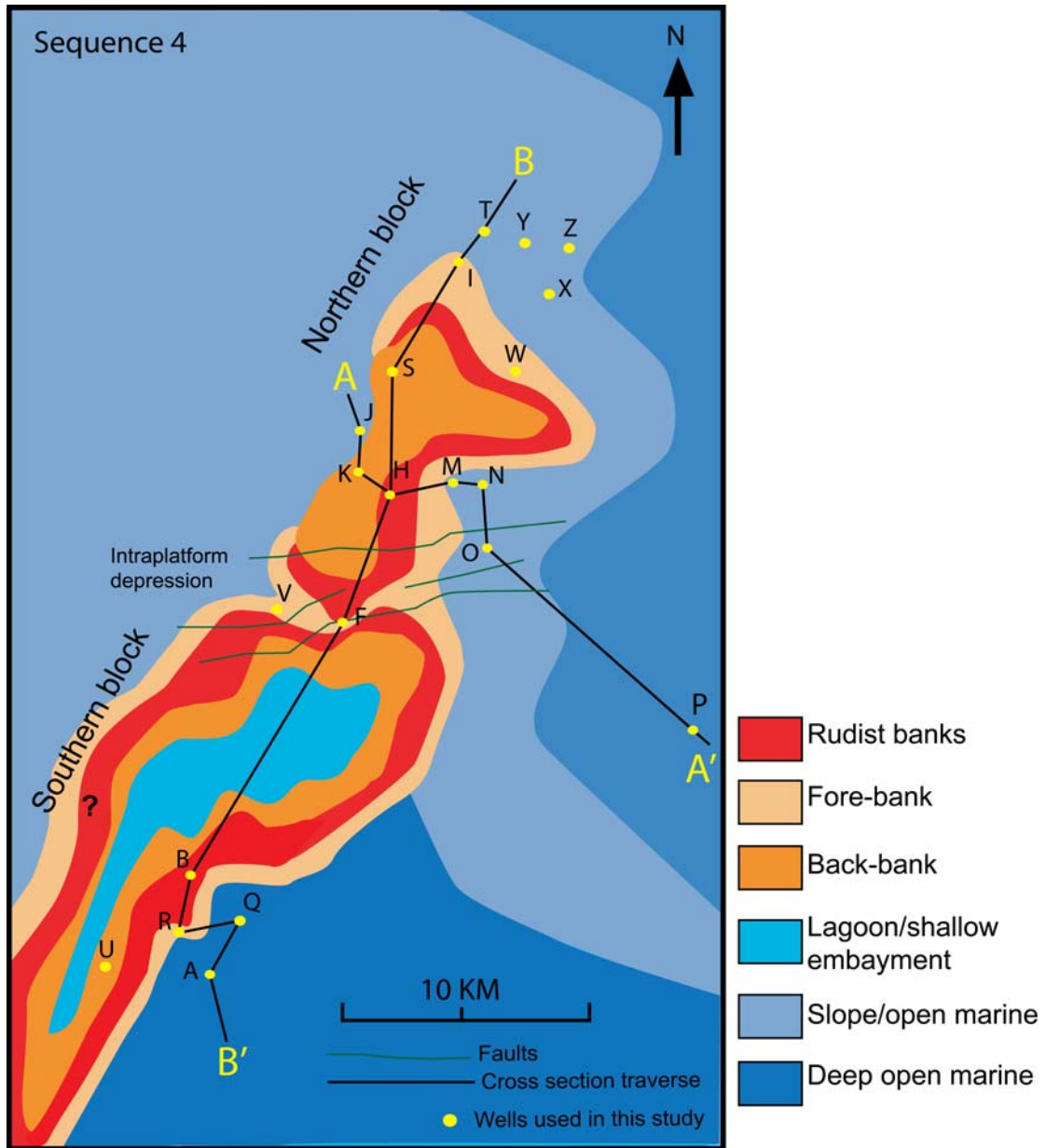


Figure 29. Base map of Shu'aiba platform showing two cross-section lines (A-A', B-B') and wells used in this study.

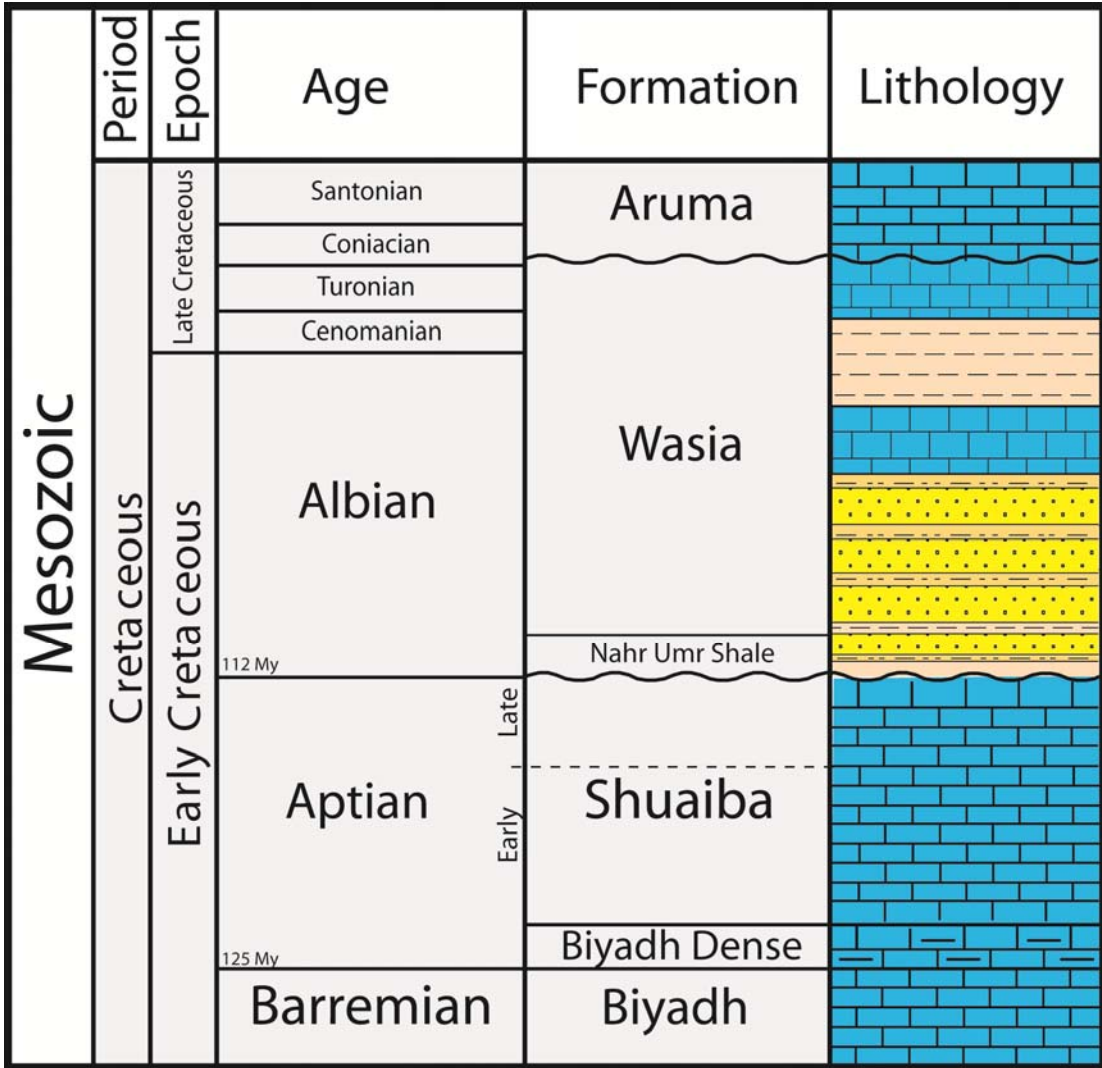


Figure 30. Stratigraphic column of the Early Cretaceous strata in Saudi Arabia.

pelagic northern Tethys records. He concluded that the similarity between the pelagic Tethyan isotope records and the Shu'aiba Formation isotope indicates global marine carbon isotope fluctuations affected both carbonate sediments at the same time resolution. The bulk carbon isotope data from the Shu'aiba Formation in the U.A.E and Oman was interpreted to represent an original ocean signature with only minor or no diagenetic effects (Vahrenkamp 1996, 2010). However, the relationship between the depositional settings and high-resolution parasequences with carbon isotope values was not investigated.

The objective of this study is to integrate high-resolution carbon isotope data with the core-based sequence stratigraphic framework for better age control of the Shu'aiba Formation and to refine the stratigraphic correlation especially on the platform edge and open marine setting. High-resolution carbon isotope data is also linked to the small scale cycles (5th-order parasequences) to test the hypothesis of using the carbon isotope curves as a proxy of sea-level changes. This paper will also discuss the relationship between the complex facies architecture of the Shu'aiba Formation and the carbon isotope values and will investigate the possible influence of variable depositional environments. The northern Tethys pelagic carbon isotope record of the Early Cretaceous (Föllmi et al., 2006) will be used in this study as the standard curve for correlation with the shallow carbonate Shu'aiba Formation.

Methodology

Core materials from 21 wells with an average thickness of 137 m (450 ft) each, housed in Saudi Aramco core lab in Dhahran, Saudi Arabia, were described using a binocular microscope to identify texture, fabric, grain size and fossil assemblages. Thin sections were also analyzed to identify microfacies to help define the environment of deposition. Facies, depositional environments and sequence stratigraphy were interpreted for each well. The interpreted core descriptions were depth shifted and tied to gamma ray logs. Sequence boundaries, maximum flooding surfaces and parasequences were then picked for each well. Carbon and oxygen isotope sample (1 per meter) were collected as whole-rock samples from the muddy matrix avoiding cements and skeletal shells or fragments.. Higher-resolution sampling (< 0.5m spacing) for better isotope resolution was performed at critical stratigraphic markers. A total of 2,397 samples were collected from 21 wells (Figure 29) representing all facies, sequences and depositional environments of the Shu'aiba Formation. The selection of these wells was based on the core quality and the representation of different environmental settings. These data were analyzed for carbon and oxygen isotopes at the isotope lab in the University of Ottawa, Canada. Isotope data of wells F and I are from previous Saudi Aramco internal studies (Lindsay and Swart, 2002; Cantrell et al., 1999). Strontium isotope data were analyzed from thirty two samples of whole-rock micrite matrix from well-M on the platform wedge to delineate the age of the Shu'aiba Formation, and especially to define the position of the Lower/Upper Aptian boundary. The use of micrite mud for strontium isotopes analysis was mainly due to the lack of continuous bivalve-or rudist-bearing

zones in the platform edge where Upper Aptian sequences may occur. Carbon isotope curves were plotted against depth with the datum being the high gamma ray marker at the base of Shu'aiba Formation. Each curve was tied to core descriptions and gamma ray logs, so that carbon isotope samples correspond to their stratigraphic markers. This is a critical step in order to link the stratigraphic boundaries to the carbon isotope values to evaluate the relationship between sea-level changes and the carbon isotope compositions.

Geological Setting

During the Aptian time, the shallow carbonate platform of the Arabian shelf was part of the large Arabian Plate that developed a passive margin facing the Neo-Tethys Ocean (Figure 28). The Arabian Plate was located several degrees south of the equator and as it separated from Africa, it moved toward the Neo-Tethys Ocean forming passive margins on its northern, northeastern, and southeastern margins (Sharland et al., 2001). Three intrashelf basins were developed during this time as a result of Neoproterozoic-Early Cambrian Hormuz salt movements. These intrashelf basins were separated from the Neo-Tethys Ocean by a carbonate barrier system (Sharland et al., 2001). The rudist buildups of the Shu'aiba Formation formed on the edge of the Bab intra-shelf basin and their positions were controlled by subtle reactivation of deep-seated fault systems (Hughes 2000; Al-Ghamdi and Read, 2010).

The Shu'aiba Formation is a prolific oil reservoir that extends regionally across the entire Arabian shelf. It is a large scale composite sequence with a total duration of

about 7 My covering the interval from earliest early Aptian at the base to the late Aptian on the platform edge (van Buchem et al., 2010). On the platform, a regional unconformity was developed limiting the duration to about 5 My. The Shu'aiba Formation was sealed by the Nahr Umr Shale which represents the lowermost part of the Albian Wasia Formation (Figure 30).

The Shu'aiba platform is a NE-trending, doubly plunging anticline and is divided into northern and southern blocks by an EW-trending fault zone that formed an intraplatform depression between the two blocks (Figure 29). This intraplatform depression was created by syn-depositional faulting that appears to have played a major role in the development of the Shu'aiba Formation stratigraphic geometry and facies architecture (Al-Ghamdi and Read, 2010).

Stratigraphic Framework

The Shu'aiba Formation (Figure 31) was divided into seven high-frequency sequences that are correlated throughout the field (Al-Ghamdi and Read, 2010). Figure 31 summarizes the evolution of these sequences along with their major depositional facies. Sequences 1 and 2 are sheet-like units that were deposited on a carbonate ramp and are equivalent to the Lower Aptian sequences 1 and 2 (AP Apt 1 and 2) in van Buchum et al., (2010). Sequences 3 to 7 record the onset of rudist buildups with the development of the intrashelf basin on the eastern side of the field. Sequences 3 to 7 on the platform are equivalent to the third-order Lower Aptian sequence 3 (AP Apt 3) in van Buchum et al., (2010). In this study, two additional sequences 8 and 9 were

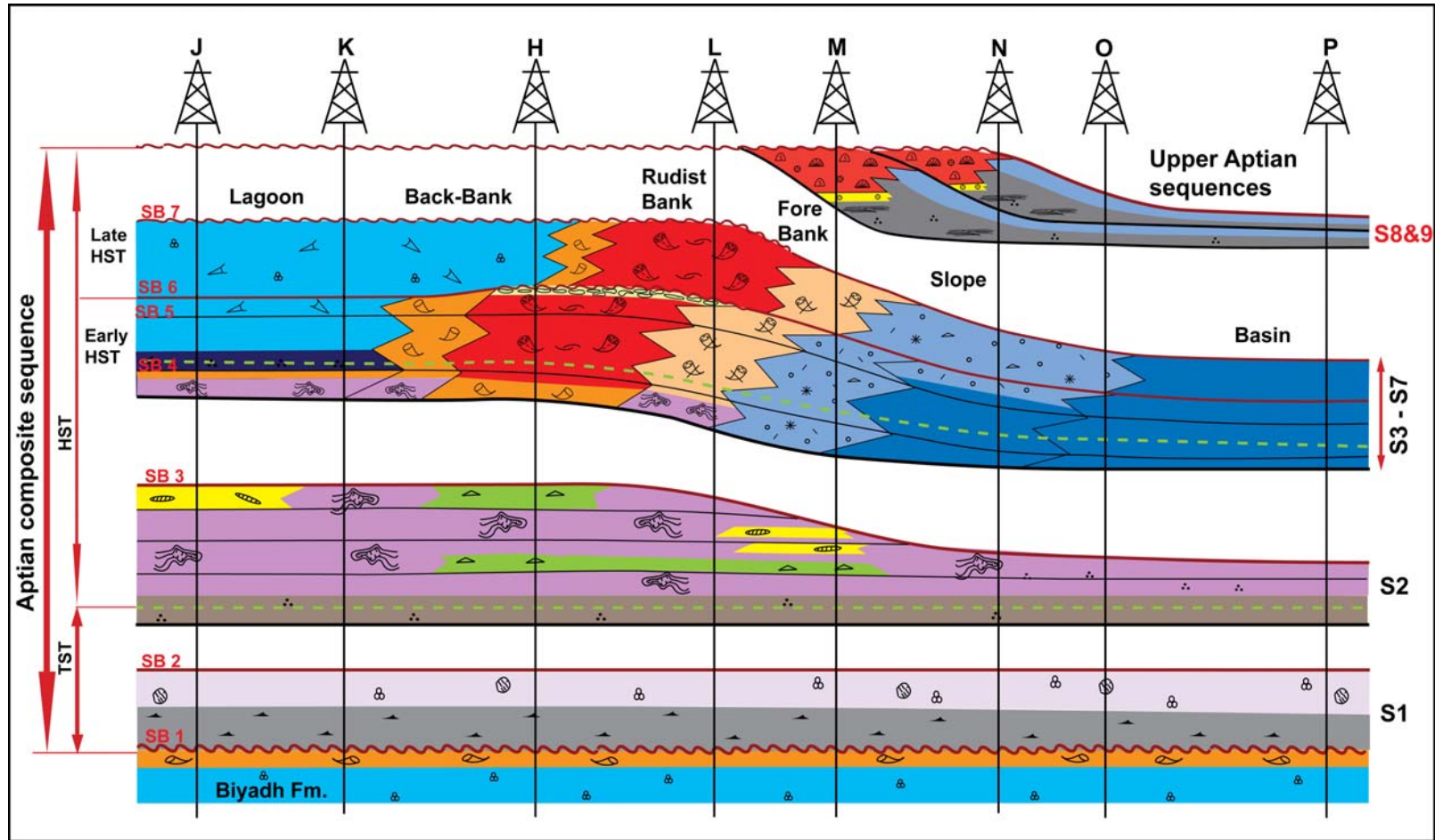


Figure 31. Two-dimensional depositional model showing the evolution of the Shu'aiba platform associated with major facies associations. Shu'aiba platform is a composite sequence with 7 sequences in lower Aptian and 2 sequences in upper Aptian.

identified on the flanks of the platforms based on isotope curves and the associated facies changes (Figure 31) and are equivalent to the Upper Aptian sequences 4a and 4b (AP Apt 4a and AP Apt 4b) in van Buchum et al., (2010), Yose et al. (2010) and Vahrenkamp, (2010). The Shu'aiba Formation platform evolved from a shallow carbonate algal platform in the earliest Aptian with the initial Transgressive Systems Tract (TST) as sequence 1 (S1) and the deposition of the dense argillaceous *Palorbitolina* packstone of Biyadh “dense” unit (equivalent to Hawar unit in the U.A.E and Oman). This was followed by deposition of oncoidal *Lithocodium/Bacinella* packstone of basal Shu'aiba Formation that represents the High Stand Systems Tract (HST) of S1. Sequence 2 started with a major flooding and deposition of deep chalky planktonic mudstone (*Hedbergella* zone) representing the regional maximum flooding unit (MFU) of the lower Aptian Shu'aiba succession (Al-Ghamdi and Read, 2010). This maximum flooding unit is equivalent to the updated K70 maximum flooding surface (MFS) of Davis et al., (2002). A thick and extensive *Lithocodium aggregatum* facies associated with platy corals and *Palorbitolina* wackestone developed above the MFU and represents the HST of sequence 2. At this time, a subtle clinof orm of the *Lithocodium* facies developed along the margin of the platform (Figure 31). Sequence 3 records the onset of rudist buildups and the formation of intrashelf basin on the eastern side of the field. Tectonic activity along a fault zone created a raised area upon which the rudists established a rimmed carbonated platform (Aktas and Hughes, 1998; Al-Ghamdi and Read, 2010). On the platform, sequences 3 to 6 are composed of skeletal rudist bank facies that are separated by back-bank and lagoonal settings on the western side from

fore-bank, slope and open marine settings on the eastern side with major clinoforms prograding toward the basin. The platform interiors are characterized by peloidal orbitolinid packstone facies and local rudist mounds. The rudist buildups formed shallowing upward sequences that are capped either by well-rounded rudist rudstone deposited in a beach environment or a local exposure surface at the top of sequence 6. Sequence 7 records a slight progradation of the rudist buildups with fine peloidal-miliolids packstone facies on the back-bank and detrital rudist packstone on the fore-bank and slope. Sequences 8 and 9 are the Upper Aptian new defined sequences that only been detected on the flanks of the northern block. These represent a time when the Shu'aiba margin was subaerially exposed and karsted during development of a regional unconformity and a global sea-level fall at the end of the Aptian. Sequences 8 and 9 represent major basinward progradation corresponding to a 3rd-order sea-level fall (Haq and Al-Qahtani, 2005). These two prograding sequences have distinctive facies characteristics that are slightly different than the Lower Aptian sequences. They start with a dense argillaceous mudstone and shallow up to a reefal facies of stromatoporoid, massive coral heads and rudists. Rudists in the upper Aptian sequences are composed mainly of the *Horiopleura* rudists that extended from early to late Aptian (Skeleton, 2008 Saudi Aramco written report). It is possible that more prograding sequences exist further east toward the intrashelf basin similar to the prograding sequences described from seismic data (Yose et al., 2006; 2010). The Bab intrashelf basin facies is present at Well-P and displays a truncation and onlapping geometry against the Shu'aiba Formation shelf margin. It is the last stage infill of mixed siliciclastic and carbonate sediment

representing the Lowstand Systems Tract (LST) of an additional sequence in the latest Aptian.

Chemostratigraphy

General Results

A type log from Well-M with its stable isotope data and strontium isotope data were plotted and calibrated against the core description and gamma ray logs (Figure 32). This well was selected as a type log, because of its good core condition and its penetration of the Lower and Upper Aptian sequences. The carbon isotope values in this well show strong variation associated with sequence boundaries picked from cores. The Oxygen isotope curve shows poor correlation with sequence boundaries and more uniform pattern with values around -4‰. However, at some stratigraphic markers, such as the contact between the Hawar unit and basal Shu'aiba Formation, $\delta^{18}\text{O}$ values shows abrupt depletion from -4‰ to -4.9‰ that gradually enriched and reach -4‰ at SB3 (Figure 32). The lack of systematic correlation between $\delta^{13}\text{C}$ and $\delta^{18}\text{O}$ is commonly used as evidence for original carbon isotope composition with little or no diagenetic alterations (Glumac and Walker, 1998). All carbon and oxygen isotope data were plotted on one diagram with samples color coded for different facies (Figure 33). The carbon isotope values of Shu'aiba Formation range from 1.5 to 6.1‰. However, these values are higher than the standard pelagic record of northern Tethys that range from 1.5 to 4‰ (Föllmi et al., 1994). Oxygen isotopes range from -2.7 to -6.7‰ and are likely to be less significant than carbon isotopes in chemostratigraphic analysis. This is due to the greater

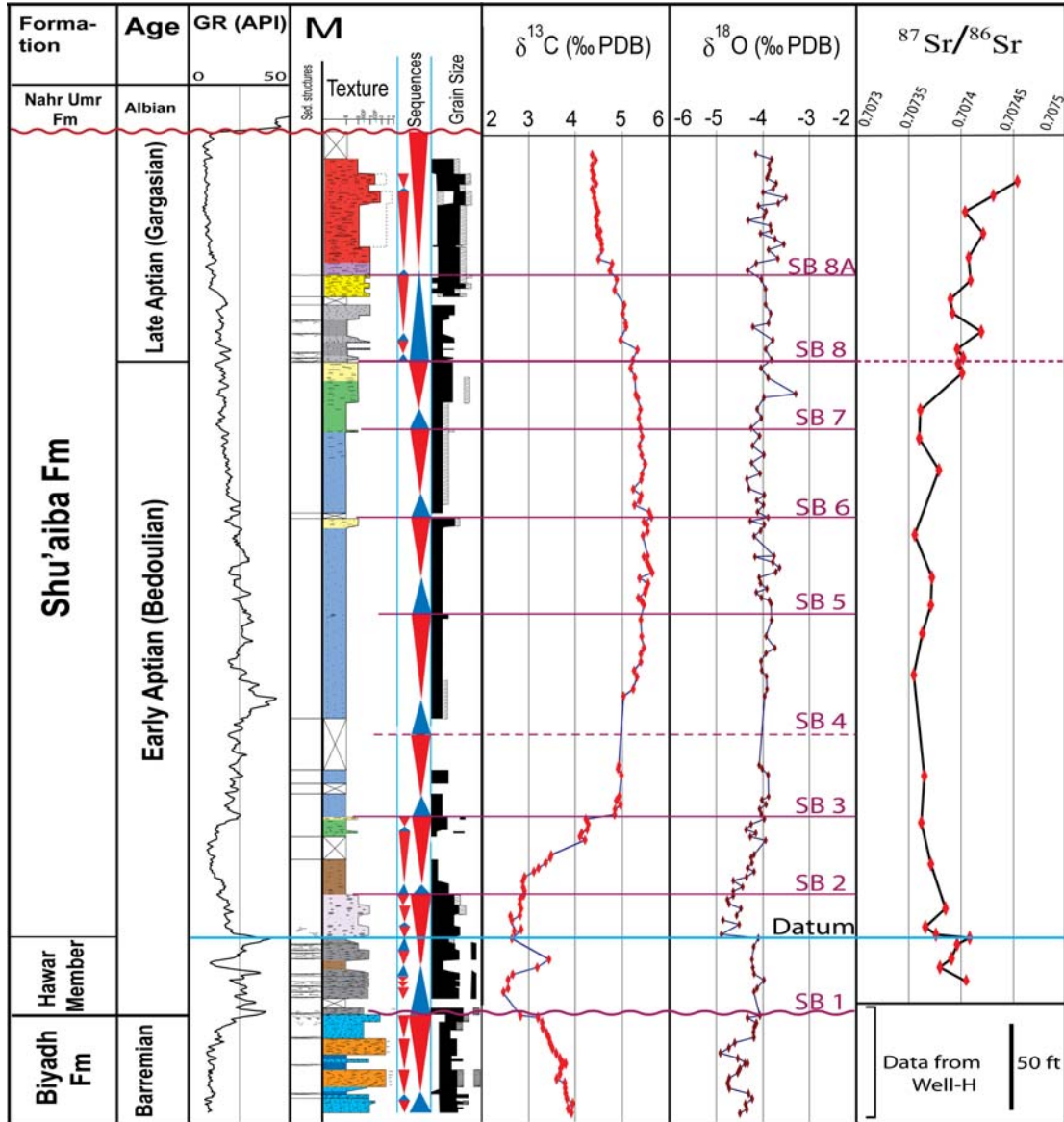


Figure 32. Type well (M) showing composite isotope data calibrated with core descriptions and gamma ray logs. Aptian sequences are shown in red. Whole-rock Strontium isotope data is plotted against core description and showing pronounced changes at the base of Shu'aiba and at the Lower/Upper Aptian boundary.

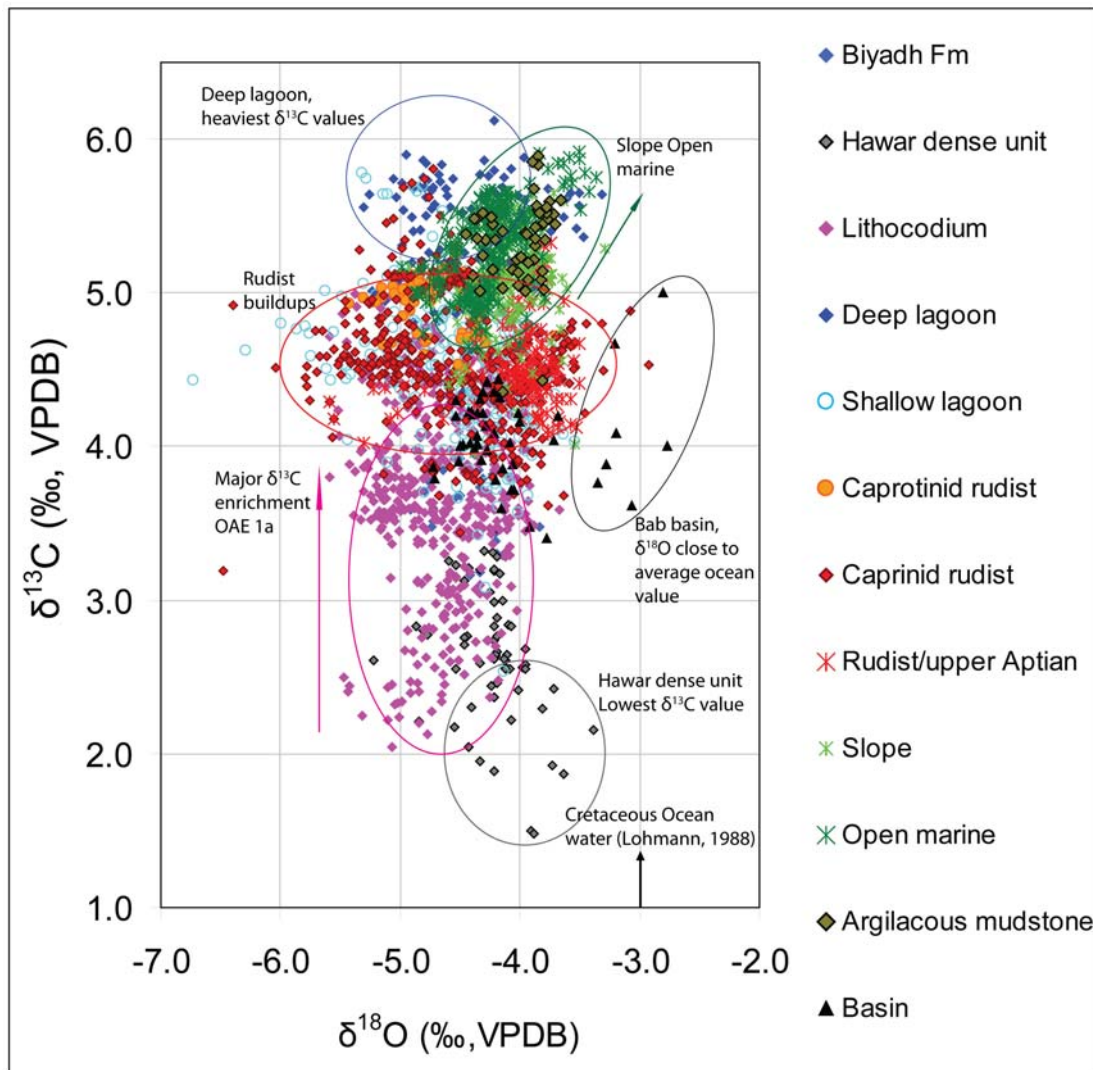


Figure 33. Carbon versus oxygen isotope plots from all 21 wells. The different colors and symbols represent different facies defined from cores and thin section analysis. General interpretations and trends are indicated by circles and arrows.

reservoir of oxygen in water (compared with carbon) that exchanges with the carbonate rocks and resets oxygen during diagenesis. The highest carbon isotope values are recorded in the deep lagoonal setting (Well-J) with a maximum value of 6.1‰ (Figure 33). Platform-margin rudist facies have relatively higher values compared to the standard Tethyan realm with average values ranging from 4.5 to 5‰. Carbon isotope values increase from platform interior to slope and open marine settings by about 1‰ (Figure 33). However, Well-P in the intrashelf basin has the lowest values ranging only from 1.5 to 4.5‰ and are very similar to the standard Tethyan curve.

Strontium isotope values of the Shu'aiba Formation are from the micrite matrix at Well-M on the eastern flank of the platform. The $^{87}\text{Sr}/^{86}\text{Sr}$ values range from 0.707356 in the middle part to 0.707454 in the upper most part (Figure 32). The $^{87}\text{Sr}/^{86}\text{Sr}$ of the Shu'aiba Formation begins at the Hawar unit with a value slightly over 0.70740 and then gradually declines to 0.70735 forming a trough associated with the lower Aptian sequences 4 - 7. $^{87}\text{Sr}/^{86}\text{Sr}$ values then abruptly rises to 0.70740 and rises to 0.70745 near the top of the section. These high values are associated with the upper/lower Aptian boundary that was picked from core description and carbon isotope data. The strontium isotope data from whole rock micrite samples do not provide an accurate age due to diagenetic effects during the recrystallization of micrite matrix (Denison et al., 2003). However, the general similarity in the pattern with slightly different values between the Shu'aiba records and Aptian records from deep sea drilling (Bralower et al., 1997), suggests that the Shu'aiba Formation record may still preserve some global ocean signature. A major decline of $^{87}\text{Sr}/^{86}\text{Sr}$ values (the trough) during the early Aptian was

mainly due to the increase in ocean-crust production and sea-floor spreading that accompanied the formation of submarine igneous province (Bralower et al., 1997; Denison et al., 2003; Jenkins, 2003).

Carbon Isotope Record

The Shu'aiba Formation carbon isotope curves of the platform-to-basin and their gamma ray logs were correlated with the pelagic Tethys curve (Figure 34). Two detailed core-based sequence stratigraphic cross sections integrated with carbon isotope curves show: a west-east dip section in the northern block that has a transition from platform interior, margin, slope and basin (Figures 28 and 35) and a north-south strike section across the intraplatform depression between the southern and northern blocks (Figures 28; 36A and 36B).

The late Barremian Biyadh Formation underneath the Shu'aiba Formation records a gradual decrease of carbon isotope values from 4.5 to 2.5‰ (Figure 34) associated with the major third-order sequence boundary (SB 1). The Biyadh "dense" unit (equivalent to the Hawar unit in the U.A.E and Oman) records a major decrease of carbon isotope values. The onset of major positive carbon excursion in the lower part of the Shu'aiba Formation is associated with the TST of sequence 2 with its chalky *Hedbergella* mudstone facies that shallow up to *Palorbitolina* and *Lithocodium* wackestone facies. This positive excursion associated with the *Lithocodium* aggregatum facies is coeval with the global Oceanic Anoxic Event OAE 1a in the early Aptian (Weissert and Lini, 1991; Föllmi et al., 1994; Weissert et al., 1998; Vahrenkamp, 2010).

Aggrading rudist bank facies with skeletal rudstone/grainstone have relatively uniform isotopic composition that ranges from 4.5 to 5‰. The upper part of the Shu'aiba Formation has a slightly negative isotope trend associated with a sea level fall during the HST. The lower/upper Aptian boundary was identified on the basis of isotopes and facies changes on the northeastern and northwestern sides of the field and was correlated with the Tethyan isotope curves (Figure 34). This boundary corresponds to the switchover from a negative to positive trend in carbon isotope values and a major shift in facies from slope derived fine skeletal packstone to relatively deeper high density dark colored argillaceous mudstone with high gamma ray values. The similarity in the carbon isotope pattern of the Shu'aiba Formation and the global Tethyan pelagic curve suggests that the Shu'aiba Formation records an original signature of the Early Cretaceous ocean composition (Vahrenkamp, 1996; 2010; Immenhauser et al., 2004). However, sedimentation rates are quite different between the shallow carbonate Shu'aiba Formation and the pelagic curve, especially at the platform margins where extensive rudist buildups developed during high sedimentation rate. This higher sedimentation rate resulted in poorly cycles buildups with almost uniform carbon trend within the marginal middle Shu'aiba Formation. This difference in sedimentation rates may explain the absence of some sequences with their carbon isotope variations between the shallow carbonate Shu'aiba Formation and deep pelagic Tethyan record. These variations must be taking into account when applying the chemostratigraphic analysis.

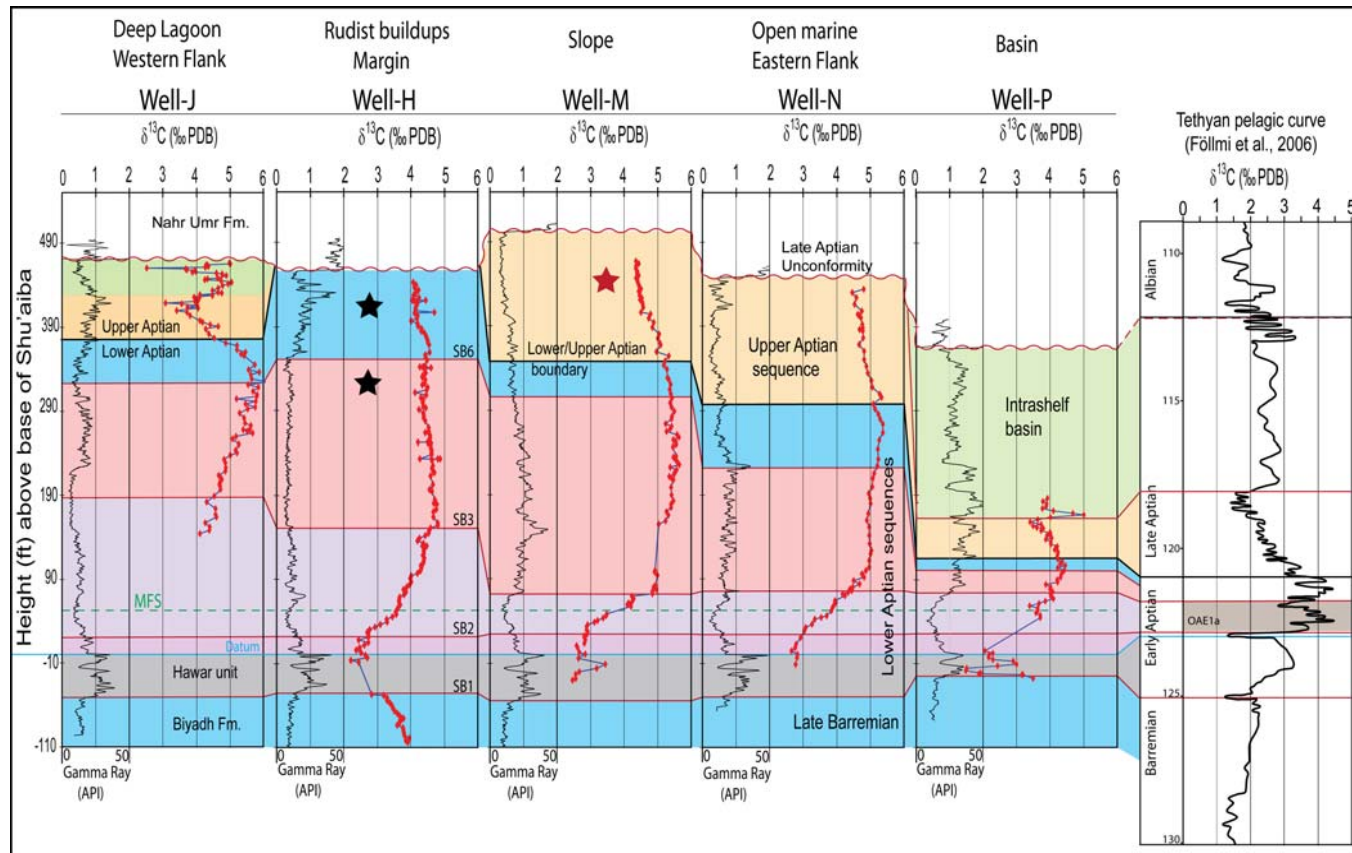


Figure 34. Type east-west chronostratigraphic cross section of the Shu'aiba Formation correlating gamma ray logs and $\delta^{13}\text{C}$ isotope curves for five wells versus the Tethyan pelagic curve of Föllmi et al. (2006). Major sequence boundaries are shown in red. The purple shaded zone is the *Lithocodium* algal platform facies that corresponds to major global positive excursion in the early Aptian that is related to Oceanic Anoxic Event 1a. Upper Aptian prograding sequences are shown in orange and green. Black stars in well-H indicate early Aptian rudist caprinid *Offneria* and caprotinid *Agriopleura*. Red star indicates late Aptian rudist *Horiopleura* of the Polyconitidae family, while black stars indicate early Aptian rudist Caprinid *Offneria* below SB6 and Caprotinid *Agriopleura* above SB6.

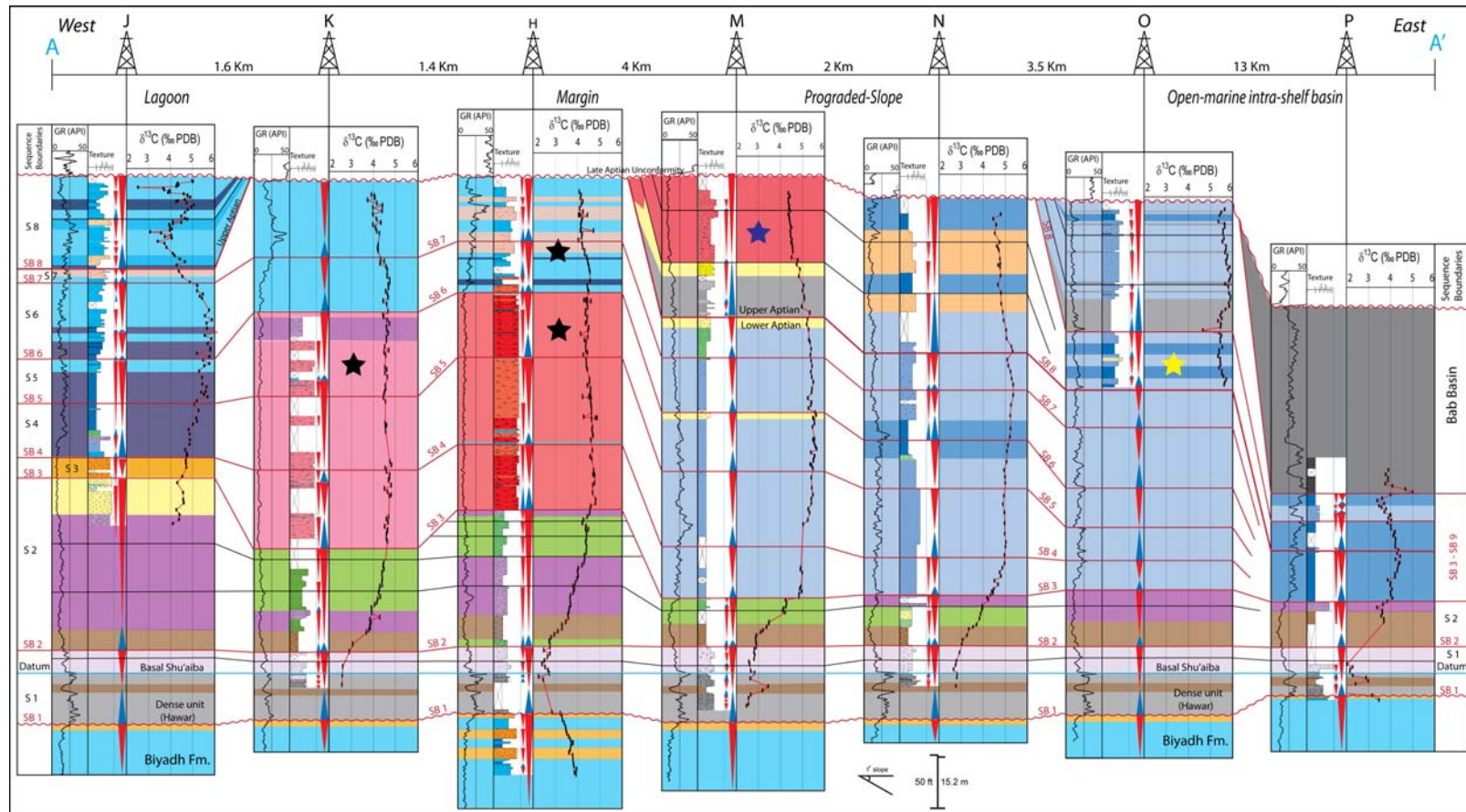


Figure 35. Integrated west-east cross section showing high-resolution stratigraphic framework, gamma ray logs and $\delta^{13}\text{C}$ isotope curves from platform to basin transition. The prograding Upper Aptian sequences occurred on the eastern platform edge clinoforming toward the basin. Yellow stars indicate the nannofossil data of late Aptian age in Well-O and late Aptian rudist in Well-M. Blue star indicates late Aptian rudist in Well M. Black stars indicate early Aptian rudists in Wells H and K.

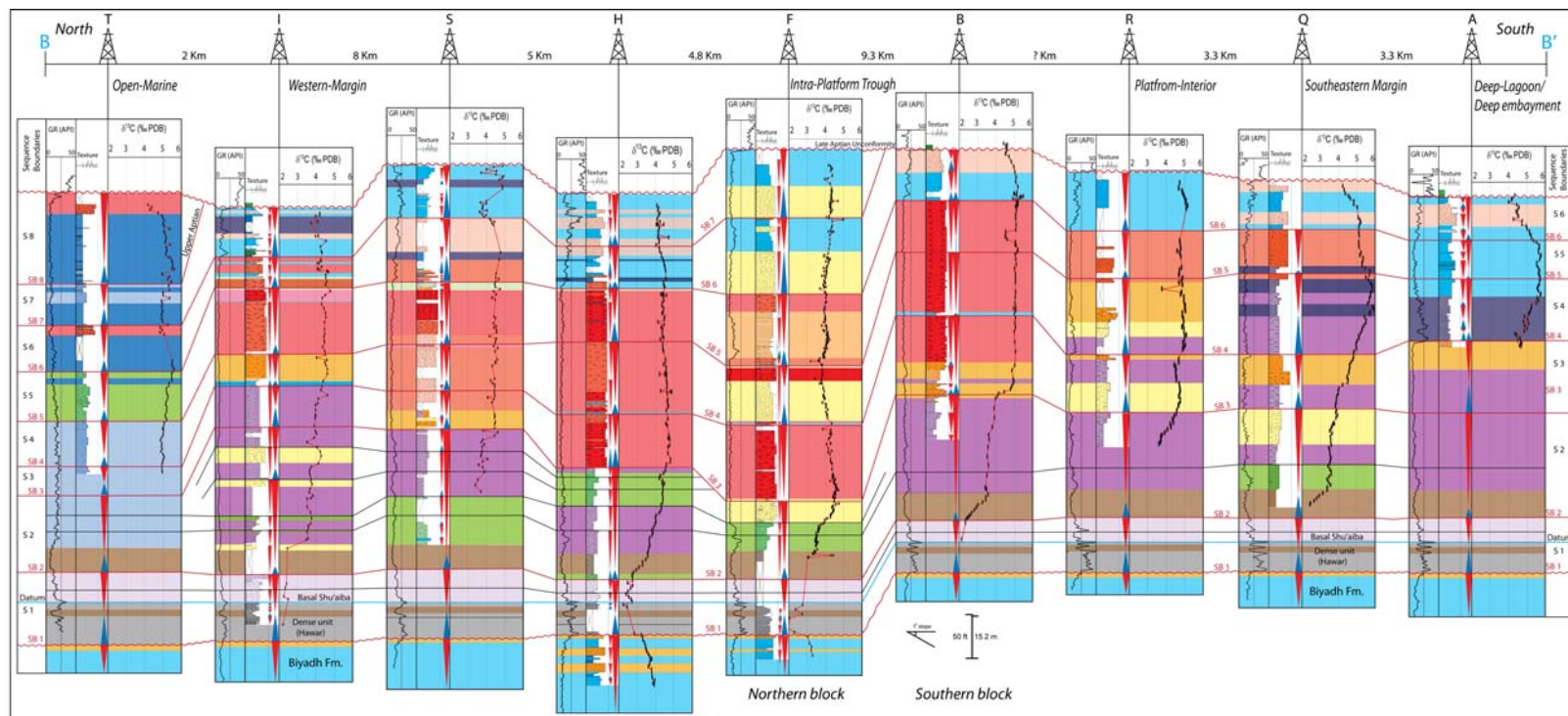


Figure 36A. Integrated north-south strike trend cross section. The intraplatform depression occurs in the middle of the section at Well-F. The northern and southern blocks are shown with the top Shu'aiba Formation being the datum between the two blocks. Upper Aptian sequences also occur on the northwestern side of the field at Well-T.

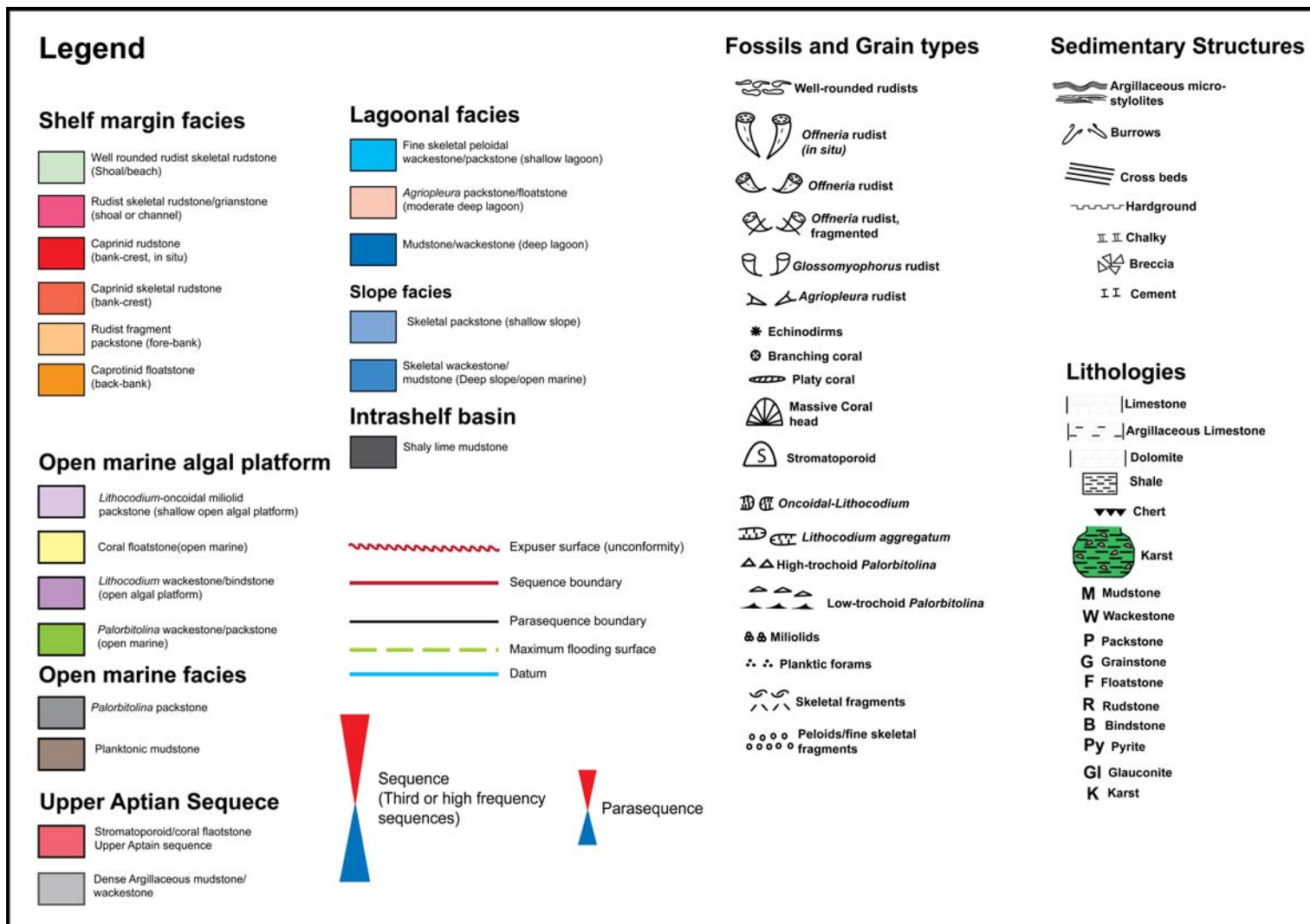


Figure 36B. Legend, symbols and color codes of lithofacies used in the above cross sections.

Oxygen Isotope Record

Although the Shu'aiba Formation oxygen isotope record has been reset during diagenesis, a general correlation between oxygen isotope and some sequence boundaries occurred, especially on the shelf margin settings (Figure 37). This is because the marginal setting is more susceptible to diagenesis than the slope and open marine settings, thus resulting a meteoric diagenesis effects on oxygen isotope record. The contact between the Biyadh Formation and the overlain Hawar unit at SB 1 coincide with a sharp increase in $\delta^{18}\text{O}$ values from -4.9‰ to -4.1‰ associated with SB 1 (Figure 37). The $\delta^{18}\text{O}$ of Hawar unit is relatively enriched with values reaching -4‰. The contact between the Hawar unit and the overlain basal Shu'aiba Formation is associated with a sharp $\delta^{18}\text{O}$ depletion of approximately 1‰. This depletion is also coincident with the onset of the OAE 1a and the deposition of the *Lithocodium/Bacinella* facies. The contact between the *Lithocodium/Bacinella* facies and the overlain rudist facies at SB3 is marked by the abrupt increase of $\delta^{18}\text{O}$ from \sim -4.2‰ to -3.45‰ associated with the onset of rudist buildups (e.g Well H) (Figure 37). The rudist buildups of sequences 3 – 6 have generally uniform trend, but with minor depletion of $\delta^{18}\text{O}$ and a value range from -4.5 to -5‰. At top of sequence 6, however a pronounced depletion of $\delta^{18}\text{O}$ (\sim 2‰) occurred, associated with the deposition of the shallowest rounded rudist rudstone of beach environment and local exposure surfaces that capped the rudist facies (yellow zone) (Figure 9). This depletion was possibly resulted from the influence of meteoric water associated with SB 6 marking the end of the rudist buildup facies. Carbon isotope values were not affected much at this surface, but still showing some minor depletion at this

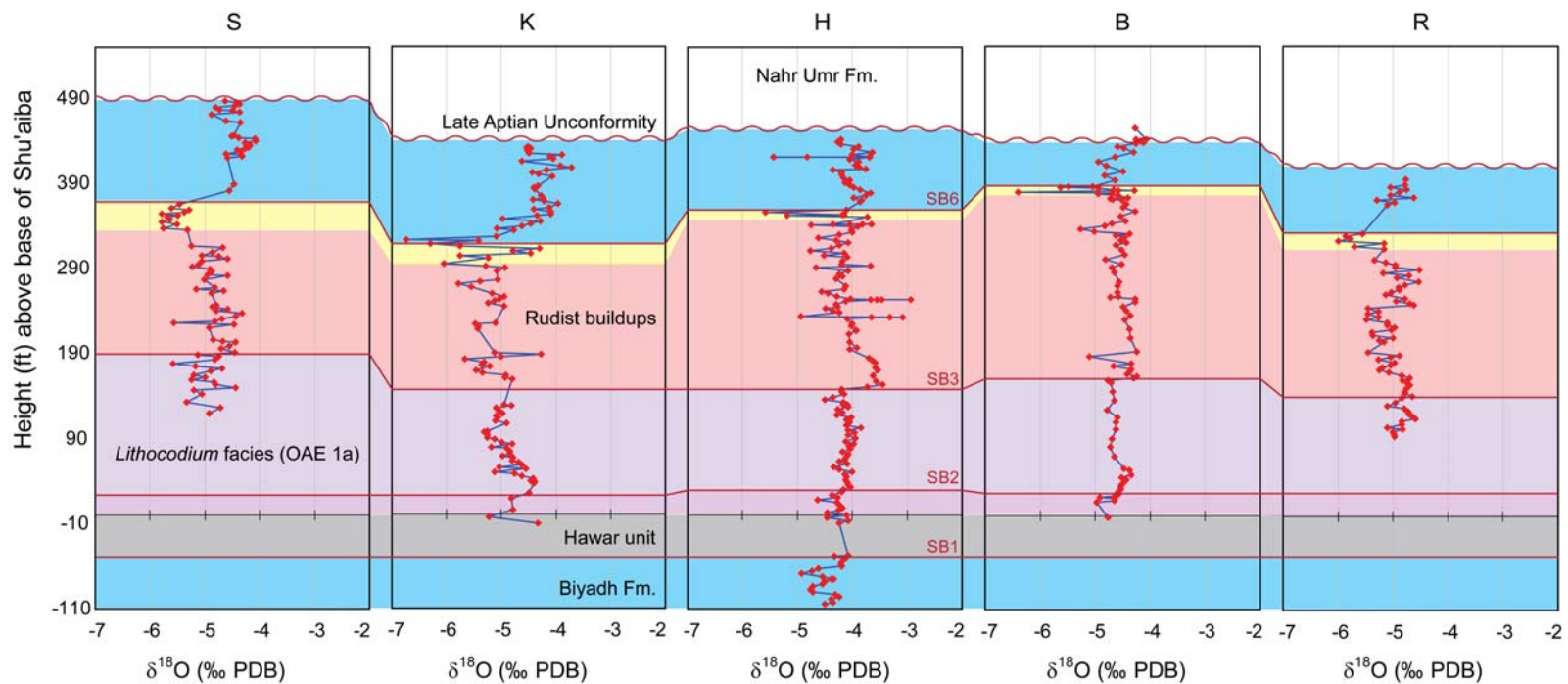


Figure 37. Correlation of oxygen isotope curves from several wells in the shelf-marginal setting showing major sequence boundaries. The yellow zone beneath SB6 shows the depletion in oxygen isotope curves due to the effects of meteoric diagenesis. Oxygen isotope curves show opposite trend at top Shu'aiba associated with the late Aptian Unconformity.

surface (Figure 8B, Well B). The upper part of the Shu'aiba Formation (sequences 6 and 7) has an overall increase of $\delta^{18}\text{O}$ from $\sim -6\text{‰}$ to $\sim -4\text{‰}$ at top of the Shu'aiba Formation. This enrichment of $\delta^{18}\text{O}$ is contradict with the core description data that show massive karsted surface on top of the Shu'aiba Formation associated with the development of late Aptian Unconformity. This contradicts between the enrichment of $\delta^{18}\text{O}$ and the karsted unconformity at the top of the Shu'aiba Formation is enigmatic and need further analysis to explain.

Sequence 1

Sequence boundary 1 (SB1) is a major surface (Figure 38) that separates the shallow subtidal caprotinid rudist rudstone/grainstone of the Biyadh Formation from the dense argillaceous *Palorbitolina* packstone facies of the overlying Hawar unit. This initial transgression corresponds to the abrupt carbon isotope depletion from 3‰ in Biyadh Formation to 2‰ or less associated with the deposition of dark-gray highly argillaceous *Palorbitolina* packstone (Figure 34). This depletion increases upward and reaches its minimum value of 1.5‰ at high gamma ray marker associated with a thin bed of argillaceous shale in the basal Shu'aiba Formation (Figure 38B). The fluctuation of $\delta^{13}\text{C}$ within the Hawar unit (Figures 35 and 36) is correlated with higher-order cycles picked from cores, where the enriched spike of about 3.5‰ occurred in the clean, chalky mudstone that represent the MFS of sequence 1 (see Wells H, M, P and F).

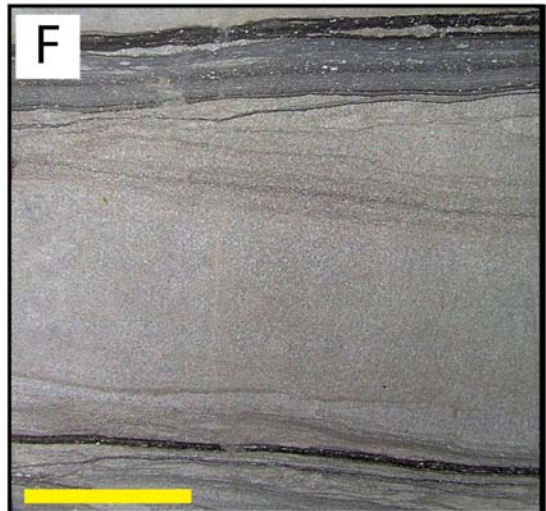
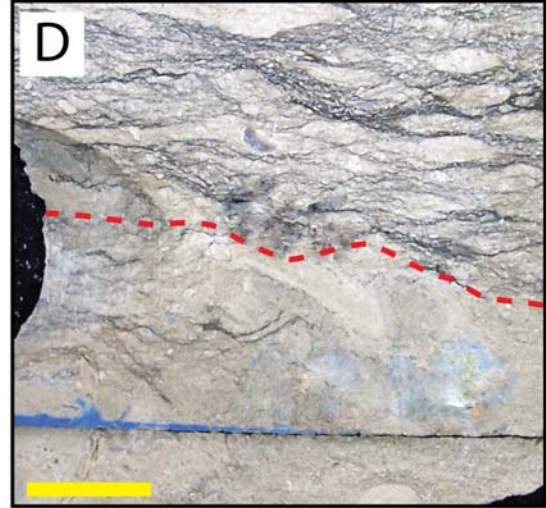
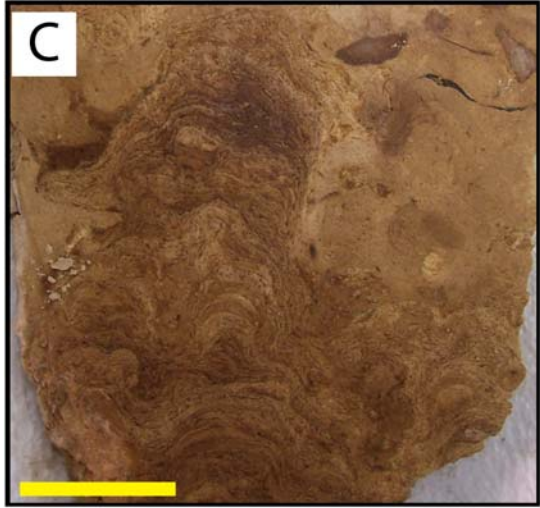
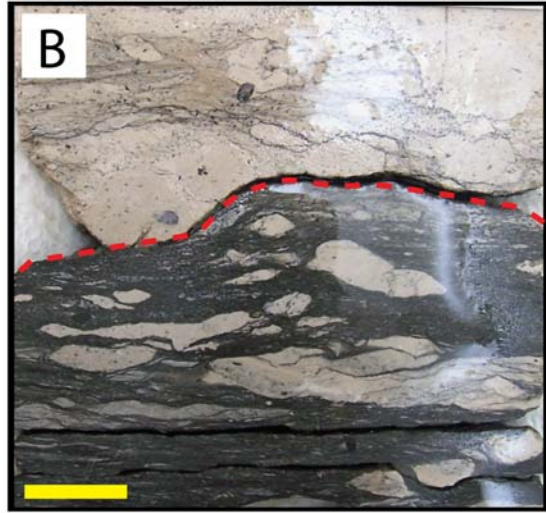
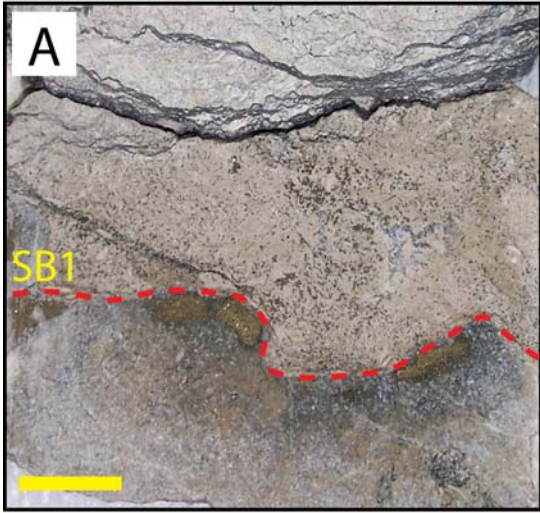
The HST of sequence 1 has a sharp contact where the facies change from argillaceous *Palorbitolina* packstone to oncoidal *lithocodium/Bacinnilla* packstone

(Figure 38B) associated with an increase of the carbon isotope values of about 0.5‰. This minor increase in $\delta^{13}\text{C}$ values of this facies marks the onset of the following high magnitude positive enrichment ^{13}C trend in the Early Cretaceous period associated with the first Oceanic Anoxic Event series (OAE 1a). The small fluctuations of carbon values in this unit also are correlated with the higher frequency parasequences (Figure 36A), with minor carbon enrichment corresponding to flooding surfaces and minor depletion corresponding to the shallow water grainy facies (Well H).

Sequence 2

Sequence 2 started with a sea-level rise associated with the deposition of chalky planktonic (*Hedbergella*) mudstone that likely represents the maximum flooding unit (MFU) of the Shu'aiba Formation composite sequence (Al-Ghamdi and Read, 2010). Hedbergellids planktonic forams have been recorded within the black shale Tethyan deposits in Italy (Luciani et al., 2006). This may suggest that this deep water facies in the Shu'aiba Formation records the onset of the coeval interval to the OAE 1a black shale interval of the pelagic Tethyes record. A major enrichment of carbon isotope values approximately 2‰ to 3‰ is associated with this flooding event and the following HST of *Lithocodium aggregatum* facies (Figures 35 and 36). The HST of this sequence has extensive *Lithocodium aggregatum*, platy corals and *Palorbitolina* wackestone facies that also records a continuous gradual increase in carbon values to about 4.5‰ at the top

Figure 38. Core sample photographs of some important boundaries and facies. The yellow scale bar represents 2 cm. (A) sequence boundary 1 (SB1) separates the lower shallow peloidal skeletal grainstone of Biyadh Formation from the overlying argillaceous *Palorbitolina* packstone of Biyadh "dense" unit (or Hawar unit). (B) major contact at basal Shu'aiba Formation separating the underlying argillaceous shale at top of Hawar unit (used as stratigraphic datum) and the overlying light-colored *Lithocodium/Bacinella* oncoidal packstone. (C) *Lithocodium* Aggregatum facies form as extensive mounds within the HST of sequence 2. This *Lithocodium* is coeval to the black shale deposited in the deep pelagic setting of the northern Tethys Ocean. (D) Lower/Upper Aptian contact (dashed line) separating the underlying fine skeletal peloidal packstone and the overlying argillaceous mudstone. It occurs on the slope and platform edge as a correlative conformity. (E) *Horiopleura* type rudist in upper Aptian sequences, extends their age from Aptian to the Lower Albian. (F) dark argillaceous mudstone/wackestone of deep lagoonal environment, which records the highest carbon isotopic values in all Shu'aiba Formation data.



of this sequence. This *Lithocodium aggregatum* facies is very distinctive in its composition and morphology (Figure 38C) and also is coeval to the black shale that formed during OAE 1a in the northern Tethys pelagic deposits of southern Europe (Immenhauser et al., 2005). The gradual long-term increase of the carbon isotope values is interrupted by several minor depletion events, similar to the four reversal trends described by Vahrenkamp (2010). These minor depletion trends are correlated with the minor flooding events associated with high frequency-cycles within the *Lithocodium* facies.

Sequences 3 - 7

Sequence 3 marks the end of the positive ^{13}C excursion associated with the onset of thick, stacked rudist buildups within the middle part of Shu'aiba Formation with their uniform carbon isotope trend. The boundary between the *Lithocodium* platform of sequence 2 and the rudist buildups of sequence 3 corresponds to the $\delta^{13}\text{C}$ value of 4.5‰. This value is well correlated from platform to slope and basin as shown in Wells H, M and N (Figure 35). The good lateral correlation from margin to basin with almost a constant value of 4.5‰ at sequence boundary 3 suggests that the $\delta^{13}\text{C}$ at this surface represents a significant chronostratigraphic time marker. Sequences 4, 5 and 6 on the platform are dominated by constant high sedimentation rate of the rudist buildups, having uniform $\delta^{13}\text{C}$ values ranging from 4.5 to 5‰ with nearly constant values of 5‰. However, toward the slope and open marine settings (e.g Wells M, N and Q), carbon values increase to more than 5‰. Moreover, the deep lagoonal setting (e.g Wells J and A) have the highest carbon isotopic values reaching its maximum of 6.1‰ in sequences

5 and 6. The sequence boundary 6 (SB 6) marks the termination of the rudist buildups facies with local subaerial exposure associated with oxidized clay materials developed at this surface (e.g Wells B and S) (Al-Ghamdi and Read, 2010). However, no concomitant carbon isotope depletion occurs here. Oxygen isotope records, on the other hand show significant depletion at this sequence boundary (Figure 37). Sequences 6 and 7 record a gradual decrease in carbon values from 5 to 4‰ at the top of Shu'aiba Formation where it is capped by the late Aptian unconformity. However, this gradual depletion is cyclic in nature and is not related to the influence of meteoric water beneath the unconformity.

Sequences 8 and 9

Newly identified sequences 8 and 9 are sequences and they only formed on the flanks of the northern block, as clinoformal sequences prograding toward the basin while the platform top was exposed and eroded by the late Aptian Unconformity (Figures 34 and 35) (Wells M, N, O & P). These two sequences are Upper Aptian in age and have distinctive facies characteristics and biota. Each has a base of dense argillaceous mudstone as a TST that shallow upward to stromatoporoids and rudist reefal facies in the HST (Wells M, N, O and T) (Figure 38D). The first occurrence of the nannofossil *Lithraphidites houghtonii* in Well-O is late Aptian (Varol, 1993, Saudi Aramco internal report). This paleontological data is calibrated with sequence stratigraphy, facies stacking patterns and isotope curves to interpret the prograding sequences in nearby wells. Rudists in sequences 8 and 9 are different than the lower Aptian rudists. Whereas, Lower Aptian rudists of sequences 3-7 are mainly caprinids in the shallow water bank-

crest settings or caprotinids in the back-bank or shallow lagoonal inner ramp setting (Figure 38E), the rudists in the upper Aptian sequences are *Horiopleura* of the Polyconitidae family (Skelton, 2008, Saudi Aramco internal report). The range of *Horiopleura* rudists extends from the Aptian to the lower Albian (Skelton and Masse, 2000).

It is possible that even more prograding sequences may have formed prograding into the basin similar to those that are interpreted from seismic data in the U.A.E (Yose et al., 2010). The Lower/Upper Aptian boundary marks a major change in facies from fine skeletal and peloidal packstone to dark argillaceous mudstone associated with increase in carbon isotope data of about 0.5 to 1.5‰. This change in $\delta^{13}\text{C}$ is similar in pattern but smaller in magnitude than the standard Tethyan curve (Wells M, N and P on the eastern flank). However, Well J on the western flank shows a strong depletion of 2‰ followed by an increase of 1.5‰ at the Lower/Upper Aptian boundary similar in pattern and magnitude with the pelagic Tethys curve (Figures 34 and 35).

Discussion

Isotopes versus Depositional Facies

The relationship between isotopic composition and facies is critical when evaluating chemostratigraphic correlations, as a strong correlation between isotope values and depositional facies may not indicate an original ocean signature (Kaufman and Knoll, 1995). To analyze the relationship between depositional facies and isotope values, a plot of all carbon and oxygen isotope data (Figure 33) associated with the

major facies of the Shu'aiba Formation was plotted. Shu'aiba Formation $\delta^{18}\text{O}$ values range from -2.7 to -6.7‰, whereas $\delta^{13}\text{C}$ ranges from 1.5 to 6‰. The Shu'aiba Formation $\delta^{18}\text{O}$ is generally more depleted than the proposed Early Cretaceous Ocean value, which is about -3‰ (Lohmann, 1988). This depletion along with the general lack of variation in the $\delta^{18}\text{O}$ values suggests diagenetically altered values, making them unreliable for chemostratigraphic correlations. Carbon isotope values on the other hand have larger variations associated with the evolution of Shu'aiba Formation platform and sequence stratigraphic architecture.

The following are brief discussions of the main Shu'aiba lithofacies that plotted in Figure 33 and their isotope signatures:

Hawar Unit and *Lithocodium/Bacinella* Facies

The most depleted $\delta^{13}\text{C}$ values (1.5‰) occur within the dark argillaceous *Palorbitolina* packstone within the Hawar unit. This depletion is corresponding to global methane hydrates in the earliest lower Aptian (e.g. Jenkyns, 1995; Weissert et al., 1998; Föllmi et al., 1994, 2006; Jahren et al., 2001; Vahrenkamp, 2010). The early Aptian nannoconid crisis defined from the Tethyan pelagic sediments (Luciani et al., 204) is possibly coeval to the Hawar unit, associated with the initial TST of Shu'aiba platform and a possible warming event during the earliest early Aptian (Föllmi et al., 1994; Jenkyns, 2003). The nannoconid crisis was associated with a reduction in calcification, due to the high atmospheric CO_2 just before the OAE 1a (Luciani et al., 2004). The higher values in this facies (> 3‰) is corresponding to the low gamma ray, white chalky

mudstone within the Hawar unit that represent the MFU of sequence 1. The *Lithocodium/Bacinella* facies (purple) associated with sequence 2 of the lower Shu'aiba Formation have a major increase in $\delta^{13}\text{C}$ and are coeval with the global OAE 1a. This large increase in $\delta^{13}\text{C}$ is one of the major carbon enrichments of the Cretaceous Period and is related to a rise in inorganic carbon as a result of increased organic carbon burial in ocean black shale during the early Aptian Oceanic Anoxic Event OAE 1a (e.g. Scholle and Arthur, 1980; Jenkyns, 1995; Weissert and Lini, 1991; Weissert et al., 1998; Föllmi et al., 1994, 2006).

Rudist Buildup Facies

The rudist buildups facies (both caprinid and caprotinid types) are shown in red (Figure 33) with most $\delta^{13}\text{C}$ values ranging from 4 to 5‰. The rudist facies that plot below 4‰ are interpreted to either have undergone minor diagenesis (e.g Well-F), or they represent local *Agriopleura* rudist buildups that formed in the upper part of Shu'aiba Formation and are associated with the general depletion of carbon (Figures 35 and 36) in the upper Shu'aiba sequences (e.g S6 and S7 in Wells J and H). The large variations in $\delta^{18}\text{O}$ values of this facies possibly indicate influence of meteoric diagenesis associated with local subaerial exposure, especially on the shallow bank-crest settings (Figure 37).

Shallow Lagoonal Facies

The shallow lagoonal facies (light blue) shows an overlap with the rudist facies isotope values, but with slightly broader clustering (Figure 33). The overlap of lagoonal

facies with rudist facies indicates that the platform interior values are time equivalent to the surrounding rudist facies (e.g S6 in Wells H and S) (Figure 36A).

Deep Lagoon Facies

The deep lagoonal facies (dark blue) have the highest carbon isotope values with over 6‰ recorded at Well-J on the northwestern flank of the field (Figure 35). Well-A on the southeastern flank has a similar carbon trend (Figure 36A). This carbon enrichment is associated with the black laminated wackestone/mudstone facies only recorded in these two wells (Figure 37F). Gamma ray signals of this facies have higher values possibly associated with higher Uranium content and organic-rich mudstone. Similar heavy isotope values were recorded in the inner platform of Bu-Hasa field, representing isolated ponds formed under partially anoxic conditions (Vahrenkamp, 2010; Amthor et al., 2010; Yose et al., 2010). The partial anoxia explains the withdrawal of light carbon by the organic matter, resulting in heavier carbon isotope values in the inorganic carbonate (Vahrenkamp, 2010).

Slope and Shallow Open Marine Facies

Although the slope and open marine facies (light and dark green), have some overlap with the rudist facies, the majority of these data have higher $\delta^{13}\text{C}$ and $\delta^{18}\text{O}$ values than the rudist buildups (Figure 33). Their $\delta^{13}\text{C}$ values range from 5 to 6‰ and is associated with slight enrichment of $\delta^{18}\text{O}$ from -4 to -3.5‰. Variations in isotope trends from the modern Bahamas and Florida platforms indicate the platform seawater may be

depleted in $\delta^{13}\text{C}$ by 4‰ relative to the open-ocean water (Patterson and Walter, 1994). This depletion occurs as a result of light CO_2 input from respiration of organic matter due to the aging of seawater on semi-restricted platforms and also to seasonal effects. The depletion of $\delta^{13}\text{C}$ from slope and shallow open marine to the rudist buildups in Shu'aiba Formation however, is only 1‰ at maximum and they show similar isotope trends as shown between Wells H and M. Therefore, the Bahamas modern platform example may not be applicable to the ancient Shu'aiba Formation platform. It is possible that the small depletion in rudist buildups is related to the alteration of the muddy matrix within the rudist facies, where the matrix is commonly composed of cemented silt-sized rudist fragments.

Deep Basinal Facies

The isotope record of the deep intrashelf basin (black) in Well-P has generally lower ^{13}C values than both the rudist buildups and the slope and shallow open marine facies (Figure 33). However, the carbon isotope curve of the intrashelf basin is close in magnitude and pattern to the Tethyan pelagic curve (Figure 34). The oxygen isotope values in the basinal section also are close to the values of Cretaceous ocean water (Figure 33). A similar trend of increased values in the shallow carbonate values relative to the basinal values was observed in the Arabian Gulf region and interpreted as resulting from the isolation of shallow water from the circulation of marine water (Vahrenkamp, 1996). However, there is no evidence of such isolation at the Shu'aiba Formation in this study. Another possible interpretation may be the vital effects of

dominant rudist bivalves in the margins/or their skeletal fragments in the slope and shallow shelf environments versus the dominant pelagic foraminifera in the intrashelf basin facies. These different organisms incorporate different amount of light isotope metabolic CO₂ into their shells, thus the resulting coeval facies may have different carbon values (Emrich et al., 1970; Grossman, 1987). Corals and red algae have larger vital effect than benthic foraminifera (Grossman, 1987) and that may explain the depletion of carbon isotope from shelf margin to slope and open marine. Well-F on the central margin of the field shows even more depletion of carbon isotopes that may be related to the dominant coral facies in this well (yellow facies, Figure 36A). Another factor affecting the carbon isotope values in the rudist buildups is the aragonite composition of rudists shells. The Early Cretaceous rudists usually have relatively thick aragonite shells covered by a thin calcite layer (Steuber, 2002). The aragonitic compositions of the rudists contribute to the enrichment of heavy carbon due to the higher fractionation rate in aragonite as the presence of 20% aragonite sediments may increase the carbon isotope values by about 0.2‰ (Godet et al., 2005).

Carbon Isotope Curves versus Stratigraphic Framework and Depositional Settings

The carbon isotope curves from all wells are plotted against depth (Figure 39). Each major depositional setting then separated into a single plot to analyze the relationship between carbon isotope trends, stratigraphic frameworks and depositional settings (Figures 40 to 44). The curves were datumed on the regional marker at top of Hawar unit, which has high gamma ray values and low carbon isotope values. All the

data below and above the datum until depth ~ 90 have similar values and trends representing a series of uniform layers of the Late Barremian Biyadh sequence, Shu'aiba Formation sequence 1 and the TST of sequence 2. The major depletion of $\delta^{13}\text{C}$ at the datum is closely correlated with the global ocean signature associated with methane hydrate dissociation in the earliest early Aptian (Jenkyns, 1995; Weissert et al., 1998; Föllmi et al., 1994, 2006; Jahren et al., 2001; Vahrenkamp, 2010). The subsequent gradual increase in values is also well correlated in all wells associated with the major flooding and OAE 1a. At depth ~ 90 with values between 4 and 4.5‰, carbon isotope curves begin to diverge from each other indicating a major change in paleoenvironment, ocean signature and/or sequence stratigraphy. This change is correlative with the onset of the rudist buildups at SB3 and with the formation of shelf margin with its slope and open marine in the front and back-bank and lagoonal settings in the back. After the divergent zone between the different curves within the middle part of Shu'aiba Formation, the carbon values in most wells converge, with decreasing values in the upper part of the Shu'aiba Formation. The prograding Upper Aptian sequences (8 and 9) have relatively similar depletion trends toward the top, but this interval is younger and they should not be compared with the platform wells that only record the Lower Aptian (Figure 45). The overall similarity in pattern and trends of these different isotopic curves along with their association with the cored-based sequence boundaries suggest that the Shu'aiba Formation carbon isotope record represents the original marine signature and thus can be used to constrain a high-resolution chronostratigraphic framework for the Shu'aiba Formation.

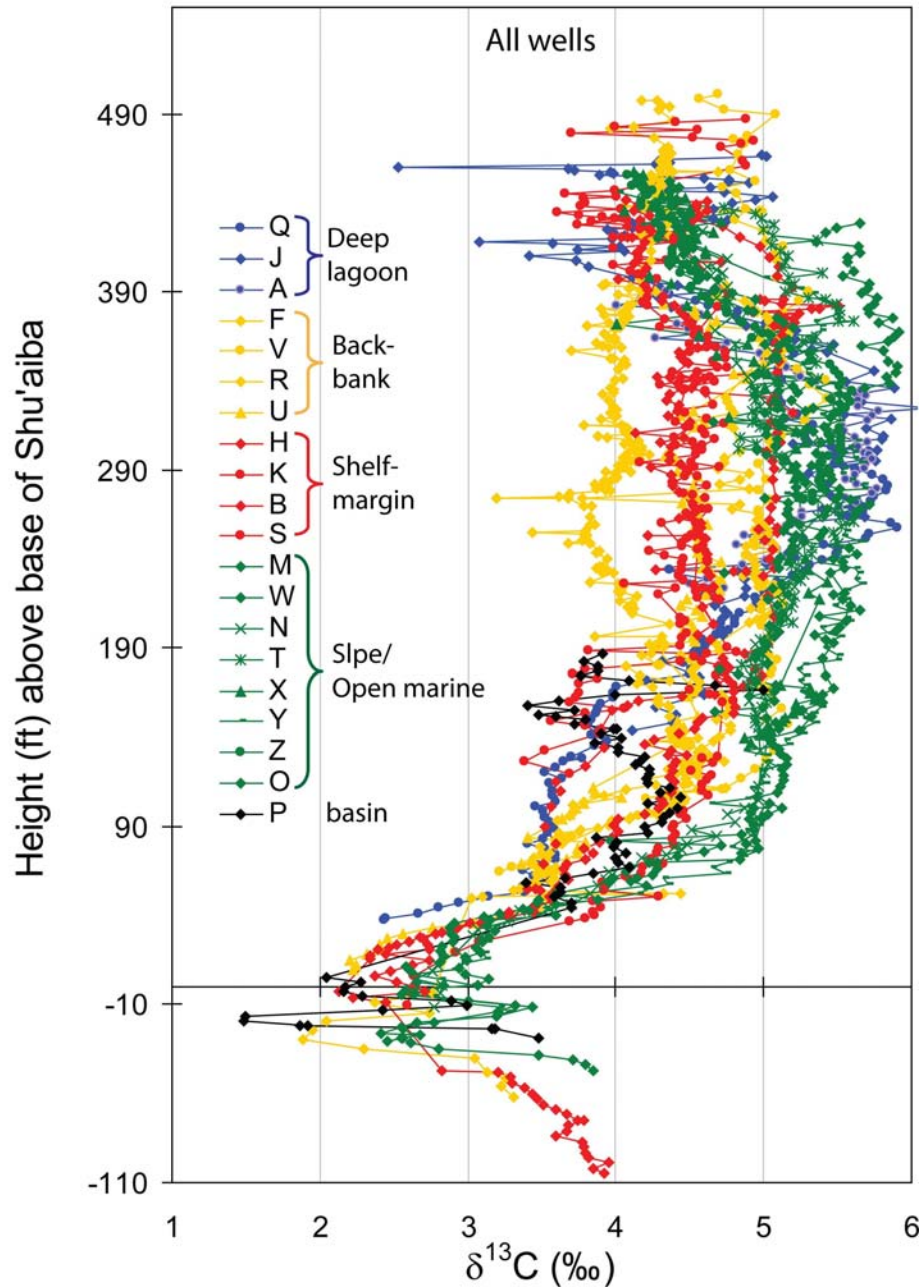


Figure 39. Carbon isotope curves from all wells plotted against depth. The datum is the basal Shu'aiba Formation associated with the negative carbon isotope spike. The datum is a depth value of zero that increases upward to 490 feet and decreases to -110 feet, which is study interval. Curves with different colors represent different depositional settings, (red is the shelf margin, yellow is back-bank/platform interior, blue is the deep lagoon or lagoon, green is slope or shallow open marine, and black is the intrashelf basin).

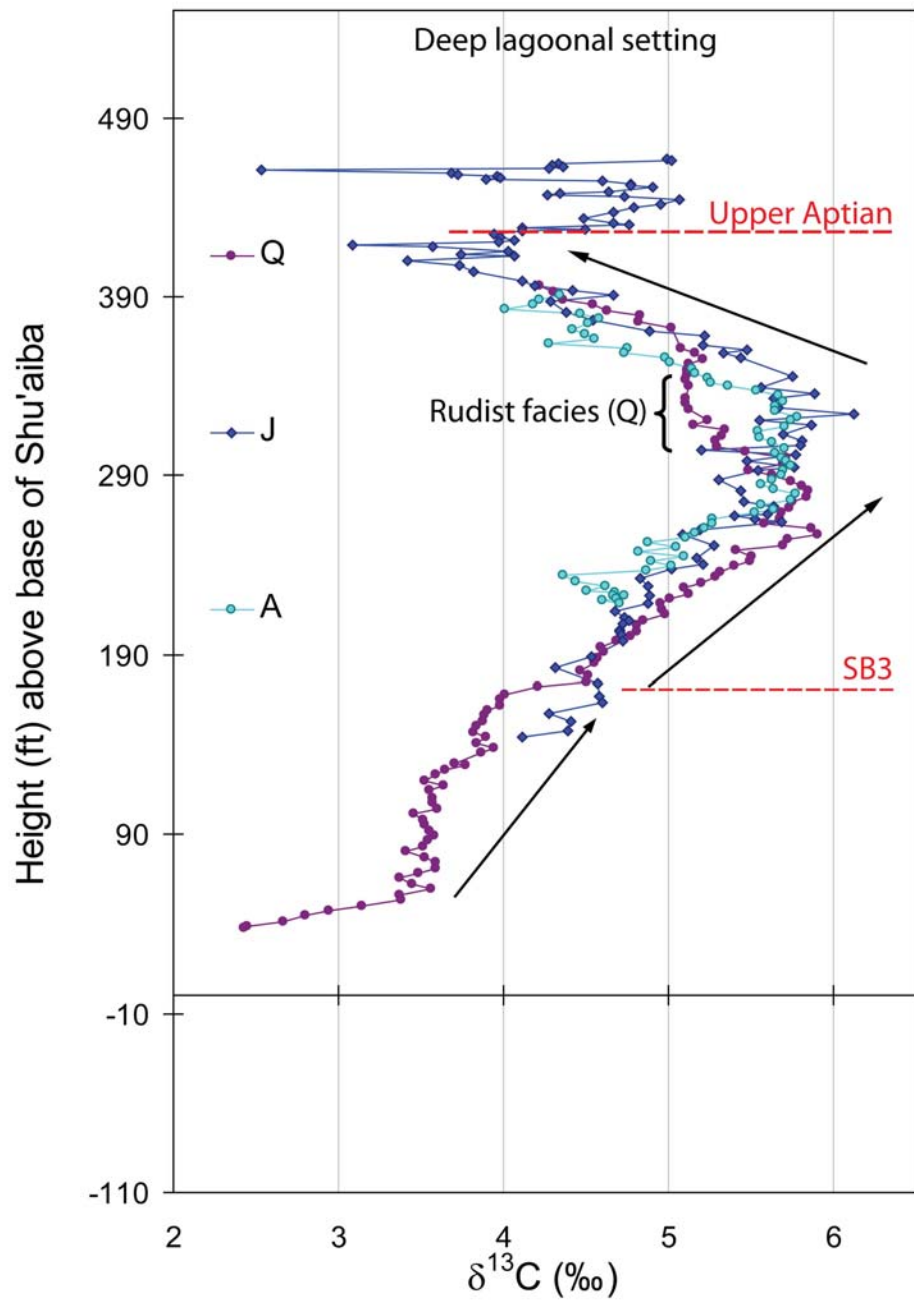


Figure 40. Carbon isotope curves from the deep-lagoonal setting. Different colors are arbitrary chosen just to differentiate between wells. Wells Q and A are located on the eastern flank of southern block, while well J is located on the western flank of northern block. Black arrows show general carbon isotope trends.

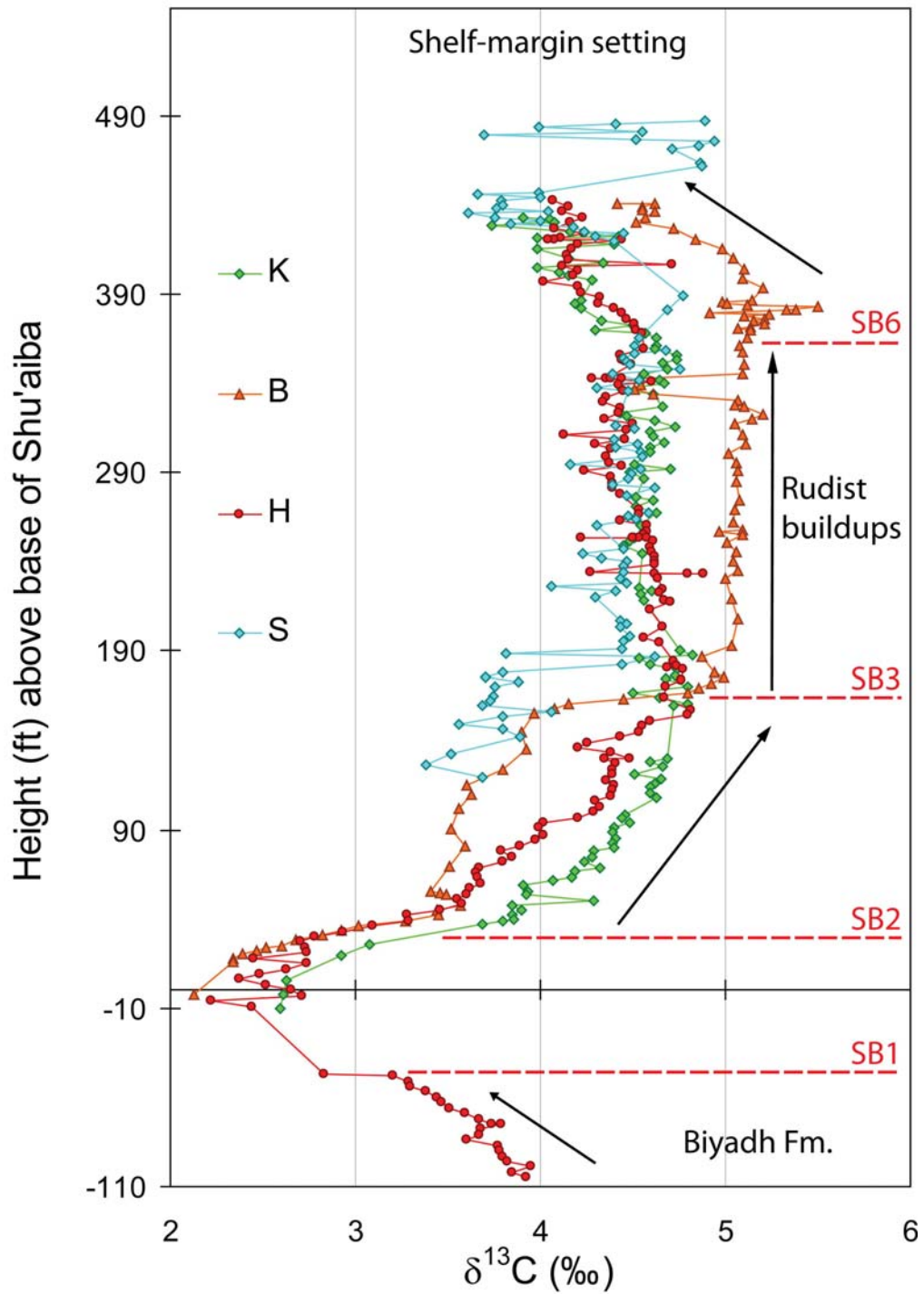


Figure 41. Carbon isotope curves from the shelf-marginal setting. Different colors are arbitrary chosen just to differentiate between wells. Black arrows show general carbon isotope trends.

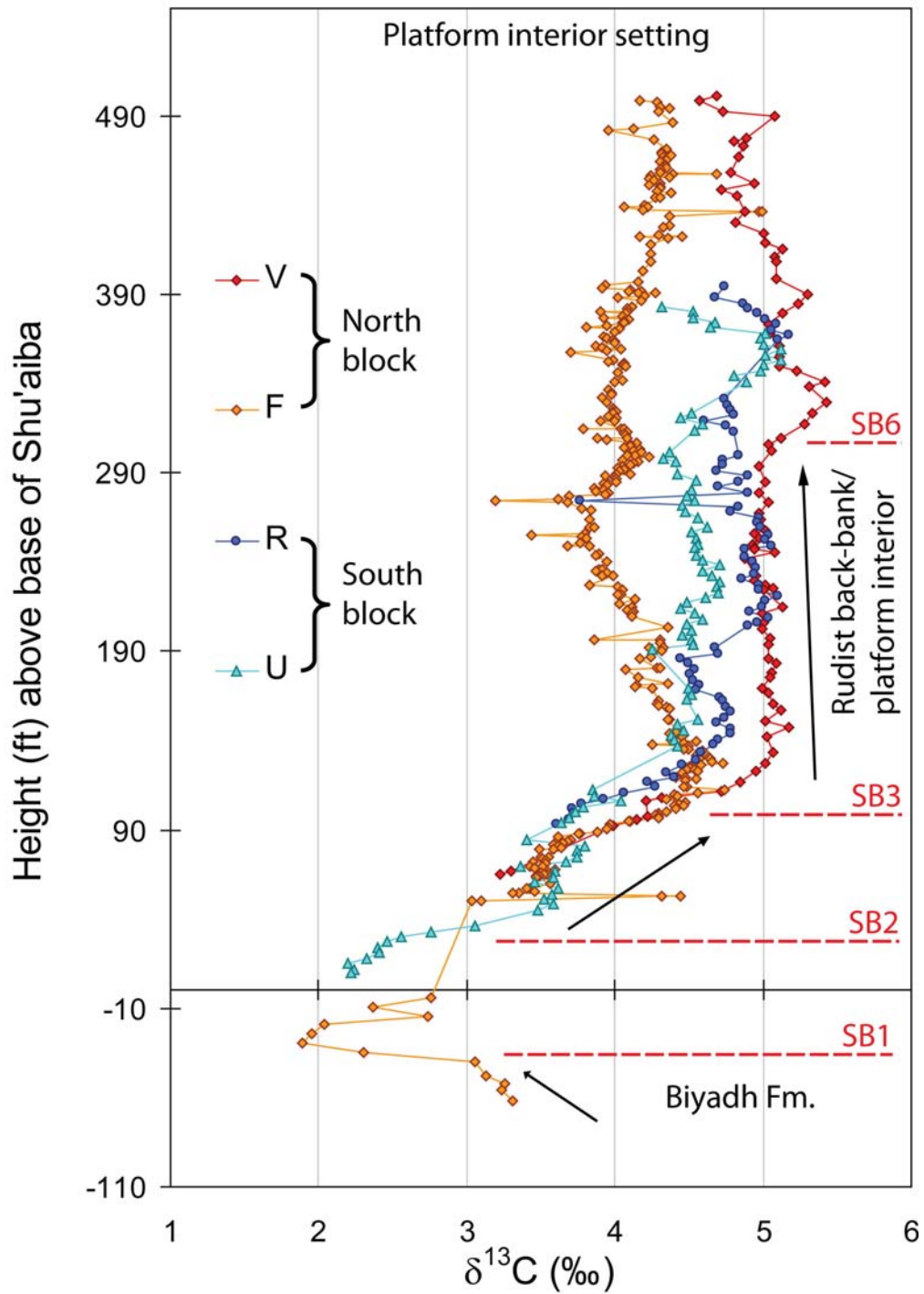


Figure 42. Carbon isotope curves from the back-bank/platform-interior setting. Different colors are arbitrary chosen just to differentiate between wells. Wells F and V are from the northern block, while wells R and U are from the southern block. Black arrows show general carbon isotope trends.

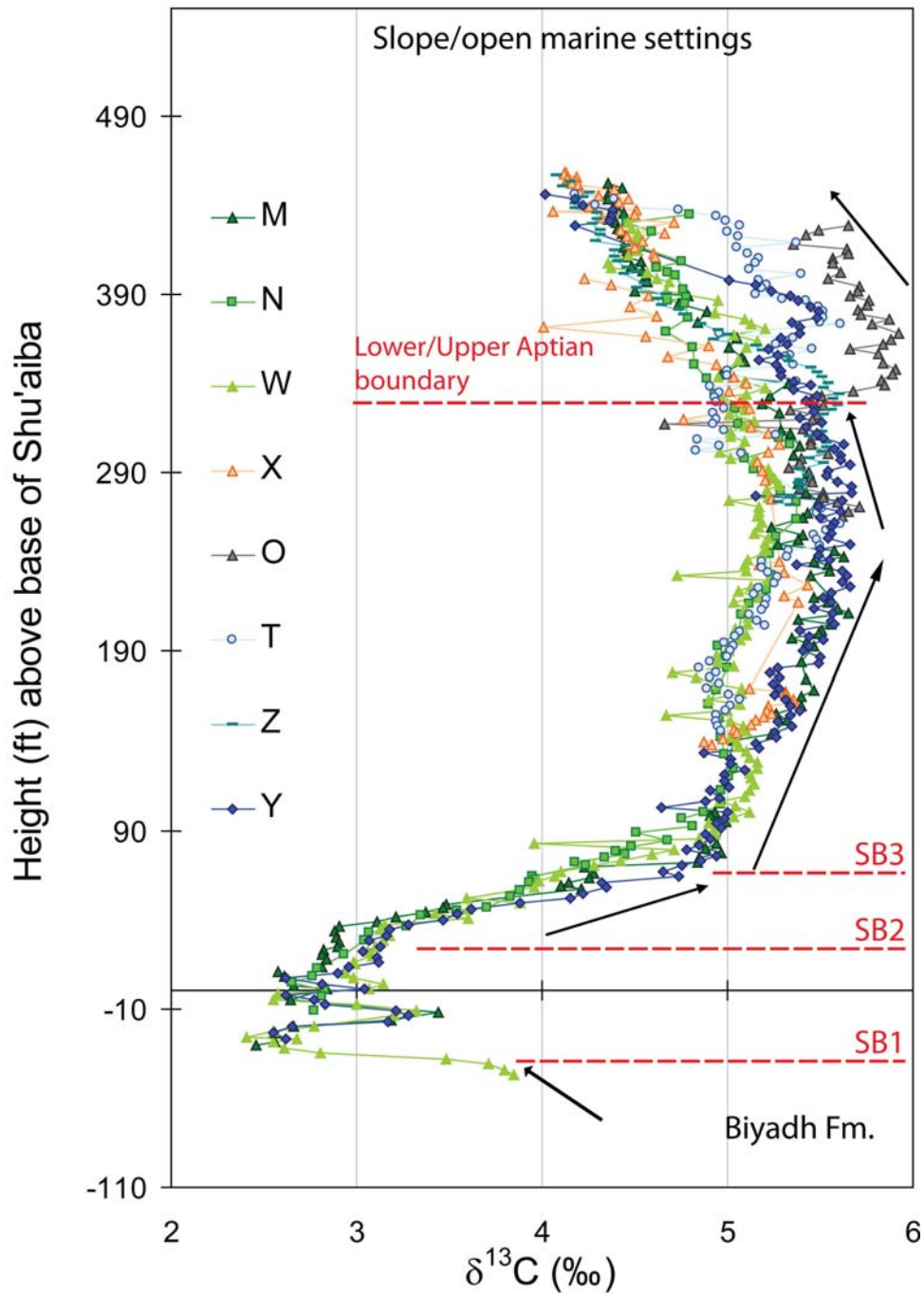


Figure 43. Carbon isotope curves from the slope and open-marine settings. Different colors are arbitrary chosen just to differentiate between wells. Upper Aptian prograding sequences occurred in most wells of these settings. Black arrows show general carbon isotope trends.

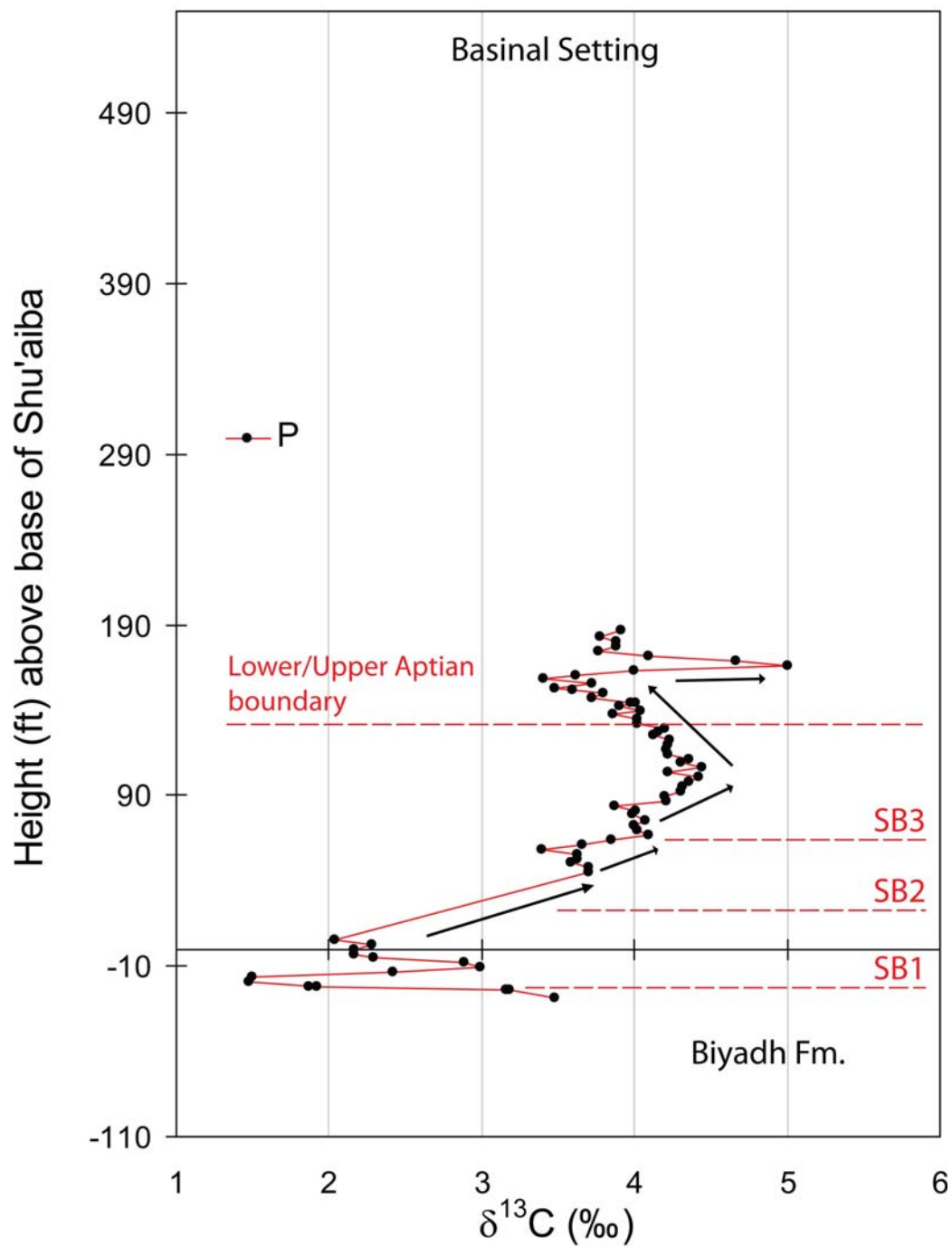


Figure 44. Carbon isotope curves from the basinal setting. Wells P is located off structure within the intrashelf basin. Black arrows show general carbon isotope trends.

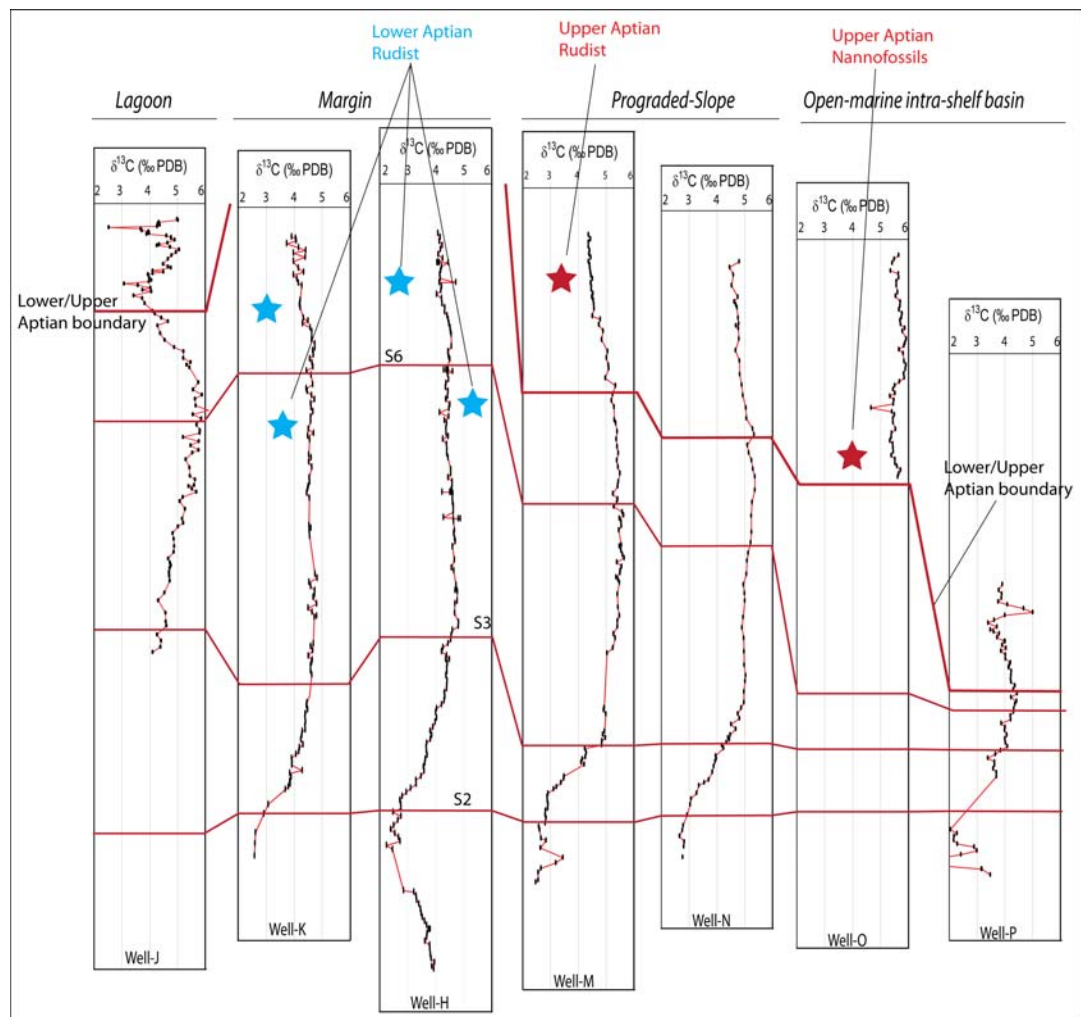


Figure 45. Carbon isotope correlation of the west-east platform to basin transition illustrating how biostratigraphy and chemostratigraphy data are integrated to determine the stratigraphic geometry of the Shu'aiba Formation and age difference between the Lower Aptian platform sequences and the Upper Aptian prograding sequences.

Five major depositional settings can be distinguished based on their carbon isotope trends, sequences architectures and facies stacking patterns. These depositional settings are: (1) deep-lagoonal setting (Wells A, Q and J) (Figure 40), (2) shelf-margin setting (Wells K, B, H, S) (Figure 41), (3) platform-interior setting (Wells V, F, R and U) (Figure 42), (4) slope and open marine setting (Wells M, N, W, X, O, T, Z and Y) (Figure 43), (5) basinal-setting (Well P) (Figure 44).

- 1) The deep lagoonal setting has distinctive $\delta^{13}\text{C}$ trends with the highest values recorded within the middle part of the Shu'aiba Formation (Figure 40). Although the wells in this setting are from different locations, they almost have identical curves. They are characterized by large increase in $\delta^{13}\text{C}$ values above SB3 with the deposition of dark-colored organic mudstone/wackestone (Figure 38F). This large increase is coeval to rudist buildups in shelf margin setting. The highest $\delta^{13}\text{C}$ in the middle at depth ~ 290 is corresponding to a deepening event of mudstone facies that possibly have high organic contents (Figure 38F). The ^{13}C curve then decline in all three wells to reach the minimum value that marks the Lower/Upper Aptian boundary at Well J. The depletion in well Q at the maximum $\delta^{13}\text{C}$ increase is due to the occurrence of small rudist facies on the upper part of S6 (Figure 36A). Despite the higher $\delta^{13}\text{C}$ magnitude of the lagoonal setting, the general trends match well with the Tethys pelagic curve, especially at the Lower/Upper Aptian boundary.
- 2) The shelf-margin setting is characterized by a dominant thick massive rudist buildup facies at sequences 3 to 6 with generally uniform ^{13}C trend, indicating

higher sedimentation rates. The $\delta^{13}\text{C}$ values of the rudist buildup range from 4.5 to 5‰, with minor depletion occurred in some wells (e.g. K, H and S) (Figure 41). This depletion is possibly associated with shallowing upward event that capped by SB6. However, no influence of meteoric diagenesis on carbon isotopes occurred associated with the subaerial exposure surface of SB6. The uniform trend occurred in well B is associated with large and massive *in situ* rudist that developed in bank-crest setting.

- 3) The platform-interior setting has similar trend to the shelf margin setting (Figure 42). This is because these wells are located on back-bank platform interior with the deposition of some local rudist buildups or skeletal rudist fragments. Well-F shows more negative values compared to other wells. This depletion is possibly related to the vital effects with the dominant coral facies and to minor diagenetic alterations associated with a highly fractured and faulted zone within the intraplatform depression (Al-Ghamdi and Read, 2010).
- 4) The slope and open marine setting have identical $\delta^{13}\text{C}$ trends of sequence 1 to sequence 3 (Figure 43). The curves above SB3 increases upward then slightly decreases at the Lower/Upper Aptian boundary. This increase is coeval to the uniform rudist buildups trend present in shelf-marginal setting. Well O was deposited in a deeper open marine setting and has higher $\delta^{13}\text{C}$ values corresponding to the additional Upper Aptian prograding sequence 9.
- 5) The basinal setting has a distinctive $\delta^{13}\text{C}$ trend that represent deep water pelagic sediments (Figure 44). The $\delta^{13}\text{C}$ values are relatively low similar to the standard

Tethys record. Despite the low sedimentation rates occurred in this setting, pronounced fluctuations of the Lower Aptian sequence are still preserved and can be correlated with coeval sequences in slope and shelf-margin settings. The distinctive positive spike in the upper part of this curve is related to the deposition of the late stage infill of Bab intrashelf basin.

Isotope Stratigraphy versus Global Sea-level Changes

The use of carbon and oxygen isotope compositions as a proxy of sea-level changes was documented on several platforms around the world (e.g., Scholle and Arthur, 1980; Föllmi et al., 1994, Stoll and Scharg, 2000). It was proposed that the positive carbon excursion during the Early Cretaceous is related to the rise of sea-level associated with increased atmospheric CO₂, whereas the negative carbon excursion is related to sea-level fall (Scholle and Arthur, 1980; Föllmi et al., 1994). Immenhauser et al. (2003), however hypothesized that during sea-level fall in the Carboniferous ice-house, the shallow carbonate platforms were exposed and underwent meteoric diagenesis resulting in a depletion of $\delta^{13}\text{C}$ and $\delta^{18}\text{O}$ values. On the other hand, during sea-level rise, the carbonate platform was flooded with open marine, well circulated waters with minimum diagenetic effects. This resulted in an enrichment of the $\delta^{13}\text{C}$ and $\delta^{18}\text{O}$ with positive shifts of the isotope curve. Therefore, shallow carbonate platforms may reflect local alterations rather than global ocean signatures (Immenhauser et al., 2003).

Although core descriptions from the Shu'aiba Formation show some evidence of exposure surfaces (e.g SB 6 at Wells B and S), there is no recorded depletion of $\delta^{13}\text{C}$

values are associated with this boundary. Oxygen isotope data, however, record depletion values at SB 6 associated with possible meteoric influence (Figure 37). This results suggest that carbon isotope data on the shallow carbonate Shu'aiba Formation were more stable and did not get affected by the meteoric water or soil gas at exposure surfaces, similar to what Vahrenkamp (1996; 2010) concluded on other Shu'aiba platform in the region. Therefore, the hypothesis of (Immenhauser et al., 2003) cannot be applied on carbon isotope data here and it should only be limited to oxygen isotopes signature. But, it is possible that short periods of dry climate prevailed during the formation of other local exposure surfaces of Shu'aiba Formation (e.g SB 4 and 5 in Wells F and B), thus no meteoric waters affected the sediments. Moreover, the top of Shu'aiba Formation has a major unconformity with extensive karstification (Al-Ghamdi and Read, 2010) but the slight depletion of $\delta^{13}\text{C}$ in the upper part of Shu'aiba Formation is well correlated with the global carbon records and is not related to meteoric diagenesis, karstification or soil gas from the unconformity. Therefore, the Shu'aiba Formation carbon isotope records strongly reflect changes in the global carbon cycles which can be tied to the global sea-level curves. Oxygen isotope data has an opposite $\delta^{18}\text{O}$ trends associated with the top Shu'aiba unconformity. The oxygen records have enrichment trend rather than depletion trend that normally recorded at major subaerial unconformities (Figure 37).

The Shu'aiba Formation carbon isotope records correlate with the third-order sea-level fluctuations of the Aptian in the following manner:

- (1) the gradual depletion in $\delta^{13}\text{C}$ in the Biyadh Formation beneath SB1 is associated with a regressive phase and sea-level fall of the latest Barremian.
- (2) the major depletion of $\delta^{13}\text{C}$ in the Hawar unit is a widespread event that has been related to the dissociation of methane hydrates and can be correlated globally.
- (3) the major positive excursion during S2 is associated with the major sea-level rise, the deposition of the maximum flooding unit (MFU, K70) and the *Lithocodium* algal platform during the global early Aptian sea-level rise and the OAE 1a (Föllmi et al., 1994).
- (4) the uniform trend of $\delta^{13}\text{C}$ in the rudist buildups reflects an aggradational phase with a very high sedimentation rate during the early HST of the Shu'aiba Formation composite sequence.
- (5) the general depletion of $\delta^{13}\text{C}$ at the upper part of Shu'aiba Formation is associated with the major third order sea-level fall during the latest early Aptian.

Carbon Isotope Stratigraphy versus High-Frequency Parasequences

Higher-order parasequences (e.g 5th-orders or more) also can be correlated to small-scale carbon isotope enrichment and depletion. Small scale parasequences of the Biyadh Formation (Figure 46) show minor positive excursion of $\delta^{13}\text{C}$ enrichment ($\sim 0.2\text{‰}$) associated with flooding surfaces. On the other hand, gradual depletion of carbon values ($\sim 0.3\text{‰}$) occurs in the grainy facies associated with the top of these shallowing

upward cycles. Two parasequences in the basal Shu'aiba Formation beneath the SB2 have good correlation with $\delta^{13}\text{C}$ fluctuations. These parasequences have increasing $\delta^{13}\text{C}$ values ($\sim 0.3\%$) at their base followed by decreasing values of similar amplitude at the cycle top. These parasequences are correlatable field wide as shown in cross sections (Figures 35 and 36) and seem to be correlating in their $\delta^{13}\text{C}$ values (e.g Wells H, F and P) despite the small magnitude of the $\delta^{13}\text{C}$ fluctuation. However, more isotope data from these zones are required to further substantiate this interpretation. These small-scale fluctuations in $\delta^{13}\text{C}$ cannot be tied to global sea-level changes or global carbon cycles due to their high resolution, but they may reflect a change in relative sea-level on a regional scale.

The major positive excursion in the early Aptian related to OAE 1a is interrupted by several small-scale negative $\delta^{13}\text{C}$ spikes (Figure 46). Some of these minor negative values appear to be related to the development of parasequence tops within the HST of S3 within the *Lithocodium aggregatum* facies. Vahrenkamp (2010) interpreted these small-scale negative spikes within the larger scale positive enrichment as a result of minor methane hydrates defrosting that episodically interrupted the prevailing oceanic anoxic environments during the early Aptian. The relationship between these small reversals and small-scale shallowing-upwards parasequences, however likely indicate that these small reversal spikes may be local rather than global events. Hochuli et al., (1999), proposed that the enhanced primary productivity is the main cause for the organic carbon accumulation during the OAE 1a with its $\delta^{13}\text{C}$ values marked by an interval of unchanged values with an absence of anoxia environment.

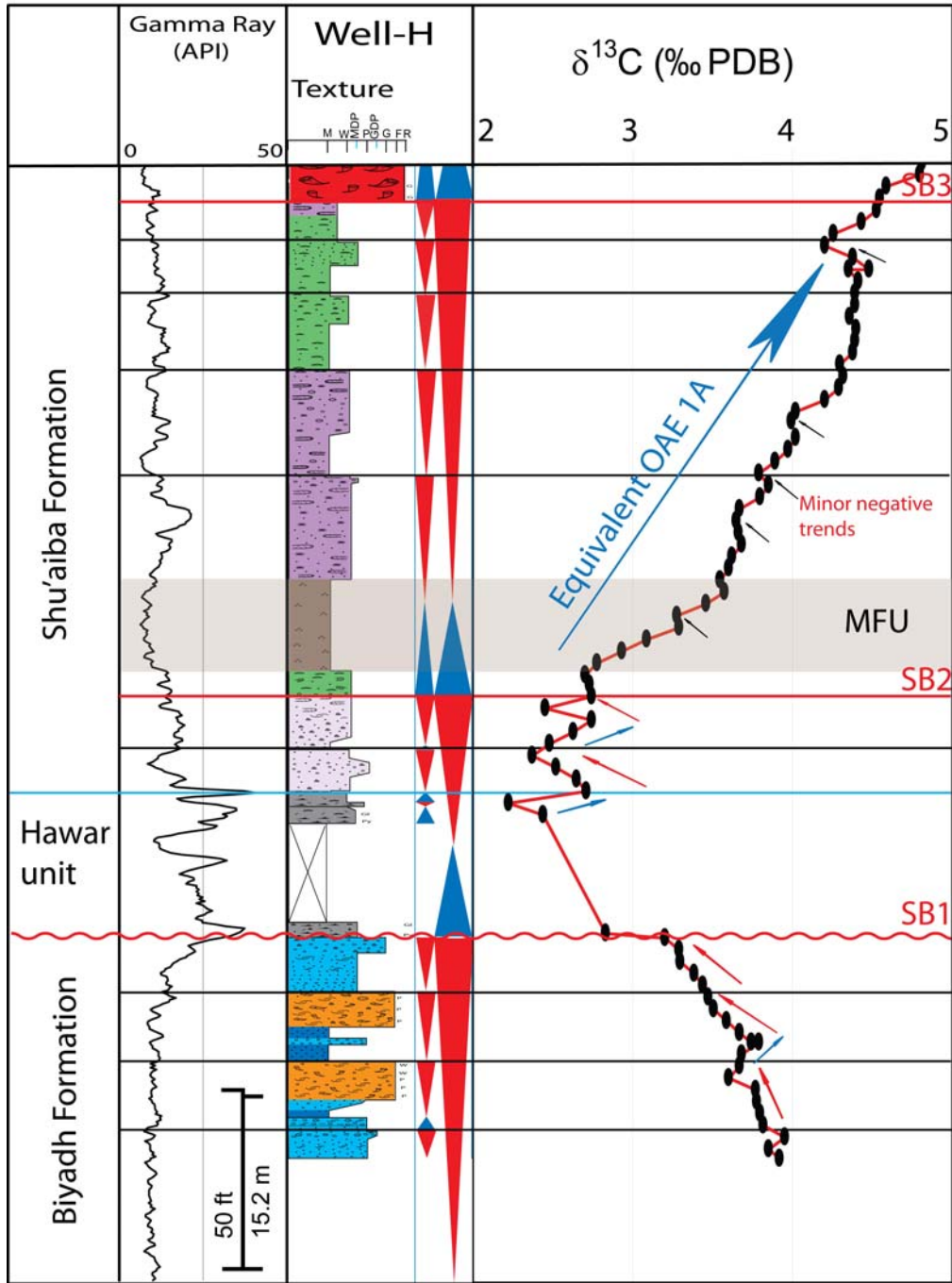


Figure 46. Carbon isotope curve in a higher resolution scale from Well H, plotted against core description of Well H. The black horizontal lines represent high resolution parasequences (possibly 5th orders) identified from cores and tied to $\delta^{13}\text{C}$. Small blue and red arrows show enrichment and depletion of ^{13}C , associated with flooding surfaces and cycle tops respectively.

Carbon Isotope and Palaeoclimate Changes

The Cretaceous Period has long been considered as a continuous warm, greenhouse climate. However, intervals of global cooling and warming have been interpreted from isotope data from different carbonate platforms, with possible development of ice-sheets in the poles (e.g Frakes, 1999; Frakes et al., 1995; Stoll and Scharg, 2000; Immenhauser and Matthews, 2004). The major carbon isotope perturbations during the Early Cretaceous were associated with rapid global climate changes (Jenkyns 2003).

The latest Barremian including the Barremian-Aptian boundary record cooling event associated with carbon isotope depletion and sea-level fall (Weissert and Erba, 2004). This event was recorded in the Shu'aiba Formation at SB1. This sequence boundary records the disappearance of the rudist buildups facies and is related to the global carbonate platform diminish recorded elsewhere in northern Tethys (Föllmi et al., 1994). This was abruptly followed by the global negative carbon isotope excursion related to dissociation of methane hydrates and deposition of the argillaceous *Palorbitolina* packstone of the Hawar unit (the initial TST of the Shu'aiba composite sequence). The Hawar unit is a condensed section composed of glauconite-and pyrite with many erosion surfaces that seems to be synchronous to the earliest Aptian condensed and phosphentic sections in northern Tethys described by Föllmi et al. (1994). These condensed sections represents widespread breakdown of carbonated production reflecting what is called the destructive sea-level rise (Föllmi et al., 1994). AT this time, the global climate changed rapidly from a cooling phase at the Barremian

to a warming in the earliest Aptian (Weissert and Erba, 2004, Jenkens, 2004). The warm climate at the earliest Aptian culminated with the deposition of the black shale in the pelagic sections and chalky *Hedbergella* lime mudstone and *Lithocodium aggregatum* wackestone in the shallow carbonate Shu'aiba platform. The OAE 1a was deposited during warm and humid climate as suggested by isotope signatures, fossil assemblages and the presence of southern provenance pollen (Hochuli et al., 1999; Jenkens, 2003; Luciani et al., 2006). OAE 1a was associated with an increase in marine biological productivity, accelerated hydrological cycling, global sea-level rise, positive carbon isotope excursion, and poor circulation of the deep ocean. This disturbance in the global carbon cycle with this rapid warming event possibly resulted from the dissociation of methane hydrates, possibly triggered by an increase in volcanism on the Ontong-Java Plateau (dated ~ 125-119 Ma) with large amount of CO₂ released to the atmosphere causing a greenhouse warm climate and warming of bottom waters continental shelves (Larson and Erba 1999; Weissert and Erba, 2004; Jenkens 2003).

The onset of the rudist buildups in the Shu'aiba Formation at sequence 3 and the development of extensive rudist-banks indicate carbonate platform recovery that possibly associated with a cooling climate and HST of the composite Shu'aiba sequence, similar to the cooling event above the OAE 1a in northern Tethys (Weissert and Erba, 2004; Jenkens 2003). This cooling event was due to the drawdown of CO₂ due to an increase in marine productivity and to the increase in carbon burial during the OAE 1a (Jenkens, 2003). The major unconformity at the top of the Shu'aiba is a global event

caused by eustatic sea-level fall in a cooling and humid climate and is associated with the overall gradual carbon isotope depletion at top of the Shu'aiba Formation.

Conclusions

The carbon isotope values of the shallow carbonate Early Cretaceous, Aptian, Shu'aiba Formation range between 1.5 and 6‰ with variations that are mimicking the Tethyan pelagic record. Carbon isotope values of the Shu'aiba Formation have not undergone major meteoric diagenesis, and likely reflect the original marine values of the Early Cretaceous shallow platform waters. Oxygen isotope values of the Shu'aiba Formation range between -2.7 to -6.7‰ and were diagenetically modified including meteoric diagenesis and so do not reflect the original marine signature of the Early Cretaceous Ocean.

In this study, the carbon isotope record of the Shu'aiba Formation was used as a correlation tool to further refine the age model beyond the resolution of the biostratigraphic age model. Carbon isotope data from 21 wells were integrated with core descriptions and gamma ray logs to define sequence boundaries, maximum flooding surfaces and the Lower/Upper Aptian boundary. Two detailed chemostratigraphic cross-section transects were generated; (1) an east-west cross-section along the dip direction showing a platform transition from lagoonal, back-bank, shelf-margin, slope, open marine and basin, (2) a north-south cross-section along strike section showing the evolution of the Shu'aiba platform from platform edge, platform interior and intraplatform depression.

The Shu'aiba Formation is a large-scale composite sequence (~ 7 My) composed of seven high-frequency sequences in the Lower Aptian and two more prograding sequences in the Upper Aptian. The Lower Aptian sequences show good correlation with the carbon isotope curves, where TST's are associated with carbon isotope enrichment and HST's are associated with carbon isotope depletion. These records of enrichment and depletion of carbon isotopes during the early Aptian are related to the change in global carbon cycles and are not related to local diagenetic effects.

The major negative excursion in the Hawar unit is a global event associated with dissociation of methane hydrates in the basal Aptian. The major positive excursion within sequence 2 is also a global phenomena related to organic carbon burial and OAE 1a. Carbon isotope values of ~ 4.5‰ represent an important chronostratigraphic time line associated with the onset of rudist buildups in the middle Shu'aiba. This value is well preserved despite major changes in facies from margin to slope and open marine. The upper Aptian sequences on the northern platform edge prograded toward the basin. These additional sequences were mainly identified on the basis of a carbon isotope trends that calibrated to facies stacking patterns and biostratigraphy. Although, isotope values of single stratigraphic time lines show some lateral variations with different environments, the general isotope trends are similar in pattern and are laterally correlative. These minor changes in carbon isotope values across environments are possibly related to changes in dominant organisms. However, overlaps of isotope values between different facies suggesting those are original carbon isotope signatures. The

deep lagoonal environment records the highest carbon values, whereas the intrashelf basinal setting records lower values similar in magnitude to the pelagic record.

Carbon isotope data can be used as a proxy for the third-order global sea-level fluctuations of the Early Cretaceous. The carbon isotope enrichment is linked to sea-level rise as shown in the maximum flooding unit (MFU) of chalky planktonic mudstone in sequence 2. The carbon isotope depletion is linked to sea-level fall in the Biyadh Formation at SB1 and in the top of the Shu'aiba Formation.

Exposure surfaces within the Shu'aiba Formation including the major unconformity at the top, lack evidence of meteoric waters adversely affecting the carbon isotope data. On the other hand, oxygen isotope record shows depletion with some exposure surfaces such as SB6. However, oxygen isotope record did not get affected by the late Aptian unconformity, despite the massive karstification observed in cores. It is not clear why the extensive karstification at the top of the Shu'aiba Formation did not alter the oxygen isotope values. The general carbon isotope depletion beneath the upper unconformity is related to global marine isotope trends and not related to meteoric diagenesis.

Strontium isotope values of the Shu'aiba Formation range from 0.707356 to 0.707454, and are slightly different from the standard Aptian record. Although there is some relationship between certain stratigraphic markers and strontium isotope shifts in the Shu'aiba Formation, the diagenetic alteration of the whole-rock strontium isotope values make them less reliable in defining the age of the Shu'aiba Formation. The uses of carbon isotope data as a correlation tool along with core data significantly enhance the

stratigraphic framework of the Shu'aiba Formation, leading to better reservoir characterization and modeling.

CHAPTER IV

**TRACE ELEMENT VARIATIONS, GEOCHEMICAL ANALYSIS AND THEIR
IMPLICATIONS ON DIAGENETIC HISTORY OF THE EARLY
CRETACEOUS (APTIAN) SHU'AIBA FORMATION**

Overview

The Early Cretaceous (Aptian) Shu'aiba Formation has undergone a complex diagenetic history resulting in a heterogeneous reservoir along with complex pore systems. Trace elements, stable isotopes and thin sections were analyzed to determine the diagenetic history of the Shu'aiba Formation and are linked to major facies, depositional settings and sequence boundaries.

The trace element composition of the Shu'aiba Formation are generally low, reflecting either low values of the original fluids (e.g. Fe and Mn) or removal of elements during diagenesis (e.g. Sr and Mg). The lower Fe and Mn contents of the original sediments indicates that no additional values were added during diagenesis, suggesting the meteoric fluids in oxidizing environment were the primary diagenetic event rather than reducing environments. Sr and Mg contents also are generally low compared to the original Cretaceous sea water or modern carbonate rocks, suggesting they were removed from the sediments during diagenesis in an open system environment. Variations of trace elements were controlled by the presence of subaerial exposure surfaces, depositional settings and lithofacies. Upper Aptian sequences on the

platform edge and basinal settings have different compositions likely reflecting different fluid chemistry associated with facies changes.

Carbon isotope values of mud matrix and cements are similar ranging from ~ 1 to 6 ‰, reflecting the original carbon isotope record of the Cretaceous. No depletion of $\delta^{13}\text{C}$ is associated with subaerial exposure or meteoric diagenesis observed from the cements, shells or mud matrix. $\delta^{18}\text{O}$ values of the cements are depleted with wide variations representing different stages of cementation. No evidence of depletion associated with deep burial diagenesis except in a few fracture fills samples. The average strontium isotope data of the Shu'aiba Formation is 0.07389. This value fall within the range of the Cretaceous Sr isotope values reflecting the original composition of the sediments with no additional radiogenic Sr added during the diagenesis further supporting meteoric diagenesis as the primary fluids affecting these rocks.

Cathodoluminescence (CL) analysis of the Shu'aiba Formation indicates four to five zones within the rudist buildups facies. CL analysis helped identify the original stable Low Magnesium Calcite (LMG) rudist with the non-luminescent zone (NL) from the recrystallized aragonitic shells that has bright luminescent. Dull luminescent zones are less common, occurred only as thin layer at the edges of the blocky calcite crystals and reflecting the general low Fe contents.

The subaerial exposure surface SB7 within the Shu'aiba Formation and the major unconformity at the top of Shu'aiba Formation are the most important events that influenced the diagenetic history of the Shu'aiba Formation. These events diagenetic including the chalkification and development of micro-rhombic calcite, microporosity

and moldic porosity occurred at this time or as the platform was exposed associated with meteoric fluids.

Introduction

The Early Cretaceous (Aptian) Shu'aiba Formation has a complex depositional and diagenetic history that impacts reservoir characterization and performance (Figure 47). Diagenetic processes played a major role in developing or occluding pore systems within the Shu'aiba Formation. The diagenetic fabrics of the Shu'aiba Formation range from the poorly cemented micro-crystalline chalky mudstone with dominant microporosity to cemented rudist rudstone with large vugs and molds. This complexity results in heterogeneous reservoir quality in both lateral and vertical scales associated with complex stratigraphic architectures. For instance, rudist debris grainstone facies deposited in shallow-water, high-energy marginal settings occurred in two forms, one as a clean porous facies and the other as a tight and cemented grainstone. To understand and characterize the temporal and spatial distribution of these two facies within the sequence stratigraphic framework, diagenetic environments and paragenetic history were identified and tied to sequence stratigraphy, to better define and predict flow and barrier units within the reservoir.

The diagenetic study presented here includes petrographic analysis of thin sections, cathodoluminescence (CL) analysis of selective thin sections, trace elements and microprobe elemental analysis from mud matrix and cements. It also includes stable isotope analysis of mud matrix and cements.

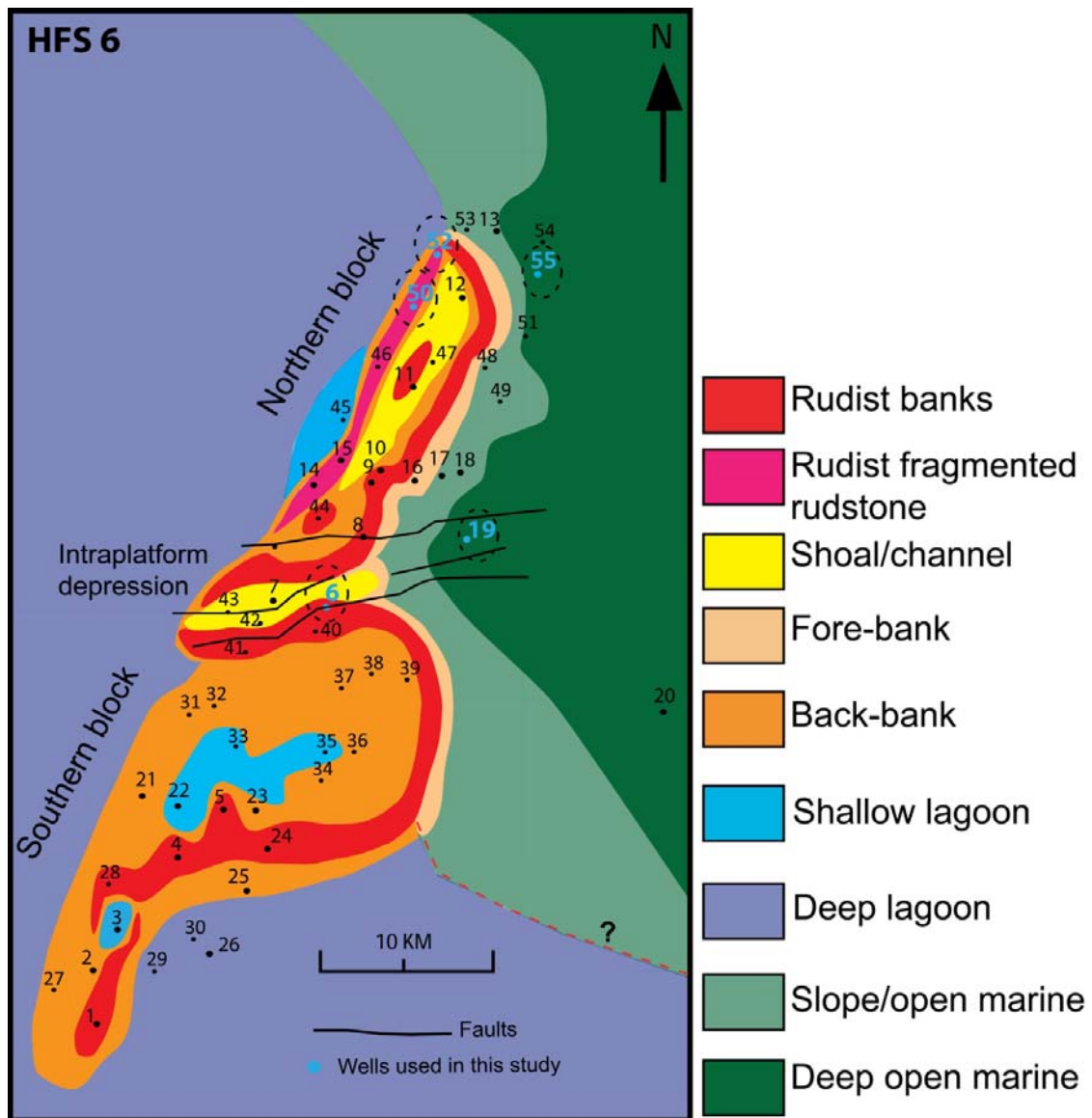


Figure 47. Base map with the Shu'aiba platform facies showing well locations. Wells in blue are used in this study.

The diagenesis history and diagenetic environments of the Shu'aiba Formation has been studied in the region (e.g Harris 1964; Litsey et al., 1986; Alsharhan and Kendall, 1991; Moshier, 1989, Budd, 1989), however, there are no published data on the diagenesis of the Shu'aiba Formation in the study area. Only two unpublished diagenetic studies were conducted for Saudi Aramco (Swart and Cantrell, 2000 and Swart and Lindsay, 2002). In addition, there is no regionally coherent conclusive diagenetic model of the Shu'aiba Formation, due to the lack of a detailed stratigraphic framework and complex geochemical data.

The chalky textures in the Shu'aiba Formation were attributed to meteoric diagenesis associated with the development of the unconformity at the top of the Shu'aiba Formation (Harris 1964). The unconformity hiatus at the top of the Shu'aiba Formation was estimated using benthic forams to represent a 1-1.5 My hiatus (Forst et al. 1983). The porosity development of the Shu'aiba Formation is related to the major sea-level fall during the latest Aptian time (Muris 1980). The lack of cementation and porosity preservation, particularly within the lower part of the Shu'aiba Formation was possibly due to early oil emplacement that inhibited subsequent diagenetic processes (Litsey et al., 1986). However, Pratt and Smewing (1993) indicate that the depleted supply of CaCO_3 fluids is the main cause of porosity preservation. Moshier et al. (1988), Moshier (1989), and Budd (1989) present two contradicting arguments for the development of the micro-crystalline chalky textures of the Shu'aiba; (1) stabilization in marine waters in shallow to intermediate burial depths (550-800) in a closed system conditions (Moshier 1989); (2) they developed in meteoric fluids by a two-step diagenetic process during

subaerial exposure Budd (1989). This study will evaluate these two theories using the advantage of the detailed and updated sequence stratigraphic frameworks that will be integrated with geochemical data to define more accurate diagenetic history. This study provides extensive data across all depositional environments and facies, including subaerial exposures surfaces within the Shu'aiba Formation that were lacking in previous studies.

Data Sets

This study used previously determined trace element analyses from Aramco internal reports for Wells 19, 50, 52, 55 (Swart and Cantrell, 2000) and Well-6 (Swart and Lindsay, 2002). These data were collected from core plugs at intervals of approximately every 1 to 3 feet (0.3 m). Mn, Sr, Mg were measured and analyzed using ICP-MS using a ratio of 1:100 and standardization was achieved using conventional methods which employed internal standard, while Fe was measured using an AA, with standardization using standards derived in Specpure calcium carbonate (Swart and Cantrell, 2000). In addition, 39 microprobe analyses from eight different thin sections were analyzed for trace elements at Texas A&M microprobe lab targeting small-scale calcite cements. This analysis was crucial to identify the paragenetic sequence and its stages of cementation. Cathodoluminescent and petrographic analysis were done on selective samples to identify the diagenetic features, type and timing of cementation.

Carbon, oxygen and strontium isotope data are also included in this study. Isotope date of the matrix was used from 26 wells across the platform (see AL-Ghamdi and Pope, 2013). Another 138 samples were analyzed for carbon and oxygen stable

isotope by micro-drilling the rudist shells, cements, and other diagenetic features. These samples provide information about the diagenetic history of the Shu'aiba Formation, where the isotope data of the matrix should provide information about the Cretaceous Ocean signature and may also provide some information about the formation of the micro-crystalline calcite and microporosity evolution.

Results

Trace Elements

Trace elements were taken from five wells (Figure 47) representing different facies and depositional settings and record the transition from marginal to platform-interior to slope and open marine settings. Table 2 shows the results of the entire data with the average and range of the main trace elements. The following is a brief summary of the results from for each well with their ranges and averages plotted as curves against depth measured from the top of the Shu'aiba Formation and integrated with the sequence stratigraphy.

Rudist Buildups (Well-52)

Well-52 is located on the northwestern flank within the high-energy rudist marginal setting (Figure 47). Fe content slightly decreases with depth from 180 ppm at the top to about 80 at the base (Figure 48). Mn is also depleted with depth from top to bottom from ~150 ppm at the top to ~70 ppm at the base. However, Sr and Mg are opposite to the Fe and Mn, being enriched from the top to the bottom (Figure 48).

Table 2. Trace elements from all wells with range and average for each trace element.

Well No.	Element	Range (ppm)	Average (ppm)
Well-52	Iron (Fe)	52-209	102
	Manganese (Mn)	38-357	112
	Strontium (Sr)	48-495	209
	Magnesium (Mg)	382-2650	1855
Well-50	Iron (Fe)	28-240	98
	Manganese (Mn)	55-446	128
	Strontium (Sr)	128-482	234
	Magnesium (Mg)	112-2989	1735
Well-6	Iron (Fe)	24-440	78
	Manganese (Mn)	49-202	90
	Strontium (Sr)	105-247	159
	Magnesium (Mg)	462-4091	1210
	Vanadium (V)	0.3-12	2
Well-55	Iron (Fe)	41-167	104
	Manganese (Mn)	24-420	125
	Strontium (Sr)	125-473	193
	Magnesium (Mg)	745-2548	1275
Well-19	Iron (Fe)	55-300	131
	Manganese (Mn)	42-512	42
	Strontium (Sr)	181-432	325
	Magnesium (Mg)	1323-3159	2532
All wells	Iron (Fe)	24-440	95
	Manganese (Mn)	24-512	113
	Strontium (Sr)	48-495	204
	Magnesium (Mg)	112-4091	1561

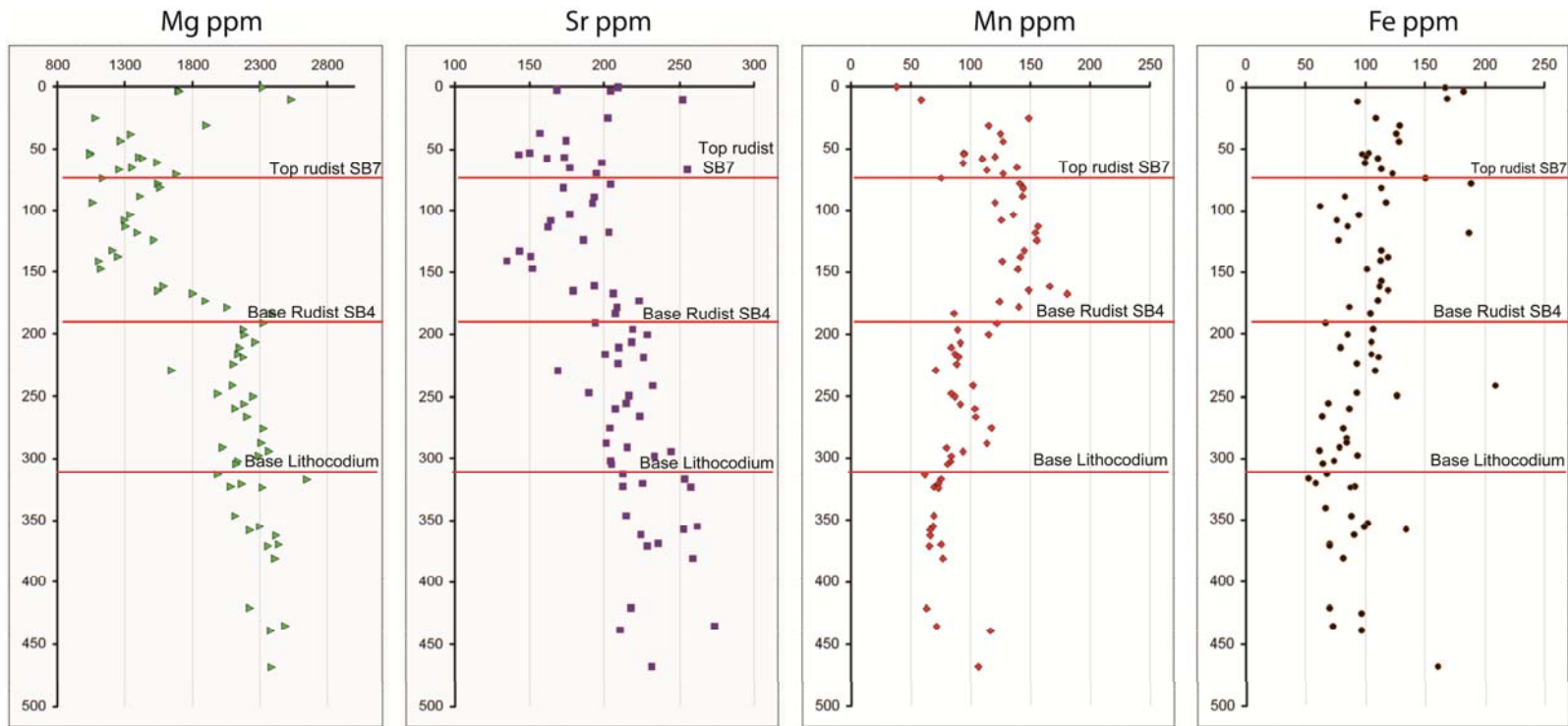


Figure 48. Trace elements from rudist buildup setting of Well-52 plotted against depth and superimposed by major sequence boundaries. Sr and Mg curves tend to positively correlated to each other and negatively correlated with Mn curve.

Fe contents in this Well do not show a clear relationship with major sequence boundaries, but subtle variations occurred associated with major facies changes. Moreover, there is no pronounced correlation between Fe and Mn in this well except the general decrease of both elements from top to bottom, but inverse correlation occurred between Mn on one hand and Sr, Mg on the other hand.

The Mn contents of Well-52 generally decreases with depth, but major increases occurred within the middle part of the Shu'aiba Formation (above SB4) associated with the rudists buildups (Figure 48). Major sequence boundaries (e.g SB4 and SB7) are correlated with abrupt changes in Mn content trends. The low Mn values at the base (~70 ppm) are associated with the deep chalky planktonic mudstone facies of the maximum flooding surface. Mn rapidly increased from ~70 ppm to ~120 ppm at the beginning of the *Lithocodium*/coral facies, then decreases to a value of ~80 ppm at the top of the *Lithocodium*/coral facies at SB4. The exposure surface occurred at SB7 has only a small decrease in the Mn value, that slightly decreases toward the top unconformity.

Sr contents are generally increase from top to bottom. An abrupt decrease of Sr occurred above SB4, above the boundary between the *Lithocodium* and rudist facies. The most Sr depletion occurred within the rudist buildups.

Mg increases with depth from ~2000 ppm at the top to ~ 2300 ppm at the bottom similar to Sr curve. Thus, Mg is positively correlated with Sr, but inversely correlated with Mn. Major enrichment and depletion of Mg are associated with major sequence boundaries with their facies changes. For instance, at SB4 with the onset of rudist

buildups, Mg is dramatically depleted from ~2300 ppm to ~1300 ppm, then get enriched more toward the unconformity at the top of the formation.

Platform Interior/Rudist Buildups (Well-6)

Well-6 is located on the platform edge of the intraplateform depression within the marginal to platform interior (Figure 49). It has a variety of depositional facies including rudist buildups, extensive massive and branching corals that are relatively more susceptible to diagenesis and severe leaching. Also, this well was affected by syn-depositional fault and fracture systems that enhanced fluid flow through this area.

Table 2 shows the average and range of trace elements in this well including Vanadium. Generally, the minimum and mean values of Fe, Sr and Mg are the lowest values comparing to other wells, whereas Mn content is relatively higher or the same as other wells (Figure 49). Fe and Mn values show generally a subtle depleted trend from top to bottom. Fe and Mn contents in this well show changes at some sequence boundaries (e.g SB5 and SB7). Fe is dramatically enriched toward the top from less than 50 ppm at SB7 to >200 ppm at SB8, and then becomes slightly depleted beneath the top Shu'aiba unconformity. The positive spikes of Fe content (e.g at SB5 and SB8) are possibly related to extensive pyrite minerals, which are common in this well. Mn shows, only a subtle increase from base to top. Sr and Mg contents are positively correlated in this well and show changes in values at or near several sequence boundaries (e.g SB3, SB6, SB7). Sr and Mg content record a major increase corresponding to the flooding

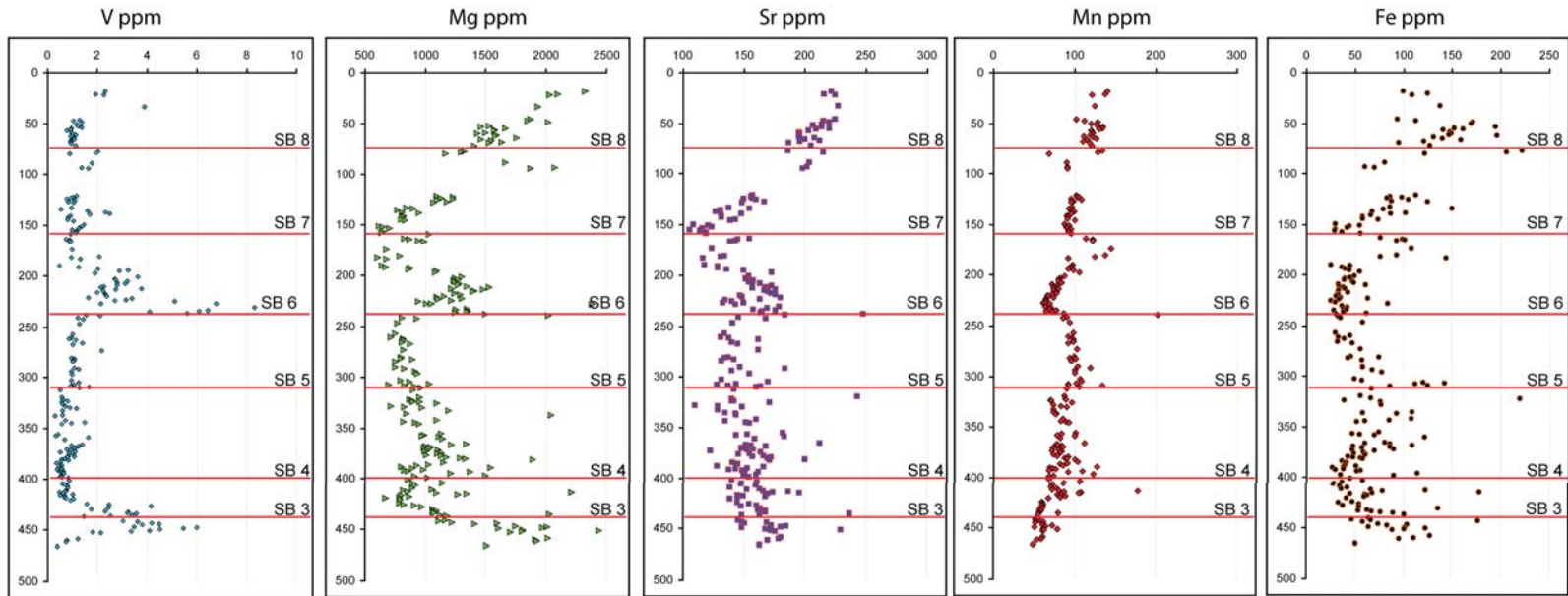


Figure 49. Trace elements from rudist buildup setting of Well-6 plotted against depth and superimposed by major sequence boundaries. This well has the lowest Fe contents recorded at the base of the section. It also records the Mn lowest maximum values. Vanadium content is recorded only in this well.

interval above SB 6, the both become depleted to their minimum values near SB 7 which is a subaerial exposure surface. Sr and Mg increase dramatically above SB 7 to their maximum values near the top of the Shu'aiba Formation.

The Vanadium (V) is only analyzed in this well with a minimum of 0.3 ppm and maximum of 12 ppm and an average of 2 ppm (Figure 49). However, two extreme values recorded for the Vanadium occur at SB 3 and above SB 6.

Slope and Platform Edge (Well-55)

Well-55 was deposited on the far eastern platform edge within slope/open marine settings (Figure 1). It is dominated by fine grained mudstone and wackestone facies in the lower part overlain by the Upper Aptian stromatoporoid and rudist buildups facies. The average and range of trace element contents in this well are shown in Table 2. Unlike other wells, Fe in well-55 is relatively homogeneous averaging ~100 ppm with no clear depletion or enrichment trends (Figure 50). Sr and Mg values are generally uniform in the base then decrease to their minimum values below the Upper Aptian rudist. The Sr and Mg contents then increase on the upper part of the Formation associated with the rudist buildups that developed marginal setting within the Upper Aptian prograding sequences then get slightly decrease at the top unconformity. Sr and Mg are positively correlated to each other, but negatively correlated to Mn.

Mn content in this well has a pronounced pattern that decreased dramatically with depth from ~ 410 ppm in the top to ~ 24 ppm at depth of 150 feet below the top, (Figure 50). Below 150 feet, the Mn values are uniform with the lowest value recorded

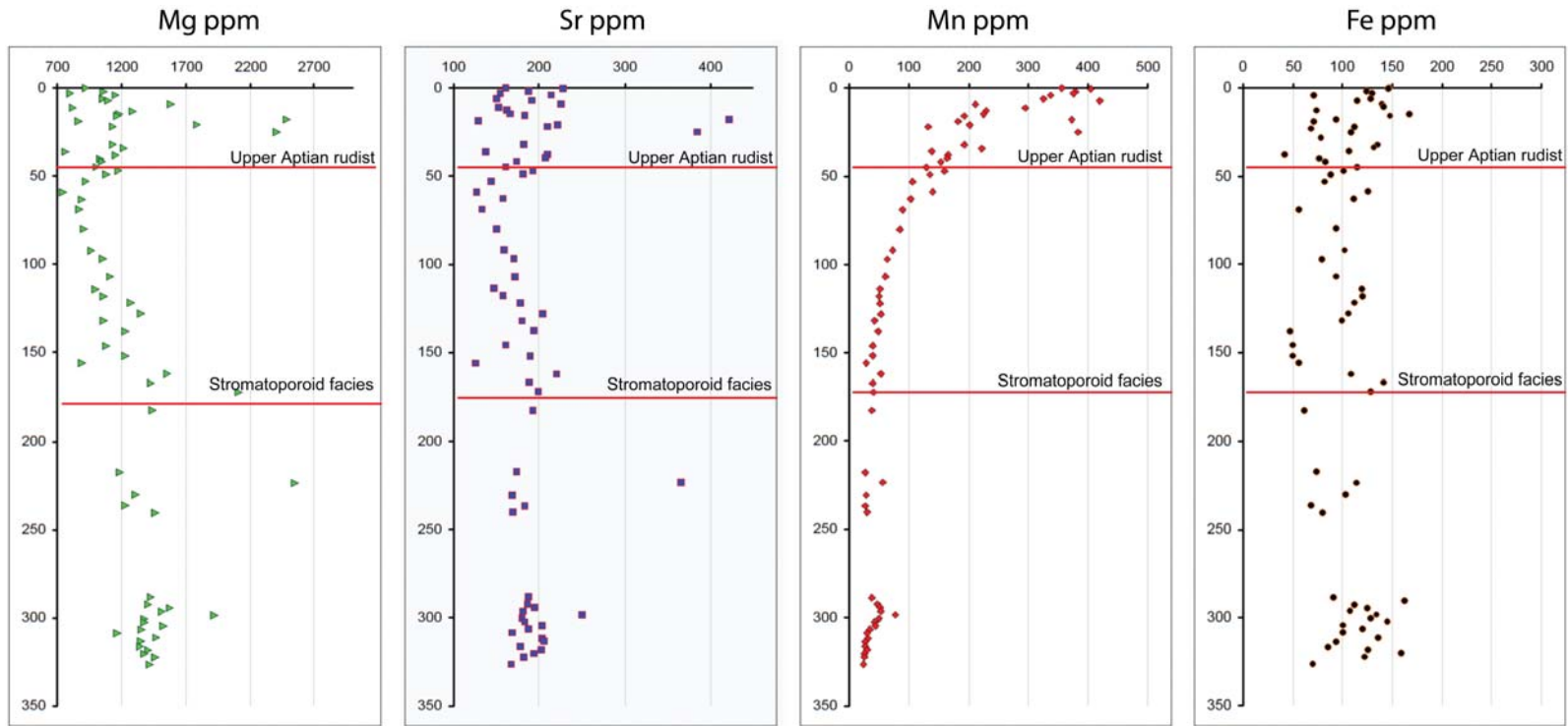


Figure 50. Trace elements from slope/shelf edge setting of Well-55 plotted against depth and superimposed by major sequence boundaries. This well records lateral facies changes associated with the Upper Aptian sequence. The Minimum Mn contents is the lowest among other wells.

in all wells corresponding to the pelagic mudstone facies. Mn values are relatively increasing along the stromatoporoids/coral facies and then rapid increase occurred at the upper Aptian rudist buildups facies.

Open Marine and Basinal Settings (Well-19)

Well 19 is located on the eastern flank of the field within the deep open marine setting (Figure 1). This well records the Upper Aptian prograding sequences 9 and 10 and is dominated by pelagic mudstone facies along with a dense argillaceous lowstand wedge that onlaps onto the Upper Shu'aiba unconformity. No rudist or grainy facies occurs in this well. The trace elements in this well are the highest of all the wells. Fe and Mn in this well have the highest mean values (131 ppm and 512 ppm respectively) of all wells and are positively correlated with similar patterns and a clear depletion trend from top to bottom (Figure 51). However, these higher values occur within the Upper Aptian sequence 10, whereas the lower part (which is open marine pelagic mudstone/wackestone) has values similar to the Lower Aptian sequences in the other wells. The argillaceous mudstone zone that represents the LST of the prograding sequence 10 does not record any particular trends or distinctive Fe or Mn values. However, major enrichment of Fe and Mn are recorded above the dense zone increasing to the maximum values at the top of the Shu'aiba Formation, similar to the trend recorded on the platform margin (Figures 49 and 50), but with higher values.

Sr and Mg contents in Well-19 also record the highest values of all wells and while their pattern is to become depleted with depth (Figure 51). In addition, Sr and Mg

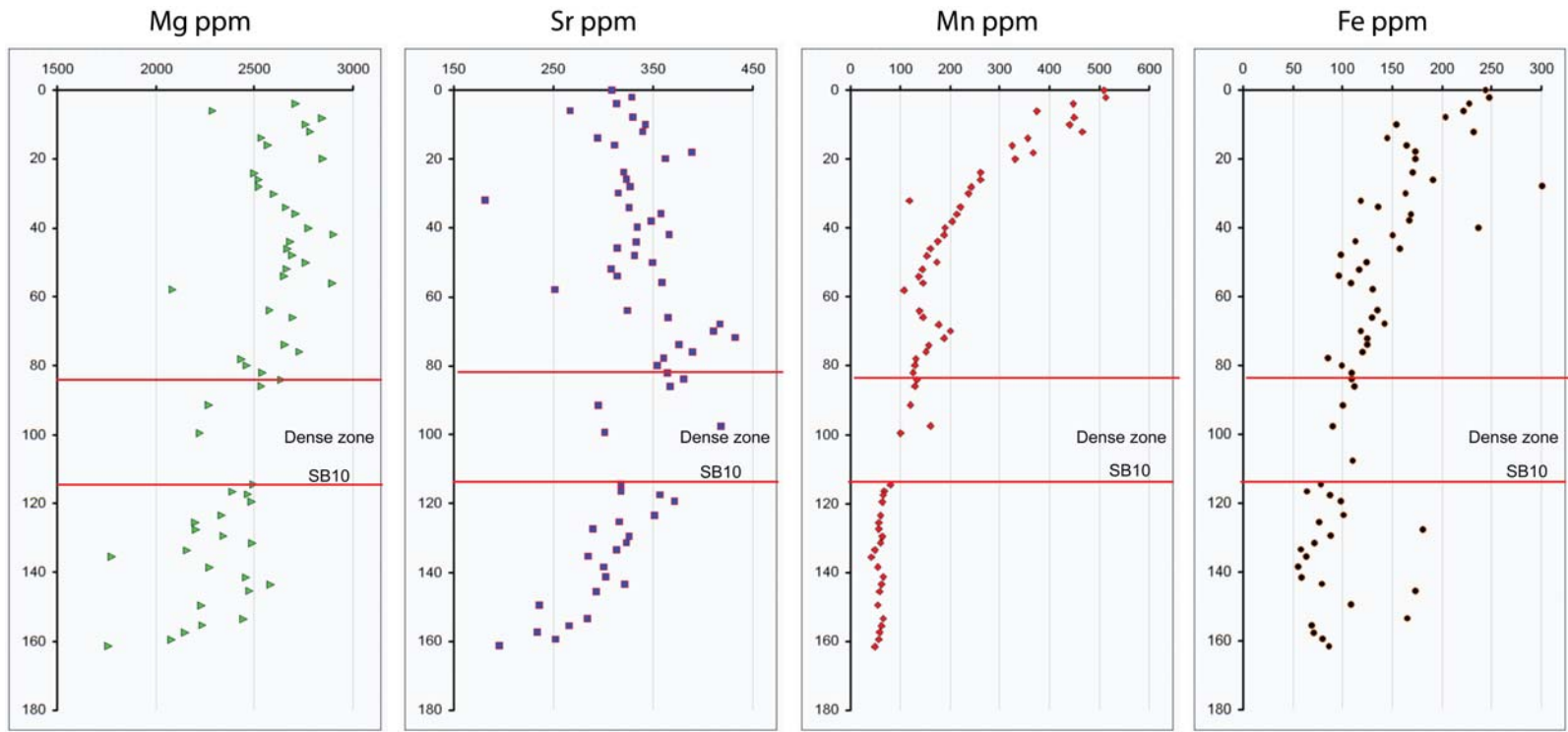


Figure 51. Trace elements from open marine setting of Well-19 plotted against depth. The dense zone in the middle part corresponding to the argillaceous mudstone marked the base of the Upper Aptian sequence 10.

have distinctive values associated with the dense argillaceous mudstone unit deposited as the lowstand wedge of the Upper Aptian sequence 10, where values tend to decrease in this zone.

Microprobe Analysis

In addition to the trace elements derived from the core plug analysis, 39 samples were analyzed by microprobe on eight thin sections for higher resolution of small-scale calcite cements and diagenetic features (Table 3; Figures 52 and 53). These eight samples (Figures 52 and 53) were taken from different depositional settings to investigate and identify the types and stages of cements, and their relationship with different Cathodoluminescence intensities (CL) zones to determine evidence of meteoric, marine or burial diagenesis.

Fe ranges from 0 to 554 ppm with an average of 87 ppm and lower detection limit of 0.010 wt%. The highest Fe value (554 ppm) occurs within the rudist fragments (Figure 52C). However, isopachous and blocky equant cements have relatively lower Fe content than micrite or rudist fragments, ranging from 100 to 159 ppm.

Mn ranges from 0 to 793 with an average of 121 ppm and lower detection limit of 0.010 wt%. Mn content of matrix, isopachous and blocky cements shows a wide variation. The matrix has the lowest values, isopachous cements have moderate values and blocky cements have higher values. The highest Mn value occurs within the large blocky cement between the rudist skeletal fragments (Figure 53B). The lowest Mn value (14 ppm) occurs within the skeletal grainstone of fore-bank setting (Figure 53A), in the

Table 3. Summary of microprobe analysis from eight thin sections of 39 samples. These thin sections were selected to represent different facies, stratigraphy and cements.

Samples	Mg ppm	Fe ppm	Mn ppm	Sr ppm	comments
7_405_pt01	2689.9	115.7	0.0	522.3	micrite rim
7_405_pt02	2542.9	0.0	62.1	652.9	cemented shell (possible original fabric)
7_405_pt03	2545.7	48.2	43.0	100.9	cemented shell
7_405_pt04	1755.8	0.0	0.0	0.0	intergranular cement
7_405_pt05	1758.7	0.0	14.3	261.1	intraskeletal cement fill (after moldic porosity)
7_405_pt06	1600.1	139.8	28.7	178.1	isopachous cements at edges
7_405_pt07	1804.8	77.1	28.7	267.1	micrite within peloids
9_111_pt01	614.1	48.2	162.5	136.5	intergranular cement
9_111_pt02	495.9	0.0	119.5	142.4	intraskeletal cement
9_111_pt03	660.2	154.3	0.0	136.5	dissolved cements at skeletal edge
9_111_pt04	351.7	159.1	148.2	136.5	blocky intergranular cement
9_111_pt05	752.5	4.8	124.3	231.5	dissolved cements at skeletal edge
18_112_pt01	1320.4	24.1	234.2	284.9	intergranular cement
18_112_pt02	743.8	0.0	148.2	243.3	micrite skeletal grains
18_112_pt03	1357.9	0.0	0.0	1044.6	cements, but with brown color (possible original)
18_112_pt04	550.7	110.9	157.7	314.6	blocky cements fill of possible large skeletal grains
14_5176_pt01	1092.7	192.8	76.5	47.5	micrite matrix, fine grains
14_5176_pt02	1320.4	173.5	148.2	207.7	micrite matrix, fine grains
14_5176_pt03	913.9	67.5	95.6	0.0	isopachous cements at edge
14_5176_pt04	1294.5	554.4	0.0	184.0	rudist shell cemented with precursor shell
14_5176_pt05	997.5	67.5	90.8	166.2	micrite matrix, fine grains
14_5176_pt06	1040.8	380.8	200.7	106.8	possible stylolites matrix between rudists
15_291_pt01	1323.3	101.2	86.0	338.3	micrite matrix, fine grains
15_291_pt02	1787.5	159.1	0.0	320.5	skeletal rudist shell
15_291_pt03	1265.7	96.4	348.9	427.3	isopachous cements at edge
15_291_pt04	1801.9	48.2	253.3	201.8	blocky cements fill within rudist
4_37_pt01	1706.8	4.8	0.0	955.6	large skeletal grains, partially dissolved
4_37_pt02	1023.5	0.0	0.0	65.3	blocky calcite fill within intergranular porosity
4_37_pt03	781.3	168.7	62.1	249.3	matrix fill, fine micrite
4_37_pt04	1023.5	9.6	66.9	0.0	cemented coral
16_4761_pt01	738.1	19.3	66.9	249.3	cemented skeletal grains
16_4761_pt02	893.8	4.8	95.6	59.4	cements between grains
16_4761_pt03	397.9	28.9	162.5	23.7	large cements between grains
16_4761_pt04	5.8	72.3	0.0	2285.0	cemented skeletal grains
9_11_pt01	1412.7	53.0	234.2	421.4	<i>Agruipura</i> rudist, possible original cement
9_11_pt02	1776.0	33.7	162.5	433.3	<i>Agruipura</i> rudist, possible original cement
9_11_pt03	1822.1	96.4	793.4	338.3	large blocky cement fill
9_11_pt04	2300.7	62.7	0.0	1056.4	<i>Agruipura</i> rudist, possible original cement
9_11_pt05	1306.0	115.7	530.5	231.5	micrite matrix with some cements
Detection limit	0.020 (wt%)	0.010 (wt%)	0.010 (wt%)	0.020 (wt%)	lower detection limit (wt%)
Mean	1271.1	87.0	121.7	333.9	
Minimum	5.8	0.0	0.0	0.0	
Maximum	2689.9	554.4	793.4	2285.0	

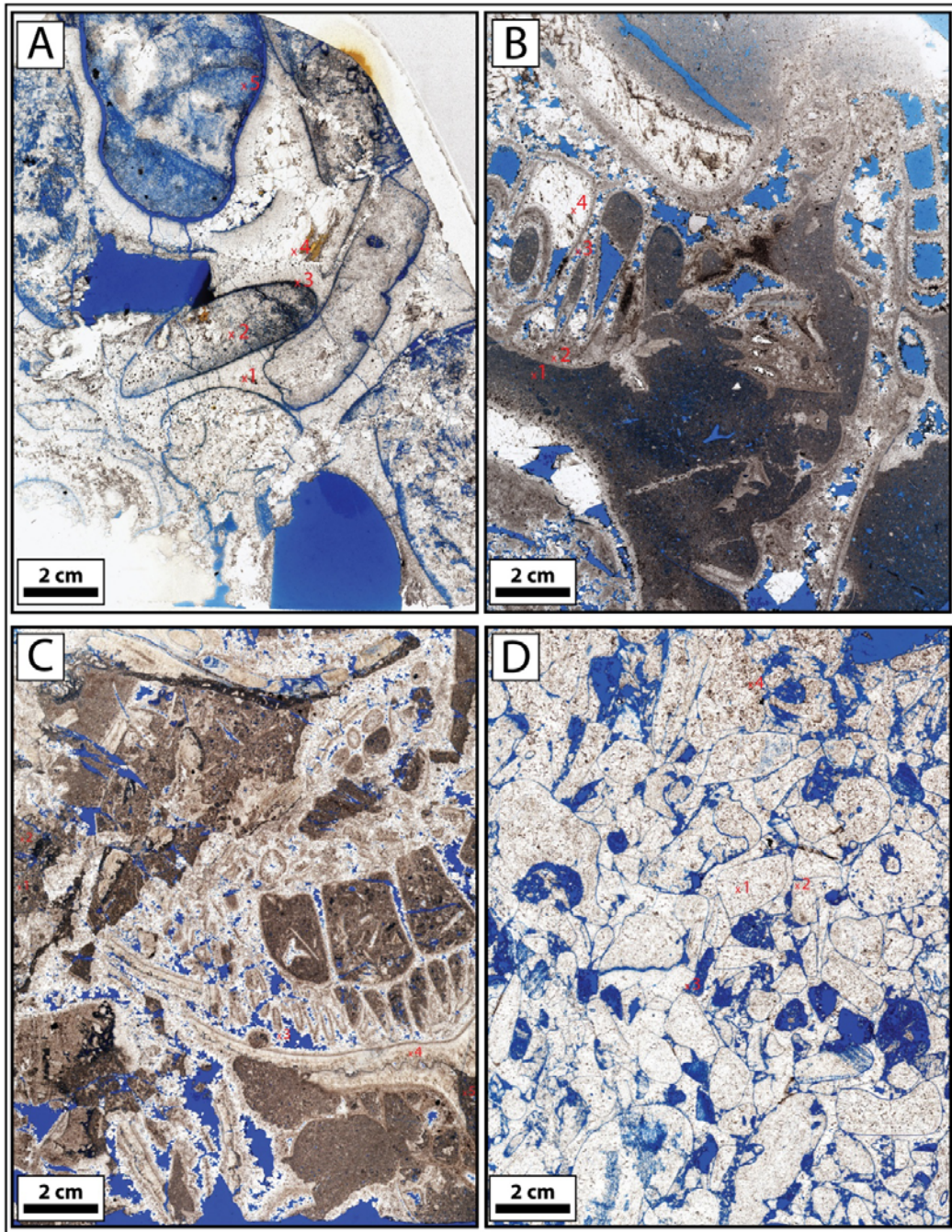


Figure 52. Thin sections samples of different cements show the location of the microprobe analysis. (A) is from rudist rudstone facies on the eastern margin. (B) is from rudist floatstone of the back bank setting. (C) is rudist fragmented rudstone facies of the western margin. (D) is from rudist debris grainstone facies near subaerial exposure surface SB 7.

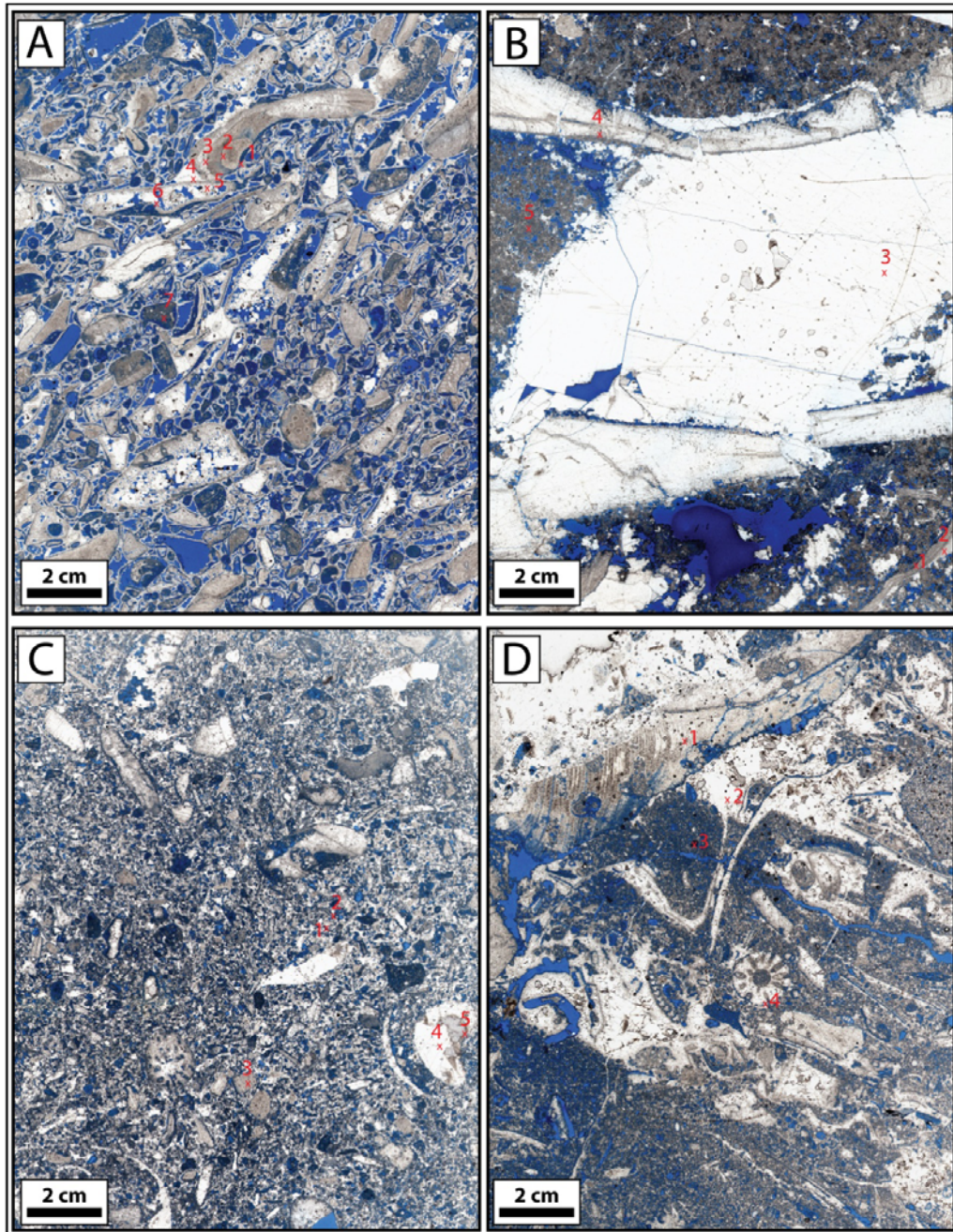


Figure 53. Thin sections samples of different cements show the location of the microprobe analysis. (A) is from rudist skeletal grainstone facies on the intraplatform depression (channel). (B) is from *Agriopleura* rudist floatstone of the shallow lagoon in the upper part of the Shu'aiba Formation. (C) is from skeletal peloidal packstone facies of slope and shallow open marine settings. (D) is from coral skeletal packstone facies of the lower part of the Shu'aiba Formation. cements filling the intraskeletal porosity.

Sr contents range from 0 to 2285 ppm with an average of 333 ppm and lower detection limit of 0.020 wt%. Generally, Sr of calcite cements are much higher than the matrix values. The highest Sr value (2285 ppm) occurs within the rudist debris grainstone facies of the beach environment at the top of the rudist buildup (Figure 52D). However, comparing this value with other lower Sr values in this rock, this value seems to be affected by the presence of pyrite (dark brown) rather than a clean calcite cements. The presence of pyrite has an impact on pore fluids by lowering the redox potential over clean calcite cements (Grover and Read, 1983). The highest group of Sr values (900 and above) correspond to the Low Magnesium Calcite (LMC) skeletal rudist shells (Figure 53B).

Mg ranges from 5 to 2689 ppm with an average of 1271 and lower detection limit of 0.020 wt%. Mg contents of cements are relatively lower than the micrite or skeletal fragments. The highest Mg value (2689 ppm) occurs in the micrite rim of the shell. Rudist fragments also have higher Mg values (e.g Well-18 points 2 and 3, well-506-11 points 4; Table 3; Figures 53A and B).

Cathodoluminescence (CL)

Diagenesis in carbonate rocks commonly is difficult to determine by just using plane light microscopy. Therefore, CL is used to provide low-cost and powerful analytical processes for determining the origin and development of cements (Fairchild, 1983). CL needs to be calibrated with other data such as trace elements and isotopes to determine the diagenetic history. Mn concentration is the most important activator of luminescence in carbonate rocks, whereas Fe is the most important quencher element.

Mn contents of 15 - 30 ppm are sufficient to activate luminescence in calcite if total Fe contents are below about 150 ppm (Hans, 2000). The intensity of the luminescence is controlled by the absolute amount of Mn and not by the Fe/Mn ratios (Have and Heignen, 1985).

CL data of the Shu'aiba Formation were analyzed from eight thin sections (Figures 52 and 53) to define different diagenetic phases, particularly within calcite cements and rudist skeletal fragments. Mud matrix of the Shu'aiba Formation generally is dominated by non-luminescent (NL) and in some cases weak luminescence, reflecting low Mn values associated with these zones. Calcite cements within the Shu'aiba Formation show subtle to moderate variations of luminescent intensities related to different cement phases of. These phases range from NL-moderate bright-high bright luminescent (Figures 54 - 56). Dull luminescent zones are less abundant and occur as thin layers at the edge of blocky calcite cements. Rudist fragments and its associated cements represent good locations for identifying multiple diagenetic phases. Four to five different diagenetic phases (zones) were determined within the *Agriopleura* rudists within on the upper Shu'aiba Formation S7 and S8 (Figure 54).

1. Zone 1 is NL phase occurred within part of the rudist fragments (No.1; Figures 54B and D).
2. Zone 2 is moderate bright and occurred as a micrite rim on the edge of the rudist (No. 2; Figure 54B).
3. Zone 3 occurred within the micritized peloidal grains of the matrix and is moderate bright with similar intensities to the previous zone (No. 3; Figure 54B).

4. Zone 4 occurred on the clear blocky calcite that filling the intergranular porosity. This zone has bright CL and can easily be distinguishable from of previous zones (No. 3; Figure 54B).
5. Zone 5 is the latest stage occurring within fractures that cut the rudist fragments and filled with calcite (No.5; Figure 54D). It has bright CL and can only be observed with cathodoluminescence.
6. In addition, the internal structure of the rudist fragments have bright CL associated with the precursor foliated fabrics (Figure 54D).

The high-energy caprinid *Offneria* rudist formed at top of rudist buildups records only two CL zones 1 and 2 (Figures 55A and B). Zone 1 is moderate bright occurred in the internal micrite sediments within the rudist cavity, whereas zone 2 is a bright CL forming in the fringing cements within the intergranular porosity.

Rudist skeletal grainstone within the intraplatform depression (Figures 55C and D) records at least four stages of diagenesis. Zone 1 is NL occurring within the micrite grains. Zone 2 is moderate bright luminescent in the fringing isopachous cements filling the intergranular porosity. Zone 3 is dully luminescent occurs in the large blocky cements filling the vugs and cavity. Zone 4 is bright cements representing the last stage cementation. These four stages of CL also recorded within the rudist rudstone facies of the shoal complex (Figure 56), with one additional stage (zone 5) that is a thin dull luminescent at the edge of the blocky calcite cements (No. 5; Figure 56B).

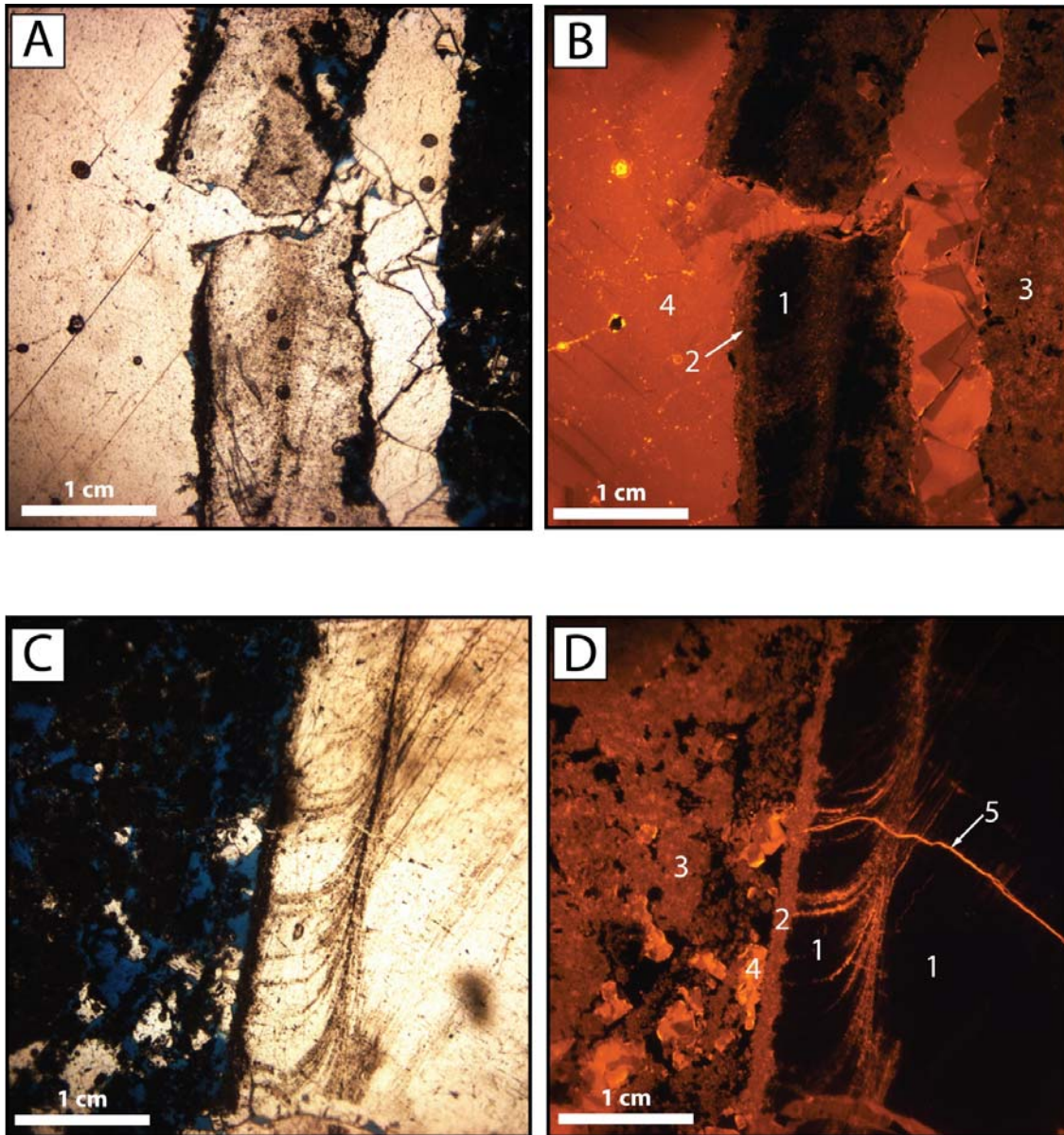


Figure 54. Plain light and Cathodoluminescence petrography zones of rudist fragments within rudist buildups. (A) Plain light of rudist fragment and blocky calcite fill. (B) Four CL zones; zone 1 is NL; zones 2 and 3 are moderate bright luminescent and zone 4 is bright luminescent. (C) Plain light of rudist shell. (D) Five CL zones; zone 1 is NL; zones 2 and 3 are moderate bright luminescent; zone 4 is bright luminescent and zone 5 is bright luminescent within fracture fill.

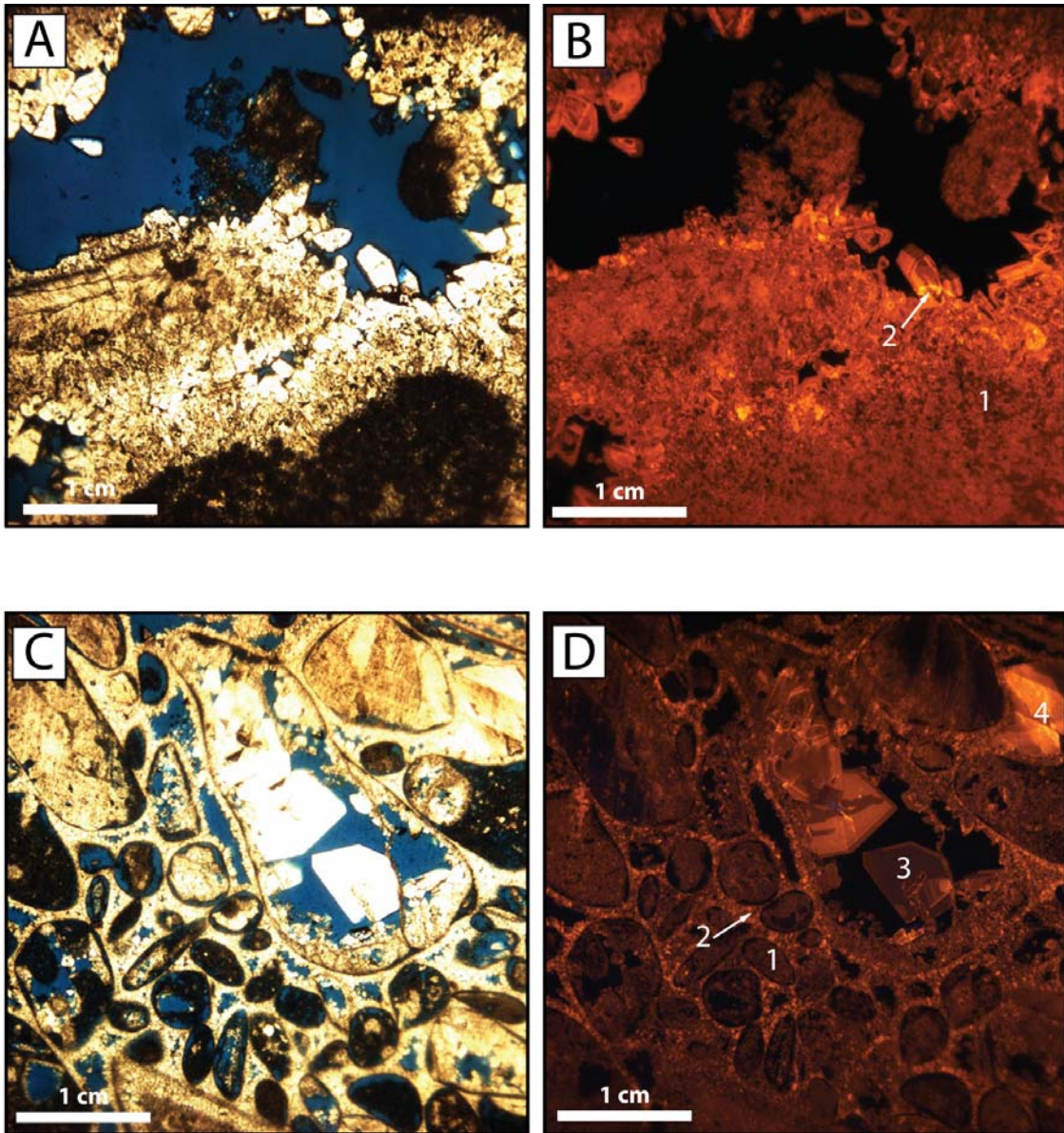


Figure 55. Plain light and Cathodoluminescence petrography zones of rudist fragments within rudist facies and slope setting. (A) Plain light of cemented rudist. (B) Two CL zones; zone 1 is moderate bright luminescent and zone 2 is bright luminescent. (C) Plain light of skeletal peloidal grainstone. (D) Four CL zones; zone 1 is NL; zone 2 is moderate bright luminescent; zone 3 is dull luminescent and zone 4 is bright luminescent.

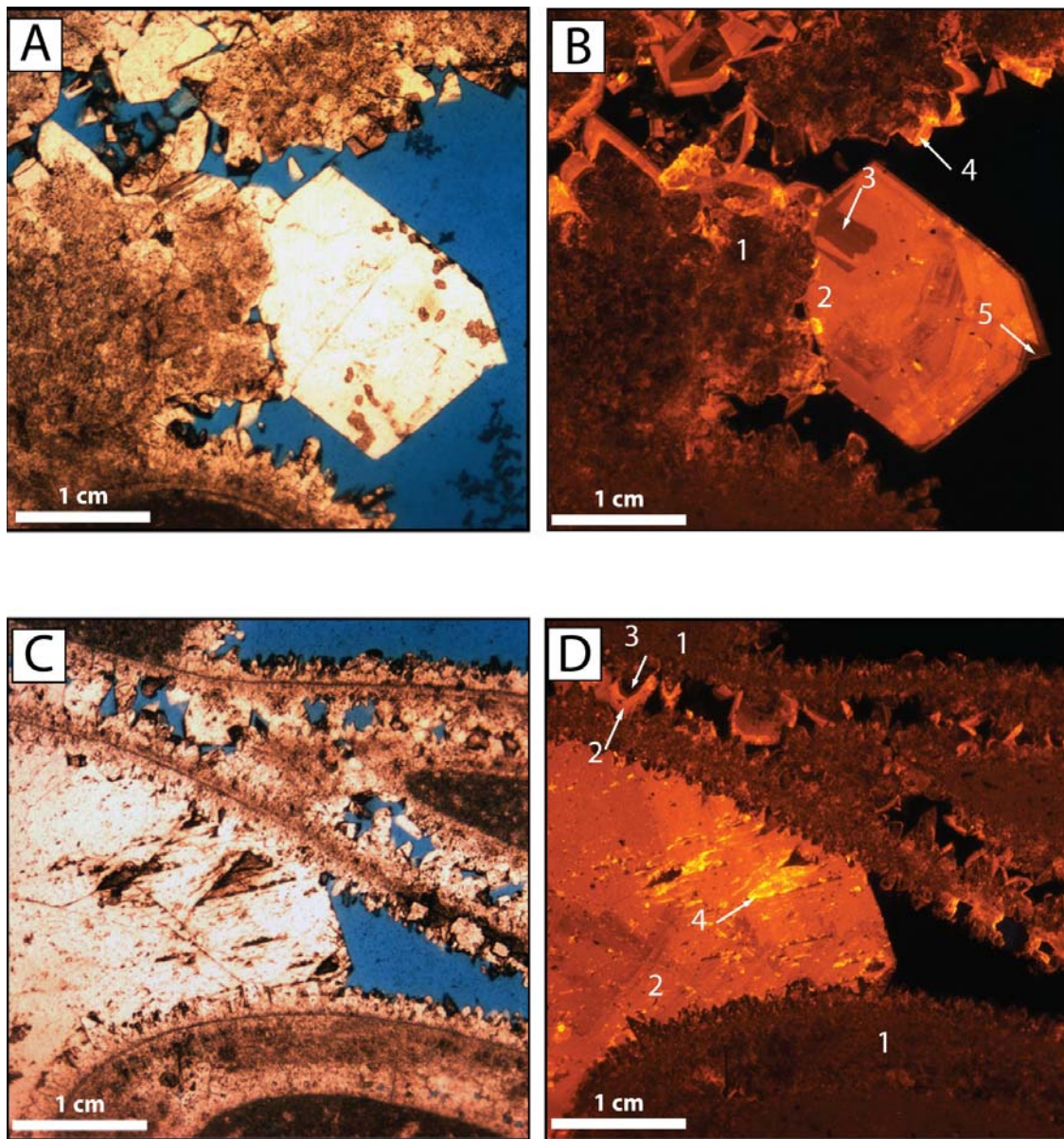


Figure 56. Plain light and Cathodoluminescence petrography zones of large blocky calcite. (A) Plain light of cemented rudist rudstone and large blocky calcite. (B) Five CL zones; zone 1 is NL; zone 2 is moderate bright luminescent; zone 3 is dull luminescent; zone 4 is bright luminescent and zone 5 is thin dull luminescent. (C) Plain light of cemented rudist rudstone and large blocky calcite. (D) Four CL zones; zone 1 is NL; zone 2 is moderate bright luminescent; zone 3 is dull luminescent and zone 4 is bright luminescent.

Isotope Geochemistry

A total of 137 micro-drill samples were collected to determine their carbon and oxygen stable isotope values of the calcite cements and other diagenetic features from eight wells representing different facies, diagenetic and depositional environments. A total of 2,397 samples (whole rock) were collected from 26 wells mainly to analyze and interpret the chemostratigraphy of the Shu'aiba Formation (AL-Ghamdi and Pope, 2013), but they will only be used here to compare with the cement values and to understand the diagenesis of the micro-rhombic calcite. Figure 57 shows a plot of all carbon and oxygen isotope data of both cements (red) and mud matrix (blue).

Carbon Isotope

The carbon isotope values of mud matrix range from 1.5 to 6.1‰ with minimal diagenetic effects. However, these values are higher than the standard pelagic record of Northern Tethys that range from 1.5 to 4‰ (Föllmi et al., 1994).

Carbon isotope values of the calcite cements range from 1.2 to 5.5‰ with an average of 4.4‰ (Figure 57). The minimum carbon isotope value of the cements (1.2‰) occurs within a fracture filled by pyrite and calcite. The heaviest carbon isotope value of the cements (5.5‰) occurs within the cemented rudist facies at top of the rudist bank-crest, beneath subaerial exposure surface SB7. Carbon isotope values of cements show more uniform clustering, have narrower variations and are similar to the carbon isotope values of the matrix; the majority of carbon isotope data plotted between 4 - 5‰ (Figure 57). This narrow range are clustered within the isotope values of shallow environments

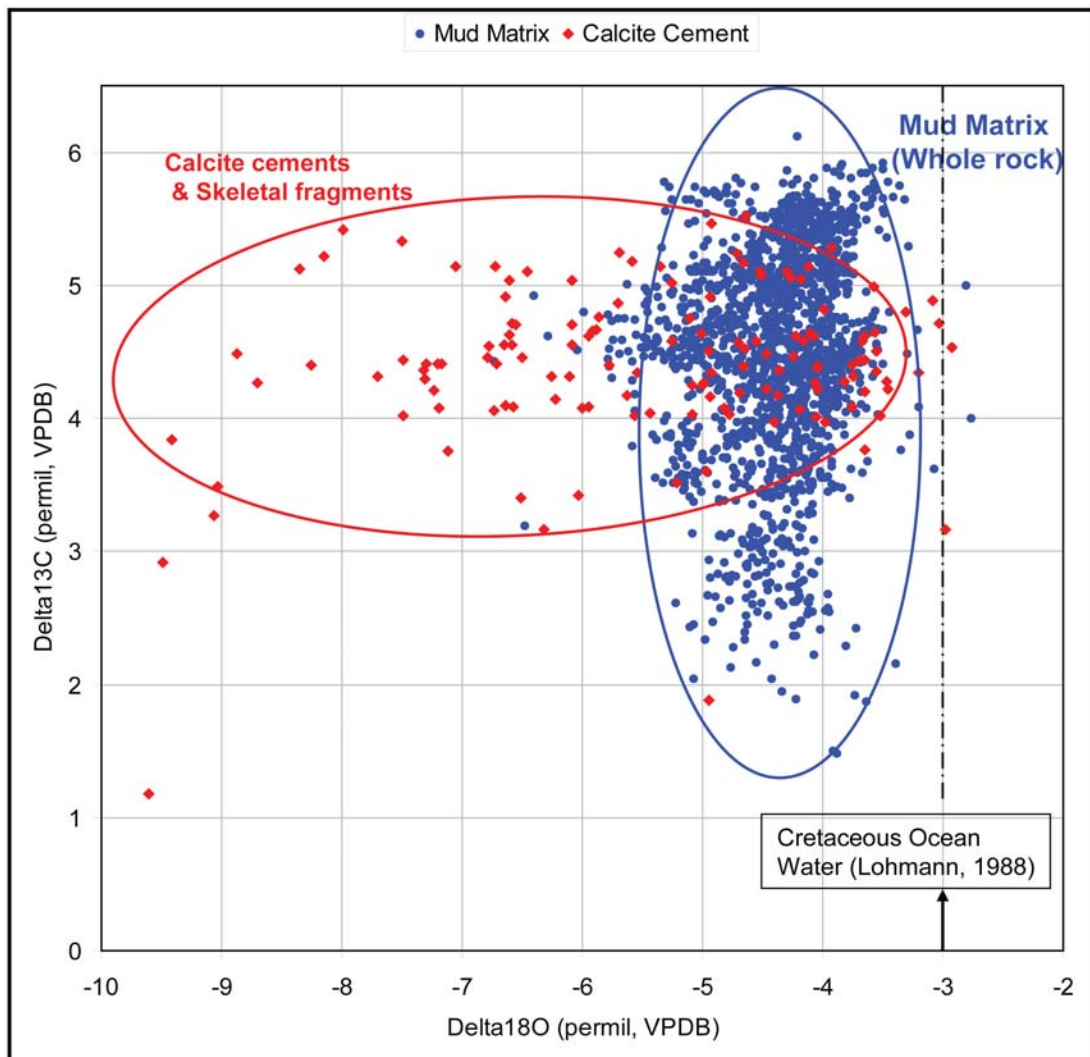


Figure 57. Cross plot of carbon and oxygen isotope data of both mud matrix (blue) and cements (red). Mud matrix values are uniform in $\delta^{18}\text{O}$, but have wide variations of $\delta^{13}\text{C}$. Cement values are uniform in $\delta^{13}\text{C}$ but have wide variation of $\delta^{18}\text{O}$.

rudist buildups of sequences 3 to 5 (Al-Ghamdi and Pope, 2013).

Oxygen Isotope

Oxygen isotope values of the matrix range from -6.7 to -2.7‰ and they were likely influenced by meteoric diagenesis (Al-Ghamdi and Pope, 2013; Figure 57). The estimated original oxygen isotope value of the Cretaceous ocean water is ~ -3‰ (Lohmann, 1988), therefore the Shu'aiba Formation oxygen isotope values of the mud matrix are depleted by 1 - 2 ‰ relative to the original ocean value. Oxygen isotope values of the calcite cements ranges from -9.6 to -2.9‰ with an average of -5.4‰ (Figure 57). The minimum oxygen isotope value (-9.6‰) occurs within a fracture filled pyrite and calcite, associated with the minimum carbon isotope value (1.5‰). The heaviest oxygen isotope value (-2.9‰) occurs within the rudist buildups of the platform margin. In contrast to the carbon, oxygen isotope values record major depletion with wide variations that ranges from -3 to -9.5‰, indicating locally strong diagenetic influence.

Strontium Isotope

Thirty samples were collected for strontium isotope analysis of the micro-rhombic mud matrix in the Shu'aiba Formation (Figure 58). The $^{87}\text{Sr}/^{86}\text{Sr}$ values range from 0.707355 to 0.707454 with an average of 0.707389. This data fall within the range of Sr isotope of the Cretaceous seawater (Bralower et al., 1997) and are similar to the values of 0.7040 and 0.70744 reported by Moshier (1989) and the value of 0.70749

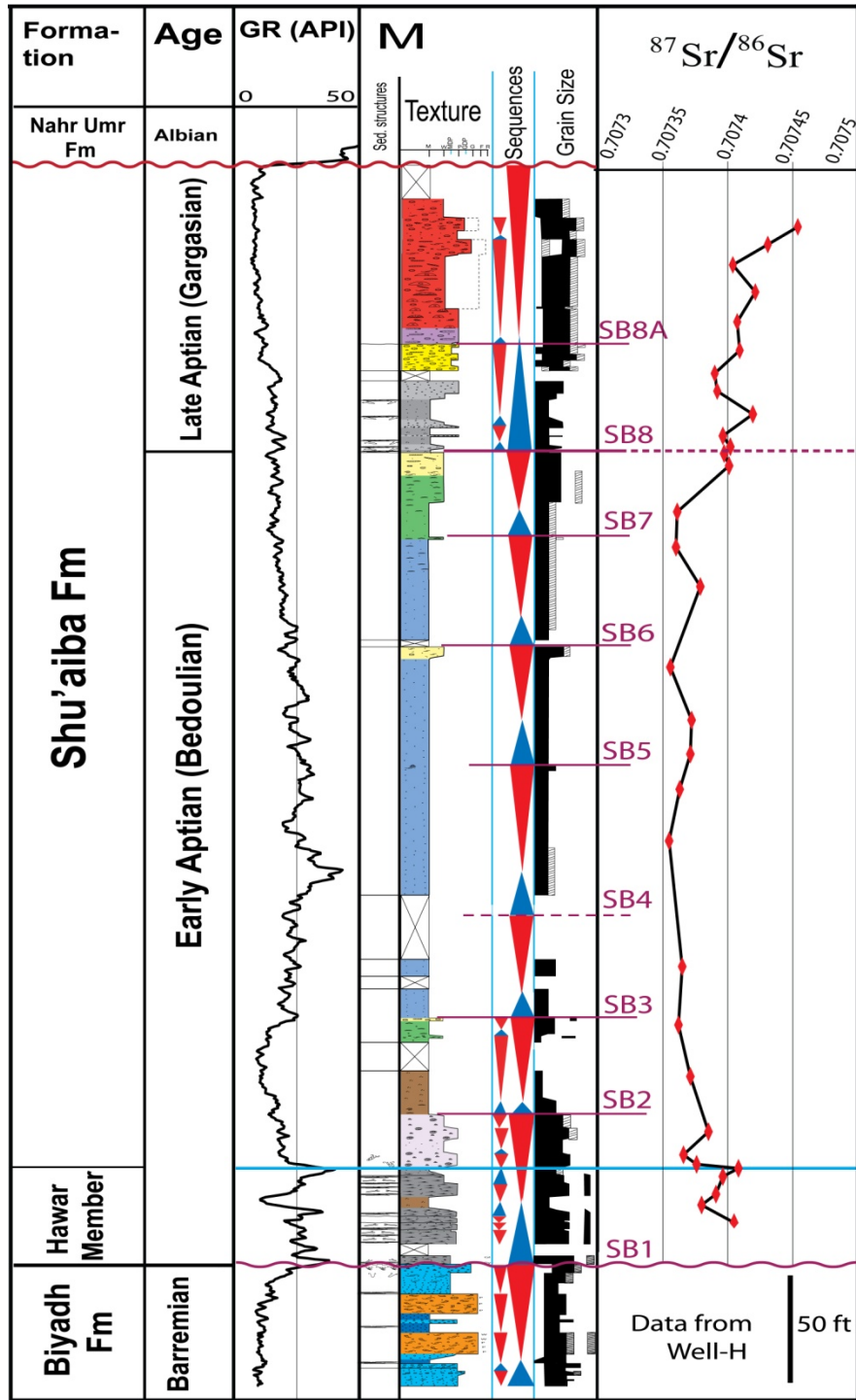


Figure 58. Strontium isotope curves ($^{87}\text{Sr}/^{86}\text{Sr}$) linked to core descriptions and sequence stratigraphy. Fluctuations of $^{87}\text{Sr}/^{86}\text{Sr}$ curve possibly reflect changes in ocean signatures.

reported by Budd (1989) for the coeval Thammama Formation.

Discussions

Trace Elements

Trace elements are used to analyze the diagenetic history, where the increase of diagenetic alterations are related to the elemental decrease of Sr and Mg and increase in Fe and Mn (Brand and Veizer, 1980). Sr and Mn elements are the most important diagenetic indicator, because of their widely divergent partition coefficient with their large composition and differences in marine and meteoric waters (Brand and Veizer, 1980).

The trace elements of the Shu'aiba Formation both matrix and cements are generally low indicating homogenous carbonate sediments. Fe and Mn contents possibly represent the original sediment with no additional values added during diagenesis. The lower Fe and Mn contents suggest that the sediment were formed in oxidizing environments where Mn and Fe are not incorporated into calcite crystals (Grover and Read, 1983). Sr and Mg content in the Shu'aiba Formation samples are very low compared to the original Cretaceous sea water (Steuber and Veizer, 2002) or modern carbonate rocks (Budd, 1998). The low Sr and Mg contents indicates their removal from the sediments during diagenesis. These lower values, particularly Fe suggest that Shu'aiba Formation was affected by pore fluids in oxidizing environments within a meteoric vadose or phreatic environment rather than deep burial or subsurface environments. The low Fe also indicates that original sediments had low values and additional Fe was not added during the diagenetic history as Fe of reducing

environments in burial diagenesis should be in order of ~1000 ppm or higher (Drever, 1982).

The relatively high Mn values recorded in the *Lithocodium*-dominated facies (Figure 48) are related to the dense, massive and platy coral heads that have large calcite spar crystals. Major increase of Mn from ~80 ppm to ~170 ppm associated with decrease of Sr and Mg (Figures 48 and 49) is often recorded where rudist buildups facies developed, reflecting a major change in both depositional and diagenetic history, where high porous and permeable zones allowed fluids to migrate freely resulting in extensive recrystallization and cementation.

Figure 59 (A,B,C and D) comparing and correlating each individual trace element from all wells to evaluate the effect of different depositional settings on diagenesis history. Fe curves are generally homogeneous with a mean value of 100 ppm, however Fe contents tends to decrease slightly with depth from top to base (Figure 59A). Mn has similar trends to Fe, but shows more pronounced enrichment near the top of the Shu'aiba Formation. The major change of Mn occurred above SB7, where the values are dramatically increased to its maximum value below the top of the Shu'aiba Formation. The karst formed during exposure of the upper part of the Shu'aiba Formation plays an important role as a conduit that enables meteoric waters to migrate. The increases of Fe and Mn in the upper part of the Shu'aiba Formation may be linked to karsting observed in this well that penetrated at least 30 feet below the top Shu'aiba unconformity (AL-Ghamdi and Read, 2010). Meteoric waters normally have low Mn and Fe contents, but their increase recorded here may be an indication of a rock-buffered system that added Mn and Fe to the meteoric waters (Brand and Veizer, 1980). Although some positive

correlation occurs between Fe and Mn values (Figure 59A and B), plotting Fe against Mn from all wells does not show a clear linear relationship (Figure 60), except Well-6 on the platform interior that shows some relationship associated with the lowest values of Mn and Fe in all wells.

The mean value of Mn in all data is about 112 ppm which is compatible with the initial estimated values of the Shu'aiba Formation (Budd, 1989). The lower Mn and Fe values were recorded at the base of the section associated with the chalky mudstone facies. These lower values are probably inherited from the original sediments and indicate lack of abundant Fe or Mn in the pore fluids during the recrystallization of this unit (Budd, 1989). The low Mn values also reflect the dominant micro-rhombic calcite crystals within these facies that underwent extensive recrystallization with dominant micro-rhombic calcite without any large equant or blocky calcite cements. Rudist buildups record an increase of Mn from ~80 ppm to ~170 ppm (Figure 48) corresponds to the development of the rudist buildups facies, reflecting major change in both depositional and diagenetic history. These rudist units record extensive dissolution and cementation stemming from the local subaerial exposure surface at the top of the rudist buildups (SB 7). However, above this exposure surface, Fe and Mn contents tend to decrease corresponding to the flooding surface with mud-dominated facies along with less diagenetic alterations.

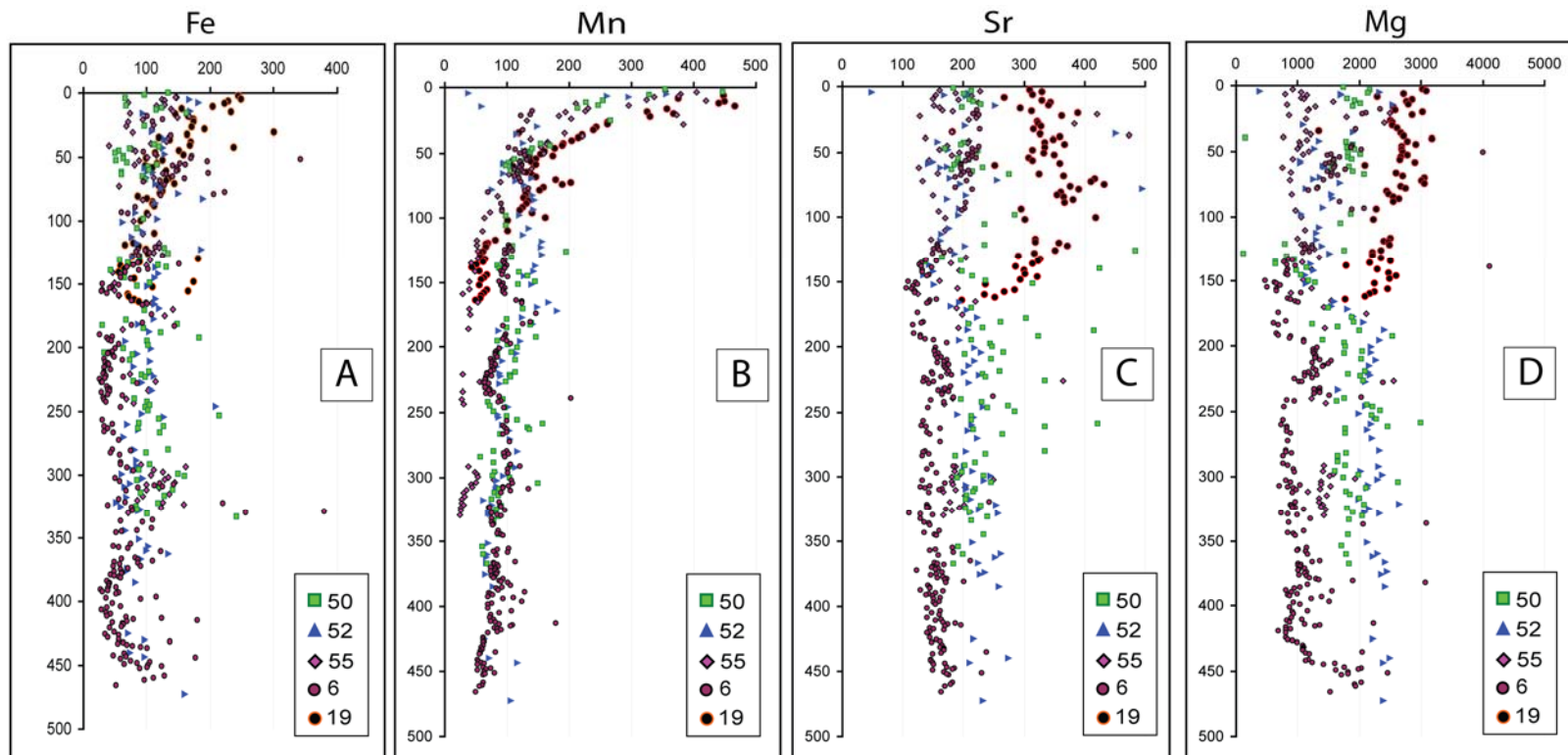


Figure 59. Major trace elements from different wells plotted against depth. (A) Fe contents plotted against depth of all five wells. The curves are generally uniform, with subtle depletion with depth. (B) Mn contents plotted against depth of all five wells. The curves show good correlation with a pronounced depletion trend with depth. (C) Sr contents plotted against depth of all five wells. Well-19 has major enrichment in the upper part associated with Upper Aptian sequence 10. (D) Mg contents plotted against depth of all five wells. Well-19 also increases in the upper part associated with Upper Aptian sequence 10.

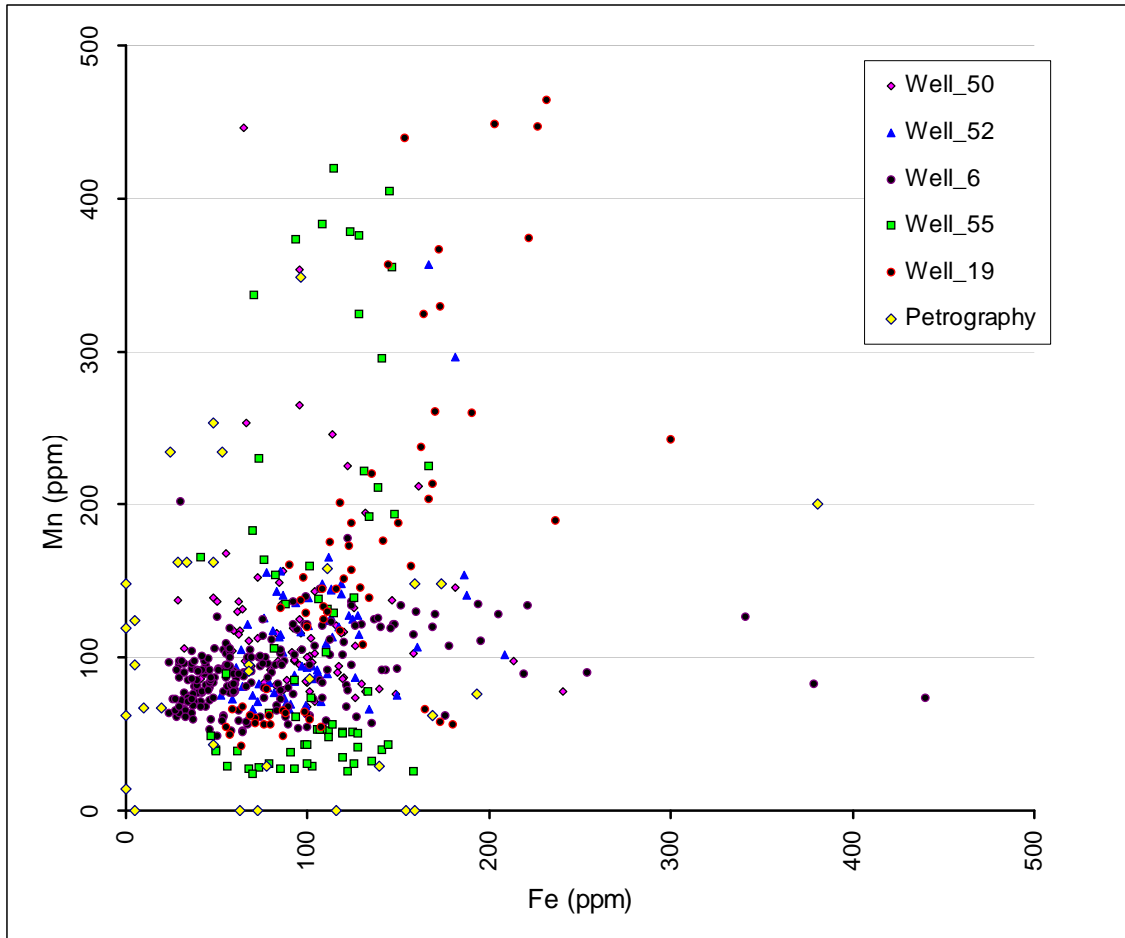


Figure 60. Cross plot of Fe and Mn from all data. No clear relationship between Fe and Mn in most wells, except Well-6 that show moderate relationship.

The Upper part of the Shu'aiba Formation records a dramatic increase of Mn in all wells associated with smaller changes in Sr and Mg that indicates a direct influence of the subaerial unconformity at top of Shu'aiba Formation. Lateral facies changes do not seem to affect the Mn and Fe values much, because the general increase of Mn and Fe patterns at the upper part occurred amongst all wells along the depositional settings including the open marine setting. This indicates that similar Fe and Mn of pore fluids chemistry affected the Shu'aiba Formation regardless of the lateral facies changes or changes in depositional settings. However, the larger increases of Mn in the upper part of the Shu'aiba Formation are recorded within open marine settings (Wells 55 and 19) (Figure 59B). This large increase of Mn values may indicate that the Upper Aptian sequences of Wells 55 and 19 may be affected by different pore fluids than the marginal settings.

Sr and Mg content of Shu'aiba Formation generally are low suggesting severe depletion during diagenesis. It was suggested that the initial Sr value of Shu'aiba was approximately 1000 ppm (Swart and Lindsay, 2002). The lower Sr concentration of the Shu'aiba Formation implies either the fluids in this unit had a lower Sr/Ca ratio than Cretaceous seawater or they formed under different temperature (Swart and Lindsay, 2002). Alternatively, the low Sr is due to the enrichment in Ca and lowering and flushing Sr of fluids during recrystallization of the Shu'aiba Formation by unconfined meteoric waters (Budd, 1989). The extensive removal of Sr and Mg must have occurred before the formation of micro-rhombic calcite that required many pore volumes of water to

remove the Sr, which suggest diagenesis formed under high water/rock ratio conditions in a diagenetic system open to fluid flow (Budd, 1989).

Sr and Mg are positively correlated to each other (e.g. Figures 49 and 50) with a linear relationship (Figure 61). This linear relationship indicates they shared a similar diagenetic history that removed them from the original lime mud during stabilization by dissolution/reprecipitation (Moshier, 1989). Sr and Mg are inversely correlated with Mn, indicating that increased Mn content was not emplaced until Sr had been removed from the sediments (Budd, 1989).

The general pattern of Sr and Mg that increased with depth (enriched at the base and depleted locally in top and mostly in the middle) is probably related to the severe influence of meteoric diagenesis from the unconformity on the upper part of the Shu'aiba Formation comparing to the less affected deeper units. In addition, the rudist buildups facies undergone extensive dissolution and cementation including local subaerial exposure surfaces at the top of the rudist buildups. Thus, Sr and Mg tends to decrease at rudist buildup zones compared to other units (e.g Figures 48 and 49).

Well-19 within platform edge and open marine settings (Wells-55 and 19) records different Sr and Mg profiles. Above the stromatoporoids facies of Well-55, trace elements are more depleted compare to other wells. This depletion may be related to facies control that are unique in this well compared to other wells. This unit contains stromatoporoids and rudist facies that are more susceptible to meteoric diagenesis, with higher primary porosity that enhanced hydraulic flow of fluids through the upper part of the Shu'aiba Formation. Well-19 in the open marine setting records the highest values of

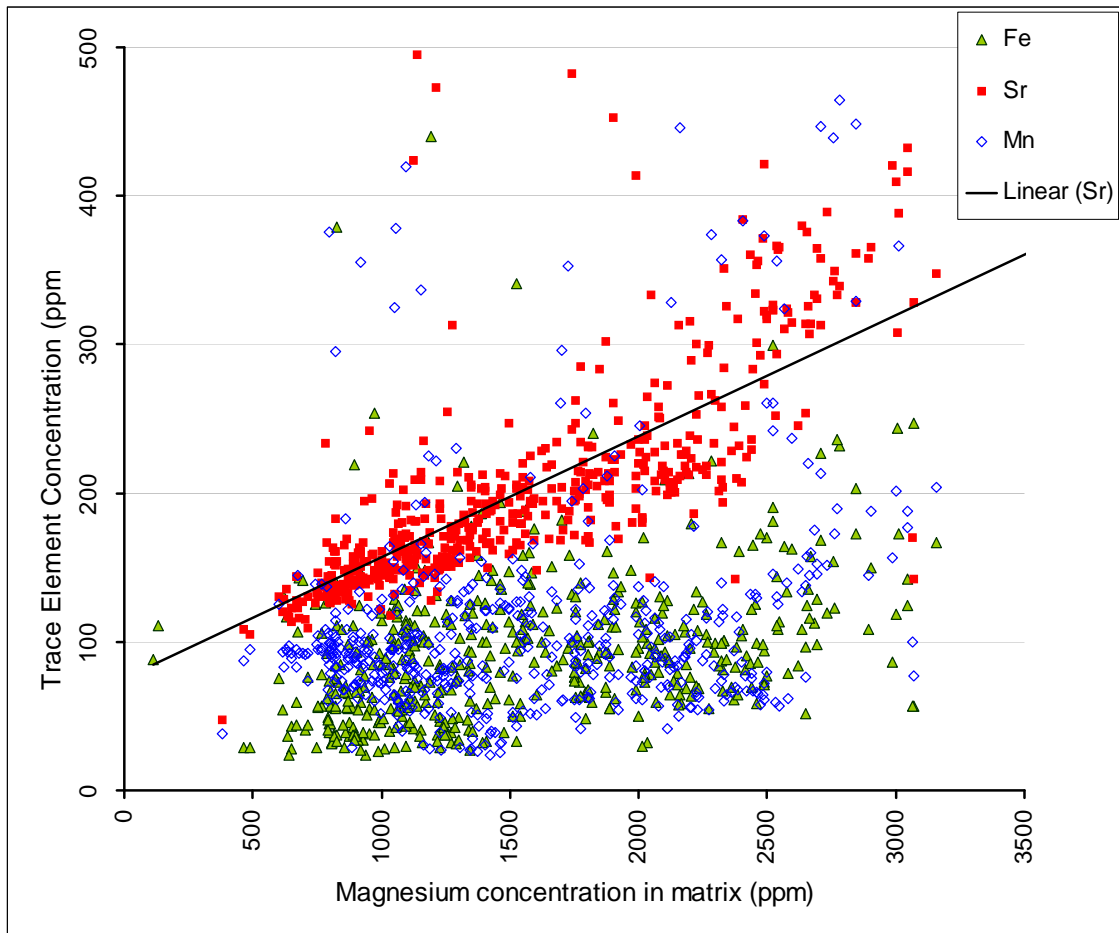


Figure 61. Magnesium concentration plotted against concentrators of Fe, Sr and Mn. Strong linear relationship occur between Mg and Sr.

Sr and Mg, presenting a gap in the pattern within the upper part of the section between the open marine and marginal settings (Figures 59C and D). This difference in trend and pattern indicates a different diagenetic history between these two settings, possibly related to the original depositional textures with their different porous matrix. The higher the porous matrix in the marginal setting (e.g Well 6 and 52), the lower the Sr and Mg. Conversely the lower the porous matrix within the deep open marine setting (e.g Well 19), the higher the Sr and Mg. In addition, the higher values of Sr and Mg in Well 19 are associated with the Upper Aptian sequences, that are diachronous compared to the Lower Aptian units marginal setting. Therefore, the increase of trace element contents particularly Sr and Mg are to some extent influence by the difference lithofacies and depositional settings.

The Vanadium (V) is only analyzed in Well-6 in the platform interior/rudist buildup setting. Two extreme values of V were recorded at SB 3 and SB 6. SB 3 records a major facies change from chalky *Palorbitolina* mudstone to coral/rudist rudstone facies, but without evidence of an exposure surface. On the other hand, SB 6 records a pronounced subaerial surface at the top of the rudist rudstone facies. Therefore, the Vanadium spikes may be associated with sequence boundaries, but not necessarily with subaerial exposure surfaces.

Microprobe Analysis

The microprobe analysis (Table 3) shows some relationship between lithofacies and trace elements. For example, the skeletal grainstone of fore-bank/channel in Well-18

(Figure 53A), deposited within the intraplatform depression generally has very low Mn and Fe content associated with higher Mg and Sr values, regardless of the type of cements. Also, the high-energy rudist fragment grainstone facies of beach environment (Figure 52D), that was completely cemented records very low values in all trace elements possibly suggesting early meteoric diagenesis. This cementation occurred at the top of rudist buildups where an exposure surface developed, and the cement formed by meteoric diagenesis during subaerial exposure. This extensively cemented facies may form a vertical flow barrier within the reservoir.

The higher Mn values recorded in the large blocky calcite cements (Figure 53B) within the rudist skeletal fragments are formed just beneath the top Shu'aiba unconformity and were likely produced during karsting as the Shu'aiba platform was subaerially exposed. Calcite cements within of the rudist fragments that were affected by meteoric waters (Figures 52A and D) have relatively moderate Sr values (~130-200 ppm) indicating extensive flushing of Sr during meteoric diagenesis. The depletion of Mg values within the cemented rudist rudstone/grainstone facies also resulted from extensive recrystallization.

The highest group of Sr values (900 ppm and above) correspond to the skeletal rudist fragments that possibly represent their original Low Magnesium Calcite (LMC) shells that were not affected by diagenesis. These higher Sr values are also compatible with the suggested initial Sr composition of the Shu'aiba, which is approximately 1000 ppm (Swart and Lindsay, 2002). These original rudist shells have high Sr and Mg values (e.g Well-18 points 2 and 3, Well-506-11 points 4; Table 3; Figures 53A, B, D) along

with the preservation of the precursor fabric of the rudist, suggesting that these rudist shells were precipitated in an equilibrium with the original Cretaceous sea water. These rudist shells are mainly *Agriopleura* rudists deposited within the shallow lagoonal environments in the upper part of the Shu'aiba Formation. The caprinid *Offneria* rudists of the marginal bank-crest settings are very poorly preserved, suggesting they were possibly original high-Mg calcite or aragonite rudists.

Although there are some differences of the trace elements between the calcite cements and the micro-crystalline matrix, both values are still low, suggesting little evidence of marine or burial diagenesis. These results strongly suggest that diagenesis of the Shu'aiba Formation was mainly influenced by oxidizing meteoric diagenesis forming during the subaerial exposure event within the Shu'aiba Formation (e.g SB7) or during the widespread development of the uppermost Shu'aiba unconformity. However, the slight increase of Mn within some blocky calcite cements may indicate they formed during shallow burial within marine phreatic environments.

Cathodoluminescence (CL)

The precipitation of dull luminescent cements indicates a change from oxidizing near-surface waters to more reducing pore fluids (Meyers, 1978). The low occurrence of a clear, dull luminescent is related to the generally low Fe concentrations indicating oxidizing waters, although relatively higher Fe values occurred locally in few samples. The dull luminescent cements typically have higher amounts of Fe and moderate amount

of Mn and are likely the results of partial quenching of the Mn luminescence by Fe amounts in excess of about 1400 ppm (Grover and Read, 1983; Savard et al., 1995).

The NL phase of the rudist fragments (No.1; Figures 54B and D) represents the original LMC that was stable during diagenesis, supported by the higher concentration of Sr (1056 ppm) and moderate Fe and Mn contents (~ 62 to 150 ppm respectively). The moderate bright luminescent of the micritized rim (Figure 54) likely occurred in early dissolution stages within marine environments. This part of the rudist fragments was very soluble compared to the first zone and was possibly deposited as aragonite (Russell, 2001). Zone 3 of moderate bright luminescent within the micritized peloidal grains are similar to zone 2 of micritization rim (Figure 54), indicating that the micritized grains occurred early, simultaneously or just after the dissolution and recrystallization of rudist rim of zone 2. Zone 4 blocky calcite cements (Figure 54), occurred later on the diagenetic histories, possibly associated with meteoric fluids during the subaerial exposure of the Shu'aiba platform. The bright CL within the internal structure of the rudist fragments indicate dissolution and cementation of the internal structures within the original rudist fragments, likely occurred during the latest phases of Mn-rich cementation.

Isopachous cements formed on substrates at the edge of the rudist micrite zone (Figures 55A and B) has similar CL to the internal micrite sediments suggesting similar diagenetic stage. The Bright CL is the last stage formed as cements filling the intergranular porosity. The diagenetic history of this facies along with little CL

variations likely resulting from the dominant meteoric diagenesis occurred underneath the subaerial exposure surface of SB 7 at the top of the rudist buildups.

The skeletal grainstone facies and rudist rudstone facies of the shoal complex record four CL phases (Figures 55C and D). The diagenetic history of these facies includes micritization and dissolution of skeletal grains forming moldic porosity, followed by cementation of intergranular porosity and then late stage cementation of cavities.

Isotope Geochemistry

Carbon isotope values of calcite cements show more uniform clustering, have narrower variations and are similar to the carbon isotope values of the matrix; the majority of carbon isotope data plotted between 4 - 5‰ (Figure 57). This narrow range cluster within the isotope values of shallow environments rudist buildups of sequences 3 to 5 (Al-Ghamdi and Pope, 2013). The uniform values of calcite cements and their similarity with the original muddy matrix strongly suggest that the carbon isotope signature of the cements were not much affected by subsequent diagenesis, or reflects a highly rock-buffered system without organic involvement (Hudson, 1977). Despite the occurrence of the subaerial exposure surfaces within the Shu'aiba platform and the karst formation at the top Shu'aiba unconformity, little depletion of $\delta^{13}\text{C}$ depletion values of either the cements or matrix within the Shu'aiba Formation, suggesting they were not extensively affected by meteoric diagenesis. The increased carbon isotope value of the cements (5.5‰) near the subaerial exposure surface SB7, indicates the absence of

organic soils (plants) influence during subaerial exposure, suggesting possible dry climate during this interval (Al-Ghamdi and Pope, 2013). The highly depleted carbon and oxygen isotope values of the fracture fills were possibly due to the influence of hydrothermal fluids formed during the latest diagenetic events (Swart and Lindsay, 2002).

The two major separation in cluster trends occurs between mud matrix and calcite cements representing two systems linked to different diagenetic pathways (Figure 57). On the one hand, the mud matrix, which is mainly dominated by micro-rhombic calcite crystal with the so called "chalky" texture record wide variations of $\delta^{13}\text{C}$ values and more uniform with narrow variations of $\delta^{18}\text{O}$ values. On the other hand, the calcite cements record more uniform with narrow variations of $\delta^{13}\text{C}$ values and wider variations with more depleted $\delta^{18}\text{O}$ values. The wide variations of $\delta^{13}\text{C}$ in the mud matrix reflect the evolution of original ocean signature from the Early-Mid-to Late Aptian (see AL-Ghamdi and Pope, 2013). The large variations of $\delta^{18}\text{O}$ values in the calcite cements reflect an influence of meteoric diagenesis; deep burial diagenesis can only be seen in the fracture fills.

The oxygen isotope record of the calcite cements are interpreted to represent five major cements types that are likely related to different diagenetic environments or phases (Figure 62). Carbon isotope trends are uniform in all these cements, except in the latest fracture cements. The heaviest oxygen isotope values (-3.2‰ to -2.9‰) occurred within the original LMC rudist shell representing the original marine signature similar original $\delta^{18}\text{O}$ values of the Cretaceous (Lohmann, 1988). Micro-rhombic calcite plots

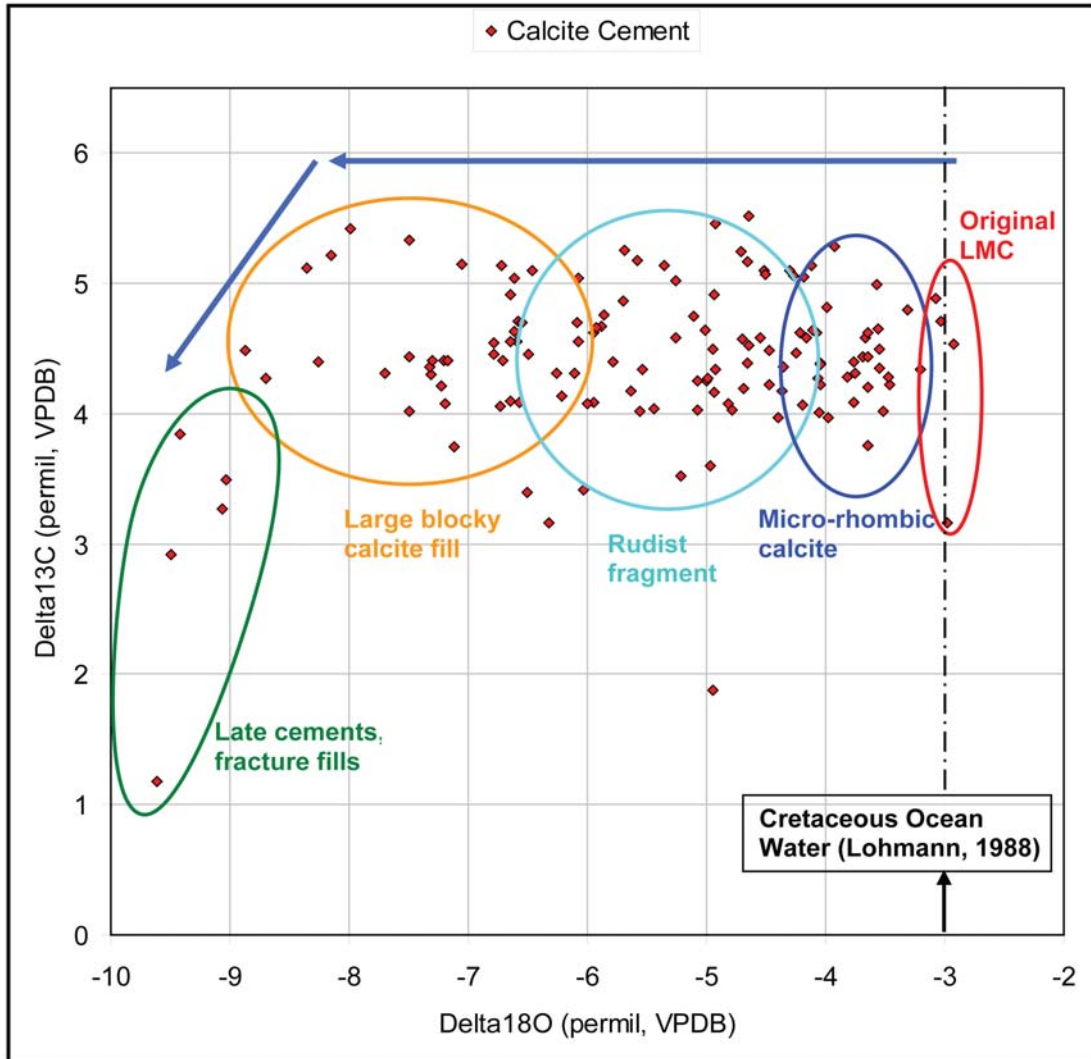


Figure 62. Cross plot of carbon and oxygen isotope data from calcite cements. Wide variations of oxygen isotope trend reflect different cement types.

within the original LMC rudist shell representing the original marine signature similar original $\delta^{18}\text{O}$ values of the Cretaceous (Lohmann, 1988). Micro-rhombic calcite plots between -4 and -3.3‰ representing the general matrix values. These relatively enriched values of the micro-rhombic calcite are due to the low permeability within the mud matrix that percolate the meteoric waters from infiltrating into the matrix, particularly within the open marine and basinal settings. Calcite cements within rudist skeletal fragments have $\delta^{18}\text{O}$ values between -4 and -5.5‰ and includes the micrite rim around the grains and the isopachous cements, both of which possibly formed during early marine that were later recrystallized by meteoric waters. Large blocky calcite cements filled the large rudist chambers, intergranular porosity, karst or caverns. These calcite cements have more depleted $\delta^{18}\text{O}$ values ranging from -5.5 to -8.7‰ and possibly formed in latest event from meteoric or possibly in very shallow burial environments. The most depleted $\delta^{18}\text{O}$ cements are the fractures filled cements that occurred in only a few samples and were possibly related to hydrothermal waters. This fractures filled cements also have depleted $\delta^{13}\text{C}$ values, thus supported the interpretation of hydrothermal waters.

Moshier (1989) and Budd (1989) concluded that the strontium isotope of the micro-rhombic calcite of the Early Cretaceous Thammama Formation reflects the initial composition of the sediment with no additional radiogenic Sr added during the diagenesis, thus suggesting a closed system diagenetic environment in either meteoric or marine diagenetic environments. Subsurface burial waters are typically enriched in $^{87}\text{Sr}/^{86}\text{Sr}$, usually higher than 0.7090. Therefore, the Shu'aiba matrix was not

diagenetically altered by deep subsurface brines (Woronick and Land; Budd, 1989). The $^{87}\text{Sr}/^{86}\text{Sr}$ data of the Shu'aiba Formation fluctuates from its base to its top possibly reflecting changes in the Early to Late Aptian ocean signature (Figure 12; AL-Ghamdi and Pope, 2013).

Paragenetic Sequence

Compiling all geochemical, trace element, CL petrography analysis, and isotope data, nine paragenetic events occurred within the Shu'aiba Formation (Figure 63). These nine events are summarized as:

1. Deposition of the Shu'aiba Formation with biodegradation and mechanical breakdown of rudist debris with both stable LMC and unstable aragonite cements.
2. Dissolution and micritization of rudist shell rims, and around the edges of peloidal grains during or just after deposition within marine environments.
3. Marine cementation of fringing isopachous cements around the skeletal and peloidal grains.
4. Dissolution and recrystallization of aragonite rudist shells.
5. Formation of large blocky calcite cements, plugging intergranular porosity. Second phase of cementation after the isopachous cements.
6. Major meteoric cementation event occurred at the time of platform exposure associated with SB7. This event mainly affected the upper part of the rudist buildup unit resulting in almost complete cementation of the rudist rudstone

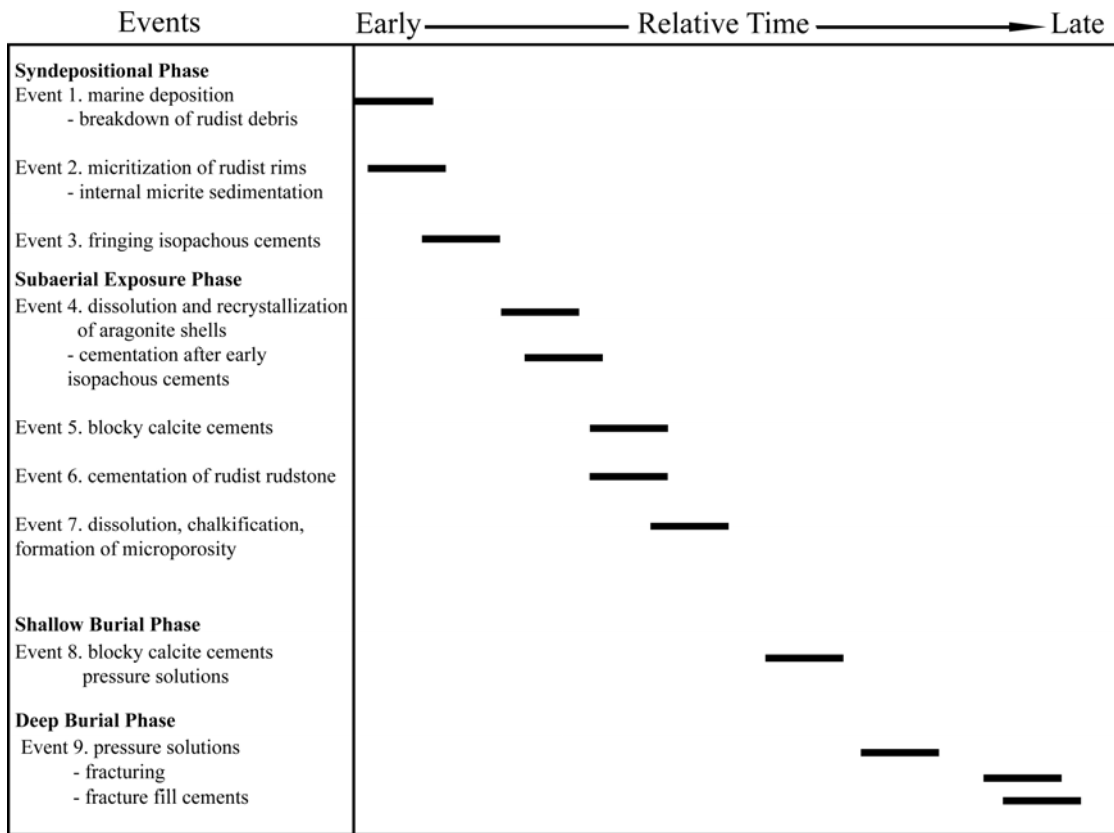


Figure 63. Paragenetic sequences of the main events from early to late diagenesis. Major diagenetic events occurred during the subaerial exposure phase.

deposited on beach environment that capped the rudist buildups. This event formed a baffle zone at this sequence boundary.

7. Major dissolution, chalkification and recrystallization event associated with the major subaerial unconformity at the top of the Shu'aiba Formation. At this time,
8. microporosity and the chalky texture were likely formed in open system meteoric environments.
9. Burial compaction associated with pressure solution and thin late stage cements fill occurred at shallow to deep burial.
10. Late stage fractures produced and filled with fracture-filling cement possibly by hydrothermal fluids.

Conclusions

The trace elements of the Shu'aiba Formation both matrix and cements are relatively low, reflecting either low values of the fluids (e.g Fe and Mn) or removal of elements during diagenesis (e.g. Sr and Mg). Fe and Mn contents represent the lower values of the original sediments with no additional values added during diagenesis, thus suggesting that the sediments were mainly influenced by meteoric fluids in oxidizing environments. Sr and Mg contents are very low compare to the original Cretaceous sea or modern carbonate rocks, indicating removal of these elements in an open system diagenetic environments. Fe and Mn trends are generally depleted with depth and following similar pattern, while Sr and Mg are positively correlated and following

similar trends. Mg and Sr are inversely correlated with Mn, but show some changes laterally reflecting changes in depositional settings.

Cathodoluminescence (CL) is best observed within the rudist buildups facies, where four to five CL zones can be identified, reflecting different stages of diagenesis. CL analysis helped identified the original stable LMC rudists with their NL zones from the recrystallized aragonite shells that have bright luminescence. Dull luminescent zones are less common, only forming thin layers at the edges of the blocky calcite crystals and reflecting the general low Fe contents.

Carbon isotopes of mud matrix and cements have similar values that range from ~ 1 to 6 ‰, reflecting the original carbon isotope record of the Cretaceous ocean. No evidence of $\delta^{13}\text{C}$ depletion associated of subaerial exposure or meteoric diagenesis observed from the cements, shells or mud matrix indicating a rock-buffered system. $\delta^{18}\text{O}$ values of the cements are very depleted with wide variations representing at least four stages of cementation from meteoric diagenesis. Deep burial diagenesis is only recorded in the late stage fracture fills. The average strontium isotope data of the Shu'aiba Formation is 0.07389, and fall within the range of Sr isotope of the Cretaceous ocean reflects the original composition of the sediments with no additional radiogenic Sr added during the diagenesis. This further support the interpretation that meteoric diagenesis was the most dominant process affecting Shu'aiba Formation.

The subaerial exposure surface occurred within the Shu'aiba Formation at the top of the rudist buildups at SB7 and the major unconformity at top of Shu'aiba Formation are the most important events that influence the diagenesis history of the Shu'aiba. The

major diagenetic stabilization events including the chalkification and development of micro-rhombic calcite occurred at the time or just after the platform exposure associated with meteoric fluids.

CHAPTER V

CONCLUSIONS

This study provides the most updated and accurate high-resolution sequence and chemostratigraphic frameworks covering the entire Shu'aiba platform using all available cored wells (50 wells), including carbon isotope profiles from 26 wells. This study also described the entire Biyadh Formation for the first time in the study area, providing the first depositional and stratigraphic model.

The Late Barremian Biyadh Formation represents one 3rd-order transgressive /regressive composite sequence (~3 My), consists of four high-frequency sequences (S1-S4). S1 and S2 are the TST of the Barremian composite sequence and are composed of deep chalky and marly limestone. S3 and S4 are the HST of the Barremian composite sequence and are composed of high-energy shallow water subtidal with Caprotinid rudist and peloidal grainstone facies. This sequence is capped by a regional subaerial boundary (SB1) corresponding to a global sea level fall.

The entire Shu'aiba Formation represents a 2nd-order composite sequence (~ 7 My duration) composed of four 3rd-order sequences (~1-2 My) and ten HFS's (S1-S10; each ~ 405 Ky - 1 My duration). S1 records the initial TST with the deposition of Hawar unit, followed by S2 that records the regional MFS (K70). S3 is the late TST of the Shu'aiba composite sequence and is characterized by the deposition of extensive *Lithocodium aggregatum*/coral facies associated with the onset of differentiated platform-to-basin settings with slight clinoform and backstepping geometries. The 3rd-

order sequence 2, consisting of sequences 4-6 and are dominated by rudist buildup facies that changed toward the platform interior into lagoonal facies and transitioned basinward into fore-bank, slope and basinal settings with pronounced clinoform geometries. This 3rd-order sequence has a transgressive lag at its base that deepens upward to the regional composite MFS (K80), then was shallowed up and capped by major sequence boundary (SB7) and exposure surface that records major changes in facies and biota. The 3rd-order sequence 3 consists of S7 and S8 and are dominated by shallow lagoonal peloidal milliolid packstone facies associated with local *Agriopleura* floatstone, representing the HST of the Shu'aiba composite sequence. The 3rd-order sequence 4 consists of the newly identified Upper Aptian sequences HFS's S9 and S10. These sequences are recorded on the northern-block within prograding platform edge and slope settings that formed during a major forced regression. Regional correlation suggests that more prograding sequences likely formed basinward.

This study proposed a refined global correlation between the Arabian Plate stratigraphic record and global stratigraphic record and global sea-level. This correlation strongly suggests a direct influence of the 3rd-order sea-level fluctuations on the Biyadh and Shu'aiba Formations. The Shu'aiba Formation records the perturbations of global carbon cycles associated with the nannoconids crisis and OAE1a. The global nannoconids crisis appears to be correlated with the deep chalky mudstone facies associated with the MFS in S2, that is coeval to the regional MFU (K70). The OAE1a with its distinctive carbon isotope values is coeval to the *Lithocodium aggregatum* facies of S3 and correlated to the TST of global sequence AP3. This correlation also suggests

that Aptian HFS's were mainly controlled by a glacio-eustatic sea-level changes and the long term eccentricity cycles (~ 405 Ky) were the main driving mechanism. The Barremian sequences record low magnitude sea-level changes with relatively thinner sequences compared to the Aptian. Moreover, the Barremian parasequences likely reflect obliquity (~ 40 Ky), whereas the Aptian parasequences are likely controlled by small scale eccentricity (~ 100 Ky) cycles. The Shu'aiba Formation records major subaerial hiatus reflecting glacial intervals, interrupted by major flooding units reflecting global warming intervals. These changes in the stratigraphic records and sea-level magnitude between the Barremian and Aptian suggest a prevailed greenhouse period during the Barremian, changed rapidly into a transitional climate period in the Aptian interrupted by glacial events.

Carbon isotope values of the Shu'aiba Formation have not undergone major meteoric diagenesis, and likely reflect the original marine values of the Early Cretaceous shallow platform waters. Therefore, carbon isotope data were integrated with well data and used as a chronostratigraphic correlation tools to refine the age model beyond the resolution of biostratigraphic age model. The fluctuations of the Shu'aiba Formation carbon isotope profile reflects global perturbation of carbon cycle that can be correlated worldwide. The major negative excursion in the Hawar unit is a global event associated with dissociation of methane hydrates in the basal Aptian. The major positive excursion within sequence 2 is also a global phenomena related to organic carbon burial and OAE 1a. Carbon isotope values of $\sim 4.5\text{‰}$ represent an important chronostratigraphic time line associated with the onset of rudist buildups in the middle Shu'aiba. This value is

well preserved and can be correlated despite major changes in facies from margin to slope and open marine. Although, isotope values of single stratigraphic time lines show some lateral variations with different environments, the general isotope trends are similar in pattern and are laterally correlative. These minor changes in carbon isotope values across environments are possibly related to changes in dominant organisms. The isotope profile of the Shu'aiba Formation can be used as a proxy for the third-order sea-level fluctuations, where carbon isotope enrichment is linked to sea-level rise and carbon isotope depletion is linked to sea-level fall.

The Shu'aiba Formation has undergone extensive diagenetic alterations that produced complex pore systems along with its complex facies architectures. The main diagenetic environments occurred during the late Aptian unconformity associated with meteoric waters. At this time major dissolution, chalkification and recrystallization events occurred possibly in open system meteoric environments.

The trace elements of the Shu'aiba Formation both matrix and cements are relatively low, reflecting either low values of the fluids (e.g. Fe and Mn) or removal of elements during diagenesis (e.g. Sr and Mg). Cathodoluminescence (CL) analysis indicates four to five CL zones, reflecting different stages of diagenesis. CL analysis helped identify the original stable LMC rudists with their NL zones from the recrystallized aragonite shells that have bright luminescence. Dull luminescent zones are less common, only forming thin layers at the edges of the blocky calcite crystals and reflecting the general low Fe contents. Carbon isotope values of mud matrix and cements are similar, reflect original carbon isotope record of the Cretaceous ocean, with no

evidence of $\delta^{13}\text{C}$ depletion associated of subaerial exposure or meteoric diagenesis. Oxygen isotope values of the cements are much depleted due to meteoric diagenesis, representing at least four stages of cementation. No evidence of deep burial diagenesis except few samples of late stage fracture fills.

REFERENCES

- Aktas, G., and G.W. Hughes, 1998, Geological framework of Shu'aiba reservoir: Sequence Stratigraphy, depositional model and reservoir quality. Saudi Aramco internal report.
- Al-Husseini, M.I., and Matthews, R.K., 2010, Tuning Late Barremian–Aptian Arabian Plate and global sequences with orbital period, *in* van Buchem, F.S.P., et al., (eds.), Barremian–Aptian stratigraphy and hydrocarbon habitat of the eastern Arabian Plate: Manama, Bahrain, Gulf PetroLink, GeoArabia Special Publication 4, v. 1, p. 199–228.
- Alley, N.F, and L.A. Frakes 2003, First known Cretaceous glaciation: Livingstone tillite member of the Cadna-Owie Formation, South Australia. Australian Journal of Earth Sciences. 50, p. 139-144.
- AL-Ghamdi, N., and J. F. Read, 2010, Facies-based sequence-stratigraphic framework of the Lower Cretaceous rudist platform, Shu'aiba Formation, Saudi Arabia. *in* Van Buchem, et al. (eds), Barremian –Aptian Stratigraphy and Hydrocarbon Habitat of the Eastern Arabian Plate. GeoArabia Special Publication 4, p. 367-410.
- AL-Ghamdi, N, M. and Pope, M., 2011, Integrated high-resolution chemostratigraphy and facies-based stratigraphic architecture of the Early Cretaceous (Aptian), Shu'aiba Formation, Saudi Arabia. Submitted to AAPG, *in review*.
- Amthor, J. E., C. Kerans and P. Gautheir, 2010, Reservoir characterisation of a Shu'aiba carbonate ramp-margin field, northern Oman. *in* Van Buchem, et al. (eds),

- Barremian –Aptian Stratigraphy and Hydrocarbon Habitat of the Eastern Arabian Plate. *GeoArabia Special Publication*, 4, v. 2, p. 549-576.
- Alsharhan, A. S., and A. E. M. Nairn, 1986, A review of the Cretaceous Formations in the Arabian Peninsula and Gulf: Part I. Lower Cretaceous (Thamama Group) Stratigraphic and Paleogeography. *Journal of Petroleum Geology*, v. 9, p. 365-392.
- Borgomano, J., Masse, J.P. and Al Maskiry, S. 2002. The Lower Aptian Shuaiba carbonate outcrops in Jebel Akhdar, northern Oman: Impact on static modelling for Shuaiba petroleum reservoirs. *AAPG Bulletin*, 86: 1513-1529.
- Bralower, T. J., P. D. Fullagar, C. K. Paull, G. S. Dwyer, and R. M. Leckie, 1997, Mid-Cretaceous Strontium-isotope stratigraphy of deep-sea sections: *Geological Society of America Bulletin*, v. 109, p. 1421-1442.
- Brand, U., and Veizer, W., 1980, Chemical diagenesis of a multicomponent carbonate-system-1: trace element: *Journal of Sedimentary Petrology*, v. 50, p. 1219-1236.
- Budd, D. A., 1989, Micro-rhombic calcite and microporosity in limestone: a geochemical study of the Lower Cretaceous Thamama Group, U.E.E. *Sedimentary Geology*, v. 63 (1989), P. 293-311.
- Carmatt, S. W., and B. St. John, 1986, Giant oil and gas fields, in M. T. Halbouty, ed., *Future petroleum provinces of the world: AAPG Memoir 40*, p. 11-53.
- Cantrell, D., P. Swart, and G. Mackenzie, 1999, The significance of the Geochemical Variation in the Shu'aiba Formation, Saudi Arabia as Diagenetic and Stratigraphic Indicators. Internal report, Saudi Aramco.

- Christian, L. 1997, Cretaceous subsurface geology of the Middle East region. *GeoArabia*, v. 2, no. 3, p. 239-255.
- Davies, R.B., D.M. Casey, A.D. Horbury, P.R. Sharland and M.D. Simmons 2002. Early to mid-Cretaceous mixed carbonate-siliciclastic shelfal systems: examples, issues and models from the Arabian Plate. *GeoArabia*, v. 7, p. 541-598.
- Denison, R. E., N. R. Miller, R. W. Scott, and D. F. Reaser, 2003, Strontium isotope stratigraphy of the Comanchean Series in north Texas and Southern Oklahoma: *Geological Society of America Bulletin*, v. 115, p. 669-682.
- Drever, J.I., 1982, *The Geochemistry of Natural Waters*. Prentice Hall, Englewood Cliffs, N. J., 388 pp.
- Droste, H. J., 2010, Sequence-stratigraphic framework of the Aptian Shu'aiba Formation in the Sultanate of Oman. In F.S.P. van Buchem, M.I. Al-Husseini, F. Maurer and H.J. Droste (Eds.). *Barremian-Aptian stratigraphy and hydrocarbon habitat of the eastern Arabian Plate*. *GeoArabia Special Publication 4*, Gulf PetroLink, Bahrain, v. 1, p. 229-283.
- Emrich K., D. H. Ehhalt, and J. C. Vogel, 1970, Carbon isotope fractionation during the precipitation of calcium carbonate. *Earth Planetary Science Letters*. V. 8, p. 363-371.
- Erbacher, J., D. Mosher, J. Bauldauf, and M. Malone, 2002, Equatorial Cretaceous and Paleogene paleoceanographic transect, western Atlantic. *Ocean Drilling Program Scientific Prospectus No. 107*.

- Fairchild, I. J., 1983, Cathodoluminescence of natural calcite and dolomites: new data and review, *Sedimentology*, v. 30, p. 579-538.
- Föllmi, K. B., H. Weissert, M. Bispin, and H. Funk, 1994, Phosphogenesis, carbon isotope Stratigraphy, and carbonate platform evolution along the Lower Cretaceous northern Tethyan margin: *Geological Society of America Bulletin*, v. 106, p. 729-746.
- Föllmi, K. B., A. Godet, S. Bodin, and P. Linder, 2006, Interactions between environmental change and shallow water carbonate buildup along the northern Tethyan margin and their impact on the Early Cretaceous carbon isotope record. *Paleoceanography*, v. 21, PA4211, p. 1-16.
- Frakes, L.A. 1999. Estimating the global thermal state from Cretaceous Seas surface and continental temperature. *In* Barrera, E. and C.C Johnson, (eds.), *Evolution of the Cretaceous Ocean-Climate System Geological Society of America. Special paper 332*. p. 49-57.
- Frakes, L. A., N. F. Alley, and M. Deynoux, 1995, Early Cretaceous ice rafting and climate zonation in Australia. *International Geology Review*, v. 37, p. 567-583.
- Frost, S. H., Bliefnick, D. M., and Harris, P. M., 1983, Deposition and porosity evolution of a Lower Cretaceous rudist buildup, Shuaiba Formation of eastern Arabian Peninsula, in *Carbonate Buildups, SEPM Core Workshop 4, Dallas*, p. 381-410.
- Glumac, B., and K. R. Walker, 1998, A late Cambrian positive carbon-isotope excursion in the southern Appalachians: Relation to biostratigraphy, sequence stratigraphy,

- environments of deposition, and diagenesis: *Journal of Sedimentary Research*, v. 68, No. 6, p. 1212-1222.
- Godet, A., S. Bodin, K. B. Föllmi, J. Vermeulen, S. Gardin, N. Fiet, T. Adatte, B. Zsolt, D. Stuben, and B. van de Schootbrugge, 2006a, Evolution of the marine stable carbon-isotope record during the Early Cretaceous: A focus on the late Hauterivian and Barremian in the Tethyan realm, *Earth and Planetary Science Letters*, 242, p. 254-271.
- Grossman, E. L., 1987, Stable isotopes in modern benthic foraminifera: A study of vital effect: *Jour. Foram. Res.*, v. 16, p. 48-61.
- Grover, G., Jr., and Read, J.F., 1983, Paleoaquifer and deep burial related cements defined by cathodoluminescent patterns, Middle Ordovician carbonates, Virginia: *Amer. Assoc. Petrologists Bull*, v. 7(8), p. 1275–1303.
- Hardenbol, J., J. Thierry, M.B. Farley, T. Jacquin, P.C. de Graciansky, and P. Vail, 1998, Mesozoic and Cenozoic sequence chronostratigraphic framework of European basins, *in* P.C. Graciansky, et al. (eds) *Mesozoic and Cenozoic Sequence Stratigraphy of European Basins: SEPM Special Publication 60*, p. 3-13, charts 1-8.
- Haq, B. U., and A. M. Al-Qahtani, 2005, Phanerozoic cycles of sea-level change on the Arabian Platform. *GeoArabia*, v. 10, no. 2, p. 127-160.
- Haq, B.U. and S.R. Shutter, 2008, A chronology of Paleozoic sea-level changes: *Science*, v. 322, October 2008, p. 64-68.

- Harris, P.M, S.H. Frost, G.A. Seiglie and N. Schneidermann 1984. Regional unconformities and depositional cycles, Cretaceous of the Arabian Peninsula. American Association of Petroleum Geologists, Memoir, v. 36, p. 67-80.
- Hillgartner, H., Van Buchem, F.S.P., Gaumet, F., Razin, P., Pittet, B., Grottsch, J., Droste, H., 2003, The Barremian-Aptian evolution of the eastern Arabian carbonate platform margin (northern Oman). Journal of Sedimentary Research 73, 756-773.
- Hochuli, P. A., A. P. Menegatti, H. Weissert, A. Riva, E. Erba, and I. Premoli Silva, 1999, Episodes of high productivity and cooling in the early Aptian Alpine Tethys. Geology, v. 27, p. 657-660.
- Huang C., Hinnov L., Fischer A.G., Grippo A. and Herbert T, 2010, Astronomical tuning of the Aptian Stage from Italian reference sections. Geology, 38, 899-902.
- Huck, S., U. Heimhofer, and A. Immenhauser, 2012, Early Aptian algal bloom in a neritic proto-North Atlantic setting: Harbinger of global change related to OAE 1a?, Geological Society of America Bulletin, doi:10.1130/B30587.1.
- Hudson, J. D., 1977, Stable isotopes and limestone lithification: Geological Society of London Journal, v. 133, p. 637-660.
- Hughes, G.W. 1997. The great pearl bank barrier of the Arabian Gulf as a possible Shu'aiba Analogue. GeoArabia, v. 2, no. 3, p. 279-303.
- Hughes, G.W. 2000. Bioecostratigraphy of the Shu'aiba Formation, Shaybah field, Saudi Arabia. GeoArabia, v. 5, no. 4, p. 545-578.

- Immenhauser, A., J. A. M. Al, Kenter, G. Ganssen, and J. E. Bahamonde, 2003, An alternative model for positive shifts in shallow-marine carbonate $\delta^{13}\text{C}$ and $\delta^{18}\text{O}$. *Sedimentology*, v. 50, p. 953-959.
- Immenhauser, A. and R. K. Matthews, 2004, Albian sea-level cycles in Oman: The 'Rosetta Stone' approach. *GeoArabia*, v. 9, no. 3.
- Immenhauser, A., H. Hillgärtner, U. Sattler, B. Bertotti, P. Schoepfer, P. Homewood, V. Vahrenkamp, T. Steuber, J. -P. Masse, H. H. J. Droste, J. van Koppen, B. van der Kooij, E. C. van Bentum, K. Verwer, E. Hoogerduijn-Strating, W. Swinkels, P. Peters, I. Immenhauser-Potthast, S.A.J. and Al Maskery, 2004, Barremian-Lower Aptian Qishn Formation, Haushi-Huqf area, Oman: a new outcrop analogue for the Kharaiib/Shu'aiba reservoirs. *GeoArabia*, 9: 153-194.
- Immenhauser, A., H. Hillgartner, and E, van Ventum, 2005, Microbial-foraminiferal episodes in the Early Aptian of the southern Tethyan margin, ecological significance and possible relation to oceanic anoxic event 1a. *Sedimentology*, v. 52, p. 77-99.
- Jahren, A. H., N. C. Arens, G. Sarmiento, J. Guerrero, and R. Amundson, 2001, Terrestrial record of methane hydrate dissociation in the Early Cretaceous. *Geology* 29 (2), p. 159-162.
- Jenkyns, H. C., 1995, Carbon-isotope stratigraphy and paleoceanographic significance of the Lower Cretaceous shallow-water carbonates of Resolution Guyot, mid-Pacific Mountains, in Winterer, E. L., et al., (eds.), *Proceedings of the Ocean*

Drilling Program, Scientific results, v. 143: College Station, Texas, Ocean Drilling Program, p. 99-104.

Jenkyns, H. C., 2003, Evidence for rapid climate in the Mesozoic-Palaeogene greenhouse world. *Phil. Trans. The Royal Society, London, A* 361, p. 1885-1916.

Kaufman, A. J., and A. H. Knoll, 1995, Neoproterozoic variations in the C-isotope composition of seawater: stratigraphy and biogeochemical implications: *Precambrian Research*, v. 73, p. 27-49.

Kerans, C., and S. Tinker., 1997, sequence stratigraphy and characterization of carbonate reservoirs: *SEPM Short Course Notes No. 40*, 130 p.

Larson, R. L., and E., Erba, 1999, Onset of the mid-Cretaceous greenhouse in the Barremian-Aptian: igneous events and the biological, sedimentary and geochemical responses. *Paleoceanography*, v. 14, p. 663-678.

Litsey, L. R., MacBride Jr., W. L., Al-Hinai, K. M., Dismukes, N. B., 1986, Shuaiba reservoir geological study, Yibal Field, Oman, in 3rd Middle East Oil Show Proceedings, Bahrain: Society of Petroleum Engineers of AIME, SPE Paper no. 11454, p. 131-142.

Klemme, H. D., and G. F. Ulmishek, 1991, Effective petroleum source rocks of the world--stratigraphic distribution and controlling depositional factors: *AAPG Bulletin*, v. 75, p. 1809-1851.

- Lohmann, K. C., 1988, Geochemical pattern of meteoric diagenetic systems and their application to the studies of paleokarst. In N.P., James and P.W. Choquette (Eds.), *Paleokarst*. New York, Springer Verlag, p. 58-80.
- Luciani, V., M. Cobianchi, and C. Lupi, 2006, Regional record of a global oceanic anoxic event: OAE1a on the Apulia platform margin, Gargano Promontory, Southern Italy. *Cretaceous Research*. v. 27, p. 754-772.
- Lucia, F. J., 2007, Carbonate reservoir characterization. Second Edition: New York, Springer-Verlag, 331 p.
- Machel, H. G., 2000, Application of cathodoluminescence to carbonate diagenesis. *Cathodoluminescence in geosciences*. P. 271-329.
- Matthews, R.K. and C. Frohlich 2002. Maximum flooding surfaces and sequence boundaries: comparisons between observations and orbital forcing in the Cretaceous and Jurassic (65-190 Ma). *GeoArabia*, v. 7, no. 3. p. 502-538.
- Meyers, W. J., 1978, Carbonate Cements: their regional distribution and interpretation in Mississippian limestones of southwestern New Mexico: *Sedimentology*, v. 25, p. 371-400.
- Moshier, S. O., Scott, R. W., Handford, C. R., and Boutell, R. D., 1988, Giant gas accumulation in a "chalky"-textured micritic limestone, Lower Cretaceous Shuaiba Fm, eastern United Arab Emirates, *SEPM Core Workshop no. 12*, Houston, p. 229-271.
- Moshier, S.O, 1989, Development of microporosity in a micritic limestone reservoir, Lower Cretaceous, Middle East. *Sedimentary Geology*, v. 63 (1989), P 217-240

- Murris, R. J., 1980, Middle East: Stratigraphic evolution and oil habitat, AAPG Bulletin, v. 64, p. 597-618.
- Patterson, W. P. and L. M. Walter, 1994, Depletion of ^{13}C in seawater CO_2 on modern carbonate platforms: Significance for the carbon isotopic record of carbonates. *Geology*, v. 22, p. 885-888.
- Pierson, B.J., G. P. Eberli, K.M. Al-Mehsin, S. Al-Menhali, G.M.D. Warrlich, H.J. Droste, F. Maurer, J. Whitworth and D. Drysdale 2010. Seismic stratigraphy and depositional history of the Upper Shu'aiba (Late Aptian) in the UAE and Oman. In F.S.P. van Buchem, M.I. Al-Husseini, F. Maurer and H.J. Droste (Eds.), Aptian stratigraphy and petroleum habitat of the Eastern Arabian Plate. *GeoArabia Special Publication 4*, Gulf Petrolink, Bahrain.
- Pittet, B., F.S.P. van Buchem, H. Hillgärtner, P. Razin, J. Grottsch and H. Droste 2002. Ecological succession, paleo-environmental change, and depositional sequences of Barremian-Aptian shallow-water carbonates in northern Oman. *Sedimentology*, v. 49, p. 555-581.
- Pratt, B. R., and Smewing, J. D., 1990, Jurassic and Early Cretaceous platform margin configuration and evolution, central Oman Mountains, in Robertson, A. H. F. and Searle, M. P., and Ries, A. C. (eds.), 1990, *The Geology and Tectonics of the Oman Region*, Geological Society Special Publication no. 49, p. 69-88.

- Russell, D.S. 2001, Reservoir characterization of the Shuaiba Formation (Lower Cretaceous) Abu Dhabi, United Arab Emirates and Jabel Akhdar, Sultanate of Oman. PHD thesis, University of Aberdeen.
- Savard, M. M., Veizer, J., and R. Hinton, 1995, Cathodoluminescence at low Fe and Mn concentrations: a SIMS study of zones in natural calcites, *Journal of Sedimentary Research*, v. A65, no. 1, p. 208-213.
- Scholle, P., and M. Arthur, 1980, Carbon isotope fluctuations in pelagic limestone: potential stratigraphic and petroleum exploration tool. *AAPG Bulletin*, v. 64, p. 67-87.
- Scott, R.W., Simo, J.A. and Masse, J.-P., 1993, Economic resources in Cretaceous carbonate platforms: An overview, *AAPG, Mem.*, 56: 15-24.
- Skeleton, P. W., and J-P. Masse, 2000, Synoptic guide to the Lower Cretaceous rudist bivalves of Arabia, *Society of Economic Paleontologists and Mineralogists, Special Publication*, v. 69, p. 85-95.
- Skelton, P. W., 2008, Identification of rudist type from Shu'aiba Formation, Saudi Aramco Internal Report.
- Sharland, P.R., R. Archer, D.M. Casey, R.B. Davies, S.H. Hall, A.P. Heward, A.D. Horbury and M.D. Simmons 2001. Arabian Plate sequence stratigraphy. *GeoArabia, Special Publication 2, PetroLink, Bahrain*, p. 371.
- Sharland, P.R., D.M. Casey, R.B. Davies, M.D. Simmons and O.E. Sutcliffe 2004. Arabian Plate sequence stratigraphy. *GeoArabia*, v. 9, p. 199-214.

- Simo, J.A. T., R. W. Scott., J.P. Masse, 1993, Cretaceous carbonate platforms: an Overview, AAPG Memoir. 56. p. 1-14.
- Steuber, T., 2002, Plate tectonic control on evolution of Cretaceous platform-carbonate production, *Geology*, v. 30, p. 259-262.
- Stoll, H. M., and D. P. Scharge, 2000a, High resolution stable isotope records from the Upper Cretaceous of Italy and Spain: glacial episodes in a greenhouse planet? *Geological Society of America Bulletin*, v. 112, p. 308-319.
- Strohmenger, C.J., L.J. Weber, A. Ghani, K. Al-Mehsin, O. Al-Jeelani, A. Al-Mansoori, T. Al-Dayyani, L. Vaughan, S.A. Khan and J.C. Mitchell 2006. High-resolution sequence stratigraphy and reservoir characterization of upper Thamama (Lower Cretaceous) reservoir of a giant Abu Dhabi oil field, United Arab Emirates, *in* P.M. Harris and L.J. Weber, eds., *Giant hydrocarbon reservoir of the world: From rocks to reservoir characterization and modeling 2006*. AAPG Annual Convention. p. 141-173.
- Swart, P., and Lindsay, R., 2002, The Development of Microporosity in the Shu'aiba Formation: A study on Shaybah well-Z. Saudi Aramco internal report.
- Ten Have, Ton, and Heignen, Wim, 1985, Cathodoluminescence activation and zonation in carbonate rocks: *Geologie en Mijnbouw*, v. 64, p. 297-310.
- Woronick, R. E., and Land, L. S., 1985, Late burial diagenesis, Lower Cretaceous Pearsall and Lower Glen Rose Formations, South Texas. *in* N. Schneidermann and P. M. Harris, Eds., *Carbonate Cements*. Soc. Econ. Paleontologists and Mineralogists Spec. Pub. No. 36, p. 265-275.

- Vahrenkamp, V. C., 1996, Carbon Isotope Stratigraphy of the Upper Kharaiib and Shu'aiba Formations: Implications for the Early Cretaceous Evolution of the Arabian Gulf Region. AAPG Bulletin, v. 80, p. 647-662.
- Vahrenkamp, V. C., 2010, Chemostratigraphy of the Lower Cretaceous Shuaiba Formation: A $\delta^{13}\text{C}$ reference profile for the Aptian Stage from the southern Neo-Tethys Ocean. *in* Van Buchem, et al. (eds), Barremian –Aptian Stratigraphy and Hydrocarbon Habitat of the Eastern Arabian Plate. GeoArabia Special Publication 4, p. 107-137.
- Van Buchem, F.S.P., Pittet, H. Hillgartner, J. Grottsch, A.I. Mansouri, I.M. Billing, H.H.J. Droste, W.H. Oterdoom and M. Van Steenwinkel 2002. High-resolution sequence stratigraphic architecture of Barremian/ Aptian carbonate in northern Oman and the United Arab Emirates (Kharaiib and Shuaiba Formations): GeoArabia, v. 7, p. 461-500.
- Van Buchem F.S.P., M.I. Al-Husseini, F. Maurer, H.J. Droste and L.A. Yose, 2010, Sequence-stratigraphic synthesis of the Barremian-Aptian of the eastern Arabian Plate and implications for the petroleum habitat. In F.S.P. van Buchem, M.I. Al-Husseini, F. Maurer and H.J. Drost (Eds.). Barremian-Aptian stratigraphy and hydrocarbon habitat of the eastern Arabian Plate. GeoArabia Special Publication 4, Gulf PetroLink, Bahrain, v. 1, p. 9-48.
- Varol, O., 1993, Nannofossil biostratigraphy of Shu'aiba Formation. Saudi Aramco Internal report.

- Weissert, H., and A. Lini, 1991, Ice age interludes during the time of Cretaceous greenhouse climate? In Muller, D. W., Mckenzie, J. A., and Weissert, H., eds., *Controversies in modern geology*: London, Academic Press, p. 173-191.
- Weissert, H., A. Lini, K. B. Föllmi, and O. Kuhn, 1998, Correlation of Early Cretaceous carbon isotope stratigraphy and platform drowning events: a possible link? *Palaeogeography. Palaeoclimatology. Palaeoecology*, v. 137, p. 189-203.
- Weissert, H., and E. Erba, 2004, Volcanism, CO₂ and palaeoclimate: a Late Jurassic-Early Cretaceous carbon and oxygen isotope record. *Journal of the Geological Society*, London, v. 161, p. 695-702.
- Witt, W. and H. Gokdag, 1994, Orbitolind biostratigraphy of the Shu'aiba Formation (Aptian), Oman - implications for reservoir development. In M.D. Simmons (Ed.), *Micropalaeontology and Hydrocarbon Exploration in the Middle East*. British Micropalaeontological Society Publication Series, Chapman and Hall, Cambridge, p. 221-242.
- Xiong, B., and P. H. Heckel, 1996, Cementation patterns and diagenesis in the Stanton Limestone/cyclothem (Missourian, Upper Pennsylvanian) in the northern Midcontinent. in Witzke, B. J., G. A. Ludvigson, and J. Day, eds., *Paleozoic Sequence Stratigraphy: Views from the North American Craton*: Boulder, Colorado, Geological Society of America, Special Paper 306.
- Yose, L. A., A. S. Ruf, C.J. Strohmenger, J. S. Schuelke, A. Gombos, I., Al-Hosani, S., Al-Maskary, G. Gloch, and Y. Al-Mehairi, 2006, Volume based characterization of a heterogeneous carbonate reservoir, Lower Cretaceous, Abu Dhabi

(U.A.E.), in P.M. Harris and L.J. Weber, (eds.), Giant hydrocarbon reservoir of the world: From rocks to reservoir characterization and modeling. 2006, AAPG Annual Convention. p. 175-214.

Yose, L. A., Strohmenger, I., Al-Hosani, G. Bloch and Y. Al-Mehairi, 2010, Sequence-stratigraphic evolution of an Aptian carbonate platform (Shu'aiba Formation), eastern Arabian Plate, onshore Abu Dhabi, United Arab Emirates. In F.S.P. van Buchem, M.I. Al-Husseini, F. Maurer and H.J. Droste (Eds.), Barremian - Aptian stratigraphy and hydrocarbon habitat of the Eastern Arabian Plate. GeoArabia Special Publication 4, Gulf Petrolink, Bahrain, v. 2, p. 309-340.

Ziegler, M.A. 1976. Rocks and fabrics in the lower Cretaceous Shu'aiba Formation of the Shaybah field and in eastern Saudi Arabia. Saudi Aramco Internal report.